Understanding and exploiting zinc toxicity in *Streptococcus pneumoniae*

Erin Bridget Brazel, BSc (Hons)

A thesis submitted for the fulfilment of the

Degree of Doctor of Philosophy



May 2020

Research Centre for Infectious Diseases

Department of Molecular and Biomedical Science

School of Biological Sciences

University of Adelaide

Adelaide, South Australia, Australia

TABLE OF CONTENTS

TABLE OF CONTENTS ii
DECLARATION v
ABSTRACT vi
ABBREVIATIONS viii
TABLE OF TABLES xi
TABLE OF FIGURES xii
ACKNOWLEDGEMENTS xv
CHAPTER 1: Introduction 1
1.1 The global threat of antibiotic resistance 2
1.2 *Streptococcus pneumoniae* 2
1.2.1 *S. pneumoniae* prevention strategies 3
1.2.2 Treatment of pneumococcal disease 5
1.3 Novel antimicrobial strategies 8
1.4 *S. pneumoniae* asymptomatic colonisation 10
1.5 Transmission of *S. pneumoniae* 13
1.6 *S. pneumoniae* invasive disease 14
1.7 *S. pneumoniae* and the immune system 16
1.7.1 Adaptive immunity 16
1.7.2 Innate immunity 17
1.8 Zinc and infectious disease 18
1.9 Metal toxicity 22
1.10 Metal ion homeostasis 23
1.10.1 Metal sensors 23
1.10.2 Metal transporters 24
1.10.2.1 Cation Diffusion Facilitator transporters 25
1.10.2.2 P-type ATPase transporters 29
1.10.2.3 ATP-binding Cassette transporters 30
1.10.3 Metal buffering systems 31
1.11 Rationale for the project and aims of the study 32
CHAPTER 2: Materials and Methods 34
2.1 Bacterial strains and oligonucleotides 35
2.2 Bacterial culturing 35
2.3 Genomic DNA isolation 35
2.4 PCR and agarose gel electrophoresis 41

2.5 DNA quantification and sequencing....41
2.6 Pneumococcal transformation....41
2.7 Growth Kinetics Assays....42
2.8 Whole cell metal accumulation....42
2.9 RNA extraction....43
2.10 Quantitative Reverse Transcription-Polymerase Chain Reaction....43
2.11 RNA sequencing....44
2.12 Cluster of orthologous group analysis....44
2.13 Membrane topology modelling....44
2.14 Structural modelling....45
2.15 Fatty acid analyses....45
2.16 Membrane fluidity studies....45
2.17 Uronic acid capsule assay....46
2.18 Metabolomics....46
2.19 Phosphofructokinase activity assay....47
2.20 6-phosphogluconate dehydrogenase activity assay....47
2.21 Cloning and mutagenesis of GlmU....48
2.22 Expression and purification of GlmU....48
2.23 Crystallisation of GlmU....49
2.24 Structure determination, building and refinement....50
2.25 GlmU acetyltransferase activity assay....50
2.26 Mice....51
2.27 Pneumococcal infection model....51
2.28 *In vivo* pneumococcal transcriptional analyses....51
2.29 Macrophage survival assays....52
2.30 Penicillin survival experiment....53
2.31 Antibiotic susceptibility analyses....53
CHAPTER 3: The role of CzcD in *Streptococcus pneumoniae* zinc resistance....54
3.1 Introduction....55
3.2 Results....57
3.2.1 Global transcriptional responses to zinc stress in *S. pneumoniae*....57
3.2.2 Bioinformatic analysis of *czcD*....64
3.2.3 *czcD* provides resistance to host-mediated zinc intoxication....69
3.2.3.1 *czcD* contributes to resistance to zinc stress....69
3.2.3.2 *czcD* protects against macrophage-mediated killing....75
3.3 Discussion....77
CHAPTER 4: Characterisation of the cellular targets of zinc toxicity....83

4.1 Introduction....84
4.2 Results....86
4.2.1 Global metabolomic responses to zinc stress in *S. pneumoniae*....86
4.2.2 Zinc disrupts glycolysis in *S. pneumoniae*....94
4.2.3 Zinc upregulates the galactose utilisation Leloir pathway....101
4.2.4 Zinc alters the pentose phosphate pathway....114
4.2.5 Zinc stress disrupts the cell wall biosynthesis pathway....118
4.2.6 Intracellular zinc alters *S. pneumoniae* membrane physiology....123
4.3 Discussion....133
CHAPTER 5: Exploiting zinc to improve antibiotic efficacy....140
5.1. Introduction....141
5.2. Results....145
5.2.1 Bioinformatic analyses of CzcD and human ZnT proteins....145
5.2.2 The ionophore PBT2 increases the potency of zinc stress....149
5.2.3 PBT2 and zinc enhances the antibiotic susceptibility of antibiotic resistant *S. pneumoniae*....152
5.2.4 The impact of zinc and PBT2 treatment on pneumococcal disease....155
5.2.5 *In vivo* studies of PBT2 and gentamicin treatment....157
5.3. Discussion....164
CHAPTER 6: Final Discussion....169
6.1 The role of CzcD in *S. pneumoniae* zinc resistance....170
6.2 The cellular targets of *S. pneumoniae* zinc toxicity....172
6.3 Exploiting zinc stress in a novel treatment strategy against *S. pneumoniae*....176
6.4 Conclusions....178
APPENDIX 1....179
APPENDIX 2....181
APPENDIX 3....183
APPENDIX 4....185
APPENDIX 5....187
APPENDIX 6....189
APPENDIX 7....194
APPENDIX 8....199
REFERENCES....202

DECLARATION

I certify that this work contains no material which has been accepted for the award of any other degree or diploma in my name, in any university or other tertiary institution and, to the best of my knowledge and belief, contains no material previously published or written by another person, except where due reference has been made in the text.

In addition, I certify that no part of this work will, in the future, be used in a submission in my name, for any other degree or diploma in any university or other tertiary institution without the prior approval of the University of Adelaide and where applicable, any partner institution responsible for the joint-award of this degree.

I give permission for the digital version of my thesis to be made available on the web, via the University's digital research repository, the Library Search and also through web search engines, unless permission has been granted by the University to restrict access for a period of time.

I acknowledge the support I have received for my research through the provision of an Australian Government Research Training Program Scholarship.

Erin B Brazel
May 2020

ABSTRACT

Antibiotic resistance is associated with increased treatment costs, longer hospital durations and higher rates of mortality. To address this globally significant challenge, novel strategies to control antibiotic resistant pathogens are essential. The world's foremost bacterial pathogen, *Streptococcus pneumoniae*, is responsible for more than one million deaths and an estimated 14.5 million cases of serious disease each year. The metal ion zinc has a critical antimicrobial role in innate immune defence and a dietary deficiency in zinc is associated with a marked increase in susceptibility to bacterial infections. Despite this association, precisely how zinc contributes to the control of bacterial infection is poorly defined. The major aim of this thesis was to understand and exploit the antibacterial action of zinc as a novel treatment against *S. pneumoniae.*

A combination of bioinformatic and structural modelling analyses drew on insights from the canonical cation diffusion facilitator family member, YiiP from *E. coli*, to explore the zinc resistance protein, CzcD, in *S. pneumoniae*. Further phenotypic analyses showed that *S. pneumoniae* CzcD directly contributes to pneumococcal zinc efflux and that this protein is important for resistance to zinc stress. Further, this work showed that CzcD contributed to survival within macrophages, indicating that the antimicrobial action of zinc is exploited to aid in the clearance of *S. pneumoniae* in phagocytic cells.

Despite the importance of zinc at the host-pathogen interface and its known antimicrobial role, the basis for zinc toxicity in *S. pneumoniae* is poorly defined. This work addressed this issue by investigating the pathways affected by zinc stress in *S. pneumoniae*. Transcriptomic and metabolomic studies showed that zinc altered key pneumococcal pathways, including central carbon metabolism, the pentose phosphate pathway, cell wall biosynthesis and *de novo* fatty acid biosynthesis. Of these pathways, further activity and phenotypic analyses showed that zinc may impair the activity of a number of putative protein targets, including glycolytic enzyme PfkA, pentose phosphate pathway enzyme Gnd, and the peptidoglycan biosynthesis enzyme GlmU. The capacity for zinc to impair these essential pathways directed studies to assess the influence of zinc on antibiotic action. Abolishment of zinc efflux via CzcD led to enhanced susceptibility to penicillin, indicating that excess intracellular zinc is capable of enhancing susceptibility to antibiotics.

Building on these findings, the ionophore activity of the safe for human use drug, PBT2, was repurposed to increase cellular zinc in *S. pneumoniae,* which rendered antibiotic resistant *S. pneumoniae* susceptible to a range of antibiotics. Despite *in vitro* success, preliminary transcriptional studies of *S. pneumoniae* from murine tissues highlighted the complexity associated with the translation of this treatment strategy. Nevertheless, this work provides a foundation for future studies to further optimise ionophore-induced bacterial zinc intoxication *in vivo* and therefore enhance pneumococcal susceptibility to antibiotic treatment.

Together, the work presented in this thesis significantly expands our understanding of the antimicrobial action of zinc, which may apply to a range of bacterial pathogens. This work describes a novel treatment approach where zinc toxicity may be harnessed to combat antibiotic-resistant *S. pneumoniae* disease. As antibiotic efficacy continues to decline, insights gained in this study may be applied to the treatment of a range of other clinically significant bacterial pathogens. Together, the improved antibiotic efficacy by zinc may provide a safety net to bridge the gap until the development of novel antimicrobial strategies to combat bacterial disease.

ABBREVIATIONS

°C	Degrees Celsius
6-PGD	6-phosphogluconate dehydrogenase
Å	Angstrom
ABC	ATP-binding cassette
ADP	Adenosine diphosphate
ADP	Alzheimer's Disease
AGRF	Australian Genome Research Facility
Ala	Alanine
ANOVA	Analysis of variance
Asp	Aspartic acid, aspartate
ATP	Adenosine triphosphate
BA	Blood agar
bp	Base pairs
BSA	Bovine serum albumin
C+Y	A semi synthetic yeast-based medium
CDF	Cation diffusion facilitator
CFU	Colony forming units
COG	Cluster of orthologous groups
CPS	Capsular polysaccharide
CSP	Competence stimulating peptide
CTD	C-terminal domain
DMSO	Dimethyl sulfoxide
DNA	Deoxyribonucleic acid
DOC	Deoxycholate
ECF	Energy-coupling factor
EDTA	Ethylenediaminetetraacetic acid
g	Gram
g	Centrifugal force
GI	Gene identifier
Glu	Glutamic acid, glutamate
GSH	Reduced glutathione
GSSG	Oxidised glutathione
HBSS	Hank's Buffered Salt Solution
His	Histidine
HIV	Human Immunodeficiency Virus
hrs	Hours
IAV	Influenza A virus
ICP-MS	Inductively coupled plasma-mass spectrometry
ID	Identification
IP	Intraperitoneal

K	Kelvin
kb	kilobase
KEGG	Kyoto Encyclopedia of Genes and Genomes
LB	Luria Bertani
M	Molar
MHB	Mueller Hinton broth
MHC-1	Major histocompatibility complex class 1
MIC	Minimum inhibitory concentration
min	Minute
ml	Millilitre
mM	Millimolar
NADPH	Nicotinamide adenine dinucleotide phosphate
NCBI	National Centre for Biotechnology Information
NET	Neutrophil extracellular trap
ng	Nanogram
nM	Nanomolar
NTD	N terminal domain
OD	Optical density
PBP	Penicillin binding protein
PBS	Phosphate buffered saline
PC	Principal component
PCA	Principal component analysis
PCR	Polymerase chain reaction
PCV	Protein conjugate vaccine
PDB	Protein Data Bank
PFK	Phosphofructokinase
PGM	Phosphoglucomutase
Ply	Pneumolysin
PMA	Phorbol 12-myristate 13 acetate
PMN	Polymorphonuclear
PPrV	Pneumococcal protein vaccines
PTS	Phosphotransferase system
qRT-PCR	Quantitative reverse transcription-PCR
RMSD	Root mean square distance
RNA	Ribonucleic acid
ROS	Reactive oxygen species
RPMI	Roswell Park Memorial Institute
RT	Room temperature
SBP	Solute binding protein
SDS-PAGE	Sodium dodecyl sulphate-polyacrylamide gel electrophoresis
SEM	Standard error of the mean
TAE	Tris acetate EDTA
THY	Todd Hewitt broth with yeast

TM	Transmembrane
TMD	Transmembrane domain
TPEN	N,N,N′,N′-Tetrakis(2-pyridylmethyl)ethylenediamine
V	Volts
v/v	Volume per volume
w/v	Weight per volume
WCV	Whole cell vaccine
µg	Microgram
µl	Microlitre

TABLE OF TABLES

Table 2.1 Bacterial strains used in this study.....36
Table 2.2 Oligonucleotide primers used in the study 37

Table 3.1 Upregulated genes in *S. pneumoniae* D39 in response to zinc stress 59
Table 3.2 Downregulated genes in *S. pneumoniae* D39 in response to zinc stress 61

Table 4.1 Metabolites with increased abundance in *S. pneumoniae* grown with 100 μM zinc relative to untreated 89
Table 4.2 Metabolites with decreased abundance in *S.s pneumoniae* grown with 100 μM zinc relative to untreated 92

Table 5.1 Sequence identity and similarity of *S. pneumoniae* CzcD with human ZnT zinc-transporting cation diffusion facilitator family members 146
Table 5.2 Putative metal binding residues of *S. pneumoniae* CzcD and human ZnT family proteins 148
Table 5.3 PBT2 minimum inhibitory concentrations for the *S. pneumoniae*^{Spain23F} strain in the presence and absence of zinc 153
Table 5.4 Antibiotic minimum inhibitory concentrations for *S. pneumoniae*^{Spain23F} with sub-inhibitory zinc and PBT2.....156
Table 5.5 Gentamicin minimum inhibitory concentrations for *S. pneumoniae* D39 with sub-inhibitory zinc and PBT2 treatment.....162

TABLE OF FIGURES

Figure 1.1 Zinc intoxication and starvation strategies are exploited by phagocytic cells to clear invading bacteria.....21
Figure 1.2 Overview of the zinc homeostatic pathways of *S. pneumoniae*.....1
Figure 1.3 Major classes of metal transporters in *S. pneumoniae*.....28

Figure 3.1 Differential gene expression in *S. pneumoniae* D39 in response to zinc stress.....58
Figure 3.2 Validation of RNA sequencing data.....62
Figure 3.3 Cluster of Orthologous Groups classification for genes altered in *S. pneumoniae* D39 by zinc stress.....63
Figure 3.4 Predicted membrane topology model for CzcD from *S. pneumoniae*.....65
Figure 3.5 Structural modelling and predicted surface charge of CzcD.....67
Figure 3.6 Sequence alignment of *S. pneumoniae czcD* with zinc-transporting cation diffusion facilitator proteins from other bacterial species.....68
Figure 3.7 Structural modelling of the CzcD metal binding site A.....70
Figure 3.8 Transcriptional response of *S. pneumoniae czcD* to zinc.....71
Figure 3.9 Growth kinetics of *S. pneumoniae* D39 wild-type and D39 Δ*czcD*.....72
Figure 3.10 Cellular zinc and manganese accumulation in *S. pneumoniae* D39 and D39 Δ*czcD*.....74
Figure 3.11 The role of CzcD in *S. pneumoniae* survival in THP-1 cells.....76

Figure 4.1 Principal component analysis (PCA) score plot of metabolic profiles in *S. pneumoniae* treated with or without zinc.....87
Figure 4.2 Zinc induces significant changes in metabolite abundance in *S. pneumoniae*.....88
Figure 4.3 Overview of the cellular pathways impacted by zinc in *S. pneumoniae*.....97
Figure 4.4 Changes in carbohydrate abundance in *S. pneumoniae* induced by zinc.....99
Figure 4.5 Zinc alters the abundance of metabolites in the glycolytic pathway.....100
Figure 4.6 Transcription of *S. pneumoniae* glycolytic genes in the presence of zinc.....102
Figure 4.7 Amino acid sequence alignment of PfkA from *S. pneumoniae* and *S. pyogenes*..103
Figure 4.8 Zinc decreases *S. pneumoniae* phosphofructokinase activity.....104
Figure 4.9 Transcription of *S. pneumoniae* galactose utilisation genes in the presence of zinc.....106

Figure 4.10 Carbon source influences growth kinetics of *S. pneumoniae* treated with zinc ..107
Figure 4.11 Confirmation of *S. pneumoniae ccpA* mutagenesis.....109
Figure 4.12 Growth kinetics of the *S. pneumoniae* D39 wild-type and Δ*ccpA* strains.....110
Figure 4.13 Transcription of galactose utilisation genes in the presence of zinc in *S. pneumoniae* D39 and Δ*ccpA* 111
Figure 4.14 Zinc treatment increases the abundance of UDP-glucose in *S. pneumoniae* 112
Figure 4.15 Zinc reduces *S. pneumoniae* total capsule production when glucose is dominant carbon source 113
Figure 4.16 Zinc-treated *S. pneumoniae* display increased 6-phosphogluconate levels 115
Figure 4.17 Zinc does not alter the transcription of *S. pneumoniae gnd* 116
Figure 4.18 Zinc impairs *S. pneumoniae* 6-phosphogluconate dehydrogenase activity.....117
Figure 4.19 Zinc alters the abundance of metabolites in the cell wall biosynthesis pathway 119
Figure 4.20 Zinc does not alter the transcription of the *S. pneumoniae* peptidoglycan biosynthesis genes 120
Figure 4.21 Zinc binds the acetyltransferase domain of GlmU 121
Figure 4.22 Zinc impacts the activity of *S. pneumoniae* GlmU 122
Figure 4.23 Zinc can enhance the susceptibility of *S. pneumoniae* to penicillin.....124
Figure 4.24 Changes in lipid metabolites in *S. pneumoniae* induced by zinc 125
Figure 4.25 Zinc alters the abundance of lipids and lipid precursor metabolites in *S. pneumoniae* 126
Figure 4.26 Excess intracellular zinc alters the fatty acid composition of the *S. pneumoniae* membrane 128
Figure 4.27 Intracellular zinc increases the relative abundance of membrane saturated fatty acids in *S. pneumoniae* 129
Figure 4.28 Zinc treatment alters the fluidity of the *S. pneumoniae* membrane.....130
Figure 4.29 Zinc does not alter the transcription of genes in the *S. pneumoniae* fatty acid synthase II pathway 131

Figure 5.1 Primary sequence alignment of *S. pneumoniae* CzcD with human ZnT4.....147
Figure 5.2 PBT2 enhances the toxicity of zinc against *S. pneumoniae* 150
Figure 5.3 PBT2 increases *S. pneumoniae* cellular zinc accumulation 151
Figure 5.4 Treatment with sub-inhibitory zinc and PBT2 reduces survival of *S. pneumoniae*^{Spain23F} ST81 strain in the presence of antibiotics 154

Figure 5.5 Changes in body weight induced by treatment with zinc and PBT2 treatment during *S. pneumoniae* infection.....158
Figure 5.6 Impact of zinc and PBT2 treatment on *S. pneumoniae* infection.....159
Figure 5.7 Impact of zinc and PBT2 treatment on transcription of *S. pneumoniae* zinc-responsive genes during infection 160
Figure 5.8 Host infection of *S. pneumoniae* following PBT2 and gentamicin treatment.....163

ACKNOWLEDGEMENTS

This thesis marks the end of my journey towards a PhD. Scientific research has been a roller coaster filled with addictive ups and inevitable downs. Reflecting on this time, I am overwhelmed with gratitude to all of the people that have contributed to this journey so far. I am thankful to those that helped further my development as a scientist, performed critical experiments that have shaped the course of this research, and provided me with unwavering support over the years. Together, this help has made the road to PhD a little less bumpy and for that I am grateful.

Firstly, to my principal supervisor, Associate Professor Christopher McDevitt, thank you for your guidance and support throughout my scientific journey. I began this journey filled with excitement and trepidation. I have learnt so much under your guidance and gained confidence and resilience in the process. I am appreciative for all of the opportunities you have provided me with throughout my time in the lab.

To my co-supervisor, Professor James Paton, thank you for your continued support over the years. Your knowledge of pneumococcal biology is unparalleled, and I am grateful to have had your feedback and expert advice to help me better understand this fascinating pathogen. Most importantly, thank you for welcoming me into the lab when I found myself without one and for providing amusing, delightful and sometimes questionable conversations over morning tea.

To Dr Bart Eijkelkamp, thank you for always being there to provide friendly guidance, for pushing me to scrutinise my results, and for inspiring me to be a better scientist. Your supervision throughout my PhD has been invaluable and I have learnt so much from your guidance. Thank you for always taking the time to help, for offering your advice when I need it, and especially for all the banter. Most of all, thank you for your endless enthusiasm and delight when looking at new results - your excitement is contagious.

To Dr Victoria Pederick, thank you for being an endless source of support, for always being there to talk through my experimental ideas, and for your encouragement over the years. Most importantly, thank you for the long chats that helped me to put things in perspective, and

for listening and allowing me to vent when there simply was no upside. I am so grateful to have had your friendship during this time, I could not have done it without you.

To Dr Jacqui Morey, thank you for being there by my side to celebrate the wins, to vent the frustrations, and to laugh in absolute hysterics. Your friendship helped me get through some of the hardest times and I am so grateful to have embarked on this journey with your help.

To Dr Stephanie Neville, thank you for all the laughs and for easing my stress with post-conference talk drinks. Thank you to all members of the McDevitt Lab that helped keep me sane, in particular members of the student squad, Marina Zupan and Saleh Alquethamy. To Dr Richard Harvey, thank you for being an infinite source of pneumococcal wisdom and for all of your helpful advice. To Dr Danny Wilson, Dr Sonja Frölich and Dr Matt Doyle, thank you for being so friendly and for taking the time to offer your guidance and support towards my career development. Thank you to all members of the Paton Laboratory, especially Dr Claudia Trappetti, Kim McLean, Dr Alex Tikhomirova, Dr Shannon David, Vik Minhas, Cathy Scougall, Dr Adrienne Paton, Dr Hui Wang and Dr Lauren McAllister for being so welcoming and providing endless laughs. Thank you to members of the Research Centre for Infectious Diseases, in particular members of the Wilson Laboratory and Morona Laboratory, for making my PhD an enjoyable experience.

This work would not have been possible without the input of critical collaborators, whose work provided fundamental insight into the project. Thank you to Dr Bart Eijkelkamp and Dr Stephanie Neville for their analyses of the transcriptomic datasets, Dr Jason Rosch and Dr Stephanie Neville for their contribution to the metabolomic studies, Associate Professor Megan Maher, Mwilye Sikanyika and Dr Saumya Udagedara for directing and performing the GlmU studies, Dr Bart Eijkelkamp for assistance with the animal infection studies, and Jonathan Whittall for assistance with the capsule experiments.

Most importantly, I am so grateful to have had such an amazing family by my side during my PhD. Thank you to Mum and Dad for all of your love and support over the years, for always being there to listen and have a drink, and for putting up with me being a student seemingly forever. Thank you to James and Greta for all the laughs, love and support. To George, thank you for keeping me sane, for bringing me teas, for being understanding when I

had late nights in the lab, and for generally making life better. I could not have done it without you all.

CHAPTER 1: Introduction

1.1 The global threat of antibiotic resistance

The discovery of antibiotics revolutionised the treatment of bacterial diseases and led to a 30-year increase in life expectancy (Adedeji, 2016). In developed countries, communicable diseases, which were the leading causes of death, were rapidly replaced by non-communicable diseases. Since then, the reliance on antibiotics has only intensified. Not only have antibiotics enabled the treatment of primary bacterial infections, they also broadened the scope of modern medicine. Routine and advanced medical procedures, ranging from surgeries to immune-based interventions, depend on the safety net that antibiotics provide (Banin *et al.*, 2017). Thus, acting either prophylactically or therapeutically, antibiotics save millions of lives each year. Despite the long-standing contribution of antibiotics to global healthcare, bacteria resistant to one or more antibiotic classes are increasingly emerging, which pose a significant threat to the effective treatment of disease (Banin *et al.*, 2017; Roca *et al.*, 2015; Ventola, 2015). Bacterial 'superbugs' harbouring extensive resistance across multiple antibiotic classes can have a devastating impact. However, the acquisition of resistance to a comparatively modest number of antibiotics can also be problematic. Resistance can delay the administration of an effective treatment strategy, which can lead to prolonged hospital stays and increased mortality (French, 2005). The issue of antimicrobial resistance is increasing and requires urgent attention. Strategies that enable efficient and comprehensive point-of-care testing may allow effective treatment options to be implemented to alleviate morbidity and mortality. However, antibiotic efficacy is rapidly diminishing. Therefore, these strategies must be complemented with the development of novel antimicrobial strategies, particularly against pathogens that continue to cause high levels of disease.

1.2 *Streptococcus pneumoniae*

Streptococcus pneumoniae (the pneumococcus) is a Gram-positive diplococcus bacterium that was identified in 1881 as a causative agent of pneumonia. Ranking highest in terms of both morbidity and mortality, *S. pneumoniae* is a pathogen of significant global concern (Henriques-Normark & Tuomanen, 2013). The high rates of pneumococcal disease are facilitated by the frequent commensal colonisation of *S. pneumoniae* in the nasopharynx, which has been observed in children at rates of up to 70% (Bogaert *et al.*, 2004; Watson *et al.*, 2006). Transition to a disease state occurs by invasion of pneumococci into deeper tissues, such as the

lungs, middle ear, brain, or bloodstream, where disease can manifest as severe invasive diseases, including pneumonia, bacteraemia and meningitis, as well as local infections such as sinusitis and otitis media (Tan, 2012). Collectively, the pneumococcus contributes to one million deaths each year, which occur predominantly in children under the age of five (O'Brien *et al.*, 2009). On a global scale, it is estimated that there are 14.5 million cases of serious pneumococcal disease each year. Although disease is observed in developed regions, the highest rates of mortality occur in developing countries, particularly in sub-Saharan Africa and Asia (Walker *et al.*, 2013). Despite current prevention and treatment strategies, pneumococcal disease remains prevalent, particularly among children, the elderly, and in instances where co-morbidities exist, such as in immunocompromised patients.

1.2.1 *S. pneumoniae* prevention strategies

Vaccines have a crucial role in the prevention of pneumococcal disease. To date, all vaccines have targeted the major pneumococcal virulence factor, the capsular polysaccharide [CPS] (Feldman & Anderson, 2014). However, the pneumococcal CPS exhibits significant diversity and 98 serologically distinct capsular serotypes have been identified to date (Bentley *et al.*, 2006; Geno *et al.*, 2017; Larson & Yother, 2017). The first pneumococcal vaccine was licensed in 1977 and was composed of purified CPS from 14 different pneumococcal serotypes (Riley *et al.*, 1977). In 1983, the same approach was used to develop Pneumovax-23 (Merck), a 23-valent pneumococcal polysaccharide vaccine that includes a larger proportion of pneumococcal serotypes. However, polysaccharide-based vaccines do not provide protection to some of the most at-risk groups. Infants and young children mount a weaker immune response and display a low complement activity, which limits the protection elicited by polysaccharide-based antigens alone (Choo & Finn, 2001). This issue has been addressed by the development of protein conjugate vaccine (PCV) formulations, where the pneumococcal CPS is covalently conjugated to a protein carrier, for example a non-toxic mutated diphtheria toxin (Durando *et al.*, 2013). The protein carrier enables the polysaccharide to be recognised as a T-cell dependent antigen, which facilitates heightened humoral immune responses. These protein-conjugate polysaccharide vaccines, such as Prevenar and Prevenar-13 (PCV-7 and PCV-13 [Pfizer]), possess a higher immunogenicity compared to their non-conjugated counterparts (Sucher *et al.*, 2011). However, these vaccine strategies remain reliant on a robust immune response and are still limited by the immune system of the host.

Studies assessing the success of PCV-7 following implementation in the United States revealed that vaccine-covered serotypes declined by 77% in children under the age of two, while pneumococcal invasive disease by all serotypes declined by 66% (Kaplan *et al.*, 2004). In Australia, inclusion of PCVs in the national immunisation program similarly led to almost an 80% reduction in pneumococcal pneumonia in children under the age of two (Roche *et al.*, 2008). A recent study estimated that 114 million people globally have received the recommended three doses of PCV-13 (Chen *et al.*, 2019). Current estimates suggest that the widespread implementation of PCV-13 will reduce pneumococcal mortality by 34%, predominately due to the impact of the vaccine in Africa (Chen *et al.*, 2019). These encouraging results are due to the combined herd immunity and vaccine-mediated immunity, as PCV implementation can also indirectly reduce the incidence of pneumococcal disease and carriage among non-targeted age groups of the population (Davis *et al.*, 2013). Despite the promising outcomes and future predictions for continued PCV use, one factor limiting the success of current vaccines is poor serotype coverage. Current PCVs provide protection against only a small subset of known pneumococcal serotypes. Although the serotypes included in the PCV formulations are based on the most prevalent disease-causing serotypes, the use of these vaccines is altering the dynamics of pneumococcal disease. The use of serotype-dependent vaccines has been associated with an increase in disease attributable to non-vaccine covered serotypes (Feikin *et al.*, 2013; Weinberger *et al.*, 2011). This process, termed serotype replacement, has driven non-vaccine serotypes that were previously responsible for a low level of invasive disease to emerge as key players in pneumococcal disease. Another limitation is the high cost associated with the purification and conjugation techniques required for PCV manufacture, which restricts its widespread use. At $US137 per dose, PCV-13 is the second most expensive paediatric vaccine recommended for use by the Centre for Disease Control (CDC, 2019; Lagousi *et al.*, 2019). Although these costs are heavily subsidised in developing countries, the manufacturing costs may constrain their widespread use, which can lead to inadequate vaccination coverage.

In light of these challenges, the development of serotype-independent vaccine strategies to reduce capsule-based selection are required. Conserved pneumococcal protein antigens have been explored for their capacity to induce serotype-independent vaccine responses. Safe and immunogenic pneumococcal protein vaccines (PPrVs) include a genetically modified pneumolysin protein (Ply) and polyhistidine triad protein D (PhtD), either singly, or combined

in a trivalent combination with pneumococcal choline-binding protein A (PcpA) (Brooks *et al.*, 2015; Kamtchoua *et al.*, 2013; Seiberling *et al.*, 2012). These protein-based vaccine strategies circumvent the issue of serotype replacement while offering the benefit of improved humoral responses and immune memory (Swiatlo & Ware, 2003). However, the process for the purification of these proteins remains expensive. Other strategies have investigated whole-cell pneumococcal vaccine approaches. As whole-cell vaccines (WCVs) expose the full array of cellular antigens, immunisation can stimulate both antibody and T-cell responses. Traditional inactivation methods involve treatment with formalin, beta-propiolactone or chloroform. One study has demonstrated that immunisation with unencapsulated pneumococci killed with either chloroform or beta-propiolactone protected against colonisation and invasive disease in mice (Lu *et al.*, 2010). Although effective, these inactivation methods can interfere with antigen presentation by MHC-1 molecules, leading to compromised immune responses (Cardoso *et al.*, 1995). Another study investigated a pneumococcal WCV killed with ethanol and demonstrated protection against colonisation and disease in mice and rats, respectively (Malley *et al.*, 2001). This vaccine formulation has recently undergone Phase I clinical trials, which demonstrated low adverse events, while preliminary analyses of protection indicate that immunisation significantly elevated antibody responses corresponding to 112 pneumococcal proteins (Campo *et al.*, 2018). Recent studies have also demonstrated serotype-independent responses following immunisation with a gamma-irradiated *S. pneumoniae* vaccine (Babb *et al.*, 2016). These responses were amplified when this vaccine was combined with a gamma irradiated Influenza A Virus (IAV) vaccine (Babb *et al.*, 2017). The improved protection conferred by simultaneous immunisation was attributed to a direct interaction between these vaccines, a phenomenon that has recently been reported during viral and pneumococcal co-infection (David *et al.*, 2019; Rowe *et al.*, 2019b). Although the future of pneumococcal vaccination strategies is promising, these vaccines remain under development and antibiotics remain critical for the treatment of invasive disease.

1.2.2 Treatment of pneumococcal disease

The most common invasive pneumococcal disease is pneumonia. Community acquired pneumonia, of which the pneumococcus is the principal cause at up to 50% of cases, is treated with antibiotics (Cilloniz *et al.*, 2018). Recommendations for the treatment of pneumonia have traditionally ranged from empirical, broad spectrum approaches to pathogen-specific

approaches. The severity of community acquired pneumonia, which is determined based on a range of imaging, clinical scoring, and the presence of comorbidities, contributes to antibiotic selection (Correa *et al.*, 2018). For patients with non-severe pneumonia, defined as those that can be treated in an outpatient setting, the etiological agent is typically left undiagnosed and initially treated by antibiotic administration with a β-lactam (amoxicillin), macrolide (azithromycin or clarithromycin), or a fluoroquinolone (moxifloxacin or levofloxacin). High severity pneumonia requires hospital or intensive care unit admission and is typically treated by antibiotic combination therapy. To inform rationalised approaches, a 2005 study compared broad spectrum and pathogen specific approaches and showed that these strategies performed comparably in terms of length of hospital stay, which indicates that either may be effective in treating pneumococcal disease (van der Eerden *et al.*, 2005). Although pathogen-specific strategies offered a minor reduction in adverse events, presumably due to their reduced disruption of commensal bacteria, the authors state that these events were not likely to be of clinical significance. However, a more recent study of over 250,000 cases of community acquired pneumonia in the United States found that over a quarter of patients prescribed β-lactam antibiotic monotherapy had treatment failure (McKinnell, 2017). Failure often occurs as a result of antibiotic resistance, although a number of other factors, such as the presence of comorbidities, can contribute to treatment failure.

The first published case of a penicillin non-susceptible strain of *S. pneumoniae* was isolated from a patient in Australia in 1967, just a few decades after the introduction of penicillin into the clinic (Hansman & Bullen, 1967). The most common mechanism of penicillin resistance in *S. pneumoniae* is the alteration of the target penicillin binding proteins (PBPs) (Chambers, 1999). Mutations in PBPs reduce the affinity of β-lactams, limiting their activity. Resistance gene acquisition is thought to be primarily driven by homologous recombination events with other pneumococci or closely related streptococcal species, such as *Streptococcus mitis* and *Streptococcus oralis*, which localise in the pharynx and serve as a reservoir for the acquisition of resistance determinants in pneumococci (Kilian *et al.*, 2008; Kilian *et al.*, 2014). However, resistance can also arise spontaneously in response to antibiotic selective pressure. A recent Australian report on antimicrobial use and resistance in human health provides a snapshot of the current state of antibiotic resistance in Australia (AURA, 2019). Although the prevalence of penicillin resistant isolates remains relatively low (3.5-4%), resistance to erythromycin, tetracycline and trimethoprim-sulfamethoxazole is more pervasive, with alarmingly high resistance rates of 24.6%, 21.9% and 24.4%, respectively (AURA, 2019). In

other regions, these numbers are substantially higher. In the United States, *S. pneumoniae* penicillin resistance ranges from 35-45% of isolates and in certain European countries this number can reach almost 50% (Ewig *et al.*, 1999; Pallares *et al.*, 1995; Whitney *et al.*, 2000). These high rates of resistance are in part aided by the global dissemination of antibiotic resistant pandemic strains, which has led to widespread resistance among pneumococci to β-lactams, macrolides, fluoroquinolones and third generation cephalosporin antibiotics. Currently, it is estimated that more than 1.2 million pneumococcal infections each year are caused by drug resistant strains (Cherazard *et al.*, 2017). Increasing antibiotic use is thought to contribute to the high rates of resistance. There is compelling evidence that high levels of resistance correlate with high rates of antibiotic prescription (Baquero, 1996, 1999). This association is more common in instances where long-term, low dose antibiotics are administered and can be minimised by a stringent approach to antibiotic administration (Schrag *et al.*, 2001). Further, there is an association between recent antibiotic exposure and carriage of resistant pneumococci (Dagan *et al.*, 1996; Dowell & Schwartz, 1997). However, the introduction of PCVs has contributed positively to the landscape of antibiotic resistance. Serotypes 6B, 9V, 14, 19F and 23F, which are included in PCV-7, are associated with high levels of both invasive disease in children and are responsible for the majority of antibiotic-resistant infections (Schrag *et al.*, 2000). The decline in carriage of these serotypes following introduction of PCV-7 has reduced the occurrence of invasive disease, primarily due to the reduction in the spread of these strains among the community. Reduction in the carriage levels of resistant isolates has been a concomitant benefit (Kyaw *et al.*, 2006).

S. pneumoniae antibiotic resistance is pervasive, widespread and independent of serotype. However, studies assessing the clinical significance of antibiotic resistance have delivered conflicting results. An early, small scale study of pneumococcal pneumonia found that over 50% of cases were caused by a resistant pneumococcal strain, with penicillin resistance accounting for the vast majority of cases (Ewig *et al.*, 1999). The same study found that drug resistance was not associated with any difference in the length of hospital stay. Moreover, although there was an observed 3-fold higher mortality in patients harbouring non-susceptible strains compared to those with no resistance (15% compared to 6%), this difference was not statistically significant. Another study assessing a larger patient sample size similarly found high levels of penicillin resistance among the pneumococcal isolates. Among more than 500 patients admitted with pneumococcal pneumonia, almost 30% were due to penicillin-resistant isolates, and penicillin resistance was associated with a statistically significant increase

in mortality at 38% compared with 24% for susceptible strains (Pallares *et al.*, 1995). However, once additional factors were incorporated into these findings, such as the presence of comorbidities, this difference failed to reach statistical significance. Another study found an association between antibiotic non-susceptibility and increased mortality (Lujan *et al.*, 2004). In cases where the antibiotic administered retrospectively showed no *in vitro* activity against the isolated strain, termed discordant therapy, there was a 50% mortality rate. This rate is significantly higher than the mortality rate observed for patients treated with antibiotics displaying *in vitro* activity. It is clear that the factors governing the effective treatment of pneumococcal disease and the associated predictors of treatment success are multifactorial and complex. Unsurprisingly, the administration of an ineffective antibiotic is a major contributor to mortality, which may account for the large variability among the current literature. To address this issue, improved point-of-care tools enabling the rapid and accurate diagnosis of the etiological agent and antibiotic susceptibility profile are required. However, as antibiotic efficacy continues to decline due to the increasing prevalence of multi-drug resistance, the advances in treatment afforded by improved diagnosis are ultimately limited. As a result, the generation of novel therapeutic strategies or adjunct therapies to use with existing antibiotics are urgently required.

1.3 Novel antimicrobial strategies

Antibiotic resistant bacteria are predicted to cause up to 10 million deaths per annum by the year 2050 (O'Neill, 2014). Despite the urgent global need for new treatments, the implementation of new antibiotic strategies into the clinic has stagnated. Only a very low number of new antibiotics are being introduced into the clinical development pipeline. From 2014 to 2019, 67 new antibiotics were in the clinical development stages (Lepore *et al.*, 2019), and throughout these five years, only ten of these candidates have been approved for clinical use.

Nearly all antibiotics in use today were discovered more than 30 years ago and are typically naturally-derived products. Today, the pursuit of natural products harbouring antimicrobial activity continues. Innovative strategies, such as isolating uncultured bacteria from soil have been used to uncover novel compounds with activity against bacteria (Bakal *et al.*, 2017; Ling *et al.*, 2015). High throughput screening approaches have also been employed

in an effort to identify novel antimicrobials, with a focus on compounds that are effective against antibiotic resistant bacteria (Rathinakumar & Wimley, 2010; Scanlon *et al.*, 2014). Other research areas have probed currently used drugs to assess their capacity to be repurposed as antibacterial compounds (Miro-Canturri *et al.*, 2019). These include a range of anthelmintic drugs (Gooyit & Janda, 2016; Lim *et al.*, 2013; Rajamuthiah *et al.*, 2015), anti-inflammatory and immunomodulatory drugs (Artini *et al.*, 2014; Thangamani *et al.*, 2015b), anticancer drugs (Ueda *et al.*, 2009; Yeo *et al.*, 2018), and statins (Parihar *et al.*, 2014; Thangamani *et al.*, 2015a). Drug repurposing is favourable from a time and financial perspective, as these compounds may have successfully satisfied many of the required safety and regulatory requirements. Furthermore, previous analyses of these drugs can provide in-depth information on the pharmacokinetic and pharmacodynamic properties, which can aid in future studies.

Other strategies have focused on combining current conventional antibiotic treatments. Combination therapy can broaden the antibacterial spectrum, which can be useful in polymicrobial infections and in instances where the bacterial agent is unknown, or act in a synergistic manner leading to increased treatment success (Weiss, 2003). Combination treatments may also reduce the emergence of resistance (Worthington & Melander, 2013). However, combination therapy must be rationally applied, which relies on an understanding of the mechanisms of drug activity. The coupling of compounds that target bacterial resistance mechanisms with antibiotics has been extremely successful. For example, the β-lactamase competitive inhibitor, clavulanic acid, is commonly prescribed with amoxicillin to suppress resistance activity (Bonvehi *et al.*, 2003). By suppressing resistance mechanisms, these compounds can effectively prolong the shelf life of conventional antibiotics. Other approaches have investigated compounds that target bacterial virulence mechanisms. Targeted approaches include inhibitors directed at pathways involved in adherence to host cells (Pinkner *et al.*, 2006), cell-cell communication (Hentzer & Givskov, 2003; LaSarre & Federle, 2013; Lu *et al.*, 2014), global regulators of virulence (Rasko *et al.*, 2008; Wilke *et al.*, 2015; Worthington *et al.*, 2013), and nutrient uptake (Bajaj *et al.*, 2015). As these strategies act to disarm pathogens, rather than inhibit their growth, their use may be associated with a decline in the selection pressure and a reduction in the development of resistance (Totsika, 2017). Targeted approaches may also be superior to conventional antibiotics as they are unlikely to destabilise the microbiome (Stone & Xu, 2017). Although these treatments may be highly successful and selective, the development of targeted antimicrobials is dependent on an understanding of bacterial pathogenesis. Thus, an improved understanding of the pneumococcus and its interaction with

the host is important for antimicrobial development. Pneumococci experience distinct lifestyles that can be divided into three phases: colonisation, transmission, and invasion (Weiser *et al.*, 2018).

1.4 *S. pneumoniae* asymptomatic colonisation

One of the major contributors to the success of *S. pneumoniae* is its capacity to asymptomatically colonise the nasopharynx. It is estimated that at any time there may be more than 2 billion individuals worldwide colonised with *S. pneumoniae* (Short & Diavatopoulos, 2015). Pneumococcal colonisation, also termed carriage, can occur at any stage in life. However, carriage is particularly prevalent in early life, where rates can reach up to 70% at ages two to three (Navne *et al.*, 2016; Watson *et al.*, 2006). In developing countries, these rates can remain as high as up to 60% with increasing age, while carriage rates in developed countries typically decline to only 5-10% of individuals in adulthood (Adetifa *et al.*, 2012; Hussain *et al.*, 2005; Roca *et al.*, 2011; Shak *et al.*, 2013). The age-dependence of pneumococcal carriage may be attributed to the development of immune memory in response to repeated exposure to antigenically different pneumococcal strains (Adler *et al.*, 2017; Ramos-Sevillano *et al.*, 2019). Several other risk factors, including attendance at childcare, recent exposure to antibiotics, and seasonal factors, have also been associated with altered colonisation rates (Wroe *et al.*, 2012). Overall, *S. pneumoniae* is highly adapted to the environment of the nasopharynx and can effectively overcome multiple host barriers.

The first line of defence against pneumococcal nasopharyngeal colonisation is a physical barrier. The nasopharynx is lined with a thick mucus layer that traps bacteria, including pneumococci, for removal (Rose & Voynow, 2006). This barrier acts to prevent access to the epithelial surface where stable colonisation occurs. The pneumococcal polysaccharide capsule, which confers the bacterial surface charge, provides protection against mucus-mediated clearance due to its high negative charge (Nelson *et al.*, 2007). Studies have shown that unencapsulated strains remain agglutinated within the mucus layer, while larger amounts of negatively charged capsule aid in limiting pneumococcal mucus-mediated clearance. As a result, the capsule facilitates translocation across the negatively charged mucus layer to the epithelial surface. The mucus is also composed of a range of antimicrobial compounds, including lysozyme, which degrades the cell wall by cleaving N-acetylglucosamine-N-

acetylmuramic acid linkages of peptidoglycan. However, *S. pneumoniae* encodes the genes for two peptidoglycan-modifying enzymes, which synergistically protect against lysozyme, an O-acetyltransferase (Adr) and an N-acetylglucosamine deacetylase (PgdA) (Crisostomo *et al.*, 2006; Davis *et al.*, 2008; Vollmer & Tomasz, 2000). Together, these enzymes control the acetylation state of the glycan residues to control susceptibility to lysozyme. Although pneumococci use these strategies to evade the physical and chemical attacks of mucus, the capsule can impede adherence to epithelial cells. Thus, the capacity to modulate capsule expression in distinct phases of colonisation is an important step to establish pneumococcal carriage (Talbot *et al.*, 1996). The pneumococcal autolysin, LytA, enables *S. pneumoniae* to shed their capsule when they are in close proximity to epithelial cells, which exposes surface adhesins to facilitate cell adherence and invasion (Hammerschmidt *et al.*, 2005; Kietzman *et al.*, 2016).

Pneumococci utilise a range of strategies to promote adherence to the respiratory tract epithelial cells. Adhesins, such as PavA, PavB and Eno, bind to host extracellular matrix proteins (Bergmann *et al.*, 2001; Holmes *et al.*, 2001; Jensch *et al.*, 2010). The pneumococcus also possesses a range of glycosidase enzymes, such as NanA and BgaA, which can modify host cell glycoconjugates to uncover additional surface receptors (Limoli *et al.*, 2011; Uchiyama *et al.*, 2009). These carbohydrates provide more than an anchor for pneumococcal adherence, as the pneumococcus is a strictly fermentative organism and relies on host-derived carbohydrates for energy generation (Paixao *et al.*, 2015). Effective acquisition and catabolism of sugars is essential for pneumococcal persistence in the host environment; however, free sugars are limited in the nasopharyngeal environment (Philips *et al.*, 2003). Typically, host sugars exist as diverse glycoconjugates, composed of a number of different sugar residues, including glucose, sialic acid, galactose, N-acetylglucosamine and mannose (Burnaugh *et al.*, 2008). Pneumococci can acquire host sugars via deglycosylation, which can be mediated by the exoglycosidases NanA, NanB, StrH and BgaA (King *et al.*, 2006). Studies have shown that the dominant carbon source in the nasopharynx and upper respiratory tract is galactose, which can be cleaved via the action of the BgaA surface protein when galactose is the terminal sugar on a glycan (Zahner & Hakenbeck, 2000; Zeleny *et al.*, 1997). Conversely, glucose is the dominant carbon source in the blood. The ability of pneumococci to adapt to these differing environmental challenges and nutrient availability is central to its capacity to survive in the host.

Pneumococci also compete with the microflora present in the host nasopharyngeal environment. Resident bacteria can include other pneumococcal serotypes and strains, as well as more than 700 different microbial species that can also occupy this niche, including *Staphylococcus aureus* and *Haemophilus influenzae* (Aas *et al.*, 2005; de Steenhuijsen Piters *et al.*, 2015). Thus, the upper respiratory tract represents a complex local microbial ecosystem. Interplay between pneumococci and the local microbiome can occur indirectly, by competition for scarce resources, such as colonisation sites and nutrients, or via dynamic relationships between nasopharyngeal-colonising microorganisms. For example, colonisation with *H. influenzae* has the capacity to stimulate the complement-dependent phagocytic clearance of *S. pneumoniae,* thereby reducing the capacity of pneumococci to colonise (Lysenko *et al.*, 2005). Conversely, carriage of *S. pneumoniae* may inhibit the carriage of *S. aureus*, which is proposed to occur primarily through the production of hydrogen peroxide (Regev-Yochay *et al.*, 2006). The deployment of a range of bacteriocins by *S. pneumoniae* for the lysis of other bacteria can also enhance dominance in the nasopharyngeal environment (Dawid *et al.*, 2007). Despite the 'arms race' between bacteria, the nasopharynx is typically a highly co-colonised niche and the complex interspecies interactions provide a source for the uptake of foreign DNA. The natural competence of pneumococci enables horizontal gene transfer, which acts a major driver of evolution and its genetic plasticity. The competence state is triggered via the production of competence stimulating peptide (CSP). This secreted peptide accumulates in the environment and is sensed by neighbouring pneumococci (Claverys & Havarstein, 2002; Tomasz, 1965). *S. pneumoniae* responds to increasing extracellular CSP levels via a two-component regulatory system, ComCDE, which impacts the transcription of many early competence genes, including *comX*, encoding a global regulator of approximately 60 late competence genes (Havarstein *et al.*, 1996; Luo & Morrison, 2003; Pestova *et al.*, 1996; Peterson *et al.*, 2004). Together, the competence regulatory system controls the expression of genes associated with DNA uptake and recombination. Genetic adaptability is a major contributor to the success of *S. pneumoniae*. For example, the natural competence of this bacterium has mediated alterations to the capsule locus, which can enable evasion of capsule-based vaccines and the host immune response (Coffey *et al.*, 1998). The acquisition of foreign DNA can also lead to the dissemination of antibiotic resistance genes or novel virulence determinants, leading to the generation of highly resistant and virulent pneumococcal strains. In addition to the source of nutrients and the hub for gene acquisition that the nasopharyngeal environment provides, the nasopharynx also serves as a reservoir for the transmission of *S. pneumoniae* to new hosts.

1.5 Transmission of *S. pneumoniae*

The capacity for pneumococci to persist in the nasopharyngeal environment is central to the high population carriage rates. However, the capacity to effectively transmit to new hosts also contributes to *S. pneumoniae* prevalence. *S. pneumoniae* is thought to spread primarily via respiratory droplets and aerosols (Henriques-Normark & Tuomanen, 2013). Animal models of pneumococcal transmission have only recently been developed, which utilise young animals housed in close contact or co-infected with Influenza A Virus [IAV] (Diavatopoulos *et al.*, 2010; McCullers *et al.*, 2010). Increased inflammation in the upper respiratory tract, such as that observed in response to IAV, has been associated with increased shedding of pneumococci and thus transmission (Richard *et al.*, 2014). In line with this observation, transmission can be reduced by decreasing inflammation, either by intranasal administration of dexamethasone or deletion of pneumococcal pneumolysin (Ply) (Matthias *et al.*, 2008; Zafar *et al.*, 2017b). Ply is a pore-forming toxin released by pneumococci, which can contribute to the lysis of host cholesterol-containing cells (Andrew *et al.*, 1997; Boulnois *et al.*, 1991; Hirst *et al.*, 2004). Ply can cause extensive tissue damage and likely contributes to transmission by triggering the release of pro-inflammatory cytokines and chemokines, which drives inflammation in the upper respiratory tract. Even at lower concentrations, Ply can induce apoptosis, complement activation, and proinflammatory responses in host immune cells, which can contribute to pneumococcal transmission (Braun *et al.*, 2002; Cockeran *et al.*, 2001; Mitchell *et al.*, 1991; Paton *et al.*, 1984).

In addition to Ply, a range of other pneumococcal proteins also contribute to transmission. *S. pneumoniae* has been shown to persist for days in human saliva, which was shown to be dependent on genes involved in cell envelope synthesis, transport, stress response and amino acid metabolism (Verhagen *et al.*, 2014). Additional proteins involved in transmission between hosts have been identified via a transposon sequencing approach in ferrets infected with IAV (Rowe *et al.*, 2019a). This study identified a range of genes that may contribute to transmission, including those with a role in genetic competence (*comD* and *comEC*), metal ion acquisition (*piaA*, *piaD* and *phtA*), surface adherence (*cbpL*), and cell wall processing (*lytA* and *lytC*). Although the molecular basis for the contribution of these proteins remains unclear, the authors have proposed that pneumococci display increased environmental stability under conditions of metabolic limitation, which can increase their transmissibility. The

application of these surface-exposed transmission factors as vaccine antigens in mice has proven effective in transmission prevention (Rowe *et al.*, 2019a). Therefore, these may be attractive targets for future pneumococcal prevention strategies as both colonisation and transmission contribute to the high levels of invasive disease.

Serotype-dependent differences in transmission rates have also been observed. Studies assessing the contribution of capsular type to transmission have found that strains expressing a thinner capsule or mutants with reduced capsule expression display reduced transmission (Zafar *et al.*, 2017a). This may be due to the increased exposure of adhesins, which enhances the association with the nasopharyngeal epithelium (Weiser *et al.*, 2018). Transmission may also be facilitated by the capacity of pneumococci to survive outside of the host environment. Under nutrient-starved conditions, the amount of capsule was correlated with environmental survival, which may be due to the source of polysaccharides that it provides (Hamaguchi *et al.*, 2018). Pneumococci can also survive for extended periods on surfaces. Following desiccation and storage on hard surfaces for up to four weeks, viable *S. pneumoniae* were recovered and retained their infectious capacity (Walsh & Camilli, 2011). The transmission of pneumococci in the population can lead to the high rates of colonisation, which has the potential to progress to serious invasive disease.

1.6 *S. pneumoniae* invasive disease

Once nasopharyngeal colonisation has been established in a host, pneumococci can disseminate into other host niches to cause a range of local and invasive diseases. In the United States, instances of invasive disease are associated with a 10% mortality rate. However, this number is greater in developing countries where resource constraints impede the effective diagnosis and treatment of disease (CDC, 2012). A comparison of the serotypes associated with invasive disease revealed that serotypes 1 and 7F frequently cause disease in previously healthy individuals and likely have a high invasive potential (Sjostrom *et al.*, 2006). However, given the opportunistic nature of *S. pneumoniae*, even strains with a low invasive potential can be associated with significant disease among immune-compromised individuals or patients with another underlying disease. Invasive pneumococcal disease is frequently associated with a preceding or co-viral infection. Invasive disease may be triggered by changes in the environment of the upper respiratory tract in response to other infectious diseases. For example,

IAV has been shown to compromise the innate response to pneumococci by impairing the recruitment of macrophages (Davis *et al.*, 2011). IAV can also promote the adherence of pneumococci to the epithelium by upregulating host receptors and by the binding of IAV directly to pneumococci, which may enable pneumococci to exploit both viral and bacterial receptors (McCullers & Rehg, 2002; Rowe *et al.*, 2019b).

Although it is established that distinct serotypes can vary in their propensity to cause invasive disease, pneumococci of the same serotype can also differ in their invasive potential and behaviour (Sa-Leao *et al.*, 2011). This highlights that non-capsular differences, for example in pneumococcal proteins, also influence the development of invasive disease and contribute to tissue tropism. The invasion into deeper host tissues requires the adaptation to a different set of environmental conditions than those of the nasopharynx (Weiser *et al.*, 2018). As a result, the translocation to distinct niches is associated with significant changes in gene expression. The capacity to deal with altered levels of critical nutrients, such as carbohydrates, is also essential for pathogenesis (Buckwalter & King, 2012). Based on observed changes in pneumococcal gene expression, the type and relative abundance of carbohydrates varies significantly between host sites (Ogunniyi *et al.*, 2012; Orihuela *et al.*, 2004). For example, glucose is abundant in the blood, while free sugars are scarce in the upper respiratory tract and nasopharynx (Al-Bayati *et al.*, 2017). Thus, the switch from commensal colonisation requires alterations in carbon source utilisation, which is mediated by a large number of pneumococcal proteins that are involved in carbohydrate uptake and metabolism. For example, the virulent *S. pneumoniae* D39 strain encodes 21 different phosphotransferase system (PTS) transporters and 8 different ATP-binding Cassette (ABC) transporters that facilitate carbohydrate import, the majority of which are highly conserved across different pneumococcal strains (Bidossi *et al.*, 2012). The transcription of genes associated with the uptake and metabolism of different sugars are controlled through both carbon catabolite repression protein A (CcpA)-dependent and independent mechanisms (Buckwalter & King, 2012). CcpA enables pneumococci to prioritise the expression of genes associated with glucose uptake and metabolism (Carvalho *et al.*, 2011). As glucose is the preferred carbon source of *S. pneumoniae*, the transcription of genes for the utilisation of other sugars is kept low when glucose is available. Conversely, when glucose is not available, CcpA alters gene expression to enable the uptake and metabolism of more abundant sugars. In addition to the uptake pathways for carbohydrates, studies have shown that a range of transition metal ion acquisition pathways are essential for pathogenesis. Notably, the genes for the uptake of iron [Fe] (*piaA*, *pitA* and *piuA*), zinc [Zn] (*adcA* and *adcAII*) and

manganese [Mn] (*psaA*) are required for virulence (Bayle *et al.*, 2011; Brown *et al.*, 2001a; McAllister *et al.*, 2004; Plumptre *et al.*, 2014). These metal ions serve important cellular roles in bacteria, with up to 50% of proteins postulated to require a metal ion for their function (Lu, 2010). The importance of metal ion uptake pathways indicates that these metal ions are not readily available in the host environment. In mice, the total levels of these metal ions are typically in the micromolar range. However, there is significant variation in the total concentration between different host niches and upon infection. Furthermore, the relative availability of these metal ions can be altered significantly by the host during disease [reviewed in (Becker & Skaar, 2014)]. For example, iron availability is limited in the host environment as it is typically bound to lactoferrin, transferrin or haemoglobin, while Zn and Mn are restricted by the metal-binding protein, calprotectin, which is released in large quantities by neutrophils at infection sites (Brown & Holden, 2002; Liu *et al.*, 2012; Weinberg, 1975). In addition to these metal-withholding strategies, a range of other immune defences are deployed by the host to combat pneumococcal disease.

1.7 *S. pneumoniae* and the immune system

1.7.1 Adaptive immunity

The immune response is critical for the effective control of pneumococcal disease. The association of pneumococcal invasive disease with age highlights that a host with a robust immune system is less likely to contract pneumococcal disease (Brooks & Mias, 2018). Individuals are repeatedly exposed to pneumococci during commensal colonisation of the nasopharynx, particularly throughout childhood. Both human and murine studies have shown that colonisation is an immunising event, inducing antibody and cellular responses (Cohen *et al.*, 2011; Ferreira *et al.*, 2013; McCool *et al.*, 2002; Wright *et al.*, 2013). Epidemiological data indicate that levels of disease progressively decline after age two and return to high levels among the elderly (Henriques-Normark & Tuomanen, 2013). This U-shaped curve is proposed to be due to the changes in susceptibility to infection observed as the immune system develops in early life and wanes over time (Ramos-Sevillano *et al.*, 2019). The importance of the adaptive immune system is further exemplified by the increased disease incidence in individuals harbouring defects impairing their capacity to mount an effective adaptive response (Janoff *et al.*, 1992). For example, invasive pneumococcal disease is 30-100-fold more common among

HIV patients (Capocci & Lipman, 2013). The adaptive immune system relies on B cells for antibody production and specialised helper (Th) or cytotoxic T cells (Richards *et al.*, 2010). Natural acquired immunity can involve the production of antibodies directed towards the capsule and protein antigens, while cellular immunity against pneumococci is mainly driven by the induction of a Th17 cell-mediated, $CD4^+$ immune response (Malley *et al.*, 2005; Ramos-Sevillano *et al.*, 2019; Trzcinski *et al.*, 2005).

1.7.2 Innate immunity

In addition to the contribution of the adaptive arm of the immune system, the first line of defence against *S. pneumoniae* is the early and non-specific innate immune response. As an extracellular pathogen, phagocytic cell clearance of pneumococci constitutes an essential part of the host innate response. In pneumonia, the first immune defence encountered by pneumococci are the alveolar macrophages that reside in the lung environment. However, pneumococcal-induced tissue damage results in inflammation, which triggers the infiltration of circulating neutrophils and macrophages to the sites of infection (Kadioglu *et al.*, 2000). These specialised cells can recognise bacteria through pattern recognition receptors, such as Toll-like receptors 2 and 4, which detect pathogen associated molecular patterns from *S. pneumoniae* (Dockrell & Brown, 2015). Upon pneumococcal recognition, physiological changes are induced in phagocytic cells, including the generation and release of inflammatory mediators, such as cytokines, and the upregulation of genes encoding antimicrobial mechanisms (Mogensen, 2009). Bacterial uptake occurs by alterations in the macrophage actin cytoskeleton, which facilitate internalisation and entrapment into the phagosome. Following the maturation of the phagosome into a phagolysosome, the destruction of internalised bacteria is mediated through a range of antimicrobial strategies. The acidification of the phagosome as well as the deployment of reactive oxygen and nitrogen species impede microbial growth and can impair bacterial metabolism. Antimicrobial proteins and peptides are also deployed in the phagolysosome, including defensins, lysozymes, lipases and proteases, which act to kill internalised bacteria (Flannagan *et al.*, 2009). Studies have also shown that phagocytic cells can also modulate the abundance of transition metal ions, such as Zn, to eliminate internalised bacteria (Botella *et al.*, 2011; Botella *et al.*, 2012). Although it is unclear whether a similar phenomenon occurs in response to pneumococcal uptake, Zn deficiency has been associated with an increased susceptibility to pneumonia.

1.8 Zinc and infectious disease

Zn deficiency is estimated to affect almost 17% of the world's population (Wessells & Brown, 2012). Malnutrition is the main driver of Zn deficiency and is often observed in cases where diets are rich in phytates that impede the absorption of Zn (Lonnerdal, 2000). Zn deficiency is a particularly prevalent condition among young children in developing countries and is associated a range of adversities, including impaired growth and immune function (Gibson & Ferguson, 1998; Shankar & Prasad, 1998). In line with these immune defects, Zn deficiency is associated with an increased susceptibility to infectious diseases, such as bacterial pneumonia and diarrheal diseases (Bahl *et al.*, 1998; Black & Sazawal, 2001). Despite the association of Zn with protection against disease, randomised control studies of Zn supplementation in the prevention of pneumonia have delivered variable results. For example, a study in infants and preschool children showed that Zn supplementation reduced respiratory disease by 45%, while another study of preschool children in rural Mexico found that Zn supplementation reduced diarrheal diseases, but had no impact on respiratory illness (Rosado *et al.*, 1997; Sazawal *et al.*, 1998). In addition to the prophylactic administration of Zn, the therapeutic benefit of Zn supplementation has also been assessed in combination with standard antibiotic treatments. A study in Bangladesh found that administration of Zn accelerated recovery from severe pneumonia when combined with antibiotics, with reduced severity of pneumonia and a one-day reduction in the length of hospital stay (Brooks *et al.*, 2004). Despite these promising results, Zn supplementation as antibiotic adjuncts is not recommended for the treatment of pneumonia, as later analyses showed no statistically significant benefit (Haider *et al.*, 2011; Howie *et al.*, 2018). One possible reason for the conflicting results is a lack of tools to effectively quantify the Zn status of individuals. Earlier studies have relied predominantly on positive results to supplementation as a marker of Zn deficiency (King, 2011). Although serum Zn concentrations have been used as a read out for deficiency, these levels are highly susceptible to changes after a meal and in response to infection or stress. This is thought to be primarily due to the capacity for Zn to be effectively redistributed from the plasma to tissues, which can confound the conclusions drawn from serum-based Zn quantitation. The Zn source can also influence absorption, for example, a greater amount of Zn is absorbed as a Zn glycine chelate at 42%, compared with Zn sulphate at 27% (Yu *et al.*, 2010). However, it remains unclear whether the relative bioavailability of Zn is altered following supplementation with

different Zn sources. Furthermore, a diet rich in phytates can impede absorption, due to the formation of complexes between phytate and Zn, which is subsequently excreted (Lonnerdal, 2000). Therefore, diet can further confound the results of Zn supplementation studies. Overall, although Zn supplementation has in some cases shown success, strategies for improved Zn uptake and quantitation in supplementation studies are required. In addition to the challenges associated with Zn supplementation, the molecular basis for the protection afforded by Zn remains poorly defined.

It is estimated that more than 300 human proteins require Zn to function. Zn serves a range of functions in humans, with roles in protein synthesis, cell growth and cell differentiation (Liberato *et al.*, 2015). The immune system is particularly susceptible to Zn deficiency. Zn deficiency impairs the infiltration of immune cells to infection sites by reducing chemotaxis of polymorphonuclear (PMN) cells and the adherence of monocytes to endothelial cells (Gammoh & Rink, 2017). In line with this observation, Zn supplementation increases PMN chemotaxis. PMN cells produce neutrophil extracellular traps (NETs) at the sites of infection, which capture and kill extracellular bacteria (Brinkmann *et al.*, 2004). Zn chelation has been shown to impair the formation of NETs, which may limit bacterial killing *in vivo* (Hasan *et al.*, 2013). Zn deficiency also impacts the adaptive immune response. A deficiency in Zn is associated with atrophy of the thymus and T cell lymphopenia, due to the reliance of Zn for the function of thymulin (Mocchegiani & Fabris, 1995). Furthermore, a deficiency in Zn is also associated with decreased premature and immature B cells, which results in impaired antibody production (Haase & Rink, 2014). Zn supplementation in mice has also been associated with enhanced phagocytosis of *E. coli* and *S. aureus* by *ex vivo* macrophages (Nowak *et al.*, 2012). A direct antimicrobial role for Zn in phagocytic cells has also been described. An elemental analysis of *Mycobacterium* species in phagosomes revealed that Zn abundance is modulated in response to infection and in the presence of TNFα or IFNγ (Wagner *et al.*, 2005). This phenomenon was further probed by fluorescence microscopy and transcriptomic studies, which showed that Zn was redistributed towards the bacteria-containing phagosome (Botella *et al.*, 2011). Together these data indicate that Zn may influence the phagocytic activity and exhibit bactericidal action in macrophages. Further analyses found that Zn exposure in macrophages led to a rapid induction of *ctpC* transcription, which encodes a heavy metal efflux pump in *M. tuberculosis.* In accordance with these findings, deletion of *ctpC* led to impaired intracellular survival in phagosomes. The importance of bacterial metal resistance strategies has since been demonstrated in a number of other clinically significant pathogens, including *Salmonella*

enterica serovar Typhimurium and *Streptococcus pyogenes* (Kapetanovic *et al.*, 2016; Ong *et al.*, 2014). While a number of successful pathogens have been shown to utilise metal-resistance strategies to subvert host-mediated Zn toxicity, the contribution of *S. pneumoniae* Zn resistance strategies to survival in the host remain poorly defined. Nevertheless, it is clear that the antimicrobial action of Zn can be exploited in the internal phagocytic environment (Figure 1.1A).

Phagocytic cells are also capable of exploiting the essentiality of Zn to aid in bacterial clearance. In a process termed 'nutritional immunity', Zn availability can be restricted by phagocytic cells via the release of the metal-binding protein, calprotectin [Figure 1.1B] (Hood & Skaar, 2012). Calprotectin is a heterodimeric protein, consisting of the S100 family members, S100A8 and S100A9, that is highly abundant in neutrophils [~40% of total cytoplasmic protein] (Leukert *et al.*, 2005 ; Zygiel & Nolan, 2018). Calprotectin has the capacity to bind calcium (Ca), which is abundant in the extracellular space. The binding of Ca to calprotectin induces heterotetramer formation, which enhances calprotectin resistance to matrix metalloproteases and increases its affinity for Zn and Mn (Brophy *et al.*, 2012; Stephan & Nolan, 2016; Strupat *et al.*, 2000). Metal chelation by calprotectin induces broad spectrum growth inhibition in *S. aureus*, *E. coli, A. baumannii, Pseudomonas aeruginosa*, and *Shigella flexneri* (Brophy *et al.*, 2012; Corbin *et al.*, 2008; Damo *et al.*, 2013). This necessitates the upregulation of bacterial high affinity metal uptake systems to ensure sufficiency in the extra-phagocytic environment. The pneumococcus possess two substrate binding proteins, AdcA and AdcAII, that facilitate Zn acquisition (Plumptre *et al.*, 2014). Biochemical studies of AdcA have revealed that this protein binds Zn with high affinity (site 1 K_d ~2.4 nM, site 2 K_d ~228 nM). However, studies exploring the interaction of calprotectin with Zn have revealed affinities in the low nanomolar (site 1 K_d ~1.35 nM, site 2 K_d ~5.6 nM) to the picomolar range (< 10 pM), depending on the Ca abundance (Brophy *et al.*, 2012; Kehl-Fie *et al.*, 2011). In line with these findings, *in vitro* studies of calprotectin have shown that 0.5 mg/ml calprotectin perturbs pneumococcal growth (Makthal *et al.*, 2017). Calprotectin concentrations of 0.25 mg/ml and below did not impair pneumococcal growth, but these studies were performed in a rich growth media unlikely to replicate the host environment. Although the precise concentration of calprotectin that pneumococci are exposed to during disease is unclear, mice infected with *S. pneumoniae* display significantly higher calprotectin abundance in the lungs and blood, compared to uninfected mice (Eijkelkamp *et al.*, 2019). Consistent with these observations, the Zn uptake pathway of the pneumococcus is essential for virulence (Bayle *et al.*, 2011). Together, this

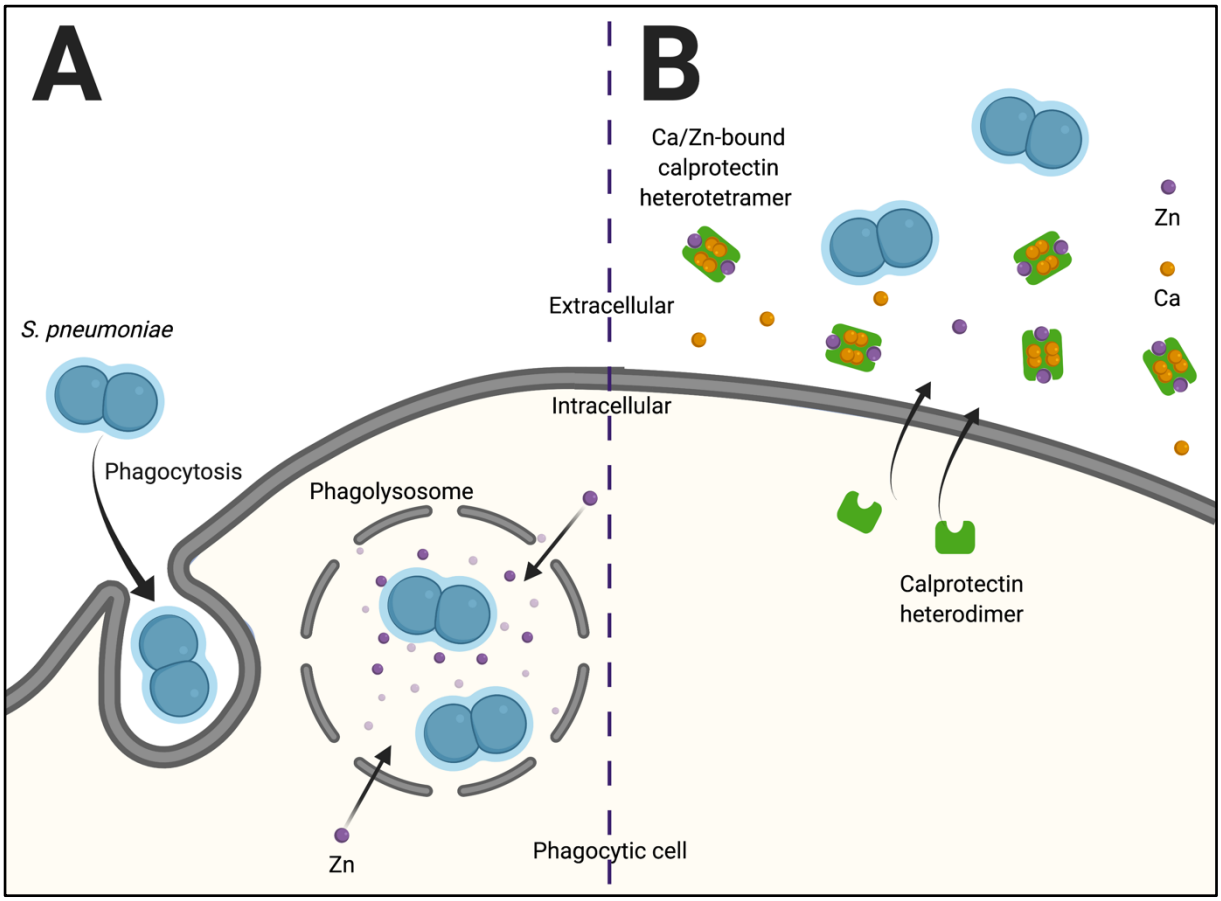


Figure 1.1 Zinc intoxication and starvation strategies are exploited by phagocytic cells to clear invading bacteria

(A) Following phagocytosis of bacteria by phagocytic cells, zinc (Zn; purple) is mobilised into the bacteria-containing phagolysosome, where high concentrations of Zn can exert antimicrobial action upon the internalised bacteria. (B) Neutrophils impart Zn starvation on bacteria via the release of calprotectin. Upon the release of calprotectin (green), calcium (Ca; yellow) in the extracellular environment promotes the formation of calprotectin heterotetramers, which have a high affinity for Zn. Heterotetrameric calprotectin sequesters Zn, rendering this nutrient less available to invading bacteria (blue).

suggests that despite the deployment of calprotectin, pneumococci are highly adapted to the environment of the host and can effectively overcome host defences to acquire Zn.

It is clear that the impact of Zn at the host-pathogen interface is complex, testing both bacterial Zn uptake and efflux mechanisms to maintain viability. Zn starvation has the capacity to impair proteins requiring Zn to exert their biological function, which represent approximately 5-6% of the prokaryotic proteome (Andreini *et al.*, 2009). Comparatively, the consequences of metal intoxication may be more complex to dissect, necessitating a systems-level approach to understand the broad impacts on a range of cellular pathways and define possible protein targets. Thus, despite the known antimicrobial role that Zn can play, the precise bacterial pathways impacted by excess Zn remain poorly defined.

1.9 Metal toxicity

Zn toxicity is understood to arise primarily due to its inappropriate binding to proteins, in a process termed mismetallation (Foster *et al.*, 2014; McDevitt *et al.*, 2011). Mismetallation is defined as the interaction of a protein with the incorrect metal (Foster *et al.*, 2014). Owing to their high degree of dynamic flexibility, proteins can be permissive to interactions with a wide range of metal ions. The major physiologically relevant metal ions, Mg^{2+}, Ca^{2+}, Mn^{2+}, Fe^{2+}, Co^{2+}, Ni^{2+}, Cu^{2+}, and Zn^{2+}, typically interact with proteins by binding to negatively charged residues, aspartate and glutamate, and polar residues, including histidine, cysteine and asparagine (Rulisek & Vondrasek, 1998). Although the precise figures are unknown, it is estimated that more than a quarter of all proteins require a metal ion to function (Waldron & Robinson, 2009). Metal ions are crucial for metalloprotein function; however, metal toxicity can arise from the interaction of a non-cognate metal ion or the inappropriate binding of a metal ion to a protein. Divalent cations display differences in their chemical properties, including their size and electron configuration. As a result, the binding of non-cognate metal ions can be detrimental to protein function by inducing an altered ligand coordination geometry via the recruitment of additional amino acid residues, which has the potential to induce structural rearrangements in a protein (Foster *et al.*, 2014). For example, the function of the Mg-dependent human placental alkaline phosphatase was impaired following an interaction with Zn (Hung & Chang, 2001). Alternatively, other metal-binding sites display a degree of promiscuity and may accommodate the binding of more than one metal ion with no discernible impact of protein

function, termed cambialistic proteins. This has been observed for the *E. coli* Fe-enzyme, ribulose-5-phosphate 3-epimerase, where the Fe is proposed to be replaced by Mn during Fe starvation and oxidative stress (Sobota & Imlay, 2011). Similarly, the *S. aureus* superoxide dismutase, SodM, possesses unchanged enzymatic activity when loaded with Mn or Fe (Garcia *et al.*, 2017). The binding of a metal ion may also lead to the inappropriate activation of a protein, which may have deleterious effects on the cell. For example, Cd causes Zn depletion in *S. pneumoniae*, which likely occurs via an inappropriate interaction of Cd with the Zn-responsive regulator, SczA (Begg *et al.*, 2015). The influence of a metal ion on the function of a protein can be varied, with examples of inhibition, activation and no alteration observed. The tendency for proteins to select metal ions is largely based on the relative stability of the metal-complexes formed. An order of preference, known as the Irving Williams series, [$Mg^{2+}/Ca^{2+}<Mn^{2+}<Fe^{2+}<Co^{2+}<Ni^{2+}<"Cu^{2+}>Zn^{2+}$], highlights the relative stability of these metals in protein complexes (Irving & Williams, 1948). Accordingly, proteins form highly stable complexes with metal ions higher on the series, such as Cu and Zn, which have a tendency to outcompete lower order metal cofactors. In order to reduce the inappropriate binding of higher order metal ions, their cellular abundance is maintained at low levels.

1.10 Metal ion homeostasis

To achieve their cognate protein metallation state, cells tightly control the intracellular abundance of competitive metal ions (Foster *et al.*, 2014). Highly competitive metal ions are buffered at low levels within a very narrow range in the cell. This favours competition between proteins for metal ions and leads to binding site selection of metals. This process is achieved through a combination of metal sensing, uptake, efflux and buffering strategies.

1.10.1 Metal sensors

Bacteria employ a range of regulatory mechanisms to control the levels of metal ions in the cell. The most well characterised of these strategies are metalloregulatory proteins that bind DNA to either activate or repress the transcription of metal homeostasis genes. These proteins bind to either a specific or range of metal ions, which typically allosterically initiates or inhibits the binding to the operator sequence of DNA (Capdevila *et al.*, 2017). DNA binding can either

promote or impair RNA polymerase binding, thereby altering transcription of downstream genes. *S. pneumoniae* possesses a range of metalloregulatory proteins to control the uptake and efflux of metal ions. The response to Mn starvation is mediated by the DxtR-family protein, PsaR (Capdevila *et al.*, 2017). Members of this family are homodimers comprised of a C-terminal domain containing two pairs of metal-binding sites per dimer and an N-terminal DNA-binding domain (Capdevila *et al.*, 2017). Pneumococcal PsaR represses the transcription of the Mn uptake pathway genes upon the binding of Mn and has been associated with pneumococcal virulence (Johnston *et al.*, 2006; Lisher *et al.*, 2013). In *S. pneumoniae*, the abundance of Fe is sensed by RitR, an orphan two-component signal transduction response regulator, which represses the transcription of genes encoding the Fe importer components (Ulijasz *et al.*, 2004). Cu abundance is sensed in *S. pneumoniae* via CopY, which is a member of the MecI/BlaI family of repressors (Fu *et al.*, 2013; Shafeeq *et al.*, 2011). The binding of Cu to CopY induces upregulation of the Cu resistance pathway genes. In *S. pneumoniae*, two metalloregulators have been identified that enable changes in Zn abundance to be sensed. The MarR-family regulator, AdcR, represses the transcription of the genes encoding the Zn-uptake machinery in the presence of Zn (Reyes-Caballero *et al.*, 2010). Proteins from the MarR family are homodimers that harbour two metal binding sites. Zn binding to AdcR initiates remodelling of the DNA-binding interface such that the N-terminal domain interacts with DNA [Figure 1.2] (Guerra *et al.*, 2011). High levels of intracellular Zn are sensed by the TetR family regulator, SczA. This metalloregulatory protein behaves distinctly from other regulators, in that SczA is proposed to bind to two distinct regions of the chromosome to either activate or repress transcription of the Zn efflux pathway genes, depending on its metal occupancy [Figure 1.2] (Kloosterman *et al.*, 2007). Collectively, metal-responsive regulators enable pneumococci to sense fluctuations in the abundance of metal ions in the cytoplasm and upregulate acquisition and resistance pathways to maintain homeostasis.

1.10.2 Metal transporters

Cells can effectively sense and respond to alterations in metal availability to maintain cellular homeostasis. As metal ions are positively charged, they cannot freely diffuse across the cell membrane. Therefore, intracellular metal ion abundance must be modulated via metal ion transporting membrane proteins to meet cellular demands. As the cellular concentration for metal ions can be higher or lower than that of the surrounding environment, the transport of

metals is driven by either the hydrolysis of ATP or coupled to the transfer of protons (Ma *et al.*, 2009). To date, metal ion transporters from the Cation Diffusion Facilitator (CDF), the P-type ATPase, and the ATP-binding Cassette (ABC) families have been identified in *S. pneumoniae* (summarised in Figure 1.3).

1.10.2.1 Cation Diffusion Facilitator transporters

In prokaryotes, the major Zn-resistance strategies involve efflux of the metal ions via the CDF family of proteins. Proteins from this family of metal ion transporters are found across all domains of life (Anton *et al.*, 1999). *S. pneumoniae* possesses two CDF proteins in the core genome, MntE and CzcD. MntE has been shown to be important for resisting Mn stress and contributes to pathogenesis, while CzcD confers resistance to Zn and Co stress [Figures 1.2 and 1.3] (Kloosterman *et al.*, 2007; Rosch *et al.*, 2009). CDF transporters exist as either homo- or hetero-dimers and use a proton-driven motive force to export metal ions out of the cell (Guffanti *et al.*, 2002; Kolaj-Robin *et al.*, 2015). Of the CDF proteins, YiiP (formerly FieF) from *E. coli* is the most extensively studied. Although early studies suggested YiiP was an Fe transporter, this protein has been since been shown to be primarily involved in Zn and Cd transport (Chao & Fu, 2004; Grass *et al.*, 2005). Structural studies of YiiP have yielded a wealth of information about this family of proteins. The first 3.8 Å crystal structure of YiiP showed that this protein possessed four metal-binding sites in each protomer, designated sites A, B and C1/C2 (Lu & Fu, 2007). A Zn ion is coordinated in a tetrahedral arrangement at site A, which is situated between transmembrane domains two and five, and is the proposed active site for metal transport. Amino acid substitution mutants at this site in several CDF members led to decreased Zn resistance and altered metal ion selectivity (Anton *et al.*, 2004; Martin & Giedroc, 2016; Wei & Fu, 2005). As a result, the site A metal-binding site is proposed to be the major site governing substrate selectivity and the capacity to discriminate between metal ions. Site B is positioned between transmembrane domains two and three in a cytoplasmic facing loop (Lu *et al.*, 2009). This metal binding site is situated adjacent to the subunit-bridging charge interlock and has been proposed to contribute to dimer stabilisation. Sites C1 and C2 are located in the cytoplasmic C-terminal domain (CTD) of the protein. The binding of metal ions to this site has been proposed to initiate a reorientation and conformational shift in the transmembrane domains (Coudray *et al.*, 2013). Studies of the inward and outward facing structures of YiiP have provided insight into the potential mechanism of CDF metal ion transport

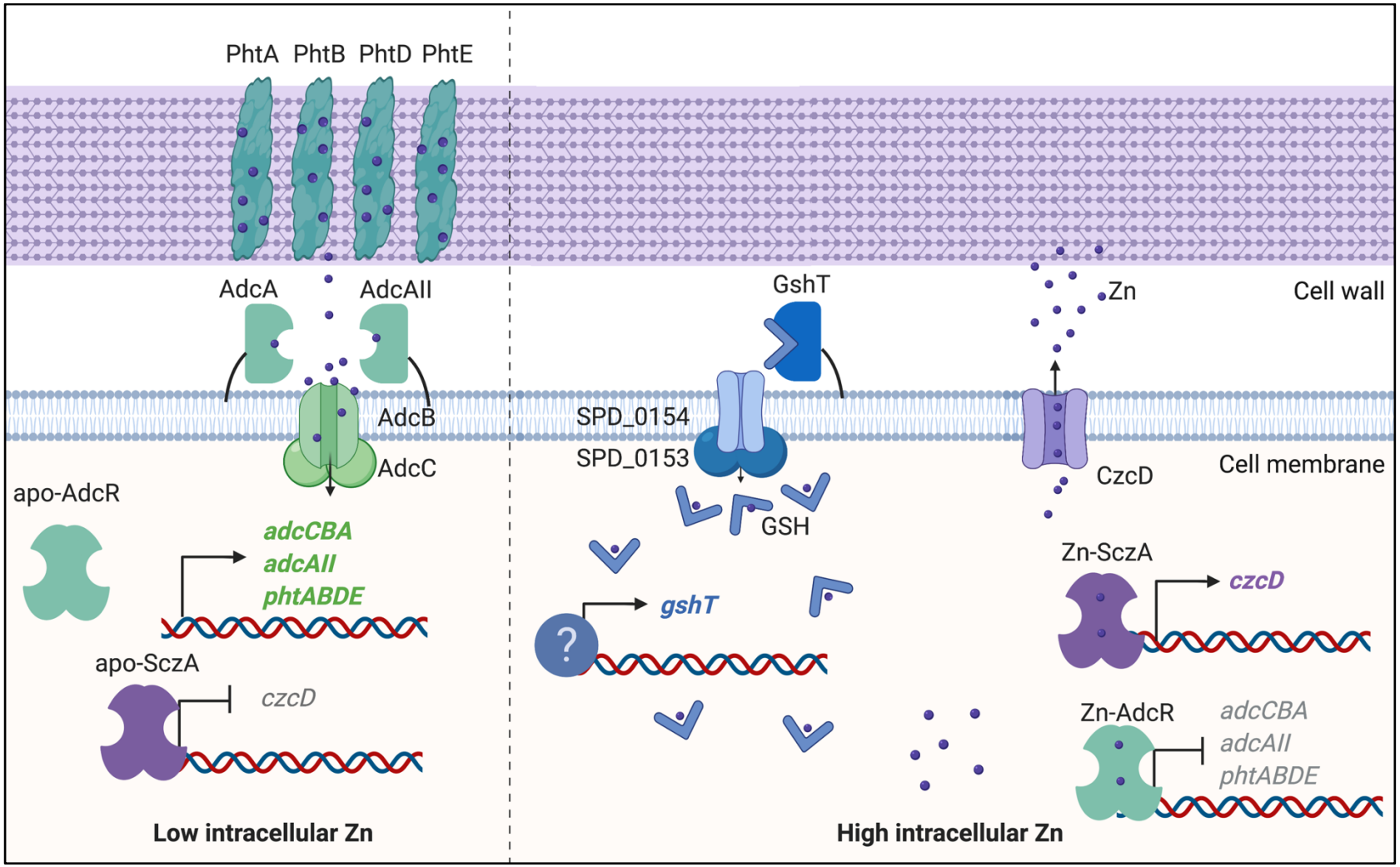

PhtA PhtB PhtD PhtE
AdcA
AdcAII
AdcB
AdcC
apo-AdcR
adcCBA
adcAII
phtABDE
apo-SczA
czcD
Low intracellular Zn
GshT
SPD_0154
SPD_0153
GSH
gshT
?
Zn
Cell wall
CzcD
Cell membrane
Zn-SczA
czcD
Zn-AdcR
adcCBA
adcAII
phtABDE
High intracellular Zn

Figure 1.2 Overview of the zinc homeostatic pathways of *S. pneumoniae*

Zinc (Zn, purple spheres) levels are controlled by Zn import, export and buffering strategies. Low levels of intracellular Zn are sensed by the metalloregulatory protein, AdcR. Apo-AdcR causes derepression of the Adc regulon, leading to the upregulation of the components of the Zn uptake machinery. The Adc regulon consists of the Pht proteins (PhtABDE), which are embedded in the cell wall and recruit Zn from the extracellular environment, and the transport machinery, which includes two membrane tethered substrate binding proteins (AdcA and AdcAII) that bind and deliver Zn to the ABC transporter permease (AdcCB). Concomitantly, the transcription of the gene encoding the Zn export protein, CzcD, is decreased via the metalloregulatory protein SczA. The interaction of apo-SczA with a motif upstream of *czcD* leads to repression of the *czcD* gene and reduced efflux of Zn. An increase in cytoplasmic labile Zn levels are sensed by SczA. Zn-bound SczA (Zn-SczA) binds to an alternative motif upstream of *czcD* to activate the transcription of *czcD.* CzcD is a member of the Cation Diffusion Facilitator family of transporters and mediates efflux of Zn from the cytoplasm. In parallel, the Zn uptake machinery are repressed by Zn-bound AdcR (Zn-AdcR), which interacts with DNA to repress the transcription of the Adc regulon and reduce the uptake of Zn. High levels of labile intracellular Zn can also be offset by the uptake of glutathione (GSH) from the extracellular environment. GSH can sequester excess Zn in the cytoplasm and enable an exchangeable pool of Zn ions. Glutathione uptake is mediated by the substrate binding protein, GshT, which likely is transported into the cell via the genetically associated ATP-binding cassette permease (SPD_0154) and ATP binding protein (SPD_0153). The regulator of the glutathione uptake pathway remains unknown.

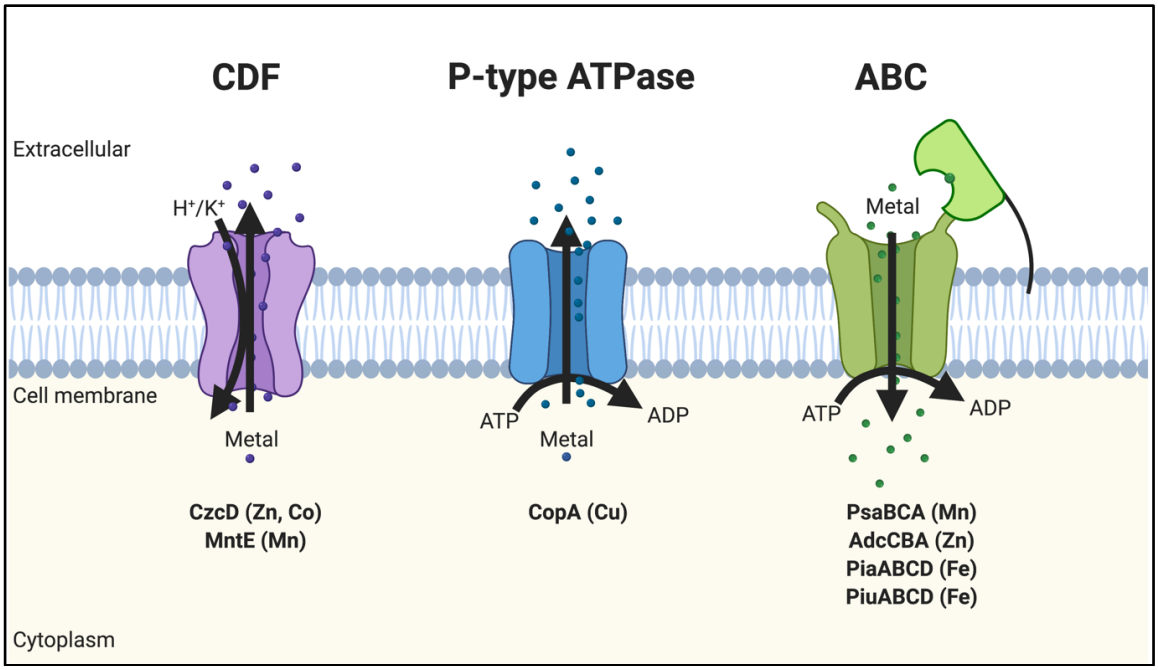


Figure 1.3 Major classes of metal transporters in *S. pneumoniae*

Transition metal homeostasis is maintained in *S. pneumoniae* by members of the Cation Diffusion Facilitator (CDF), the P-type ATPase, and the ATP-binding Cassette (ABC) families of proteins. CDF transporters use a proton-antiport mechanism to drive the export of metal ions from the cytoplasm (CzcD, Zn/Co; MntE, Mn). The Cu-transporting protein, CopA, is a member of the P-type ATPase family, which relies on ATP hydrolysis to power metal ion transport. Metal ion import is achieved via members of the ABC family of transporters, which are coupled with a substrate binding protein and utilise ATP to drive the import of metals against the concentration gradient (PsaCBA, Mn; AdcCBA, Zn; PiaABCD, Fe; PiuABCD, Fe).

(Lopez-Redondo *et al.*, 2018). YiiP is hypothesised to use an alternating access mechanism for metal transport. In the current model, the binding of Zn to the cytoplasmic CTD sites C1 and C2 induces reorientation of the transmembrane transport region, which may facilitate the cycling between inward and outward facing states. Although this model may apply to typical members of this family, CDF proteins lacking the CTD have also been identified (Russell & Soulimane, 2012). These proteins are functional and stable; however, it remains unclear whether the mechanism of transport deviates significantly from canonical members of this family. Therefore, although YiiP is the archetype of the CDF family, these proteins can be highly diverse. In bacteria, CDF proteins have been shown to contribute to virulence. For example, deletion of *czcD* in *S. pyogenes* resulted in reduced virulence in a murine model and impaired survival in human neutrophils (Ong *et al.*, 2014). Similarly, deletion of *aitP* or *czcD* from *Pseudomonas aeruginosa* led to decreased fitness in an *Arabidopsis thaliana* infection model (Salusso & Raimunda, 2017). The contribution of the pneumococcal Zn-resistance gene, czcD, to virulence and survival in phagocytic cells remains unknown.

1.10.2.2 P-type ATPase transporters

Metal ion transport can also be mediated by members of the type 1_B subfamily of the P-type ATPase transporters (Arguello *et al.*, 2007; Axelsen & Palmgren, 1998). Members of this family have been identified in both prokaryotes and eukaryotes and have been implicated in the transport of Cu, Zn, Cd, Co, lead (Pb), and silver (Ag) ions (Arguello, 2003; Axelsen & Palmgren, 1998; Lutsenko & Kaplan, 1995; Rensing *et al.*, 1999; Solioz & Vulpe, 1996; Williams & Mills, 2005). *S. pneumoniae* Cu efflux is mediated by the action of the P_{1B}-ATPase family protein, CopA [Figure 1.3] (Fu *et al.*, 2013; Shafeeq *et al.*, 2011). P_{1B}-ATPases typically possess an architecture consisting of six or eight transmembrane regions and three conserved domains (Arguello *et al.*, 2011). These include the ATP-binding domain, where ATP hydrolysis is coupled to energise metal ion transport, an energy transduction domain, and the N- or C-terminal metal-binding domain, which contributes to controlling the rate of transport. The current model of metal transport via P_{1B}-ATPases is based on the well-characterised members of this family, the Cu^+-ATPases (Arguello *et al.*, 2011; Fan & Rosen, 2002; Hatori *et al.*, 2007; Mandal *et al.*, 2002). In the absence of ATP, these proteins are posited to assume two major conformations (E1 and E2). The E1 conformation is favoured upon metal binding to the cytoplasmic metal-binding domain. Upon the binding of metal ions at this site, ATP

phosphorylation at a conserved aspartate residue drives the conformational change required for metal transport. Finally, after release of the metal ion and dephosphorylation, P_{1B}-ATPases adopt the E2 conformation. Members of the P_{1B}-ATPase family have also been shown to contribute to bacterial host survival and virulence. For example, deletion of *copA* in *S. pneumoniae* led to compromised virulence in a murine pneumococcal pneumonia model and deletion of the gene encoding the *E. coli* Cu-transporting P_{1B}-ATPase, CopA, led to enhanced susceptibility to macrophage-induced Cu-mediated killing (White *et al.*, 2009).

1.10.2.3 ATP-binding Cassette transporters

Uptake of Zn, Mn and Fe in *S. pneumoniae* is mediated by members of the ABC transporter family of transporters (Figure 1.3). Members of this family share a core architecture, composed of two transmembrane domains, which form the translocation machinery, and two ATP-binding domains (ter Beek *et al.*, 2014). ABC transporters can be broadly classified into four main groups; exporters, and type I, type II and type III importers (also known as energy coupling factor [ECF] transporters). ABC exporters are ubiquitous across all domains of life. Although traditionally only thought to be associated with prokaryotes, the three types of importers have been identified in bacteria, archaea and plants. Type I and II importers rely on an extra-cytoplasmic or lipid anchored solute binding protein (SBP) to recruit and deliver the cargo to the transport machinery (Lewinson & Livnat-Levanon, 2017). The general working model for Type I and II importers involves the binding of ligand by the SBP, an interaction that is postulated to transmit a signal via the transmembrane regions that increases the affinity of the nucleotide binding domain for ATP (van der Heide & Poolman, 2002). Finally, ATP hydrolysis induces an opening and release of the substrate into the cytoplasm (Davidson *et al.*, 1992). By contrast, ECF importers uniquely lack a dedicated SBP and instead rely on a membrane-embedded protein (S-component) that both confers substrate selectivity and participates in transport. These transporters also possess an ATP-binding component (A-component) and a transmembrane-component (T-component) (Zhang, 2013). Although relatively less is known about the mechanism of transport by ECF transporters, structural studies have provided some insight. A toppling mechanism of substrate transport has been described, in which the membrane bound S-component rotates to expose its binding site to the exterior or interior (Rodionov *et al.*, 2006). A conformational change in the T-component is proposed to enable the S-component to return back to its outward facing state (Swier *et al.*,

2016). *S. pneumoniae* Mn acquisition occurs via the PsaBCA system, composed of the PsaA SBP and the PsaBC permease. Abolishing Mn uptake by deletion of any component of this system led to compromised virulence in a murine infection model following intraperitoneal or intranasal challenge (Johnston *et al.*, 2004; McAllister *et al.*, 2004). Uniquely associated with two SBPs, AdcA and AdcAII, *S. pneumoniae* Zn uptake occurs via the AdcCB permease (Figure 1.2). Zn uptake via this pathway was shown to be critical for survival in the lungs, blood and nose of murine infection models (Bayle *et al.*, 2011; Plumptre *et al.*, 2014). Fe uptake in *S. pneumoniae* is similarly mediated by ABC import systems (Figure 1.3). The uptake of Fe via PiuBCDA and PiaABCD has also been associated with virulence, as mutants deficient in these pathways are attenuated in mice (Brown *et al.*, 2001a; Brown *et al.*, 2001b). Many bacterial metal ion ABC importers have been found to be essential for virulence. Deletion of components of the Zn uptake pathway, ZnuABC, from *E. coli* and *Acinetobacter baumannii,* led to decreased virulence in murine urinary and pneumonia models, respectively (Hood *et al.*, 2012; Sabri *et al.*, 2009).

1.10.3 Metal buffering systems

In addition to the action of metal ion import and export pathways, labile metal abundance in cells can also be controlled by metal buffering systems. These strategies can restrict the availability of cytoplasmic metal ions through a range of storage and sequestration proteins, as well as smaller molecules, such as amino acids, peptides, organic and inorganic acids (Chandrangsu *et al.*, 2017). The production or import of low molecular weight thiols serves as a common strategy for overcoming metal excess. Metal-buffering low molecular weight thiols that aid in the sequestration of metal ions include the tripeptide, glutathione, which is capable of binding Zn and Cu ions, and the analogous Zn-binding thiol, bacillithiol (Ma *et al.*, 2014; Potter *et al.*, 2012). *S. pneumoniae* intracellular Zn is buffered by reduced glutathione (GSH) [Figure 1.2]. Although *S. pneumoniae* lacks the genes required for GSH biosynthesis, the SBP GshT has been shown to facilitate the uptake of glutathione from the extracellular environment (Potter *et al.*, 2012). The amino acid histidine has also been shown to be important in *A. baumannii* for buffering excess Zn (Nairn *et al.*, 2016). These systems are likely important to offset small fluctuations in metal abundance, or to enable adaptation during the expression of metal efflux proteins.

1.11 Rationale for the project and aims of the study

Zn is an essential micronutrient; however, this metal ion can be toxic in excess. Zn is a highly competitive metal ion and has a versatile coordination geometry. These properties enable Zn to interact with a wide range of proteins, which can be detrimental to protein function. Zn has an important function in immune competence, with a major antimicrobial role in phagocytic cells (Botella *et al.*, 2012). *S. pneumoniae* remains a leading cause of death and antibiotic resistance is an issue for the effective treatment of invasive disease. As the efficacy of antibiotics continues to decline, harnessing the antimicrobial action of Zn may offer an alternative therapeutic strategy. However, in order to exploit the toxicity of Zn against *S. pneumoniae*, an improved understanding of how the pneumococcus mitigates Zn stress is required. Although CzcD has been implicated as the primary Zn resistance pathway in *S. pneumoniae*, the exact contribution of this protein to alleviating high levels of Zn and resisting phagocytic cell-mediated Zn toxicity remains unclear.

While high levels of Zn are known to limit the growth of *S. pneumoniae*, the exact pathways impacted by Zn remain poorly understood. Previous studies have shown that treatment of *S. pneumoniae* with Zn reduced the cellular accumulation of Mn (Eijkelkamp *et al.*, 2014; McDevitt *et al.*, 2011). Mn is an essential metal ion required for pneumococcal growth and also is a cofactor for the superoxide dismutase enzyme, SodA, which is required for oxidative stress tolerance. At moderate concentrations, Zn-induced Mn depletion led to compromised growth, which could be rescued upon the addition of an equimolar concentration of Mn. The Mn-specific SBP, PsaA, which interacts with the PsaBC permease to facilitate Mn uptake was identified as a target of Zn toxicity in *S. pneumoniae*. Structural studies revealed that binding of Zn to PsaA locked this protein in its closed conformation, which restricted the uptake of Mn (Couñago *et al.*, 2014). Although this pneumococcal surface protein is susceptible to mismetallation by Zn, it is unclear whether intracellular Zn levels are skewed sufficiently to induce the mismetallation of cytoplasmic proteins. Although supplementation with equimolar concentrations of Mn rescued the growth defect induced by Zn, Mn was unable to restore pneumococcal growth at higher concentrations of Zn (Eijkelkamp *et al.*, 2014). This suggests that there are additional targets of Zn mismetallation in *S. pneumoniae* that are yet to be defined.

A thorough characterisation of the targets of Zn mismetallation in *S. pneumoniae* may enable Zn toxicity to be harnessed in a rational manner. The targeting of the Zn resistance protein, CzcD, or the application of metal-modulating drugs may be effective strategies to enhance bacterial Zn accumulation in the host. Metal-modulating drugs are a topic of intense interest in medicine, particularly for the treatment of cancer and neurodegenerative diseases (Barnham & Bush, 2014; Helsel & Franz, 2015; Robert *et al.*, 2015; Santini *et al.*, 2014). Therefore, these metal-modulating drugs may be repurposed for their metal-modulating properties to induce Zn stress in clinically significant bacterial pathogens, such as *S. pneumoniae*.

The specific aims of this study are:

(1) To explore the Zn resistance strategy in *S. pneumoniae* and its role in resisting phagocytic cell clearance.
(2) To determine the *S. pneumoniae* pathways impacted by Zn and identify cellular protein targets of Zn toxicity.
(3) To investigate novel Zn-based therapeutic strategies against *S. pneumoniae* disease.

CHAPTER 2: Materials and Methods

2.1 Bacterial strains and oligonucleotides

The bacterial strains and oligonucleotide primers used throughout this study are listed in Tables 2.1 and 2.2 respectively. Unless otherwise stated, the oligonucleotides were purchased from Sigma Aldrich.

2.2 Bacterial culturing

S. pneumoniae were routinely grown at 37 °C, 5% CO_2 overnight on blood agar (BA) plates [39 g/L Columbia base agar (Oxoid), 5% v/v defibrinated horse blood]. *S. pneumoniae* was routinely grown in liquid culture in Todd-Hewitt Broth supplemented with yeast extract [Todd-Hewitt Broth (Oxoid), 0.5% w/v Bacto yeast extract (Beckman Dickinson and Company); THY]. For phenotypic characterisation, *S. pneumoniae* were cultured in a in semisynthetic media containing casein hydrolysate with 0.5% yeast extract according to the protocol of Lacks and Hotchkiss (Lacks & Hotchkiss, 1960), with the $ZnSO_4$, $CuSO_4$ and $FeSO_4$ omitted and supplemented with 1 μM $MnSO_4$ [C+Y] (Lacks & Hotchkiss, 1960). The metal content of C+Y was measured by inductively coupled plasma-mass spectrometry (ICP-MS) on an Agilent 8900 instrument (Adelaide Microscopy, University of Adelaide). For bacterial growth prior to animal experiments, *S. pneumoniae* were cultured in serum broth [10% v/v horse serum, 10 g/L peptone (Oxoid), 10 g/L Lab Lemco (Oxoid), 5 g/L NaCl]. Bacterial stocks were stored at -80 °C in THY media with 25% glycerol. Where required, BA plates were supplemented with antibiotics at the following concentrations, erythromycin (0.2 μg/ml), kanamycin (200 μg/ml), and gentamicin (5 μg/ml).

2.3 Genomic DNA isolation

Genomic DNA was isolated from *S. pneumoniae* following growth to mid-log phase. Cells were harvested from 10 ml culture by centrifugation at 3273 × *g* for 15 min, prior to resuspension in PBS containing 1% sodium deoxycholate (DOC; BDH Biochemicals). DNA was isolated using the DNeasy Blood and Tissue Mini Kit (Qiagen) according to the manufacturer's instructions.

Table 2.1 Bacterial strains used in this study

Strain	Description	Reference/source
S. pneumoniae D39	Serotype 2	Avery et al 1944
S. pneumoniae D39 Δ*czcD*	Replacement of *czcD* gene with an erythromycin resistance cassette	CL Ong
S. pneumoniae D39 Δ*ccpA*	Replacement of *ccpA* gene with a kanamycin resistance cassette	This study
S. pneumoniae^{Spain23F}	ATCC 700669 multidrug-resistant Spain 23F ST81 lineage	NJ Croucher, 2009

Table 2.2 Oligonucleotide primers used in the study

Name	Sequence 5' → 3'	Purpose
qgyrA_F_EB_1	ACTGGTATCGCGGTTGGGAT	qRT-PCR
qgyrA_R_EB_1	ACCTGATTTCCCCATGACAA	qRT-PCR
qSPD0382_F	GGCTGGCTTTATGCTAGGTG	qRT-PCR
qSPD0382_R	CGAACAGCATGACCAAAGTG	qRT-PCR
qSPD0890_F	AGCACCTCAAGGAAATGGTG	qRT-PCR
qSPD0890_R	TAGGGTCACTCCCCACATTC	qRT-PCR
qSPD1636_F	TGTCGCACCTGACTCCATAG	qRT-PCR
qSPD1636_R	TGTTCAAAAAGGGGACAAGG	qRT-PCR
qSPD1384_F	TCAAGTTAGCTGAGCGTGGA	qRT-PCR
qSPD1384_R	TAAGAGGGCCACATTTCCAA	qRT-PCR
qSPD1463_F	AGCCTATGGTGTTCCAAGTG	qRT-PCR
qSPD1463_R	GTTTTCATTGGACGGTCATC	qRT-PCR
qSPD1637_F	TCCCTTTTGGTAGAGCGACA	qRT-PCR
qSPD1637_R	GGTCTTGTGCCACCGATTAC	qRT-PCR
qSPD1638_F	TTGGTTCTAGCGCTGTTCTT	qRT-PCR
qSPD1638_R	AGGCTCCTAGCAGGCTAAAC	qRT-PCR
qSPD_0580_F_gki	GGGACTGTTATCGGTGCCTA	qRT-PCR
qSPD_0580_R_gki	TAAAGACAACGTCTGGTTGG	qRT-PCR
qSPD_1897_F_pgi	AAGTTTTAGACAAATTTGTT	qRT-PCR
qSPD_1897_R_pgi	AGATGCGGTCAAATTCTTCG	qRT-PCR
qSPD_0789_F_pfkA	AGGGGACATCATTTCTCGTG	qRT-PCR
qSPD_0789_R_pfkA	ACGCATAGCGCCGTGGTAAG	qRT-PCR
qSPD_0526_F_fba	GACGGTTCACACCTTCCAGT	qRT-PCR
qSPD_0526_R_fba	GCTTTAGCGTCTTCGATTGG	qRT-PCR
qSPD_1404_F_tpiA	ATCTTATCGATAGCGTCCAT	qRT-PCR
qSPD_1404_R_tpiA	CTGAGGCAGCAACTTGTTCA	qRT-PCR
qSPD_1823_F_gap	TTGGTATTAACGGTTTCGGA	qRT-PCR
qSPD_1823_R_gap	CAGTACCGTCGAAACGACCT	qRT-PCR
qSPD_0445_F_pgk	GATGCATTCGGTACAGCTCA	qRT-PCR
qSPD_0445_R_pgk	TGTCTGAAACTTTTGAACCA	qRT-PCR
qSPD_1468_F_gpmA	TCCAGTTGAAAAATCATGGC	qRT-PCR

qSPD_1468_R_gpmA	GGTCTGTGTGAGCTGAGTGC	qRT-PCR
qSPD_1012_F_eno	CTCGTTACGGTGGTCTTGGT	qRT-PCR
qSPD_1012_R_eno	ATAGACACACCGAGGATTGC	qRT-PCR
qSPD_0790_F_pyk	TGCTCGTGGTGATATGGGTA	qRT-PCR
qSPD_0790_R_pyk	TCTGATACTTCTGAACGAGT	qRT-PCR
qSPD_0071_F_galM	ATACGCTGGTCAATCCAACC	qRT-PCR
qSPD_0071_R_galM	GACCACATCACGGTTGGCTT	qRT-PCR
qSPD_1634_F_galK	CAGTTTGCTATTGGTATGGG	qRT-PCR
qSPD_1634_R_galK	CTCAGCACGACGTTCATTGT	qRT-PCR
qSPD_1432_F_galE-1	TTACAAAGCAGACTCAGAAT	qRT-PCR
qSPD_1432_R_galE-1	TCGTCTCCAAACACTTGCAC	qRT-PCR
qSPD_1433_F_galT-2	CGCAGCAACCACCGGATTAT	qRT-PCR
qSPD_1433_R_galT-2	CGATAGCCAACAGACGTTCA	qRT-PCR
qSPD_1326_F_pgm	TTTCGCAGGTATCATGGTCA	qRT-PCR
qSPD_1326_R_pgm	TCCACATCAGCAACTTCAAC	qRT-PCR
qSPD_1053_F_lacA	CGTGATTGATGCTTATGGAG	qRT-PCR
qSPD_1053_R_lacA	AGCCAATTCATCACCAACAAG	qRT-PCR
qSPD_1052_F_lacB	AAATGAGAATTGCAATTGGA	qRT-PCR
qSPD_1052_R_lacB	TTGGCCGCTAGTTACAGCTT	qRT-PCR
qSPD_1051_F_lacC	TGAATGGATTATCGTTTCAC	qRT-PCR
qSPD_1051_R_lacC	TGCATCCGATTCTTTGTGAA	qRT-PCR
qSPD_1050_F_lacD	AAACGCTTGCCAGACTGCTT	qRT-PCR
qSPD_1050_R_lacD	CCACACACTCAGAACCGATG	qRT-PCR
qSPD_0874_F_glmU	GGTAAAGGGACTCGCATGAA	qRT-PCR
qSPD_0874_R_glmU	TTCAGCCAAGACCTCCTCAA	qRT-PCR
qSPD_0248_F_glmS	CTGCGGGAATTTTTGTCCTA	qRT-PCR
qSPD_0248_R_glmS	CTCAGAGCGGTGTGGGTGAG	qRT-PCR
qSPD_1390_F_glmM	AAAAAGAAGCAGAAATTGAA	qRT-PCR
qSPD_1390_R_glmM	CAAGGCAACCTTCATTCCAT	qRT-PCR
qSPD_1078_F_ldh	TGTTGCTGCTAACCCAGTTG	qRT-PCR
qSPD_1078_R_ldh	GCGTGCACTGAACGAGCATC	qRT-PCR
qSPD_0621_F_lctO	TGCGATGTTGAAAATCCAAG	qRT-PCR
qSPD_0621_R_lctO	GAACTGGTTGTATAAAGAGA	qRT-PCR

qSPD_1853_F_ackA	TTCAACTGTAAAATTTGACG	qRT-PCR
qSPD_1853_R_ackA	TTCTCCACCAGCAACAACAC	qRT-PCR
qSPD_0235_F_pfl	TGAAAAGCGTGATGGAGATG	qRT-PCR
qSPD_0235_R_pfl	AATTCATCTTACCTTCCATA	qRT-PCR
qSPD_0343_F_gnd	AGATGGCAAACCATGTGTGA	qRT-PCR
qSPD_0343_R_gnd	AGATTTCAGCCATATCTTCT	qRT-PCR
ccpA_F1	GGCATCCTGCTGACTTATG	*ccpA* mutagenesis
ccpA_R1	CCATACTTTTGTGCCCGTTCCTTTTCC TGTCCTTTCTATCT	*ccpA* mutagenesis
ccpA_F2	GAATTGTTTTAGTACCTAGAATTCACC AAAAAATCAGGGAATCGAG	*ccpA* mutagenesis
ccpA_R2	TGATTGCTAGTGGTAATGTGC	*ccpA* mutagenesis
kanR_F	ACGGGCACAAAAGTATGG	Kanamycin^R gene
kanR_R	GGTGAATTCTAGGTACTAAAACAATTC	Kanamycin^R gene
seq_ccpA_F	GTGGTAGCAAGGAGCTAAAC	*ccpA* sequencing
seq_ccpA_R	TGAAAGACTATATGGAAGGCTAATAC	*ccpA* sequencing
glmU forward*	GGGCCCCTGGGATCCATGTCAAATTTT GCCATTATTTTA	*glmU* cloning
glmU reverse*	CGGCCGCTCGAGTCGCTACTGGTTCT TAGCATG	*glmU* cloning
glmU-E315A forward*	GGGCCCCTGGGATCCATGGGTAAATA TTTTGGGACTG	*glmU* site directed mutagenesis
glmU-E315A reverse*	CGGCCGCTCGAGTCGTTAGTCAATCC CAATTTCAGC	*glmU* site directed mutagenesis

glmU-H330A forward*	GGGCCCCTGGGATCCATGTCAAATTTT GCCATTATTTTA	*glmU* site directed mutagenesis
glmU-H330A reverse*	CGGCCGCTCGAGTCGCTACTGGTTCT TAGCATG	*glmU* site directed mutagenesis

*Purchased from IDT Oligos

2.4 PCR and agarose gel electrophoresis

PCR was performed using Phusion High Fidelity DNA polymerase (ThermoFisher) according to the manufacturer's instructions on a MasterCycler Nexus thermos cycler (Eppendorf). Oligonucleotides used for PCR were purchased from Sigma Aldrich, unless otherwise stated, and sequences are shown in Table 2.2. Standard cycling conditions were 95 °C for 5 mins, followed by 30 cycles of 95 °C for 30 secs, 63 °C for 30 secs and 72 °C for 1 min 30 secs. Annealing temperature was modulated based on the recommendations on the New England BioLabs website and an extension time of 30 secs per kb was used. For overlap extension PCR, oligonucleotides were added after 3 PCR cycles. DNA was mixed with 5 × GelPilot DNA Loading Dye (Qiagen) prior to electrophoresis on gels composed of 1% agarose dissolved in TAE [40 mM Tris, 20 mM acetic acid, 1 mM ethyenediaminetetraacetic acid (EDTA)], with RedSafe Nucleic Acid Solution (Intron Biotechnology) at 1:10,000. Electrophoresis was performed in TAE at 180 V. DNA was visualised by transillumination with short wavelength ultraviolet light using the Gel Doc XR system (Bio-Rad, NSW, Australia). DNA was purified from PCR reactions using a QIAquick PCR purification kit (Qiagen) according to the manufacturer's instructions.

2.5 DNA quantification and sequencing

The quantity and quality of purified DNA was assessed either using a Nanodrop 1000 spectrophotometer or using the LVis plate on a PHERAstar spectrophotometer (BMG Labtech). The purity of the DNA was assessed by calculating the A_{260}/A_{230} and A_{260}/A_{280} values, to indicate the level of salt and protein contamination, respectively. Samples with values >1.8 were of sufficient quality for downstream applications. Sanger sequencing of purified DNA was performed by the Australian Genome Research Facility (AGRF).

2.6 Pneumococcal transformation

S. pneumoniae was grown in THY media to OD_{600} = 0.2 and diluted 1:10 in warm transformation media (THY media with 0.2% [w/v] bovine serum albumin, 0.02% [w/v] glycerol, 0.02% [w/v] $CaCl_2$). Competence was induced by the addition of competence

stimulating peptide 1 (CSP-1) at a final concentration of 100 ng/ml, and cells were incubated for 10 mins at 37 °C. DNA was added to the tubes and the cells were incubated for a further 2-3 hrs at 37 °C. Transformants were selected by plating onto BA plates supplemented with the appropriate antibiotic. Successful transformants were confirmed based on size by PCR and agarose gel electrophoresis, and by Sanger sequencing at the Australian Genome Research Facility.

2.7 Growth Kinetics Assays

For analyses with Zn and PBT2, cellular material from overnight growth on BA plates were used to inoculate 7 mL of C+Y to a starting OD_{600} of 0.05. The cells were grown to mid-log phase (OD_{600} = 0.3) and pelleted by centrifugation at 3273 × *g* for 15 mins. The cell pellets were resuspended in fresh C+Y to an OD_{600} of 0.02. A volume of 100 µL of the inoculum was then diluted 1:2 into a 96-well flat bottom plate (Costar), containing 100 µL of C+Y with the appropriate Zn and PBT2 supplementation, to a final OD_{600} of 0.01. For carbon source analyses, cells from overnight growth on BA plates were washed once with PBS and resuspended in C+Y media supplemented with either 0.2% (w/v) glucose or 0.2% galactose (w/v) to a final OD_{600} of 0.1. A volume of 1 ml of the inoculum was then diluted 1:2 into a 96-well flat bottom plate (Costar) containing 1 ml of the same growth media to a final OD_{600} of 0.05. For Δ*ccpA* growth, cells from overnight growth on BA plates were resuspended in C+Y media to a final OD_{600} of 0.1. A volume of 1 ml of the inoculum was then diluted 1:2 into a 24-well flat bottom plate (Costar) containing 1 ml C+Y media to a final OD_{600} of 0.05. All plates were sealed with gas-permeable seals (Breathe-Easy, Diversified Biotech) and incubated in a FLUOStar Omega spectrophotometer with an atmospheric control unit (BMG Labtech) at 37 °C, 5% CO_2. Readings of the OD_{600} were recorded every 30 mins using the well scan function.

2.8 Whole cell metal accumulation

Analysis of metal content was conducted following growth of *S. pneumoniae* until mid-log phase (OD_{600} = 0.3) in C+Y media with or without supplementation with 50 µM ZnSO4, 0.4 µM PBT2.2HCl, either singly or in combination. The cells were pelleted by centrifugation at 7000 × *g* for 7 mins at 4 °C, washed 3 times with PBS with 5 mM EDTA to remove

extracellular metals, followed by 3 washes with PBS to remove residual EDTA. The cell pellet was resuspended in 1 mL of PBS, transferred to a microcentrifuge tube, and pelleted by centrifugation. The cell pellets were desiccated by heating at 96 °C overnight, and the dry pellet weight was recorded. The cell pellets were resuspended in 35% HNO_3 (Seastar Chemicals) and boiled at 96 °C for 1 hr. The samples were cooled, and the insoluble material was pelleted by centrifugation at 21,130 × *g* for 30 mins. Samples were diluted 1:10 in milliQ water and the metal content of the samples was assessed by ICP-MS on an Agilent 8900 QQQ-ICP-MS (Adelaide Microscopy, University of Adelaide).

2.9 RNA extraction

For analyses with Zn supplementation, growth of *S. pneumoniae* in C+Y and C+Y with metal supplementation was monitored until OD_{600} = 0.3. For analyses comparing D39 with the Δ*ccpA* mutant strain, growth of *S. pneumoniae* in C+Y and C+Y with metal supplementation was monitored until OD_{600} = 0.15. A 300 µL aliquot of the culture was incubated for 5 mins at room temperature with 600 µL of RNAProtect Bacterial Reagent (Qiagen), before harvesting the cell pellets by centrifugation at 21,130 × *g* for 5 mins. The supernatant was removed, and cell pellets were stored at -80 °C until required. To extract the RNA, pellets were enzymatically lysed by resuspension in a solution of 10 mg/ml lysozyme (Sigma Aldrich) in Tris-EDTA buffer and 50 Units of mutanolysin (Sigma Aldrich). The RNA was extracted using the RNeasy Mini Kit (Qiagen) and DNA was depleted from the samples through an on-column treatment using the RNase-Free DNase Set (Qiagen) according to the manufacturer's instructions. The quantity and quality of purified RNA was assessed using an LVis plate on a PHERAstar spectrophotometer (BMG Labtech). The purity of the RNA was assessed by calculating the A_{260}/A_{230} and A_{260}/A_{280} values, to indicate the level of salt and protein contamination, respectively. Samples with values >1.8 were of sufficient quality for downstream applications.

2.10 Quantitative Reverse Transcription-Polymerase Chain Reaction

The quantitative reverse transcription-polymerase chain reaction (qRT-PCR) analyses were performed essentially as previously described (Plumptre *et al.*, 2014). The oligonucleotides for qRT-PCR were designed using Primer3 (Unipro UGENE) to amplify

products of 140-160 nucleotides and are presented in Table 2.3. The qRT-PCR was performed on a QuantStudio 6 Flex Real-Time PCR System (Thermofisher Scientific) using a SuperScript III One-Step RT-PCR kit (Invitrogen). The levels of gene transcription were normalised relative to the transcription of the *gyrA* gene (SPD_1077).

2.11 RNA sequencing

S. pneumoniae was grown in biological triplicate until mid-log phase (OD_{600} = 0.3) in C+Y media with or without supplementation with 100 μM $ZnSO_4$. RNA was extracted as described above and RNA from biological replicates was pooled and analysed on a Bioanalyzer 2100 (Agilent) according to manufacturer's instructions to confirm a RIN value >8. RNA was submitted to AGRF for sequencing. The Epicentre Bacterial Ribozero Kit (Illumina) was used to deplete ribosomal RNA content before the generation of barcoded libraries using the Ultra Directional RNA kit (New England Biolabs). Prepared libraries were sequenced using an Illumina HiSeq2500 with Version 3 SBS reagents and 2 × 100 bp paired-end chemistry. Reads were aligned to the *S. pneumoniae* D39 genome (GenBank accession number NC_008533) using BOWTIE2 version 2.2.6 (Langmead & Salzberg, 2012). Counts for each gene were obtained using SAMtools version 1.2 (Li *et al.*, 2009) and BEDtools version 2.24.0 (Quinlan & Hall, 2010), and differential gene expression was determined using R (DESeq Library) version 3.2.2 (Anders & Huber, 2010).

2.12 Cluster of orthologous group analysis

The *S. pneumoniae* D39 reference sequence (NC_008533) was obtained from NCBI and the cluster of orthologous groups (COG) classification of the proteins were applied based on computational analyses of sequenced genomes (Tatusov *et al.*, 2000). The available COG classifications were mapped to the data from the RNA sequencing results and the percentage of genes with 2-fold or greater increased or decreased transcription relative to untreated were determined for each COG classification.

2.13 Membrane topology modelling

The amino acid sequence of *S. pneumoniae czcD* (SPD_1638) was obtained from the NCBI database. Membrane topology predictions were performed by analysis of the amino acid sequence using the TMHMM server (Krogh *et al.*, 2001). Membrane topology was graphically presented using the graphics program, TOPO2 (Johns S.J., TOPO2, Transmembrane protein display software)

2.14 Structural modelling

The amino acid sequence of *S. pneumoniae* CzcD (SPD_1638) was obtained from the NCBI database and input into SWISS-MODEL (Biasini *et al.*, 2014). A homology model of *S. pneumoniae* CzcD was generated based on the 2.9 Å Zn-bound structure of *E. coli* YiiP (PDB: 3h90) (Lu *et al.*, 2009). The cartoon representation of the CzcD homology model and aligned YiiP template structure was generated in PyMOL version 2.3.3 (Schrödinger) and the surface electrostatic potential of the CzcD homology model was calculated using the Adaptive Poisson-Boltzmann Solver package (Baker *et al.*, 2001).

2.15 Fatty acid analyses

S. pneumoniae was grown in C+Y with or without supplementation with 50 µM $ZnSO_4$ to mid-log phase (OD_{600} = 0.30). Cells were washed twice in PBS and 10 ml culture was harvested by centrifugation at 7000 × *g* for 7 mins at 4 ºC. The cell pellets were resuspended in 300 µl PBS and mechanically lysed by sonication using a Bioruptor system (Diagenode) for 30 cycles (30 secs on, 30 secs off), and stored at -80 ºC. The fatty acid content was analyzed by gas chromatography-mass spectrometry by Waite Lipid Analysis Service (University of Adelaide) as described previously (Eijkelkamp *et al.*, 2018).

2.16 Membrane fluidity studies

S. pneumoniae cultures were grown in C+Y media or C+Y media supplemented with 50 µM $ZnSO_4$ to mid-log phase (OD_{600} = 0.3). Cells were washed in PBS, resuspended in 500 µL PBS and 40 µM 1,6-diphenyl-1,3,5-hexatriene (DPH) in tetrahydrofuran was added. The

samples were incubated on a shaking incubator (200 rpm) at 37 °C for 30 mins. A volume of 100 µl of the samples were transferred in triplicate into a 96-well microtiter tray (Costar) and the fluorescence polarization (excitation/emission 350/450 nm) was measured on a PHERAstar spectrophotometer (BMG Labtech), where the sample fluorescence polarization = (parallel – perpendicular) / (parallel + perpendicular).

2.17 Uronic acid capsule assay

S. pneumoniae cultures were grown mid-log phase (OD_{600} = 0.3) in C+Y media with or without supplementation with 50 µM $ZnSO_4$. Cells were pelleted by centrifugation at 3273 × g for 15 mins and resuspended in 500 µl buffer (1 mM $MgCl_2$ in Tris-HCl pH 7.0). Cells were lysed by the addition of 0.1% w/v DOC and incubated at 37 °C for 30 mins. DNase I and RNase A at final concentration of 100 µg/ml and mutanolysin (100 Units) were added and the lysates were incubated overnight at 37 °C. Proteinase K was added at a final concentration of 100 µg/ml and the samples were incubated at 56 °C for 4 hrs. A volume of 100 µL of the capsular polysaccharide samples were transferred in duplicate to safe-cap Eppendorf LoBind tubes and cooled on ice. While on ice, 600 µl sodium tetraborate solution in concentrated sulphuric acid (12.5 mM $Na_2B_4O_4$ in concentrated H_2SO_4) was added. Samples were vortexed, boiled for 5 mins and cooled on ice. A volume of 10 µL of 3-phenylphenol solution (0.15% phenylphenol in 0.5% NaOH) was added to one tube and 10 µL 0.5% NaOH was added to the duplicate. Samples were shaken and 200 µl was immediately transferred to a 96-well microtitre tray (Costar) in duplicate. The absorbance at 520 nm (OD_{520}) was measured using a PHERAstar spectrophotometer (BMG Labtech).

2.18 Metabolomics

S. pneumoniae cultures were grown in C+Y media with or without supplementation with 100 µM $ZnSO_4$ to mid-log phase (OD_{600} = 0.3). Cells were harvested by centrifugation at 7000 × *g* for 7 mins at 4 ºC, flash-frozen using liquid nitrogen to preserve the metabolite profile and stored at -80 ºC. Metabolomic analyses were performed by Metabolon®, North Carolina, USA. Statistical analysis was performed using the MetaboAnalyst package (Chong *et al.*, 2018).

2.19 Phosphofructokinase activity assay

S. pneumoniae cultures were grown in C+Y media to mid-log phase (OD_{600} = 0.3). Cells from a 4 ml culture were pelleted by centrifugation at 3273 × *g* for 15 mins. Cells were washed twice in PBS, resuspended in 300 µL PFK assay buffer (Phosphofructokinase Activity Colorimetric Assay Kit, BioVision) and transferred to a microcentrifuge tube. Cells were mechanically lysed by sonication using a Bioruptor system (Diagenode) for 30 cycles (30 secs on, 30 secs off). Insoluble material was pelleted by centrifugation at 21,130 × *g* for 5 mins and the supernatant was collected. The total protein concentration was determined using the DC protein assay (Bio-rad) using bovine serum albumin (BSA) as a standard. The phosphofructokinase activity was determined using a colorimetric assay linked to the production of NADH (BioVision). The activity assay was performed essentially according to the manufacturer's instructions, with the exception of the lysis procedure detailed above and a total of 250 ng protein was added per well. A standard curve with known concentrations of NADH (2-10 nmol) was generated and the production of NADH in the samples was monitored by measuring the absorbance at 450 nm (A_{450}) every 30 seconds at 37 °C. To calculate the sample PFK activity the samples were corrected based on background (no substrate) controls and the activity as determined based on the change in OD_{450} over time (PFK activity = $\mathbf{B}/[\Delta\mathbf{T} * \mathbf{w}] *$ dilution factor = nmol/min/mg = mU/mg, where **B** is the NADH amount from standard curve [nmol], $\Delta\mathbf{T}$ is the reaction time [min] and **w** is the protein concentration [mg] added to the reaction well).

2.20 6-phosphogluconate dehydrogenase activity assay

S. pneumoniae cultures were grown in C+Y media to mid-log phase (OD_{600} = 0.3). Cells from a 4 ml culture were pelleted by centrifugation at 3273 × *g* for 15 mins. Cells were washed twice in PBS, resuspended in 300 µL 6-PGD assay buffer (6-Phosphogluconate Dehydrogenase Activity Colorimetric Assay Kit, BioVision) and transferred to a microcentrifuge tube. Cells were lysed through the addition of 0.1% w/v DOC and incubated at 37 °C for 15 mins. Insoluble material was pelleted by centrifugation at 21,130 × *g* for 5 mins and the supernatant was collected. The total protein concentration was determined using the DC protein assay (Bio-rad)

using bovine serum albumin (BSA) as a standard. The 6-phosphogluconate dehydrogenase activity was determined using a colorimetric assay linked to the production of NAPDH (BioVision). The activity assay was performed essentially according to the manufacturer's instructions, with the exception of the lysis procedure detailed above and a total of 10 ug protein was added per well. A standard curve with known concentrations of NADPH (2-10 nmol) was generated and the production of NADPH in the samples was monitored by measuring the absorbance at 460 nm (A_{460}) every 30 seconds at 37 °C. To calculate the sample 6-PGD activity the samples were corrected based on background (no substrate) controls and the activity as determined based on the change in OD_{460} over time (6-PGD activity = $\mathbf{B}/[\Delta\mathbf{T} * \mathbf{w}] *$ dilution factor = nmol/min/mg = mU/mg, where **B** is the NADH amount from standard curve [nmol], $\Delta\mathbf{T}$ is the reaction time [min] and **w** is the protein concentration [mg] added to the reaction well).

2.21 Cloning and mutagenesis of GlmU

The GlmU analyses were performed in collaboration with Associate Professor Megan Maher (University of Melbourne). The *S. pneumoniae glmU* gene was amplified and ligated into the pGEX-6P-3 plasmid by Gibson Assembly using the Gibson Assembly Cloning Kit (New England Biolabs) with minor modification to the manufacturer's instructions. Briefly, insert DNA (150 ng) was incubated with plasmid DNA (50 ng) in a reaction volume of 10 µl. Samples were incubated at 50 °C for 30 mins in a T100 Thermal Cycler (Bio-Rad). The E315A/H330A amino acid substitution mutants were generated by site directed mutagenesis using the Q5 Site Directed Mutagenesis kit (New England Biolabs). The pGEX-6P-3-GST-GlmU and pGEX-6P-3-GST-GlmU-E315A/H330A plasmids were confirmed by Sanger sequencing (Macrogen).

2.22 Expression and purification of GlmU

The pGEX-6P-3-GST-GlmU and pGEX-6P-3-GST-GlmU-E315A/H330A plasmids were transformed into *E. coli* One Shot BL21 (DE3) chemically competent cells. The cells were grown at 37 °C in Luria Broth (LB) media overnight cultures (1% [w/v] tryptone, 0.5% [w/v] yeast extract, 1% [w/v] NaCl) containing ampicillin (100 µg/ml), shaking overnight at 180 rpm.

The overnight cultures were used to inoculate LB media and grown to reach an OD_{600} of ~0.6 (2-3 hrs, 37 °C) before induction with IPTG (0.2 mM). Induced cells were grown for 20 hrs at 18 °C and harvested by centrifugation at 5,000 × g for 15 min at 4 °C.

The cells were resuspended in resuspension buffer (20 mM MOPS pH 7.0, 150 mM NaCl, 10% glycerol) followed by the addition of one cOmplete EDTA free Protease Inhibitor Cocktail Tablet (Life Science Roche) and DNase I (Sigma). Cell suspensions were lysed at 35 kpsi by a single pass through a TS Series Benchtop cell homogeniser (Constant Systems Ltd) and the soluble fraction was isolated by ultracentrifugation at 35,000 × g for 35 min at 4 °C). The supernatant was incubated with 1 ml of Glutathione Sepharose 4B resin (GE Life Sciences) for 1 hr at 4 °C. The supernatant-resin suspension was applied to a gravity column, and the resin was washed with 10 column volumes of resuspension buffer before being incubated overnight in 10 column volumes of resuspension buffer and 3C protease (0.3 μM). For the elution of GST-GlmU, the resin was re-applied to the gravity column and the tag-cleaved GlmU protein was eluted. The eluted protein was concentrated and loaded onto a Superdex 200, 16/60 column (GE Life Sciences) equilibrated in resuspension buffer and eluted at a flow rate of 1 ml/min in resuspension buffer. Fractions containing the target protein were analysed by SDS-PAGE, pooled, aliquoted and frozen at -80 °C.

2.23 Crystallisation of GlmU

Purified *S. pneumoniae* GlmU was concentrated to 15 mg/ml and crystallised by hanging drop vapour diffusion in 24-well plates. The conditions for crystallisation of GlmU in complex with acetyl-CoA and Zn were optimised based on the crystallisation conditions used for *S. pneumoniae* GlmU bound to acetyl-CoA and calcium (PDB: 1HM8; (Sulzenbacher *et al.*, 2001). Briefly, GlmU was incubated with 20 mM acetyl-CoA prior to crystallisation with reservoir solution (20% [v/v] PEG 400, 50 mM NaCl, 300 mM $CaCl_2$ at pH 7.25 by Tris HCl and 1 mM $ZnCl_2$) via hanging drop vapour diffusion method at 293 K. Rhombohedral crystals typically appeared overnight. Crystals were mounted with 0.2-0.3 mm loops (Hampton) before being flash cooled in liquid nitrogen. The crystals from GlmU co-crystallised with acetyl-CoA and Zn^{2+} were collected at 100 K using the MX2 beamline at the Australian Synchrotron at a wavelength of 1.23 Å on a Quantum 315r Detector (Area Detector Systems Corporation). Diffraction data was similarly collected at wavelengths 1.28 Å and 1.30 Å. Data sets were auto

processed by XDS at the beamline. Data collected at wavelengths 1.28 Å and 1.30 Å, near the Zn absorption edge at 1.2837 Å, was also performed at the Australian Synchrotron. For each dataset, the data was scaled and auto processed by XDS.

2.24 Structure determination, building and refinement

The crystal structure of *S. pneumoniae* GlmU bound to acetyl-CoA and Zn was solved using the CCP4 program suite unless otherwise specified (Winn *et al.*, 2011). The structure was solved by molecular replacement using the program PHASER using *S. pneumoniae* GlmU co-crystallised with acetyl-CoA (PDB ID: 1HM8) as the search model (McCoy *et al.*, 2007; Sulzenbacher *et al.*, 2001). The model was prepared by removing acetyl-CoA and the two Ca^{2+} ions before it went through refinement with REFMAC5 and iterative model building in COOT, where water molecules were incorporated into the model (Emsley *et al.*, 2010; Murshudov *et al.*, 2011). Anomalous difference Fourier electron density maps were created and calculated with phases from SFALL, SigmaA and FFT. After an initial round of refinement, a Zn atom was modelled into the positive feature of the difference Fourier electron density map (> 30 σ) adjacent to the positions of residues Glu315 and His330. Structural geometry was analysed by MOLPROBITY and all structural figures were generated using PyMOL(Chen *et al.*, 2010; Schrödinger). The quality of the model was validated using MOLPROBITY (Chen *et al.*, 2010).

2.25 GlmU acetyltransferase activity assay

Acetyltransferase activity of GlmU was assessed by a colorimetric acid assay as described previously (Ellman, 1958). Briefly, the acetylation of glucosamine-1-phosphate with acetyl-CoA was measured spectrophotometrically by monitoring the breakdown of acetyl-CoA using 5, 5' -dithio-bis-(2-nitrobenzoic acid) [DTNB, Ellman's reagent; Sigma Aldrich]. For samples including Zn, 5, 10, or 20 µM $ZnCl_2$ was added with 0.2-1.2 mM acetyl-CoA to 5 ng purified GlmU for 15 mins prior to the addition of glucosamine-1-phosphate. A master reaction mixture containing 50 mM Tris HCl pH 7.5, 5 mM $MgCl_2$ and 0.8 mM glucosamine-1-phosphate was added, and the mixture was incubated with in a 96-well microtiter plate for 10 mins at 37 °C. Over the 10 min reaction time, 50 µL aliquots were taken at 2 min intervals and 50 µL of stop solution (50 mM Tris–HCl pH 7.5 and 6 M guanidine hydrochloride) was added

to terminate the reaction. The samples were then incubated with 50 µL of Ellman's reagent solution (0.2 mM DTNB, 50 mM Tris–HCl pH 7.0 and 1 mM EDTA). The samples were transferred to a 96-well plate and the absorbance at 412 nm was measured.

2.26 Mice

Four-week-old CD1 (Swiss) mice were obtained from the University of Adelaide Laboratory Animal Services breeding facility. All experiments were approved by the University of Adelaide Animal Ethics Committee (Project approval number S-2016-183). The procedures performed for this study were conducted in compliance with the Australian Code of Practice for the Care and Use of Animals for Scientific Purposes (8th Edition, 2013) and the South Australian Animal Welfare Act 1985.

2.27 Pneumococcal infection model

Mice were anaesthetized by intraperitoneal injection of sodium pentobarbitone (Ilium) at a dose of 66 µg/g body weight. A total of 1×10^7 CFU of *S. pneumoniae* D39 suspended in a total volume of 50 µL serum broth was administered directly into the anterior nares. The challenge dose was retrospectively enumerated by serial dilution and plating on BA plates. Mice were treated with either single or combination treatments of 4 mg/kg PBT2.2HCl and 125 µg/kg $ZnSO_4$, 20 mg/kg gentamicin sulphate, or a vehicle control (water and dimethyl sulfoxide; DMSO) at 12 hourly intervals. Mice were monitored closely for signs of illness and animal weight was recorded at 12 hourly intervals. At 48 hrs post infection, the mice were humanely killed by CO_2 asphyxiation. Blood was harvested by syringe from the posterior vena cava and the pulmonary vasculature was perfused with PBS through the heart. The lungs, spleen, brain and liver were excised, transferred to 1 ml PBS and homogenized using a Precellys 24-tissue homogenizer (Bertin Technologies). All samples were serially diluted in serum broth, plated onto BA plates supplemented with 5 µg/ml gentamicin, and the CFU were enumerated after overnight growth at 37 C, 5% CO_2.

2.28 *In vivo* pneumococcal transcriptional analyses

For *in vivo* analyses of bacterial transcriptional responses, pneumococci from the infected mice was diluted in RNAprotect Bacteria Reagent (Qiagen) and centrifuged at 400 × g for 5 mins to remove tissue debris and eukaryotic cells. The supernatant was collected, and pneumococci were pelleted by centrifugation at 3273 × g for 15 mins. Bacterial RNA was extracted using a hot phenol–chloroform method as described previously (Eijkelkamp *et al.*, 2019). Briefly, the pellets were resuspended in 300 µl of phenol-chloroform at 65 °C and incubated at 65 °C for 5 mins. A volume of 300 µL NaES solution (50 mM sodium acetate, 10 mM EDTA, 1% SDS) at 65 °C was added and the samples were incubated at 65 °C for 5 mins. The samples were placed on ice for 1 min and centrifuged at 15000 × g for 1 min. The upper layer was transferred to a new tube and The RNA was extracted using the RNeasy Mini Kit (Qiagen) according to the manufacturer's instructions.

2.29 Macrophage survival assays

THP-1 cells (ATCC TIB-202) were routinely grown in cell culture flasks (BD Falcon) at 37 °C 5% CO_2 in complete RPMI medium (RPMI with phenol red [Gibco], supplemented with 10 mM HEPES, 10% [v/v] foetal calf serum [FCS], 30 µg/ml penicillin and 50 µg/ml streptomycin). THP-1 cells were differentiated by the addition of 100 ng/ml phorbol 12-myristate 13 acetate (PMA; Sigma) and a total of 1×10^5 THP-1 cells were seeded into each well of a 48-well plate (Costar). Cells were differentiated during incubation at 37 °C 5% CO_2 for 3 days. Differentiated THP-1 cells were washed and incubated for two days with RPMI media without PMA. *S. pneumoniae* was grown in THY media to mid-log phase (OD = 0.30). The *S. pneumoniae* cells were washed twice with HBSS with 10% [v/v] FCS and resuspended to a final concentration of 4×10^7 CFU/ml. The THP-1 cells were washed twice with Hank's Balanced Salt Solution (HBSS; Gibco) with 10% [v/v] FCS. A volume of 250 µL of *S. pneumoniae* was added to the THP-1 cells at a multiplicity of infection of 100, the plate was centrifuged at 100 × g for 5 mins, and the *S. pneumoniae* and THP-1 cells were co-incubated for 90 mins at 37 °C 5% CO_2. The THP-1 cells were washed in HBSS with 10% FCS and the extracellular bacteria were removed by incubation with 200 µg/ml gentamicin and 10 µg/ml penicillin for 30 mins at 37 °C, 5% CO_2. THP-1 cells were lysed using 0.0625% Triton X-100 and intracellular survival was determined by serial dilution and plating on BA plates.

Intracellular survival was determined by enumerating the CFU after overnight growth at 37 °C, 5% CO_2.

2.30 Penicillin survival experiment

S. pneumoniae D39 and Δ*czcD* strains were grown in C+Y media to mid-log phase (OD_{600} = 0.30). Cells were pelleted by centrifugation at 3273 × *g* for 15 min and resuspended in C+Y media with or without 100 μM $ZnSO_4$ and 0.1 μg/ml penicillin, either singly or in combination. Cells were incubated at 37 °C 5% CO_2 and the CFU were measured at 5 hrs by serial dilution and plating on BA plates. Sensitivity was assessed based on the survival relative to the untreated D39 wild-type strain.

2.31 Antibiotic susceptibility analyses

Antibiotic minimum inhibitory concentrations (MIC) were determined based on the guidelines of the Clinical Laboratory Standards Institute and as described previously (CLSI, 2015; Wiegand *et al.*, 2008). *S. pneumoniae* D39 and ATCC 700669 were grown on BA plates for 18-20 hrs at 37 °C 5% CO_2. Cells were resuspended in Mueller Hinton II (cation adjusted) media (BD) supplemented with 5% [v/v] horse blood (MHB) to 1 × 10^8 CFU/ml and diluted a further 1:100 into MHB with or without $ZnSO_4$, DMSO, and PBT2.HCl. MIC plates were prepared by performing two-fold serial dilutions of the appropriate antibiotic and control wells in 50 μL in MHB and adding 50 μL of cells to a final concentration of 5 × 10^5 CFU/ml. The plates were sealed with opaque gas-permeable seals (Aeraseal, Sigma Aldrich) and incubated at 37 °C for 20 hrs. The MIC was recorded as the antibiotic concentration of the well displaying no visible growth. Bacterial survival was assessed by serial dilution and plating on BA plates. CFU were enumerated after overnight growth at 37 °C, 5% CO_2.

CHAPTER 3: The role of CzcD in *Streptococcus pneumoniae* zinc resistance

3.1 Introduction

Zn is an essential micronutrient for all cells. It is estimated that Zn interacts with ~3000 human proteins, fulfilling a range of catalytic and structural roles (Andreini *et al.*, 2006; Andreini *et al.*, 2008). Zn deficiency is estimated to affect almost 2 billion individuals worldwide and is associated with a range of adversities, including an increased susceptibility to infectious disease (Prasad, 2013; Strand *et al.*, 2003; Walker *et al.*, 2013). Although the association between host nutritional status, Zn and susceptibility to infectious diseases is established, it remains poorly understood. Recently, it has been shown that phagocytic cells could exploit the antimicrobial activity of Zn to aid in the clearance of bacterial pathogens. Phagocytic cells, such as neutrophils and macrophages, are an important part of the non-specific, innate response against invading bacteria. Following phagocytosis of bacteria, these cells employ a combination of factors to kill internalised pathogens, including reactive oxygen and nitrogen species, antimicrobial proteins and peptides, and manipulation of the ionic composition of the phagolysosome (Flannagan *et al.*, 2009). The role of Zn in macrophages was first demonstrated with the intracellular bacterium, *M. tuberculosis*, where Zn was shown to be mobilised towards the phagolysosome (Botella *et al.*, 2011). The contribution of Zn in phagocytic cell killing of bacterial species has since been expanded to include *S. pyogenes, E. coli*, and *Salmonella enterica* serovar Typhimurium (Kapetanovic *et al.*, 2016; Ong *et al.*, 2014). However, this antimicrobial strategy does not apply to all pathogens as was shown for the fungal pathogen, *Histoplasma capsulatum*, where Zn deprivation was implicated as the macrophage's killing mechanism (Winters *et al.*, 2010). These findings show that the modulation of Zn abundance is an important component of antimicrobial defence, with species-specific responses of phagocytic cells requiring elucidation.

The molecular basis for how Zn mediates toxicity towards pathogenic species is not yet fully understood. As Zn lacks the capacity for direct redox activity, current models suggest that Zn toxicity arises from the inappropriate binding of Zn to proteins, a process termed mismetallation (Foster *et al.*, 2014; McDevitt *et al.*, 2011). Mismetallation of proteins can impact their function, resulting in reduced or abrogated activity, or inappropriate activation. In this way, accumulation of excess intracellular Zn can alter gene expression, affect key cellular pathways, and exert deleterious cellular effects. To prevent toxicity, bacteria tightly regulate the cellular abundance of Zn. In the pneumococcus, metal ion efflux proteins represent the primary metal ion tolerance mechanisms. The most prominent pathways used in related

streptococcal species belong to the CDF family of metal ion transport proteins. CDF transporters are homodimeric, proton-driven antiporters present in all domains of life (Guffanti *et al.*, 2002; Nies, 2003; Paulsen & Saier, 1997). The most extensively characterised exemplar of the CDF family is *E. coli* YiiP, for which both functional and structural data is available, discussed earlier in section 1.10.2.1 (Chao & Fu, 2004; Grass *et al.*, 2005).

S. pneumoniae is highly adapted to the host environment and utilises a range of virulence factors to evade the host immune response (Kadioglu *et al.*, 2008). As an extracellular pathogen, *S. pneumoniae* survival is dependent on resisting and evading the killing mechanisms of phagocytic cells (Martner *et al.*, 2008). Recent studies of the related streptococcal species, *S. pyogenes,* revealed the importance of the CDF transporter CzcD in Zn homeostasis and resisting neutrophil-mediated killing (Ong *et al.*, 2014). Based on these findings, the present study aimed to investigate the pathways by which *S. pneumoniae* resists host-mediated Zn toxicity. *S. pneumoniae* possesses an orthologous protein to *S. pyogenes* CzcD (70% similarity, 49% identity) that has previously been implicated in Zn resistance (Kloosterman *et al.*, 2007). LacZ fusion studies showed that *S. pneumoniae czcD* was upregulated following exposure to Zn, Co and Ni stress. Further growth analyses of mutant strains deficient in *czcD* showed reduced biomass following growth in the presence of Zn and Co. In this chapter, the response of *S. pneumoniae* to Zn stress and the role of CzcD in phagocytic cell survival was further investigated. This study provides insight into the transcriptional changes induced by Zn, the pathway by which pneumococci overcome Zn toxicity, and the important role of CzcD in survival in phagocytic cells.

3.2 Results

3.2.1 Global transcriptional responses to zinc stress in *S. pneumoniae*

The changes in gene expression induced by exposure to extracellular Zn were examined in the *S. pneumoniae* D39 strain. Analysis of the differential gene transcription by RNA sequencing following logarithmic growth in C+Y media or C+Y media supplemented with 100 μM $ZnSO_4$ revealed that 65 genes were substantially altered by Zn (Figure 3.1) [RNA sequencing data generated and processed by Dr Stephanie Neville and Dr Bart Eijkelkamp]. Overall, 57 genes were upregulated >2-fold in response to Zn stress, with 17 of these genes upregulated >4-fold (Table 3.1). Comparatively, only a small number of genes were downregulated following growth in the presence of Zn. Eight genes were downregulated by >2-fold, with three of these genes downregulated by >4-fold (Table 3.2). The RNA sequencing results were validated by assessing the transcription of two biological replicates of ten genes by quantitative reverse transcription-PCR (qRT-PCR) (Figure 3.2). A strong correlation (R^2 = 0.9886) was observed between the results for the RNA sequencing analysis and the qRT-PCR.

The differentially expressed genes were categorised based on their predicted function by aligning the RNA sequencing results with the classification system in the protein Clusters of Orthologous Groups (COG) database (Figure 3.3). The COG database failed to prescribe putative roles for 42% of the differentially expressed genes with ~8% corresponding to genes of unknown function. Nevertheless, this annotation revealed that Zn induced changes in 12 of the 25 COG categories. The largest number of differentially transcribed genes (14%) belonged to the carbohydrate metabolism and transport group. These genes encoded putative galactose-specific PTS transporters (SPD_1057, SPD_0559, SPD_0560, and SPD_0561), the Leloir pathway genes (*galK, galT-2* and *galR),* and a β-galactosidase (*bgaA*), which facilitate galactose uptake and metabolism, a putative lactose-specific (*celB*) and putative mannose-specific (SPD_0293) PTS. Although dispersed among multiple COG groups, 14 genes associated with genetic competence (*comA, comB, comEA, comEC, coiA, comGA, comBG, comGC, comGD, comFC, comFA, comE, comD,* and *comC1*) were increased by >2-fold in transcription in Zn treated *S. pneumoniae*. Approximately 6% of the genes altered by Zn were classified into the inorganic ion transport and metabolism COG group. Notably, *czcD* was the most upregulated gene under Zn stress.

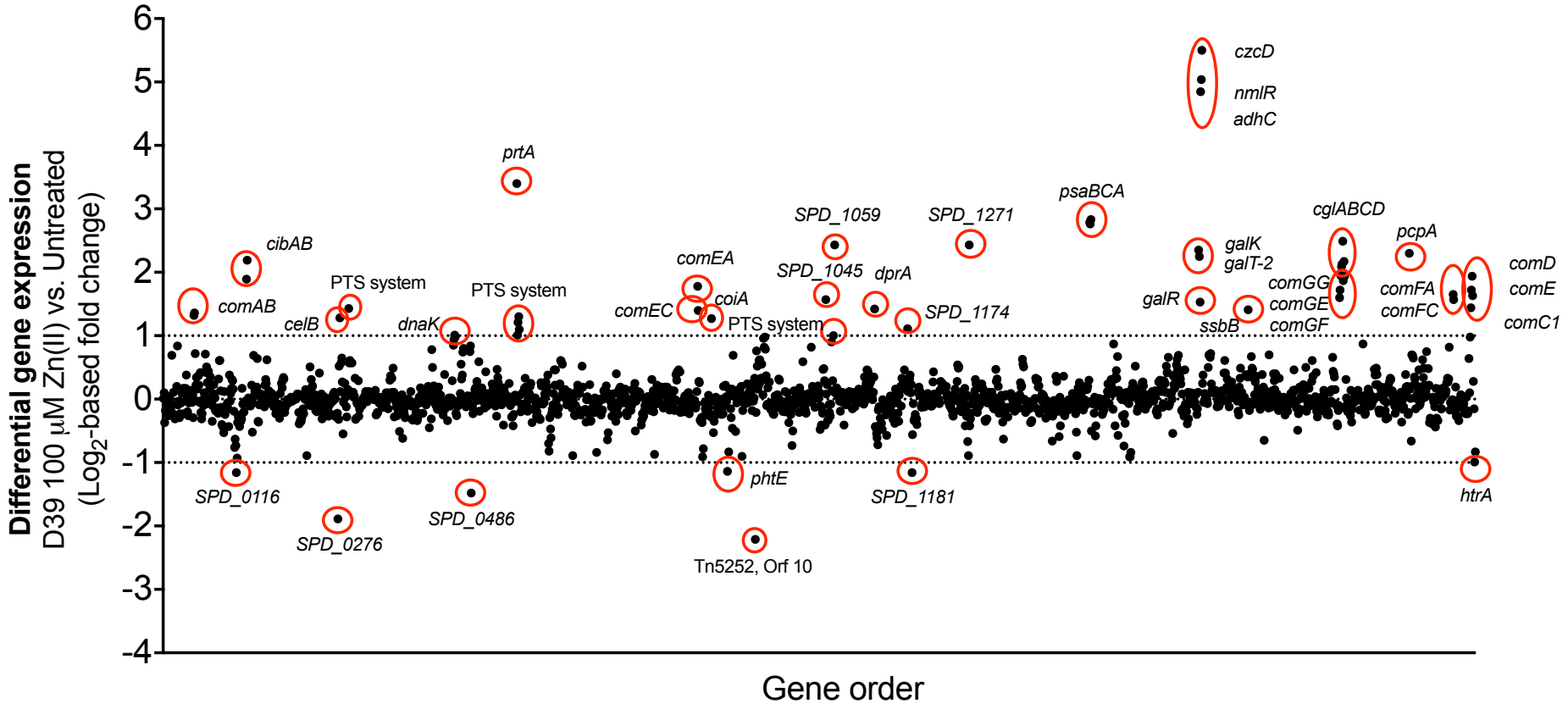


Figure 3.1 Differential gene expression in *S. pneumoniae* D39 in response to zinc stress

Log_2-based fold change in gene expression in *S. pneumoniae* D39 wild-type following growth with 100 μM $ZnSO_4$, compared with untreated. Each dot represents a single gene plotted along the x-axis based on locus tag. Genes that were increased and decreased in transcription greater than 2-fold relative to untreated were considered significant and annotated with their gene names or, if unnamed, the locus tag.

Table 3.1 Upregulated genes in *S. pneumoniae* D39 in response to zinc stress

Gene name	Locus ID	Protein function	Fold-change (Log_2)
comA	SPD_0049	Competence factor transporting ATP-binding protein ComA	1.32
comB	SPD_0050	Competence factor transport protein ComB	1.36
cibC	SPD_0132	Bacteriocin-type signal sequence domain protein	1.89
cibAB	SPD_0133	Class IIb bacteriocin, lactobin A/cerein 7B family	2.19
celB	SPD_0279	PTS-Lactose system, IIB component	1.28
SPD_0293	SPD_0293	PTS-Mannose system	1.43
dnaK	SPD_0460	Chaperone protein DnaK (HSP70)	1.01
prtA	SPD_0558	Cell wall-associated serine protease PrtA	3.40
SPD_0559	SPD_0559	PTS system IIA component, putative	1.01
SPD_0560	SPD_0560	PTS system, IIB component, putative	1.21
SPD_0561	SPD_0561	PTS system, IIC component, putative	1.30
bgaA/lacZ	SPD_0562	bgaA; Beta-galactosidase	1.10
comEA/celA	SPD_0843	Competence protein CelA	1.78
comEC/celB/cilE	SPD_0844	Competence protein CelB	1.40
coiA	SPD_0865	Competence protein CoiA	1.27
SPD_1045	SPD_1045	Uncharacterized protein	1.57
SPD_1057	SPD_1057	PTS system, IIB component, putative	1.00
SPD_1059	SPD_1059	Uncharacterized protein	2.43
dprA/smf/cilB	SPD_1122	DNA processing protein DprA, putative	1.42
SPD_1174	SPD_1174	Uncharacterized protein	1.11
SPD_1271	SPD_1271	Uncharacterized protein	2.43
psaB	SPD_1461	Mn ABC transporter, ATP-binding protein	2.79

psaC	SPD_1462	Mn ABC transporter, permease protein	2.76
psaA	SPD_1463	Mn ABC transporter, substrate binding protein	2.83
galT-2	SPD_1633	Galactose-1-phosphate uridylyltransferase	2.35
galK	SPD_1634	Galactokinase	2.25
galR	SPD_1635	Galactose operon repressor	1.53
adhC	SPD_1636	Alcohol dehydrogenase, Zn-containing	4.85
nmlR	SPD_1637	Transcriptional regulator, MerR family protein	5.04
czcD	SPD_1638	Cation efflux system protein	5.50
ssbB/cilA	SPD_1711	Single-strand binding protein family protein	1.41
SPD_1855	SPD_1855	Methyltransferase small domain superfamily	1.60
SPD_1856	SPD_1856	Uncharacterized protein	1.72
comGG	SPD_1857	Uncharacterized protein	1.95
comGF	SPD_1858	Competence protein ComGF	2.09
comGE	SPD_1859	Uncharacterized putative membrane protein	2.13
cglD/comGD	SPD_1860	Competence protein CglD	2.49
cglC/comGC	SPD_1861	Competence protein CglC	1.87
cglB/comBG	SPD_1862	Competence protein CglB	2.17
cglA/comGA/cilD	SPD_1863	Competence protein CglA	1.94
pcpA	SPD_1965	Choline binding protein PcpA	2.30
comFC	SPD_2034	Competence protein ComF	1.65
comFA	SPD_2035	Competence protein ComFA	1.57
comE	SPD_2063	Response regulator; ComE	1.72
comD	SPD_2064	Putative sensor histidine kinase ComD	1.94
comC1	SPD_2065	Competence-stimulating peptide type 1	1.63

Table 3.2 Downregulated genes in *S. pneumoniae* D39 in response to zinc stress

Gene name	Locus tag	Protein function	Fold change (Log_2)
SPD_0116	SPD_0116	Uncharacterized protein	-1.16
SPD_0276	SPD_0276	Uncharacterized protein	-1.89
SPD_0486	SPD_0486	Uncharacterized protein	-1.48
phtE	SPD_0890	Pneumococcal histidine triad protein E	-1.14
SPD_0891	SPD_0891	Pseudogene	-2.31
SPD_0934	SPD_0934	Tn5252, Orf 10 protein	-2.21
SPD_1058	SPD_1058	Pseudogene	-3.48
SPD_1181	SPD_1181	Uncharacterized protein	-1.16

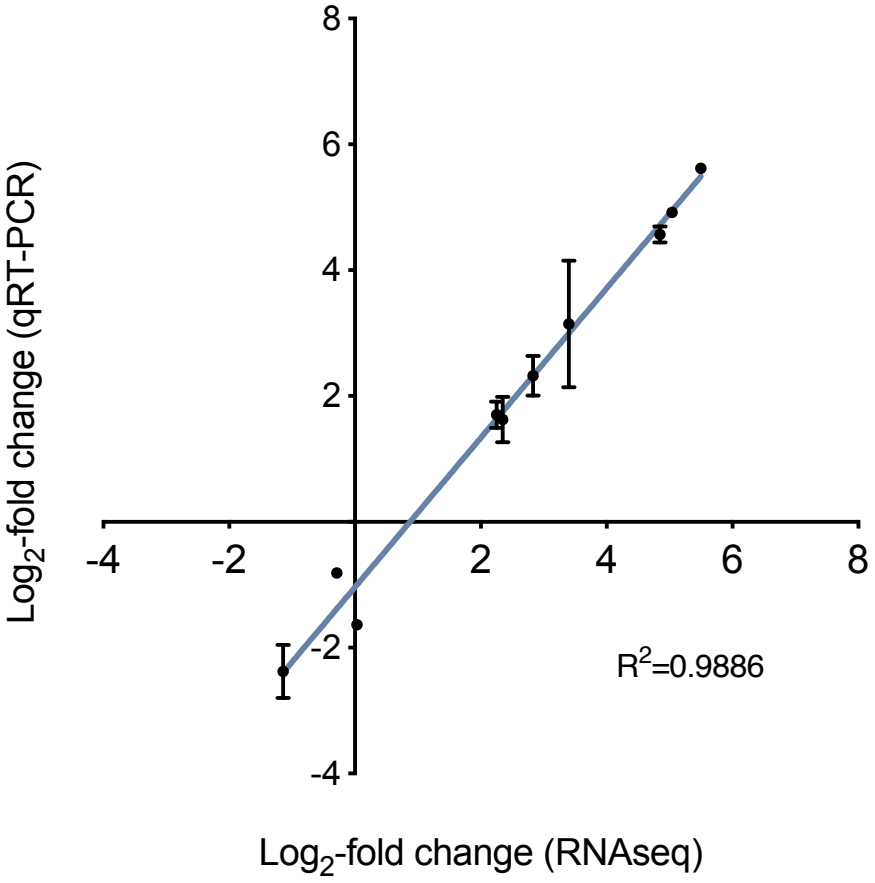


Figure 3.2 Validation of RNA sequencing data

S. pneumoniae D39 was grown to mid-log phase (OD_{600} = 0.3) in C+Y or C+Y supplemented with 100 µM $ZnSO_4$. RNA was extracted and the expression of ten genes (SPD_0382, SPD_0890, SPD_0558, SPD_1384, SPD_1463, SPD_1633, SPD_1634, SPD_1636, SPD_1637, and SPD_1638) was assessed by quantitative real time-PCR (qRT-PCR) analysis relative to the transcription of the *gyrA* (SPD_1077) internal control. Data for RNA sequencing (RNAseq) is presented as the log_2-based fold change for the Zn-treated sample relative to untreated (output from six pooled replicates). Data for the qRT-PCR are the mean ± SEM, n ≥ 2 biological replicates, of the log_2-based fold change for the Zn-treated samples relative to the untreated samples. A strong correlation coefficient (R^2=0.9886) was observed between the two techniques.

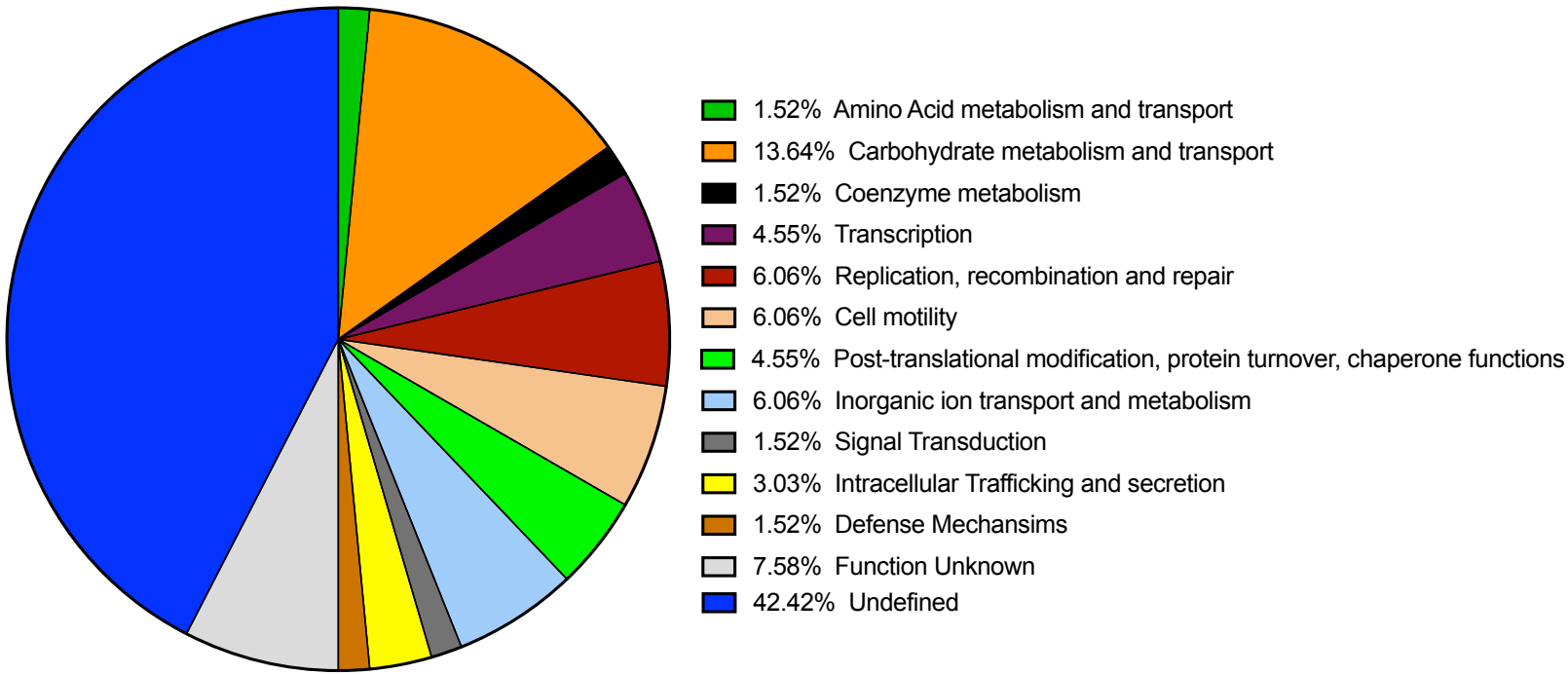


Figure 3.3 Cluster of Orthologous Groups classification for genes altered in *S. pneumoniae* D39 by zinc stress

Genes in *S. pneumoniae* D39 differentially transcribed following growth in the presence of 100 μM $ZnSO_4$ classified based on their Cluster of Orthologous Group (COG) annotation (Tatusov *et al.*, 2000). Data are the percentage of genes in each category of the total genes with increased or decreased transcription greater than 2-fold relative to untreated.

Furthermore, *phtE*, a gene associated with the known Zn uptake pathway was downregulated by >2-fold. In addition to pathways associated with Zn homeostasis, genes encoding the characterised Mn import pathway, *psaBCA,* and the co-regulated genes, *prtA* and *pcpA,* were upregulated following growth in the presence of Zn. Analysis of the transcriptomic response to Zn treatment did not reveal any additional Zn export gene candidates. As *czcD* likely encodes the major Zn efflux pathway of *S. pneumoniae,* features of this gene were investigated in greater detail using a range of bioinformatics tools.

3.2.2 Bioinformatic analysis of *czcD*

CzcD is a member of the CDF family of membrane proteins. Transmembrane topology analysis predicted that CzcD possesses six transmembrane regions and an extended 113 amino acid cytoplasmic C-terminal domain (CTD) containing six histidine, eight glutamate and ten aspartate residues (Figure 3.4). Comparison of CzcD to *E. coli* YiiP, the only CDF protein for which high resolution structural data (2.9 Å) is available (Coudray *et al.*, 2013; Lu *et al.*, 2009; Lu & Fu, 2007), revealed that the two proteins are 23% identical and have 50% similarity. A homology model of *S. pneumoniae* CzcD was generated based on the structure of *E. coli* YiiP (PDB: 3h90) using SWISS-MODEL (Biasini *et al.*, 2014) (Figure 3.5A-B). Structural comparisons revealed that CzcD followed the overall Y-shaped organization of YiiP with minimal deviations from the structure for an intrinsic membrane protein (RMSD 1.822 Å). Electrostatic analyses reveal the presence of highly negatively charged patches, which likely correspond to metal binding sites (Figure 3.5C-D). While largely obscured in the dimeric structure, analysis of the protomeric structure of CzcD revealed negatively charged regions buried within the transmembrane domains, at the dimer interface, and within the C-terminal domain of the protein. A primary sequence alignment of *S. pneumoniae* CzcD with characterised CDF proteins associated with Zn transport, YiiP (50% similarity, 23% identity) and ZitB (51% similarity, 27% identity) from *E. coli*, CzcD from *S. pyogenes* (70% similarity, 49% identity), CzcD from *Cupriavidus metallidurans* (51% similarity, 26% identity), and CzcD from *A. baumannii* (54% similarity, 32% identity) was generated (Figure 3.6). This alignment showed that in contrast to *E. coli* ZitB, *C. metallidurans* CzcD and *A. baumannii* CzcD, *S. pneumoniae* CzcD possesses a relatively short N-terminal domain with no histidine residues. Based on YiiP, alignment of the sequence of CzcD highlighted the putative site A ligands,

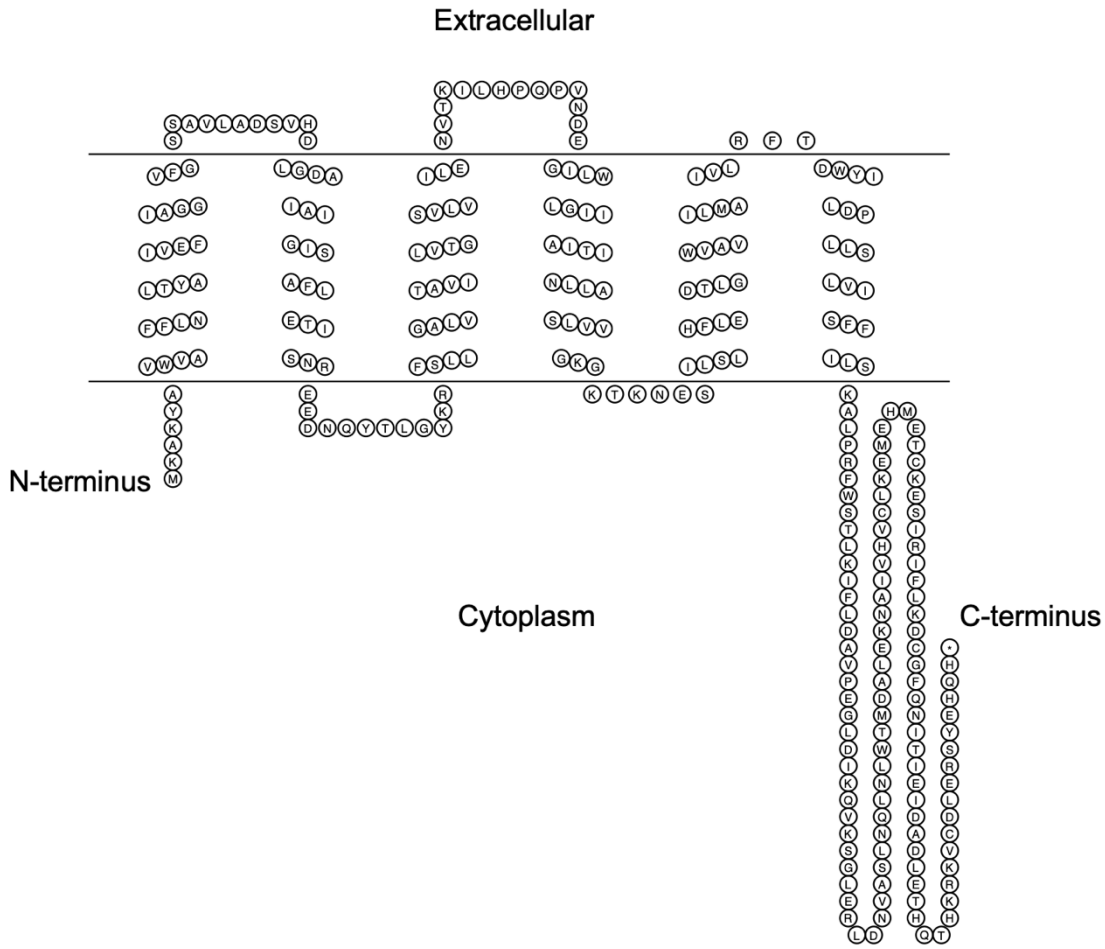


Figure 3.4 Predicted membrane topology model for CzcD from *S. pneumoniae*

Membrane topology prediction was performed for the amino acid sequence of *S. pneumoniae* CzcD (SPD_1638) using the TMHMM server (Krogh *et al.*, 2001). Membrane topology was graphically presented using the graphics program, TOPO2 (Johns S.J., TOPO2, Transmembrane protein display software, http://www.sacs.ucsf.edu/TOPO

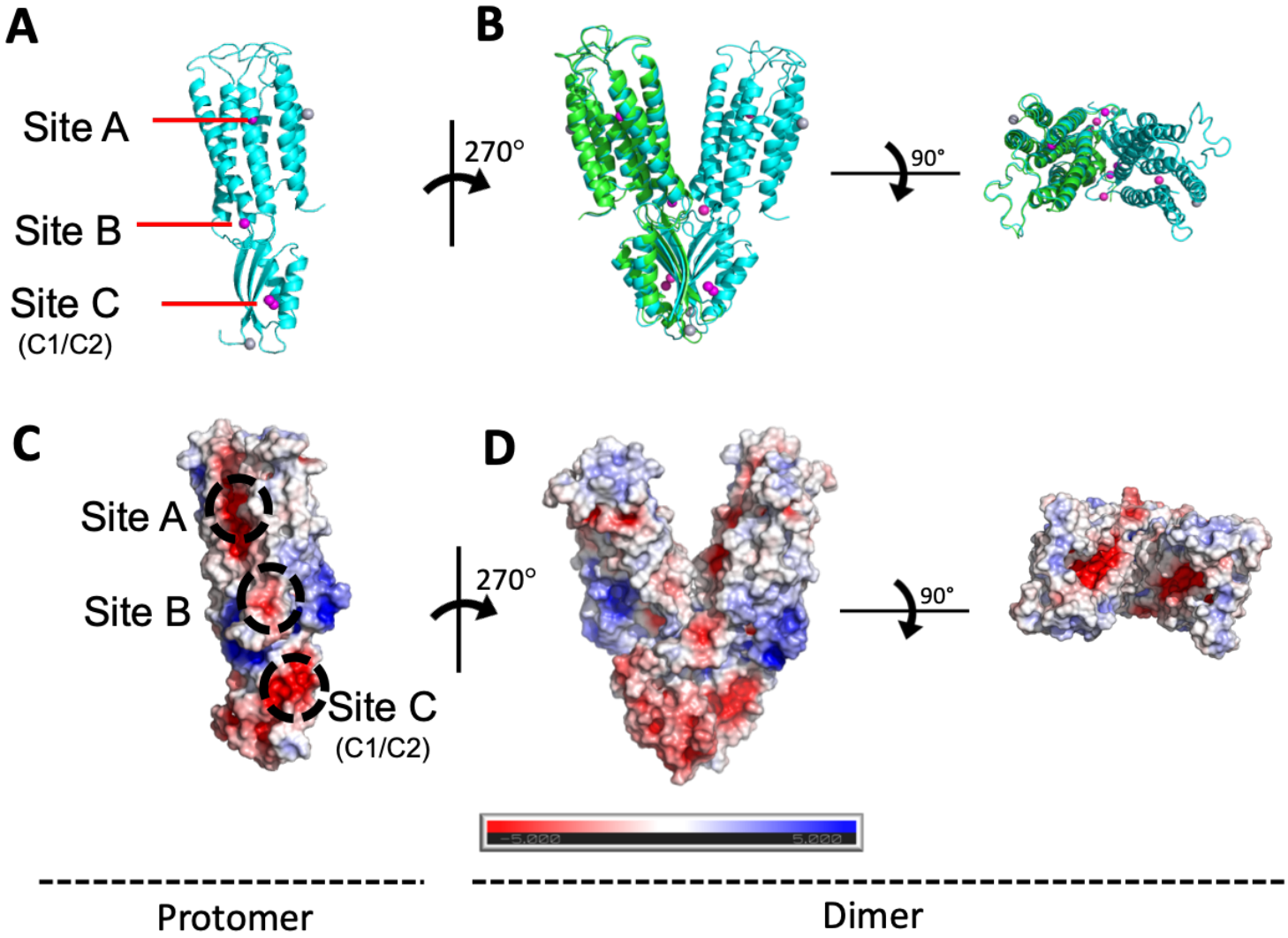

A
Site A
Site B
Site C
(C1/C2)
B
270°
90°
C
Site A
Site B
Site C
(C1/C2)
D
270°
90°
-5.000
5.000
Protomer
Dimer

Figure 3.5 Structural modelling and predicted surface charge of CzcD

(A) Cartoon representation of the CzcD homology model (cyan) based on the crystal structure of *E. coli* YiiP (3h90) viewed from the membrane plane. The bound Zn^{2+} and Hg^{2+} ions are shown as magenta and grey spheres, respectively. (B) Cartoon representation of CzcD dimeric homology model (cyan) and the crystal structure of YiiP (3h90; green). (C) Surface electrostatic potential of CzcD homology model viewed from the same orientations as in (A) and (B). Positive and negative potentials are shown in blue and red, respectively, coloured continuously between -5 and 5 kT/e. Surface electrostatic potential was calculated using the Adaptive Poisson-Boltzmann Solver package (Baker *et al.*, 2001).

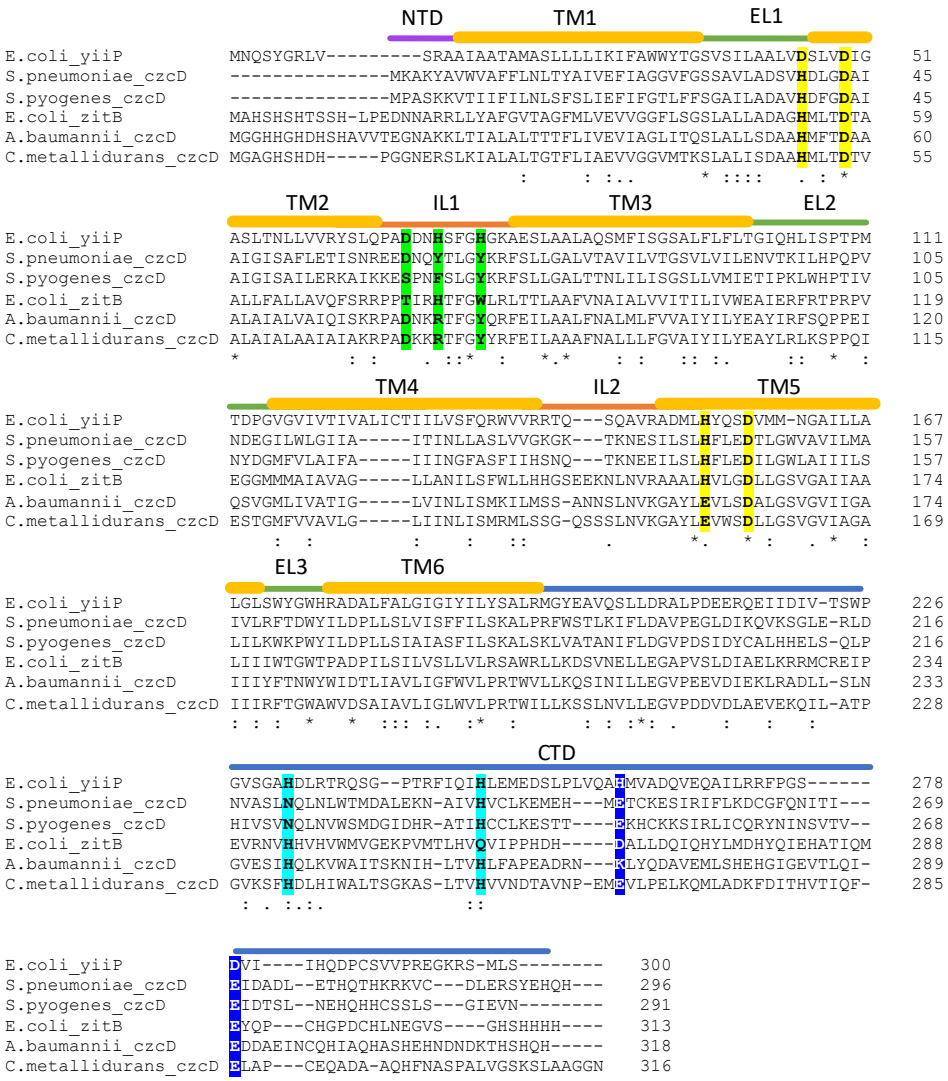


Figure 3.6 Sequence alignment of *S. pneumoniae czcD* with zinc-transporting cation diffusion facilitator proteins from other bacterial species

Amino acid sequences of *E. coli* YiiP (GI: 60392291*), S. pneumoniae* CzcD (SPD_1638; GI: 116077533), *S. pyogenes* CzcD (GI: 94547648), *E. coli* ZitB (GI: 16128720), *A. baumannii* CzcD (GI: 672214288) and *C. metallidurans* CzcD (GI: 3170388) were extracted from NCBI and aligned using Clustal Omega (Sievers *et al.*, 2011). The putative N-terminal domain (NTD, purple line), transmembrane (TM, yellow lines) regions, extracellular loops (EL, green lines), intracellular loops (IL, orange lines) and C-terminal domain (CTD, blue line) are based on membrane topology predictions for CzcD (Krogh *et al.*, 2001). Putative metal binding residues predicted based on alignment with the YiiP residue locations for site A (yellow shading), site B (green shading), site C1 (aqua shading), and site C2 (blue shading) (Lu *et al.*, 2009). * denotes fully conserved residue, : denotes conservation between groups of strongly similar properties, . denotes conservation between groups of weakly similar properties.

His39, Asp43, His142, and AspD146 in TM2 and TM5. The residues of this site in *E. coli* YiiP have previously been proposed to be responsible for the substrate specificity of CDF transporters. The CzcD site A site differs from that of YiiP by the most N-terminal histidine residue (His39), which aligns to an aspartate residue in YiiP. Further analysis of the coordination residues of the CzcD model (HD-HD) compared to YiiP (DD-HD) showed that a histidine residue at this site leads to a smaller binding pocket (Figure 3.7). While less conserved, the proposed site B ligands in the intracellular loop region 1 of CzcD were Asp62, Tyr65, Tyr69 and Arg71 (Figure 3.6). Putative residues in the cytoplasmic CTD region of CzcD for site C1 corresponded to Asn222 and His239, while site C2 aligned with Glu249 and Glu270 (Figure 3.6). The contribution of these residues was not assessed further as a publication showing that mutation of these residues compromised Zn resistance was released during the course of this study (Martin & Giedroc, 2016). Given the lack of information on the role of CzcD in survival within phagocytic cells, the role of this protein in Zn homeostasis was investigated further.

3.2.3 *czcD* provides resistance to host-mediated zinc intoxication

3.2.3.1 *czcD* contributes to resistance to zinc stress

Building on the RNA sequencing, the expression of *czcD* was analysed by qRT-PCR to enable confirmation of the initial observations. Consistent with the transcriptomic analyses, growth of *S. pneumoniae* D39 in the presence of Zn induced a 38-fold ($P < 0.0001$, two-tailed unpaired *t*-test) increase in *czcD* transcription (Figure 3.8). Transcription of *czcD* was then assessed following growth in the presence of the Zn chelator, N,N,N′,N′-Tetrakis(2-pyridylmethyl)ethylenediamine (TPEN). Here, *czcD* transcription was decreased by 4.8-fold ($P = 0.0079$, two-tailed unpaired *t*-test), consistent with a transcriptional response to Zn limitation (Figure 3.8).

To examine the role of *czcD* in resistance to Zn toxicity, the growth of an isogenic Δ*czcD* deletion strain was measured relative to the parental strain. Comparable growth was observed between the mutant and parental strains in un-supplemented C+Y media, with maximal absorbance readings of ~0.35 reached within 3.5 hrs of growth (Figure 3.9). In un-supplemented media, the mutant and wild-type strains also showed reductions in absorbance during stationary phase growth, most likely attributable to autolysis. Supplementation with Zn

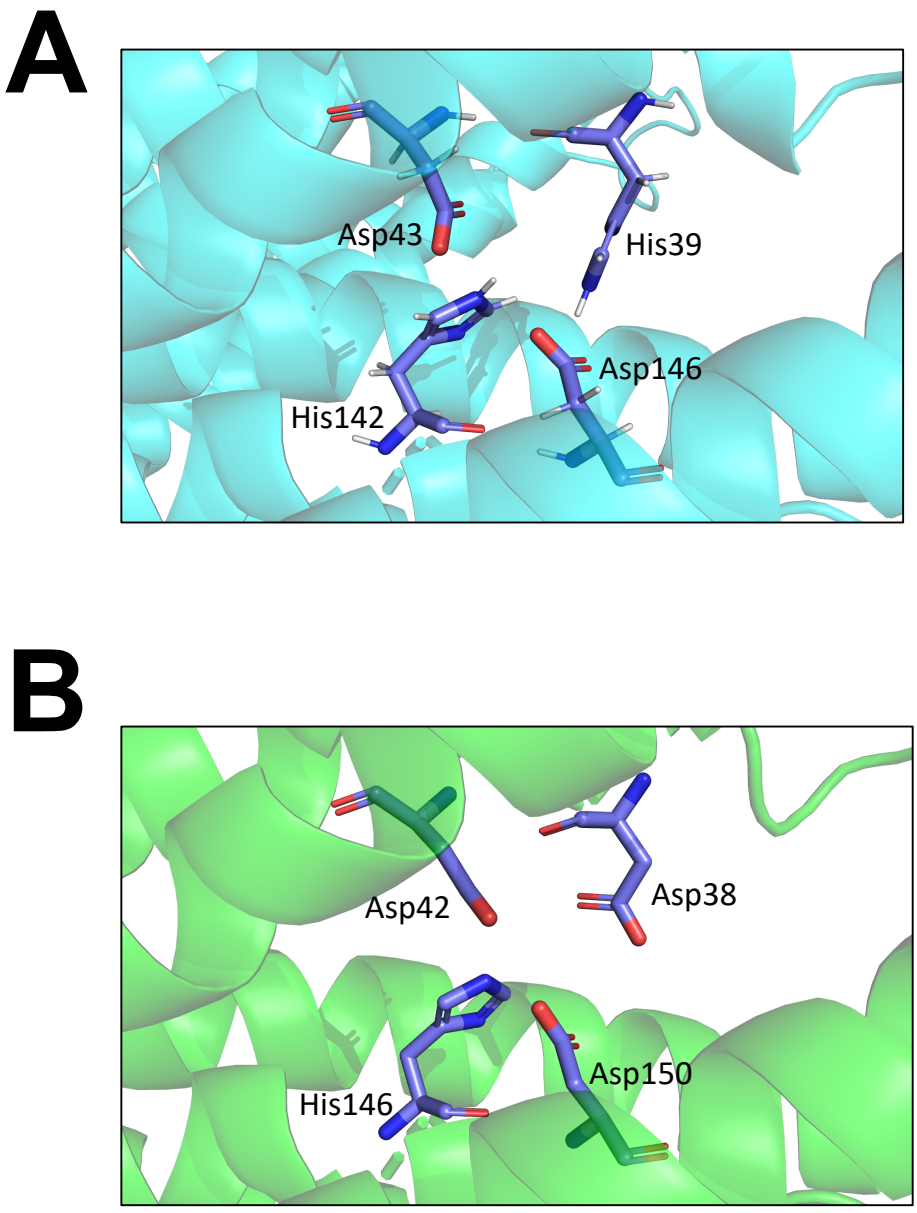


Figure 3.7 Structural modelling of the CzcD metal binding site A

(A) Cartoon representation of the Site A residues of the CzcD homology model (cyan) based on the crystal structure of *E. coli* YiiP (3h90) and (B) cartoon representation of the Site A residues of *E. coli* YiiP (PDB 3h90; green). The site A residues of CzcD (HD-HD; His39, Asp43, His142 and Asp146) and YiiP (DD-HD; Asp38, Asp42, His146 and Asp150) are coloured based on element in blue.

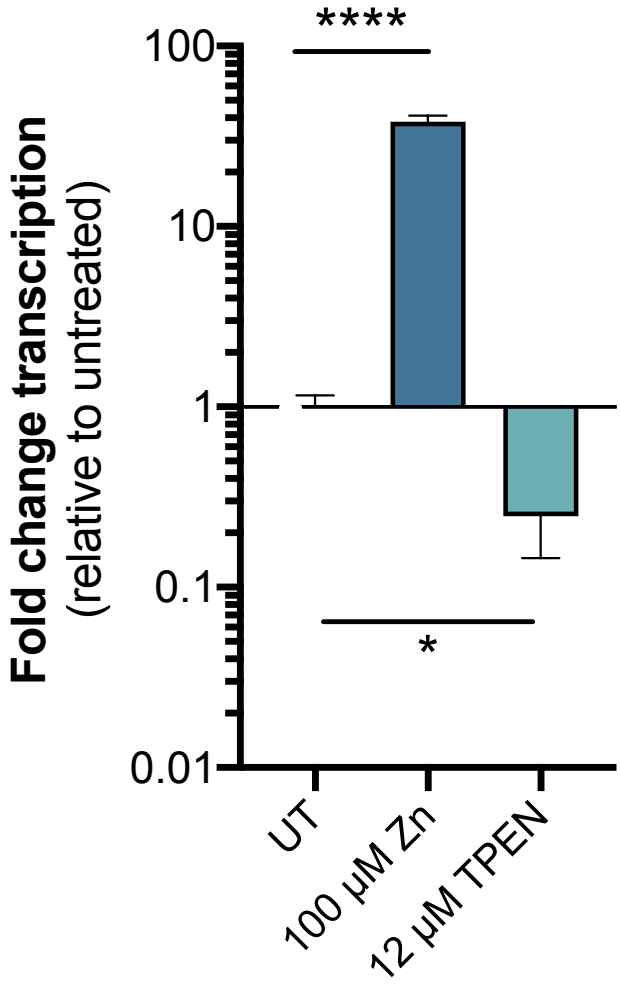


Figure 3.8 Transcriptional response of *S. pneumoniae czcD* to zinc

Transcription levels of *czcD* in *S. pneumoniae* D39 wild-type were assessed following growth in C+Y medium (untreated; UT), C+Y supplemented with 100 µM $ZnSO_4$, or C+Y supplemented with 12 µM N,N,N′,N′-Tetrakis(2-pyridylmethyl)ethylenediamine (TPEN). The data are normalised against the transcription of the *gyrA* (SPD_1077) internal control and presented as the differential transcription relative to UT. Data are the mean ± SEM, from n ≥ 2 biological replicates. Statistical significance was assessed using the Student's two-tailed *t*-test, where * represents $P < 0.05$, **** represents $P < 0.0001$.

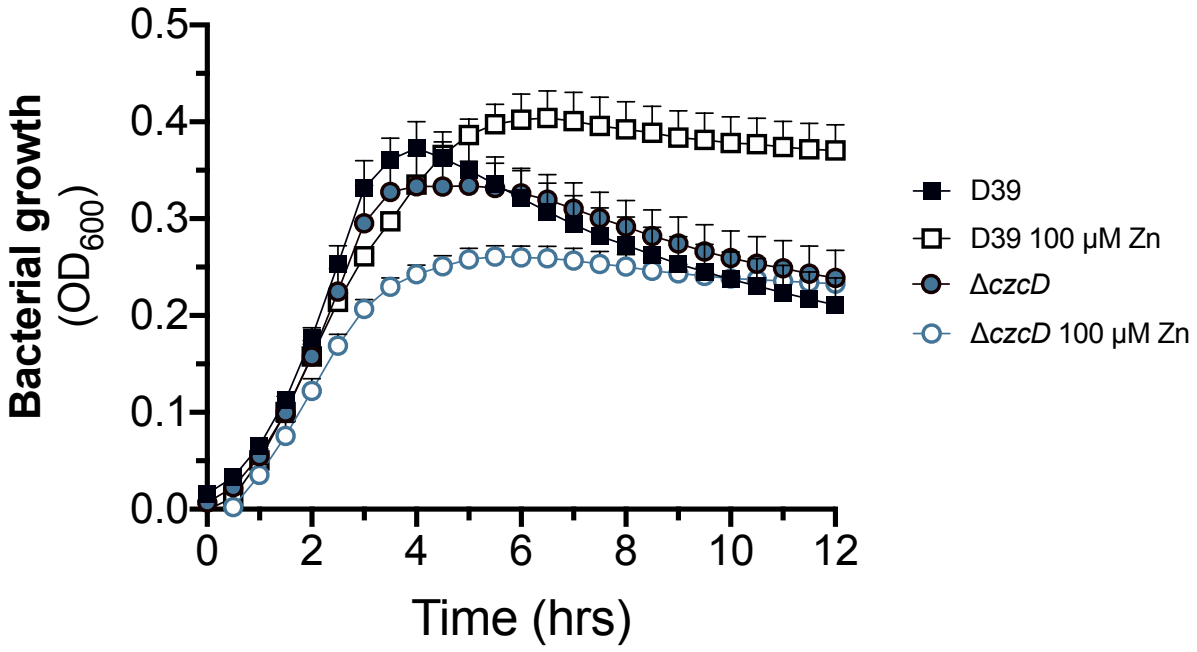


Figure 3.9 Growth kinetics of *S. pneumoniae* D39 wild-type and D39 Δ*czcD*

S. pneumoniae D39 wild-type and Δ*czcD* were grown in C+Y medium or C+Y supplemented with 100 µM $ZnSO_4$. Growth was monitored by readings of the optical density at 600 nm (OD_{600}) every 30 mins. The data are the mean absorbance + SEM, from n ≥ 3 biological replicates. Where not visible, error bars are overlapped by the representative symbols.

resulted in strain-specific growth differences. During logarithmic phase, the Zn-supplemented wild-type strain displayed only a minor growth delay compared to un-supplemented conditions. The maximal absorbance for growth reached OD_{600} ~0.40, which was marginally more than that observed in un-supplemented media and was maintained for at least 12 hours post inoculation. Although the Δ*czcD* strain displayed comparable growth kinetics to the parental strain for the first two hours of growth, the mutant reached a maximal absorbance of only OD_{600} ~0.25 by five hours. Therefore, loss of *czcD* reduced resistance to extracellular Zn, manifested as an impact on the growth of *S. pneumoniae* during logarithmic and stationary phase.

To complement the growth experiments and to define the contribution of *czcD* in protection against Zn stress, the cellular Zn content of *S. pneumoniae* was determined. Here, direct comparisons between the wild-type and Δ*czcD* strains were facilitated by growth to the same cell density (OD_{600} = 0.30), in the presence and absence of 50 μM $ZnSO_4$. Subsequently, the cellular metal content was measured by inductively coupled plasma-mass spectrometry (ICP-MS). The strains showed cellular Zn levels that were not significantly different after growth in un-supplemented media (Figure 3.10A). Upon supplementation with Zn, the wild-type strain showed a significant ($P < 0.001$, two-tailed unpaired *t*-test), 1.5-fold increase in Zn accumulation compared to the untreated strain, while the Δ*czcD* strain accumulated 2.2-fold more Zn ($P < 0.001$, two-tailed unpaired *t*-test), compared to the un-supplemented mutant strain. By comparison with the wild-type, the mutant Δ*czcD* strain showed a significant ($P < 0.001$, two-tailed unpaired *t*-test) 1.6-fold increase in Zn abundance relative to the wild-type strain under identical conditions. Therefore, these data show that *czcD* has a key role in maintaining pneumococcal intracellular Zn abundance. The cellular abundance of Mg, Ca, Mn, Fe, Co, Ni and Cu were also assessed. The levels of Co, Ni and Cu fell below the detection limit (data not shown) and no significant differences were observed under the different test conditions and strains for Mg, Ca or Fe (Appendix 1). Cellular Mn abundance was not significantly different between the wild-type and Δ*czcD* strains grown in un-supplemented media (Figure 3.10B). However, treatment with Zn influenced the abundance of cellular Mn. Consistent with prior studies, the Zn-treated wild-type strain accumulated 2.5-fold less cellular Mn compared with the untreated strain ($P < 0.0001$, two-tailed unpaired *t*-test). A similar trend was observed for the Δ*czcD* strain, where Zn treatment induced a 3.6-fold decrease in Mn accumulation ($P < 0.0001$, two-tailed unpaired *t*-test). By comparison with the wild-type, the mutant Δ*czcD* strain showed a further 1.3-fold decrease in Mn accumulation after growth in the

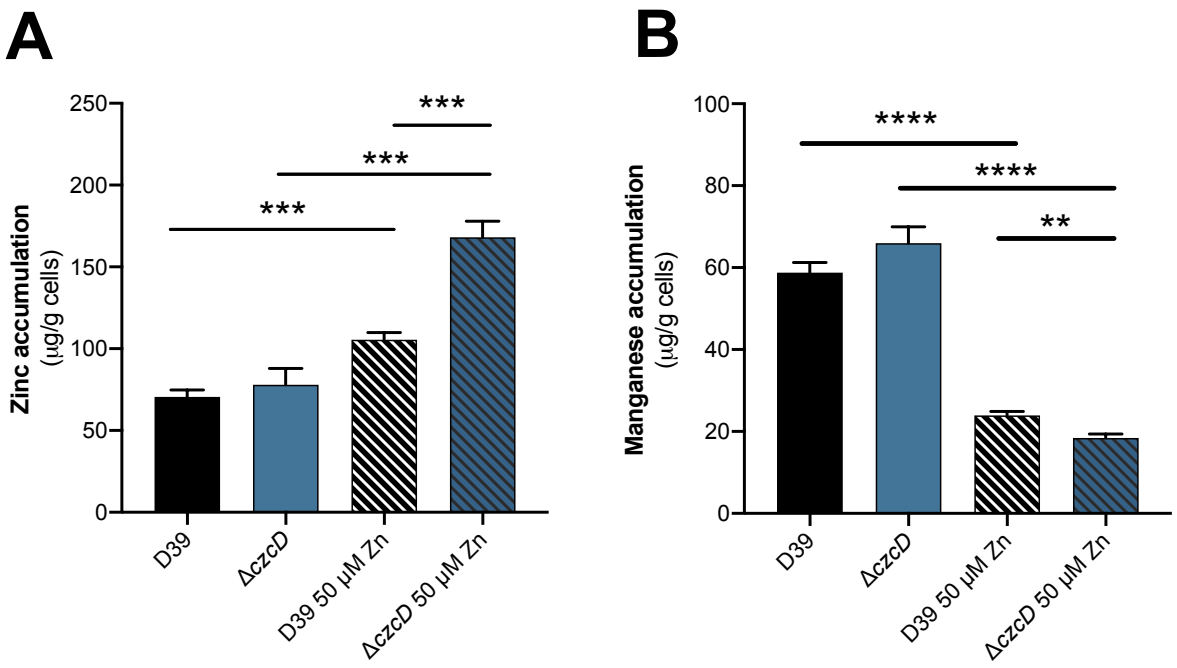


Figure 3.10 Cellular zinc and manganese accumulation in *S. pneumoniae* D39 and D39 Δ*czcD*

Zn and Mn content were assessed in *S. pneumoniae* D39 wild-type and the mutant strain Δ*czcD* following growth in the presence of absence of 50 μM $ZnSO_4$. Cellular content of (A) Zn and (B) Mn were determined based on the dried cell pellets of cells grown to mid-log phase by ICP-MS. Data are the mean + SEM, n ≥ 3 biological replicates. Statistical significance was assessed using the Student's two-tailed *t*-test, where ** represents $P < 0.01$, *** represents $P < 0.001$, and **** represents $P < 0.0001$.

presence of Zn ($P < 0.01$, two-tailed unpaired *t*-test). Taken together, these data indicate that an increase in both extracellular and intracellular Zn has the capacity to reduce pneumococcal Mn levels.

3.2.3.2 *czcD* protects against macrophage-mediated killing

During disease, *S. pneumoniae* is subjected to a broad arsenal of immune defences. Emerging evidence suggests that Zn intoxication in phagocytic cells is an important feature of the innate immune response (Botella *et al.*, 2011; Kapetanovic *et al.*, 2016; Ong *et al.*, 2014). Given the importance of *czcD* in the maintenance of cellular Zn concentrations, the contribution of *czcD* to macrophage-mediated killing was investigated. Here, the human THP-1 monocyte cell line was differentiated with phorbol 12-myristate 13-acetate to induce cells with macrophage-like properties. The *S. pneumoniae* wild-type and Δ*czcD* strains were incubated with the THP-1-derived macrophages and the intracellular survival was measured by enumerating the colony forming units (CFU) 1 hr post infection (Figure 3.11). Survival of the Δ*czcD* strain was severely compromised in THP-1 monocyte-derived macrophages. Compared to the wild-type strain, the Δ*czcD* mutant survival was significantly reduced by 95% ($P < 0.01$, two-tailed unpaired *t*-test) (Figure 3.11). This observation indicates that the hyper-susceptibility of the mutant to Zn stress leads to decreased survival in THP-1-derived macrophages. Therefore, consistent with recent findings, these data indicate that the antimicrobial activity of Zn is exploited by macrophages to prosecute antibacterial clearance.

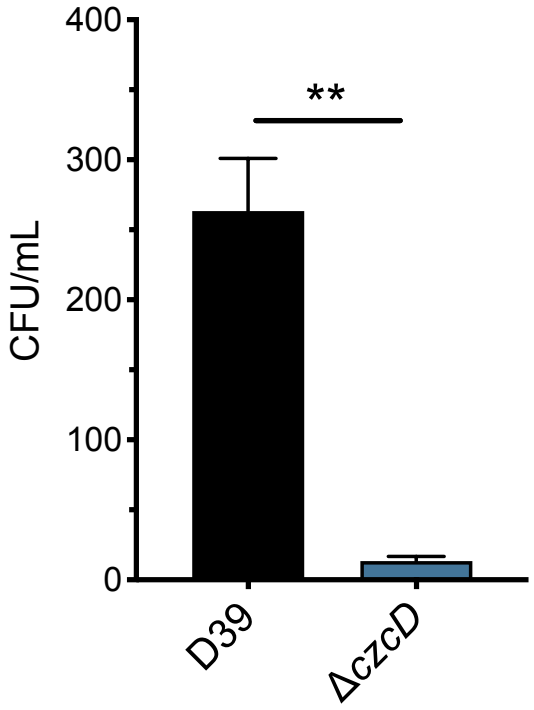


Figure 3.11 The role of CzcD in *S. pneumoniae* survival in THP-1 cells

Survival of wild-type *S. pneumoniae* and the mutant derivative strain Δ*czcD* in THP-1 monocyte-derived macrophages. Bacterial colony forming units (CFU) were determined after 1 hr treatment. Data are the mean + SEM, from n = 3 biological replicates. Statistical significance was assessed using the Student's two-tailed *t*-test, where ** represents $P < 0.01$.

3.3 Discussion

Zn deficiency has long been associated with an increased incidence of bacterial disease (Fischer Walker & Black, 2004). While the mechanism(s) underlying the protective role of Zn remain to be fully understood, recent studies have highlighted the importance of Zn in the innate immune response. Zn mobilisation in phagocytic cells towards bacteria captured within the phagolysosomes is associated with enhanced antimicrobial clearance. Although this phenomenon was first described for intracellular pathogens such as *M. tuberculosis* and *S.* Typhimurium, it is emerging as a generalised feature of bacterial clearance following phagocytosis (Botella *et al.*, 2011; Kapetanovic *et al.*, 2016; Ong *et al.*, 2014). Resistance to this innate killing mechanism has led to the evolution of Zn-resistance pathways in bacterial pathogens (Capdevila *et al.*, 2016). Metal tolerance and resistance pathways include mechanisms such as intracellular buffering pools and efflux machinery. *S. pneumoniae* is a host-adapted bacterial pathogen that subverts host immune responses to survive and proliferate within host niches. Nevertheless, how the pneumococcus resists phagocytic cell-mediated Zn intoxication had not been elucidated prior to this investigation. This study has shown, through a combination of bioinformatic, transcriptomic and cell-based analyses, that CzcD in *S. pneumoniae* provides resistance to Zn stress in media and to phagocytic cell clearance.

CDF transporters are present in all domains of life and serve important roles in the cytoplasmic efflux of cations. The CDF family protein, CzcD, had previously been implicated in *S. pneumoniae* Zn efflux (Kloosterman *et al.*, 2007). By analysing the transcriptomic response of *S. pneumoniae* to Zn stress, the present study showed that *czcD* was the only gene upregulated in response to Zn that possessed a putative metal export function. It is likely that CzcD represents the major Zn resistance pathway. However, the possibility that other transporters are capable of Zn efflux cannot be excluded. Further studies assessing the transcriptome following growth with Zn upon deletion of *czcD* may highlight alternative transporters capable of contributing to Zn resistance. Bioinformatic studies predicted that *S. pneumoniae* CzcD possesses six transmembrane regions and an extended cytoplasmic C-terminal domain possessing many histidine, aspartate and glutamate residues with the potential to interact with Zn. A homology model and surface charge analysis based on the archetype of this family, YiiP from *E. coli*, suggests that CzcD possesses regions of high negative charges that may accommodate the binding of a divalent metal cation. In particular, highly negatively charged regions were observed in pockets located within the transmembrane domains, which

likely correspond to the metal binding residues of site A. While occluded from the dimeric structure, the surface charge structure of protomeric CzcD viewed from the dimer interface revealed a negatively charged region that could accommodate metal binding, likely corresponding to site B. In addition, patches within the C-terminal domain displayed a high negative charge. These regions likely harbour the metal binding residues for site C1 and C2, as well as other putative Zn-binding residues that may act to recruit Zn from the cytoplasm. Alignment of *S. pneumoniae* CzcD against characterised Zn-transporting members of the CDF family revealed only a moderate level of overall homology, with some of the highest levels of conservation at the metal binding site A. Based on the location of the characterised metal-binding residues of YiiP, putative metal binding residues were highlighted for *S. pneumoniae* CzcD and the other Zn-transporting CDF proteins. A study has since characterised the contribution of the putative Zn-binding site residues in *S. pneumoniae* Zn resistance and selectivity (Martin & Giedroc, 2016). This study experimentally demonstrated that, with the exception of Asn222, the putative metal coordinating residues of CzcD contributed to pneumococcal Zn resistance. In contrast to the DD-HD site A of YiiP, CzcD possesses HD-HD site A residues. A previous study has shown that mutation of the most N-terminal Asp residue (Asp45) of the YiiP site A to His reduces the capacity of YiiP to transport Cd (Hoch *et al.*, 2012). In another study, growth analyses of *S. pneumoniae* revealed that CzcD does not contribute to protection against Cd stress (Begg *et al.*, 2015). Together, these data suggest that the His39 site A residue may be responsible for the inability of CzcD to transport Cd and mediate selectivity for Zn.

Transcription of *czcD* is regulated by SczA, which is a member of the MerR transcriptional regulator family of proteins (Kloosterman *et al.*, 2007). SczA is proposed to bind one of two distinct DNA motifs upstream of *czcD*, based on its metallation state, to either repress or activate *czcD* transcription. This model of regulation by SczA is unusual as metalloregulatory proteins typically regulate transcription in a binary manner depending on their metal occupancy. Nevertheless, consistent with a Zn-dependent regulation, the present study showed that *czcD* transcription is responsive to Zn abundance. Upon treatment with Zn, the growth phenotypes of the D39 wild-type and the Δ*czcD* mutant strain are affected. In corroboration with previous work, upon mutation of *czcD, S. pneumoniae* displayed a reduced growth yield at 6-8 hrs of growth compared with the parental strain in the presence of Zn stress (Kloosterman *et al.*, 2007; Martin & Giedroc, 2016). Consistent with these findings, this study showed that growth of the *czcD* mutant with Zn increased cellular Zn to significantly higher

levels than in the D39 wild-type strain. The present study has expanded these findings to reveal that CzcD contributes to pneumococcal survival within monocyte-derived macrophages, highlighting the significant role of Zn toxicity in macrophages to kill invading *S. pneumoniae*. Despite these findings, the possibility that phagocytosis of the Δ*czcD* mutant strain may be compromised cannot be excluded. Future studies to assess the contribution of *czcD* to both uptake and clearance by phagocytic cells are required. Nevertheless, these data support the role of CzcD in *S. pneumoniae* Zn export and resistance to phagocytic cell killing.

This work also provided insight into the physiological responses of *S. pneumoniae* to exogenous Zn. Interestingly, despite a minor growth delay for the Zn-treated D39 wild-type strain, these cells displayed an extended period of high cell density during stationary phase. Pneumococci typically undergo a characteristic autolytic response during stationary phase, a period of cell lysis that is primarily mediated by the autolysin, LytA (Mosser & Tomasz, 1970). The cytoplasmic material and fragments released by cell wall degradation during autolysis have previously been proposed to aid in the prevention of phagocytosis and thus contribute to the pathogenesis of pneumococci (Martner *et al.*, 2009). The results of this study indicate that Zn treatment rendered pneumococci more resistant to autolysis. These findings corroborate those of a recent study, where Zn was shown to protect against deoxycholate-induced autolysis (Brown *et al.*, 2017). The authors proposed that excess Zn may inhibit autolysis in a LytA-dependent manner via an unknown mechanism. Here, no differences were observed in the transcription of *lytA* upon Zn treatment, which indicates that a LytA-dependent impact of Zn on autolysis is likely occurring at a post-transcriptional level. As LytA possesses a Zn-containing active site, it is possible that additional Zn in the cytoplasm may alter the function of LytA (Mellroth *et al.*, 2014). The catalytic Zn ion is octahedrally coordinated in LytA via interactions with residues His26, His133 and Asp149 and three water molecules (Mellroth *et al.*, 2014). It is possible that this site may be susceptible to overloading by excess Zn, which may inhibit the catalytic activity of this protein. However, future structural, mutational and biophysical studies are required to resolve these phenotypic observations by determining how Zn interacts with LytA and whether this interaction is physiologically relevant.

The transcriptomic analyses of Zn-treated pneumococci revealed changes in genes associated with the Mn uptake pathway. An increase in the expression of the Mn uptake system and co-regulated genes upon treatment with Zn have previously been reported (Kloosterman *et al.*, 2008). Exogenous Zn can impair Mn uptake via irreversible competitive binding to PsaA,

the Mn substrate binding protein, directly impacting cellular Mn accumulation (Couñago *et al.*, 2014; McDevitt *et al.*, 2011). The Mn-bound regulator of the Mn uptake system, PsaR, has a high affinity for the Psa operator sequence, leading to transcriptional repression of the genes encoding the Mn transporter *psaBCA*, a choline binding protein, *pcpA*, and a cell-wall associated serine protease, *prtA* (Johnston *et al.*, 2006). The transcriptional upregulation of these genes is consistent with the observed decrease in cellular Mn abundance upon Zn treatment, which results in the derepression of these genes. Interestingly, the results presented herein indicate that high levels of intracellular Zn observed in the *czcD* mutant may compound the influence of extracellular Zn, leading to a further decrease cellular Mn abundance. Previous findings have shown that Zn is capable of interacting with PsaR (Jacobsen *et al.*, 2011; Kloosterman *et al.*, 2008). PsaR harbours two pairs of metal-binding sites, designated site 1 and site 2. Site 1 is typically occupied by Zn, while the binding of Mn at site 2 changes the conformation such that PsaR exhibits increased affinity of the regulator for the operator, leading to repression of the Psa regulon. Conversely, when site 2 is not occupied by a metal ion, the affinity of PsaR for the Psa operator sequence is reduced, leading to derepression of these genes. Interestingly, the binding of Zn at site 1 and site 2 leads to an increase in the affinity of PsaR for the DNA, albeit to a lesser extent than Mn binding at site 2. Thus, sites 1 and 2 of PsaR may be occupied by Zn in the Zn-overloaded *czcD* mutant, which may lead to further repression than observed when only site 1 is occupied by Zn. These findings suggest that extracellular Zn treatment reduces the uptake of Mn via PsaA, reducing cellular Mn and leading to derepression of this pathway. Conversely, high levels of intracellular and extracellular Zn, leads to impaired uptake via PsaA and a reduced capacity for PsaR to derepress the Psa regulon to respond to the Mn defect. However, further transcriptional analyses of the Psa regulon in the Zn-treated *czcD* mutant are required to assess whether there is a reduction in the upregulation of these genes compared with wild-type.

Genes encoding a β-galactosidase, a putative galactose-specific PTS, and components of the Leloir pathway, which facilitate the cleavage, uptake and metabolism of galactose, respectively, were highly upregulated in the presence of Zn. Despite the high abundance of the preferred sugar glucose in the growth medium, exposure to Zn appeared to cause a shift in pneumococcal metabolism to galactose utilisation. The minor Zn-induced growth delay may arise from the transition to catabolism of a slowly metabolised, non-preferred and low abundance sugar in the medium. A metabolic shift to galactose utilisation induced by Zn treatment has been previously reported in *S. pyogenes* (Ong *et al.*, 2015). The authors proposed

that Zn inhibited the essential glycolytic enzymes, phosphofructokinase (PFK), glyceraldehyde-3-phosphate dehydrogenase (GAPDH), and phosphoglucomutase (PGM) (Ong *et al.*, 2015). Although *S. pyogenes* lacks an intact Leloir metabolic pathway, genes in the alternative galactose utilisation pathway, the tagatose-6-phosphate (T6P) pathway, were upregulated. In *S. pyogenes*, galactose utilisation via this pathway was proposed to enable this bacterium to bypass the Zn-inhibited enzymes, thereby preserving energy production and central metabolism. Despite this, evidence to demonstrate that deletion of the T6P genes from *S. pyogenes* increases susceptibility to Zn is lacking, which limits the conclusions that may be drawn. As the PFK, GAPDH and PGM enzymes are highly conserved in *S. pneumoniae* it is reasonable to speculate that these enzymes may also be inhibited by Zn. In contrast to *S. pyogenes*, the transcriptomic analyses in the present study showed no alteration the T6P pathway genes, *lacABCD*, upon Zn treatment. Furthermore, the metabolism of galactose via the Leloir pathway in *S. pneumoniae* is unlikely to circumvent the PfkA enzymatic step of glycolysis as metabolic flux from the Leloir pathway enters the glycolytic pathway at step preceding PfkA. Thus, further work is required to assess the impact of Zn on carbohydrate metabolism and the function of the PFK, GAPDH and PGM enzymes in *S. pneumoniae.*

Genetic competence is a complex pathway in bacteria that mediates the uptake and incorporation of DNA into their genomes. The uptake of foreign DNA can offer bacterial pathogens a competitive advantage through the acquisition of novel virulence and antibiotic resistance determinants (Kadioglu *et al.*, 2008). In *S. pneumoniae*, the competence pathway is well characterised and is initiated through a CSP-mediated quorum sensing system (Shanker & Federle, 2017). In this study, a number of competence genes involved in DNA uptake or recombination were upregulated by Zn. These included genes encoding the ABC exporter and accessory protein, *comAB*, which secrete and process CSP, and the *comCDE* genes that encode the CSP precursor, a CSP receptor histidine kinase, and cognate response regulator, respectively, which further induce the expression of the *comAB* and *comCDE* operons. The upregulation of this pathway typically induces an accumulation of CSP, which leads to an increase in the expression of the alternate sigma factor, *comX.* Interestingly, while *comX* expression was slightly elevated in the Zn-treated cells, as these levels were increased by less than 2-fold, this increase may not be physiologically relevant. ComX impacts the expression of more than 100 genes responsible for the incorporation of DNA. However, only 14 of the late competence genes were increased in expression upon Zn treatment. Late competence genes upregulated by Zn included the DNA uptake machinery, *celAB*, *comGA*, *comBG*, *comGC*, and

comGD, the single-strand binding protein, *cilA,* and the DNA processing protein, *dprA*. Zn-treated cells also showed increased expression of the two-peptide bacteriocin, *cibAB* and its immunity factor, *cibC*. These fratricide effectors are important for intraspecies competition, whereby secreted peptides lyse non-competent pneumococci, which further increases the availability of exogenous DNA (Rice & Bayles, 2008). An association between Zn and competence has previously been reported, where pneumococcal transformation efficiency was reduced in a mutant lacking a component of the Zn uptake pathway, AdcC (Dintilhac *et al.*, 1997). As the transformation defect was restored through the addition of exogenous Zn, the authors proposed that this phenomenon may be due to the importance of Zn as a co-factor to a competence protein, or the requirement of Zn for the phosphorylation of ComE by ComD, a role that magnesium typically fulfils. While this work indicates that the competence pathway is activated by Zn, further studies are required to assess the impact of Zn on transformation efficiency and the phosphorylation status of ComE. Furthermore, a recent study investigated the transcriptomic changes induced by a range of different *S. pneumoniae* experimental growth conditions (Aprianto *et al.*, 2018). This work highlighted that the competence genes were dynamically expressed and responsive to a number of different growth conditions. As a result, it is possible that the upregulation of the genes of the competence pathway constitutes a broad response to environmental stress and the extent to which Zn may directly influence the transcription of these genes remains unclear. Further work to discern whether DNA uptake and recombination are increased in *S. pneumoniae* upon treatment with excess Zn is required to determine whether these transcriptional changes translate into increased genetic competence.

Overall, this study demonstrates that CzcD is capable of Zn efflux and has an important role in resistance to clearance by phagocytic cells. Furthermore, exogenous Zn was shown to alter the expression of genes involved in carbon metabolism, competence, and autolysis, which may have broader implications for pneumococcal pathogenesis. Further characterisation of pneumococcal metabolism and physiology is required to understand the impact of Zn on *S. pneumoniae* and to provide insight into the mechanism of Zn-mediated macrophage clearance.

CHAPTER 4: Characterisation of the cellular targets of zinc toxicity

4.1 Introduction

Metal-protein interactions are important for a variety of biological processes. Metal ions can contribute to the correct folding and structure of proteins or act as a catalytic cofactor for enzymes (Andreini *et al.*, 2006; Andreini *et al.*, 2008). However, while the binding of a metal ion can promote the activity of a protein, the interaction of a metal ion also has the capacity to perturb or inhibit protein function (Foster *et al.*, 2014). The interaction of essential divalent cations with proteins generally follows an order of stabilities, referred to as the Irving-Williams series, [Mg^{2+}/Ca^{2+}<Mn^{2+}<Fe^{2+}<Co^{2+}<Ni^{2+}<Cu^{2+}>Zn^{2+}] (Irving, 1953). Accordingly, metal ions higher in the series have a tendency to outcompete lower order metal ions for the binding sites of proteins. One major strategy used by cells to ensure metal-protein selectivity is by restricting the levels of the higher order metals intracellularly such that the competition between proteins is the main driver of selection, rather than between metal ions (Foster *et al.*, 2014). This is reflected in the relative cellular abundance of these divalent cations, where the cellular abundance is inversely correlated with their relative stability and position in the Irving-Williams series (Lisher & Giedroc, 2013). The levels of intracellular metal ions are coordinated by a series of metal sensors, exporters, importers, and buffering strategies that maintain the relative concentrations of metal ions within a tight range (Reyes-Caballero *et al.*, 2011).

S. pneumoniae is exposed to high concentrations of Zn during disease. During infection, the host modulates the abundance of Zn (Eijkelkamp *et al.*, 2019; McDevitt *et al.*, 2011) and the previous chapter highlighted the contribution of Zn to bacterial clearance via phagocytic cells. Zn is high on the Irving Williams series and has a versatile coordination geometry, which readily permits its competitive interaction with proteins (Laitaoja *et al.*, 2013). The previous chapter showed that Zn treatment increased the cellular Zn in *S. pneumoniae* and that CzcD contributes to protection against Zn intoxication. Although Zn can exert significant stress, the cellular targets of Zn toxicity remain poorly understood. The most well-characterised target of Zn toxicity in *S. pneumoniae* is the Mn uptake SBP, PsaA. Studies have shown that treatment with Zn perturbed growth and reduced the cellular Mn levels of *S. pneumoniae* (Eijkelkamp *et al.*, 2014; McDevitt *et al.*, 2011). Biochemical and structural studies provided a molecular mechanism for the Zn-dependent reduction in Mn levels by demonstrating that Zn irreversibly binds to PsaA, trapping it in a closed conformation, such that acquisition of Mn is prevented (Couñago *et al.*, 2014). However, a key finding of these studies was that while supplementation of Zn-treated cells with equimolar concentrations of Mn rescued growth of *S. pneumoniae*, at

higher concentrations, the growth perturbation could not be recovered by additional Mn supplementation (Eijkelkamp *et al.*, 2014). This indicated that additional cellular pathways, independent of the Mn uptake pathway, were also impacted by Zn.

The previous chapter highlighted that a number of pneumococcal genes are responsive to treatment with excess Zn. In addition to Mn uptake, altered expression was observed for the genes involved in carbon metabolism and competence. While these transcriptional changes provide some insight into the pathways impacted by Zn, transcriptomic analyses alone are insufficient to define the broader consequences of protein mismetallation. The present study aimed to explore the metabolic pathways impacted by Zn to characterise the protein targets of Zn toxicity in *S. pneumoniae.* These studies provide further insight into the impact of Zn on carbohydrate metabolism, and reveal that fatty acid abundance, the pentose phosphate pathway (PPP), and cell wall biosynthesis are also influenced by Zn stress. Together, this study provides a foundation for future mechanistic studies of the putative targets of Zn mismetallation and has the potential to inform the development of new Zn-based therapeutic strategies.

4.2 Results

4.2.1 Global metabolomic responses to zinc stress in *S. pneumoniae*

To investigate the impact of Zn stress on *S. pneumoniae* metabolic pathways, the changes in metabolic profiles following exposure to Zn were assessed. *S. pneumoniae* D39 was grown in C+Y media, with and without supplementation with 100 μM Zn, and the non-polar cellular metabolites were quantitated (Samples prepared by Dr Stephanie Neville and metabolomic studies performed in collaboration with Dr Jason Rosch by Metabolon®). Statistical analysis of the metabolomic data was performed using the online platform MetaboAnalyst (Chong *et al.*, 2018). To assess the sample grouping and variance between the two groups, an unsupervised multivariate Principal Component Analysis (PCA) was performed (Figure 4.1). The PCA model was generated with five principal components (PCs), with a variance of 72.5% for PC1 and 14.1% for PC2. Although the PCA plot revealed that the samples for each treatment group clustered together, one sample in the D39 untreated group displayed deviation from the others. Nevertheless, the lack of overlap between the 95% confidence intervals of the Zn-treated and untreated samples indicate that there is relatively minimal technical variation. Further analysis of the untreated sample displaying some deviation from the other replicate samples revealed that this sample showed approximately 60% reduced total protein concentration compared to the other samples. As a result, this untreated sample and its corresponding Zn-treated sample were omitted to reduce the impact of this anomaly on further studies. A subsequent PCA analysis following exclusion of these data revealed that omitting this sample did not reduce the clustering of these samples into the treatment groups (Appendix 2).

To identify the metabolites displaying significantly altered abundance following Zn treatment, the statistical significance (*P*-value, Two-stage linear step-up procedure of Benjamini, Krieger and Yekutieli) was plotted as a function of the fold-change metabolite abundance in the Zn-treated samples compared to untreated (Figure 4.2). The most significantly altered metabolites included an enrichment in metabolites involved in glycolysis and the PPP, and a decreased abundance of metabolites involved in fatty acid biosynthesis. Metabolites reaching statistical significance ($P < 0.05$) and displaying greater than a 1.5-fold increase or decrease in abundance are shown in Tables 4.1 and 4.2, respectively. Overall, Zn altered the abundance of metabolites from a wide range of pathways in *S. pneumoniae*. By combining the

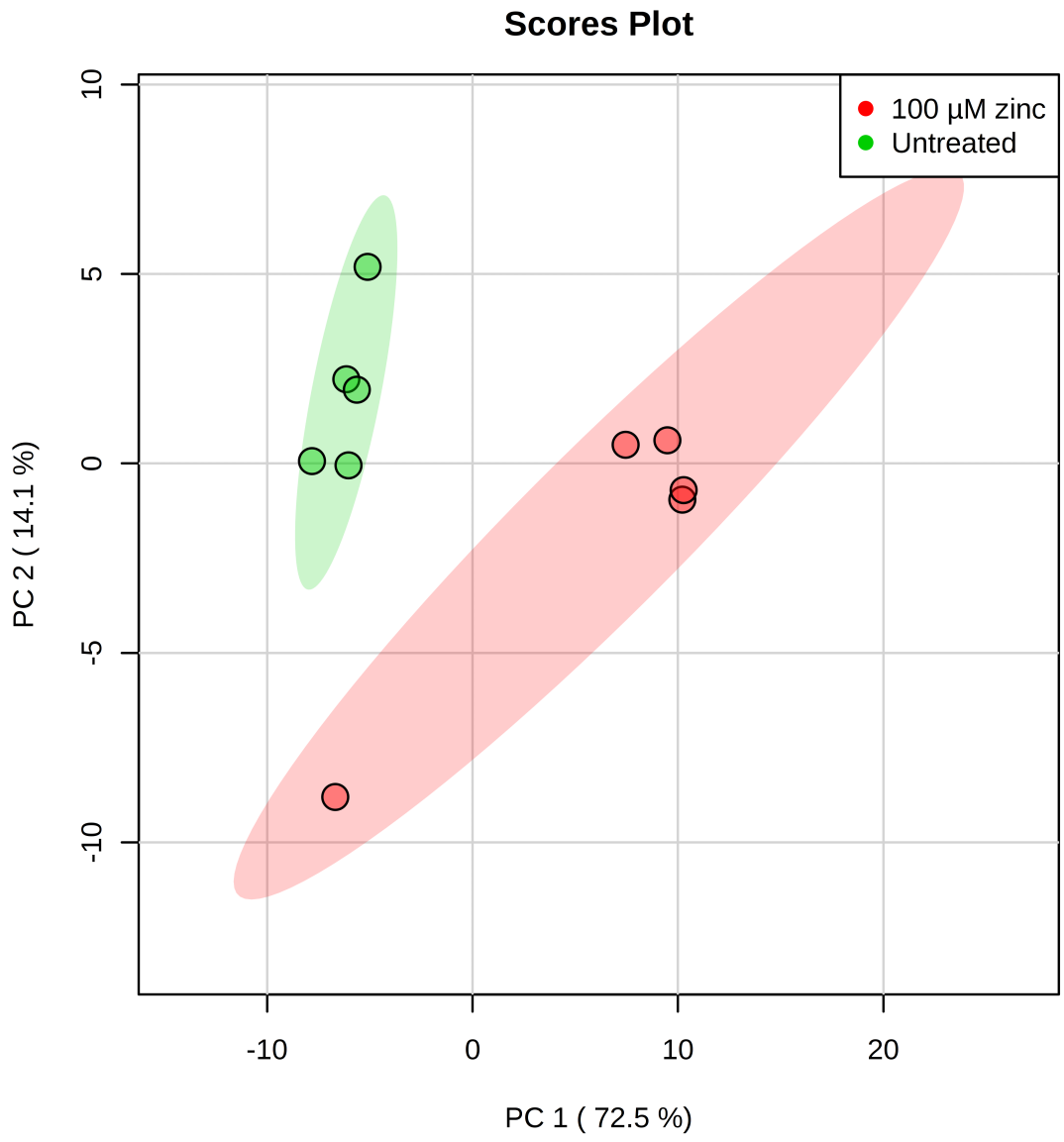


Figure 4.1 Principal component analysis (PCA) score plot of metabolic profiles in *S. pneumoniae* treated with or without zinc

S. pneumoniae were grown to mid-log phase (OD_{600} = 0.30) in the presence or absence of 100 µM $ZnSO_4$. Samples were harvested, the metabolic profile was examined by Metabolon®, and statistical analyses performed using MetaboAnalyst (Chong *et al.*, 2018), n = 5 biological replicates. The clustering of Zn treated samples (red) and untreated samples (green) in the PCA plot indicate significant metabolic differences in *S. pneumoniae* induced by Zn.

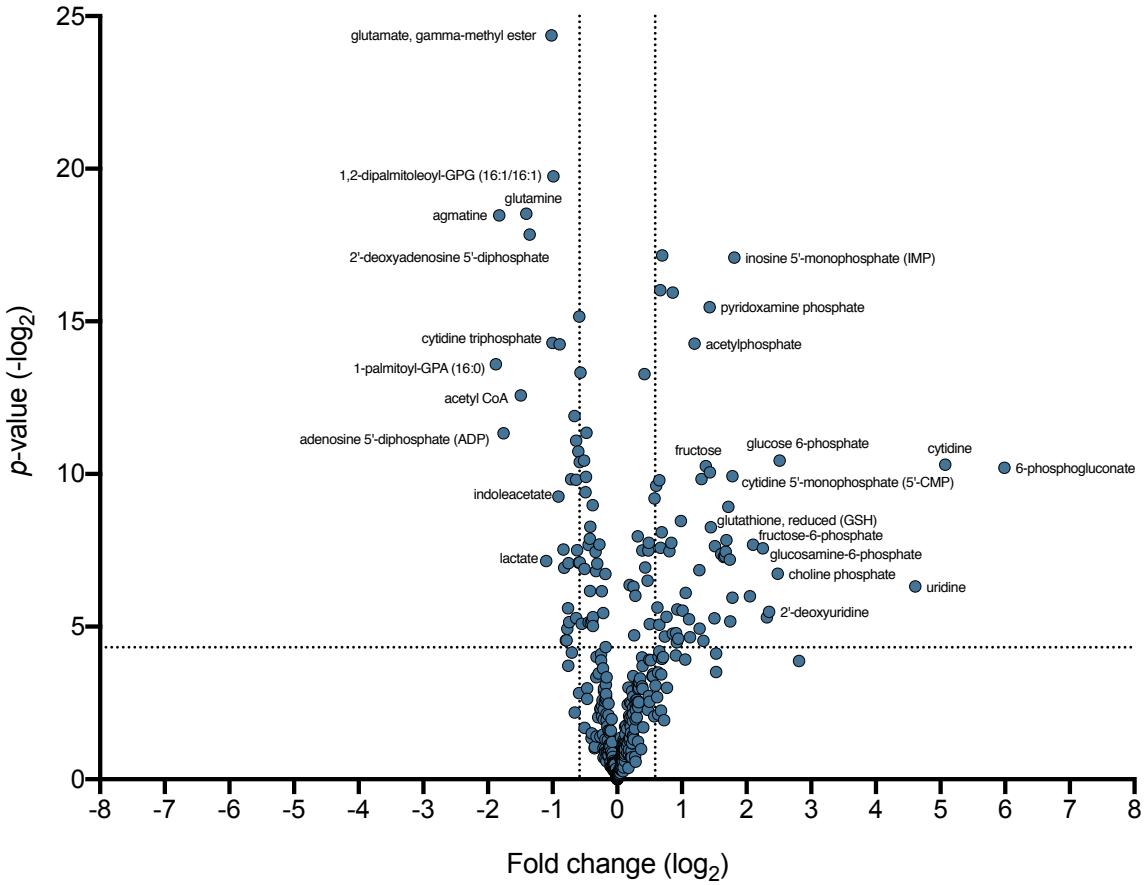


Figure 4.2 Zinc induces significant changes in metabolite abundance in *S. pneumoniae*

S. pneumoniae were grown to mid-log phase (OD_{600} = 0.30) in the presence or absence of 100 µM $ZnSO_4$. Samples were harvested and the metabolic profile relative to protein concentration was determined by Metabolon® n = 4. The fold change (log_2) and relative significance (-log_2 *P*-value) were plotted to highlight the metabolites displaying the most significant increases and decreases in abundance. Each dot represents the average fold change in Zn-treated compared to untreated and *P*-values were determined using the Two-stage linear step-up procedure of Benjamini, Krieger and Yekutieli, with Q = 1% in GraphPad Prism 7. The horizontal dotted line corresponds to a *P*-value of 0.05 and the vertical dotted lines represent -1.5 and 1.5-fold change thresholds. Selected increased and decreased metabolites displaying significant changes are labelled.

Table 4.1 Metabolites with increased abundance in *S. pneumoniae* grown with 100 µM zinc relative to untreated

Biochemical	Sub-pathway	Log_2-Fold Change	*P*-value
Amino acid			
Glutathione, reduced (GSH)	Glutathione metabolism	1.450	0.00327
N-acetylmethionine sulfoxide	Methionine, cysteine, SAM and taurine metabolism	1.330	0.04306
Ophthalmate	Glutathione metabolism	0.860	0.03666
Glutathione, oxidized (GSSG)	Glutathione metabolism	0.740	0.03904
O-methyltyrosine	Phenylalanine and tyrosine metabolism	0.700	6.82E-06
Carbohydrate			
6-phosphogluconate	Pentose phosphate pathway	5.990	0.00085
Glucose 6-phosphate	Glycolysis, gluconeogenesis, and pyruvate metabolism	2.510	0.00072
Glucosamine-6-phosphate	Aminosugar metabolism	2.250	0.00527
Fructose-6-phosphate	Glycolysis, gluconeogenesis, and pyruvate metabolism	2.100	0.00487
Mannose-6-phosphate	Fructose, mannose and galactose metabolism	1.740	0.0068
UDP-glucose	Nucleotide sugar	1.670	0.00635
Galactose 1-phosphate	Fructose, mannose and galactose metabolism	1.610	0.00603
UDP-galactose	Nucleotide sugar	1.510	0.00503
Fructose	Fructose, mannose and galactose metabolism	1.370	0.00081
N6-carboxymethyllysine	Advanced glycation end-product	1.010	0.02175
Erythronate	Aminosugar metabolism	0.920	0.04446

Pyruvate	Glycolysis, gluconeogenesis, and pyruvate metabolism	0.690	0.00367
N-acetylglucosamine/N-acetylgalactosamine	Aminosugar metabolism	0.650	0.00113
Ribose	Pentose metabolism	0.600	0.00128
Trehalose 6-phosphate	Disaccharides and oligosaccharides	0.500	0.02953
Cofactors/vitamins			
Riboflavin (Vitamin B2)	Riboflavin metabolism	1.720	0.00206
Pantothenate	Pantothenate and CoA metabolism	1.650	0.00641
Pyridoxamine phosphate	Vitamin B6 metabolism	1.430	2.21E-05
Xanthopterin	Pterin metabolism	1.130	0.03971
Pterin	Pterin metabolism	0.940	0.04101
Thiamin (Vitamin B1)	Thiamine metabolism	0.930	0.02111
Nicotinate	Nicotinate and nicotinamide metabolism	0.670	0.00522
Energy			
Acetylphosphate	Oxidative phosphorylation	1.190	5.06E-05
Lipid			
Choline phosphate	Phospholipid metabolism	2.480	0.00942
Cytidine 5'-diphosphocholine	Phospholipid metabolism	2.310	0.02531
1,2-dipalmitoyl-GPG (16:0/16:0)	Phospholipid metabolism	1.300	0.00109
Palmitoyl-palmitoyl-glycerol (16:0/16:0)	Diacylglycerol	0.860	1.59E-05
Glycerophosphoglycerol	Glycerolipid metabolism	0.760	0.02504
Arachidate (20:0)	Long chain fatty acid	0.620	0.02028
Stearate (18:0)	Long chain fatty acid	0.580	0.0017
Nucleotide			

Cytidine	Pyrimidine metabolism, cytidine containing	5.070	0.00079
Uridine	Pyrimidine metabolism, uracil containing	4.610	0.01257
2'-deoxyuridine	Pyrimidine metabolism, uracil containing	2.350	0.0223
Xanthosine	Purine metabolism, (hypo)xanthine/inosine containing	2.050	0.01565
Inosine 5'-monophosphate (IMP)	Purine metabolism, (hypo)xanthine/inosine containing	1.810	7.16E-06
Cytidine 5'-monophosphate (5'-CMP)	Pyrimidine metabolism, cytidine containing	1.780	0.00103
Orotate	Pyrimidine metabolism, orotate containing	1.690	0.0044
Uracil	Pyrimidine metabolism, uracil containing	1.680	0.0057
Xanthosine 5'-monophosphate (xmp)	Purine metabolism, (hypo)xanthine/inosine containing	1.500	0.02592
Thymidine	Pyrimidine metabolism, thymine containing	1.430	0.00094
5-methyluridine (ribothymidine)	Pyrimidine metabolism, uracil containing	1.270	0.00867
Xanthine	Purine metabolism, (hypo)xanthine/inosine containing	1.110	0.02639
Adenylosuccinate	Purine metabolism, adenine containing	0.830	0.00467
Uridine 5'-diphosphate (UDP)	Pyrimidine metabolism, uracil containing	0.800	0.00562
Cytosine	Pyrimidine metabolism, cytidine containing	0.660	1.51E-05
Peptide			
Valylglutamine	Dipeptide	1.780	0.01622
Phenylalanylalanine	Dipeptide	1.750	0.02776
Tyrosylglycine	Dipeptide	1.270	0.03262
Gamma-glutamyl-alpha-lysine	Gamma-glutamyl amino acid	0.910	0.03629
Xenobiotics			
Gluconate	Food component/plant	1.060	0.01451
4-hydroxybenzoate	Benzoate metabolism	0.990	0.00283
Homocitrate	Food component/plant	0.650	0.02998

Table 4.2 Metabolites with decreased abundance in *S. pneumoniae* grown with 100 µM zinc relative to untreated

Biochemical	Sub-pathway	Log_2-Fold Change	*P*-value
Amino acid			
Agmatine	Polyamine metabolism	-1.830	2.75E-06
Glutamine	Glutamate metabolism	-1.410	2.65E-06
Glutamate, gamma-methyl ester	Glutamate metabolism	-1.020	4.63E-08
Indoleacetate	Tryptophan metabolism	-0.910	0.00163
Spermidine	Polyamine metabolism	-0.760	0.00741
3-(4-hydroxyphenyl)lactate	Phenylalanine and tyrosine metabolism	-0.740	0.02817
N-acetylglutamine	Glutamate metabolism	-0.640	0.00046
Cystine	Methionine, cysteine, SAM and taurine metabolism	-0.630	0.00111
Phenyllactate (PLA)	Phenylalanine and tyrosine metabolism	-0.600	0.00732
N-acetyl-cadaverine	Lysine metabolism	-0.510	0.00072
Carbohydrate			
Lactate	Glycolysis, gluconeogenesis, and pyruvate metabolism	-1.100	0.00705
Adenosine-5'-diphosphoglucose	Pentose metabolism	-0.760	0.0206
UDP-N-acetylglucosamine	Nucleotide sugar	-0.590	2.73E-05
Cofactors/vitamins			
Nicotinate ribonucleoside	Nicotinate and nicotinamide metabolism	-0.890	5.13E-05
Coenzyme A	Pantothenate and CoA metabolism	-0.790	0.04276
3’-dephospho-acetyl-coenzyme A	Pantothenate and coa metabolism	-0.770	0.03288
Thiamin diphosphate	Thiamine metabolism	-0.570	9.77E-05

Lipid			
1-palmitoyl-GPA (16:0)	Lysolipid	-1.880	8.08E-05
Acetyl CoA	Fatty acid metabolism	-1.490	1.64E-04
1,2-dipalmitoleoyl-GPG (16:1/16:1)	Phospholipid metabolism	-0.990	1.13E-06
Caproate (6:0)	Medium chain fatty acid	-0.800	0.04273
1-myristoyl-2-palmitoleoyl-GPG (14:0/16:1)	Phospholipid metabolism	-0.710	0.0011
Malonate	Fatty acid synthesis	-0.660	0.00026
Palmitoleate (16:1n7)	Long chain fatty acid	-0.640	0.02573
Myristoleate (14:1n5)	Long chain fatty acid	-0.620	0.00552
3-hydroxypalmitate	Fatty acid, monohydroxy	-0.600	0.00059
1-palmitoyl-2-palmitoleoyl-GPG (16:0/16:1)	Phospholipid metabolism	-0.500	0.00843
Nucleotide			
Adenosine 5'-diphosphate (ADP)	Purine metabolism, adenine containing	-1.760	0.00039
2'-deoxyadenosine 5'-diphosphate	Purine metabolism, adenine containing	-1.350	4.25E-06
Cytidine triphosphate	Pyrimidine metabolism, cytidine containing	-1.000	4.99E-05
Methylphosphate	Purine and pyrimidine metabolism	-0.830	0.00542
N6-methyladenosine	Purine metabolism, adenine containing	-0.580	0.00074
Uridine 5'-triphosphate (UTP)	Pyrimidine metabolism, uracil containing	-0.550	0.02925
Peptide			
Lysylleucine	Dipeptide	-0.820	0.00819
Tryptophylglycine	Dipeptide	-0.580	0.00726

transcriptomic data of the previous chapter, the global changes in metabolite and gene expression induced by Zn were mapped to several overlapping metabolic pathways (Figure 4.3). These included the PPP, Leloir, glycolytic, peptidoglycan biosynthesis, capsule biosynthesis, fatty acid biosynthesis and pyruvate metabolic pathways. The genes displaying altered transcription and metabolites with varying abundance were mapped to their corresponding pathways, which revealed several metabolic fluxes induced by Zn and putative protein targets of Zn mismetallation (Figure 4.3). Together, these data suggest that Zn stress may induce changes to the synthesis of nucleotides, aromatic amino acids, NADPH, and the production of energy, cell wall, cell membrane and capsule in *S. pneumoniae*. To elucidate the molecular targets of Zn stress, the metabolic fluxes induced by Zn for a number of pathways were dissected in greater detail. Although the transcriptomic and metabolomic studies were performed following growth in media supplemented with 100 μM Zn, subsequent analyses were performed with 50 μM Zn to enable the inclusion of the Δ*czcD* deletion strain where required. This enabled comparisons between the D39 and Δ*czcD* strain to be performed, which was not possible with 100 μM Zn supplementation due to the significant growth perturbation observed for Δ*czcD* (Figure 3.9).

4.2.2 Zinc disrupts glycolysis in *S. pneumoniae*

The metabolic profile of Zn treatment highlighted distinct changes in the abundance of metabolites associated with carbohydrate metabolism. A heatmap of metabolites related to carbohydrate metabolism was constructed to present the alterations in cellular abundance following exposure to Zn (Figure 4.4). Distinct decreases in the abundance of a number of metabolites were observed upon Zn treatment. These included lactate, adenosine-5'-diphosphate, N-acetylglucosamine-1-phosphate, and UDP-N-acetylglucosamine. Conversely, an increased abundance of metabolites, including N-acetylglucosamine, UDP-glucose, UDP-galactose, glucose-6-phosphate, 6-phosphogluconate, glucosamine-6-phosphate, pyruvate, fructose, glucose, fructose-6-phosphate and galactose-1-phosphate were observed upon Zn treatment. Many of these correspond to metabolites of the glycolytic pathway of *S. pneumoniae.* Notably, the 6.2-fold increase in glucose-6-phosphate (Figure 4.5A; $P < 0.0001$, two-tailed unpaired *t*-test), 4.9-fold increase in fructose-6-phosphate (Figure 4.5B; $P < 0.01$, two-tailed unpaired *t*-test), and the lack of concomitant change in fructose-1,6-bisphosphate abundance

(Figure 4.5C) indicates that this step in the glycolytic pathway may be disrupted by Zn. An overview of the changes in transcription and metabolite abundance in glycolysis are presented in Figure 4.3. The enrichment of glucose-6-phosphate and fructose-6-phosphate indicates that PfkA may be either reduced in expression or inhibited as a result of Zn mismetallation. PfkA is a phosphofructokinase enzyme responsible for the conversion of fructose-6-phosphate to

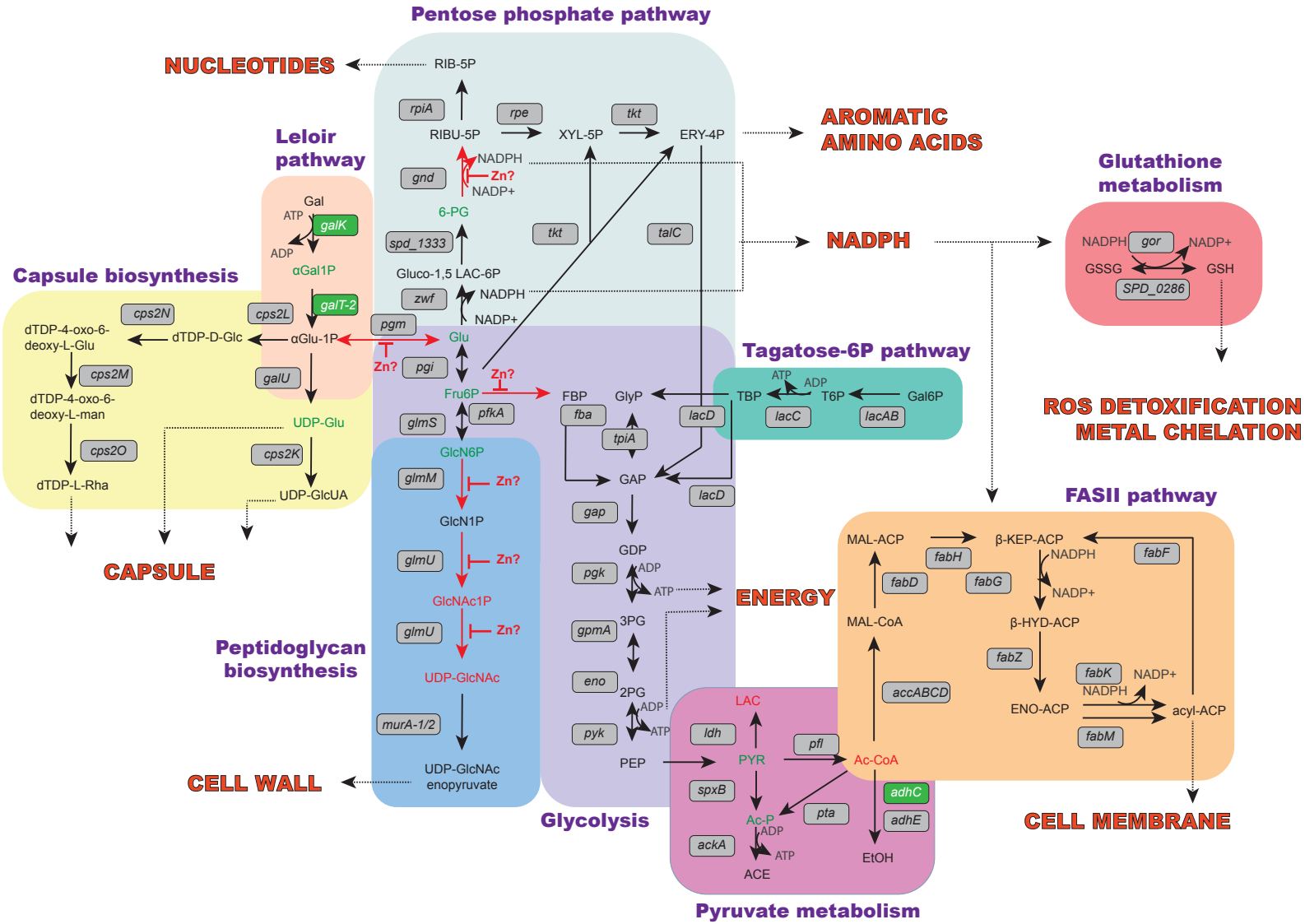

Pentose phosphate pathway
NUCLEOTIDES
RIB-5P
rpiA
rpe
tkt
RIBU-5P
XYL-5P
ERY-4P
AROMATIC AMINO ACIDS
Leloir pathway
NADPH
Zn?
NADP+
gnd
6-PG
Glutathione metabolism
Gal
ATP
galK
ADP
αGal1P
spd_1333
tkt
talC
NADPH
Capsule biosynthesis
Gluco-1,5 LAC-6P
zwf
NADPH
NADP+
NADPH
gor
NADP+
GSSG
GSH
SPD_0286
cps2N
cps2L
galT-2
dTDP-4-oxo-6-deoxy-L-Glu
dTDP-D-Glc
αGlu-1P
pgm
Glu
Zn?
pgi
Zn?
Tagatose-6P pathway
ATP
ADP
TBP
T6P
Gal6P
lacC
lacAB
cps2M
galU
Fru6P
pfkA
FBP
GlyP
fba
lacD
ROS DETOXIFICATION
METAL CHELATION
dTDP-4-oxo-6-deoxy-L-man
UDP-Glu
glmS
tpiA
GAP
cps2O
cps2K
GlcN6P
glmM
Zn?
lacD
FASII pathway
dTDP-L-Rha
UDP-GlcUA
GlcN1P
gap
GDP
MAL-ACP
β-KEP-ACP
fabH
fabF
CAPSULE
glmU
Zn?
pgk
ADP
ATP
fabD
fabG
NADPH
NADP+
GlcNAc1P
ENERGY
MAL-CoA
β-HYD-ACP
glmU
Zn?
gpmA
3PG
fabZ
Peptidoglycan biosynthesis
UDP-GlcNAc
eno
2PG
accABCD
fabK
NADP+
NADPH
ENO-ACP
acyl-ACP
LAC
ADP
ATP
fabM
murA-1/2
ldh
pyk
PEP
pfl
PYR
Ac-CoA
UDP-GlcNAc enopyruvate
CELL WALL
spxB
adhC
pta
adhE
Ac-P
ADP
ackA
ATP
EtOH
ACE
Glycolysis
CELL MEMBRANE
Pyruvate metabolism

Figure 4.3 Overview of the cellular pathways impacted by zinc in *S. pneumoniae*

Metabolic steps depicted with genes (grey boxes) encoding proteins with a putative or characterised role. Metabolites increased in abundance and upregulated genes are shown in red, metabolites decreased in abundance and downregulated genes are shown in green. Putative Zn-inhibited steps are annotated as Zn with red arrows. The proposed pathways were constructed based on information from KEGG and partially adapted from (Carvalho *et al.*, 2011). Genes: *rpiA* (SPD_0723; ribose-5-phosphate isomerase A), *rpe* (SPD_1780; ribulose-phosphate 3-epimerase), *tkt* (SPD_1839; transketolase), *gnd* (SPD_0343; 6-phosphoglyconate dehydrogenase), *spd_1333* (SPD_1333; 6-phosphoglyconolactonase), *zwf* (SPD_1100; glucose-6-phosphate1-dehydrogenase), *pgm* (SPD_1326); phosphoglucomutase), *galK* (SPD_1634; galactokinase), *galT-2* (SPD_1633; galactose-1-phosphate uridyltransferase), *galU* (SPD_1919; UTP-glucose-1-phosphate uridyltransferase), *cps2K* (SPD_0326; UDP-glucose-6-dehydrogenase), *cps2L* (SPD_0328; glucose-1-phosphate thymidylyltransferase), *cps2N* (SPD_0330; dTDP-glucose 4,6-dehydratase) *cps2M* (SPD_0329; dTDP-4-dehydrorhamnaose 3,5-epimerase), *cps2O* (SPD_0331; dTDP-4-dehydrorhamnaose reductase), *pgi* (SPD_1897; glucose-6-phosphate isomerase), *glmS* (SPD_0248; glutamine-fructose-6-phosphate transaminase), *glmM* (SPD_1390; phosphoglucosamine mutase), *glmU* (SPD_0874; bifunctional UDP-N-acetylglucosamine phosphorylase/glucosamine-1-phosphate N-acetyltransferase), *murA-1* (SPD_0967; UDP-N-acetylglucosamine 1-carboxyvinyltransferase), *murA-2* (SPD_1764; UDP-N-acetylglucosamine 1-carboxyvinyltransferase), *pfkA* (SPD_0789; ATP-dependent 6-phosphofructokinase), *fba* (SPD_0526; fructose 1,6-bisphosphate aldolase), *lacA* (SPD_1053; galactose-6-phosphate isomerase subunit), *lacB* (SPD_1052; galactose-6-phosphate isomerase subunit), *lacC* (SPD_1051; tagatose-6-phosphate kinase), *lacD* (SPD_1050; tagatose 1,6 -diphosphate aldolase), *tpiA* (SPD_1404; triosephosphate isomerase), *gap* (SPD_1823; glyceraldehyde-3-phosphate dehydrogenase), *pgk* (SPD_0445; phosphoglycerate kinase), *gpmA* (SPD_1468; 2,3-bisphosphoglycerate-dependent phosphoglycerate mutase), *eno* (SPD_1012; enolase), *pyk* (SPD_0790; pyruvate kinase), *ldh* (SPD_1078; lactate dehydrogenase), spxB (SPD_0636; pyruvate oxidase), *ackA* (SPD_1853; acetate kinase), *pta* (SPD_0985; phosphate acetyltransferase), *pfl* (SPD_0235; pyruvate formate-lyase), *adhC* (SPD_1636; alcohol

dehydrogenase, Zn-containing), *adhE* (SPD_1834; alcohol dehydrogenase, iron-containing), *accA* (SPD_0390; acetyl-coenzyme carboxylase carboxyl transferase subunit), *accB* (SPD_0386; acetyl-CoA carboxylase), *accC* (SPD_0388; acetyl-CoA carboxylase), *accD* (SPD_0389; acetyl-coenzyme carboxylase carboxyl transferase subunit), *fabD* (SPD_0383; malonyl CoA-acyl carrier protein transacylase), *fabH* (SPD_0380; 3-oxoacyl-acyl carrier protein synthase), *fabG* (SPD_0384; 3-oxoacyl-acyl carrier protein reductase), *fabZ* (SPD_0387; 3-hydroxyacyl-acyl carrier proteindehydratase), *fabK* (SPD_0382; trans-2-enoyl-acyl carrier protein reductase), *fabM* (SPD_0378; enoyl-coA hydratase/isomerase), *fabF* (SPD_0385; 3-oxoacyl-acyl carrier protein synthase). Intermediates: Gal, galactose; αGal1P, alpha-D-Galactose 1-phosphate; G1P, glucose 1-phosphate; UDP-G, UDP-glucose; UDP-GlucU, UDP-glucuronate, dTDP-D-Glu, dTDP-D-glucose; dTDP-4-oxo-6-deoxy-L-Glu, dTDP-4-oxo-6-deoxy-L-Glucose; dTDP-L-Rha, dTDP-L-rhamnose; RIB5P, ribose-5-phosphate; RIBU5P, ribulose-5-phosphate; XYL5P, xylulose-5-phosphate; Ery4P, erythrose-4-phosphate; 6PG, 6-phosphogluconate; Gluco-1,5-Lac-6P, glucono-1,5-lactone-6-phosphate; Glu6P, Glucose-6-phosphate; Fru6P, fructose-6-phosphate; GlcN6P, glucosamine-6-phosphate; GlcN1P, glucosamine-1-phosphate; GlcNAc1P, N-acetylglucosamine-1-phosphate; UDP-GlcNAc, UDP-N-acetylglucosamine; UDP-GlcNAc EnoP, UDP-N-acetylglucosamine enoylpyruvate; FBP, fructose 1,6-bisphosphate; GlyP, glycerine phosphate; Gal6P, galactose-6-phosphate; T6P, tagatose-6-phosphate; TBP, tagatose 1, 6-bisphosphate; GAP, glyceraldehyde-3-phosphate; GDP, glyceraldehyde 1,3-diphosphate; 3PG, 3-phosphoglycerate; 2PG, 2-phosphoglycerate; PEP, phosphoenolpyruvate; PYR, pyruvate; LAC, lactate; Ac-P, acetyl phosphate; ACE, acetate; etOH, ethanol; Ac-CoA, acetyl-CoA; MAL-coA, malonyl-coA; MAP-ACP, malonyl acyl carrier protein; β-KET-ACP, β-ketoacyl-acyl carrier protein; ENO-ACP, trans-2-enoyl-acyl carrier protein; acyl-ACP, acyl-acyl carrier protein.

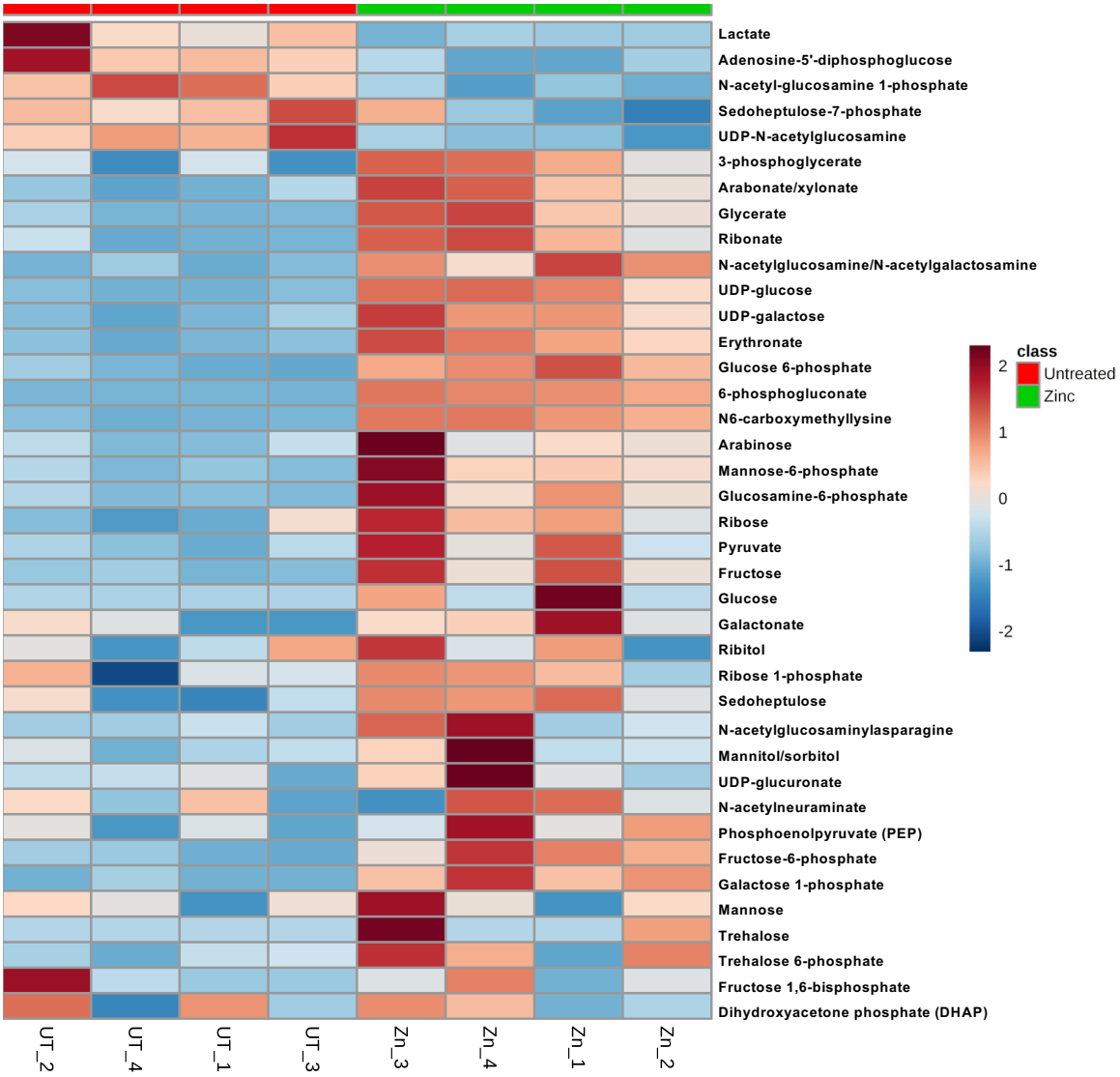


Figure 4.4 Changes in carbohydrate abundance in *S. pneumoniae* induced by zinc

S. pneumoniae were grown to mid-log phase (OD_{600} = 0.30) in the presence or absence of 100 µM $ZnSO_4$. Samples were harvested and the metabolic profile was examined by Metabolon®. A heatmap was generated by analysis of the normalised abundance of carbohydrate metabolites using MetaboAnalyst 4.0 (Chong *et al.*, 2018). Each row represents a metabolite and each column represents a sample. The scaled expression value of each sample metabolite is plotted in red-blue colour scale, where the red colour of the tile represents high abundance and blue indicates low abundance, n = 4.

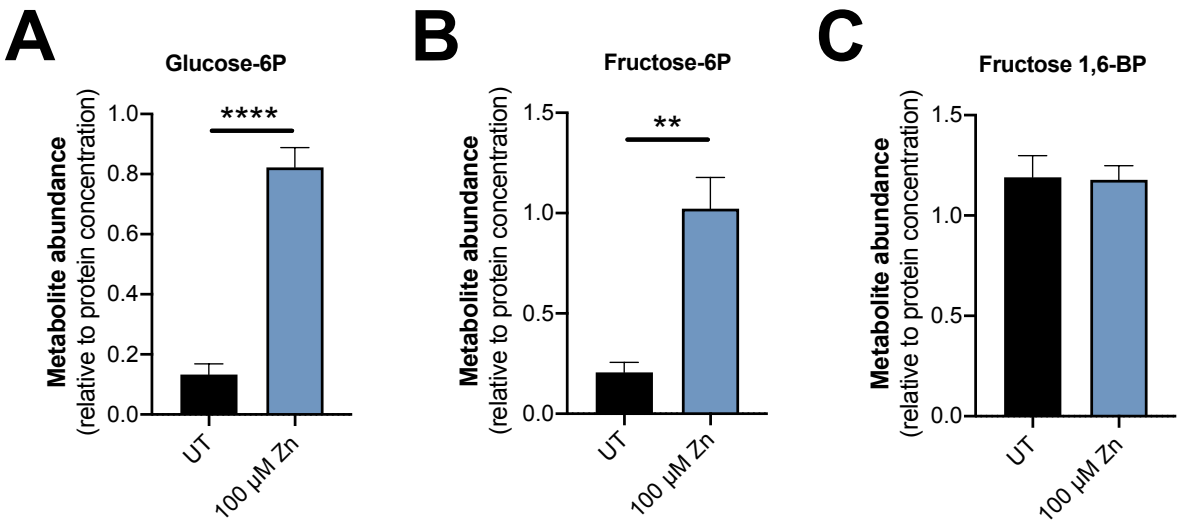


Figure 4.5 Zinc alters the abundance of metabolites in the glycolytic pathway

S. pneumoniae were grown to mid-log phase (OD_{600} = 0.30) in the presence or absence of 100 µM $ZnSO_4$. Samples were harvested, the metabolic profile was examined by Metabolon®. Data are the mean + SEM, n = 4, of the median-adjusted abundance of (A) glucose-6-phosphate, (B) fructose-6-phosphate and (C) fructose 1,6-bisphosphate relative to sample protein concentration. Statistical significance was assessed using the Student's two-tailed unpaired *t*-test, where ** represents $P < 0.01$, and **** represents $P < 0.0001$.

fructose 1,6, bisphosphate. Previous studies of the closely related bacterium *S. pyogenes* have shown that Zn treatment reduces the transcription of the glycolytic genes, including the *pfkA* homologous gene, *pfk*, which encodes a phosphofructokinase (Ong *et al.*, 2015). Although the transcriptomic data did not indicate an alteration in the expression of the glycolytic genes, further targeted analyses were performed to examine whether Zn induced significant changes in the transcription of these genes. In corroboration with the transcriptomic data of the previous chapter, treatment of *S. pneumoniae* with Zn did not significantly alter the transcription of the glycolyic genes, *gki, pfkA, fba, gap, pgk, gpmA, eno* and *pgm* (Figure 4.6). However, the changes in metabolite abundance may be explained by a Zn-dependent decrease in PfkA protein abundance or an inhibition in protein function. A study in *S. pyogenes* found that PFK activity is impaired following treatment with Zn (Ong *et al.*, 2015). Therefore, it is possible that an interaction of Zn with PfkA may inhibit enzymatic activity, leading to the accumulation of glucose-6-phosphate and fructose-6-phosphate. A primary sequence alignment of PfkA from these closely related bacteria (Figure 4.7) revealed a high degree of homology between these proteins (79% identity, 89% similarity), which indicates that Zn may disrupt *S. pneumoniae* PfkA in a similar manner. Based on these findings, *S. pneumoniae* phosphofructokinase (PFK) activity was assessed in the presence and absence of Zn. *S. pneumoniae* D39 was grown in C+Y media and mechanically lysed. Following incubation with either 0, 100, or 200 μM Zn, the PFK activity was assessed (Figure 4.8A). Treatment with 100 μM Zn did not alter *S. pneumoniae* PFK activity. However, treatment with 200 μM Zn induced a significant 20% reduction in PFK activity (Figure 4.8B; $P < 0.05$, two-tailed unpaired *t*-test). These data show that Zn can impair PfkA activity in *S. pneumoniae,* which may impede energy production via the glycolytic pathway.

4.2.3 Zinc upregulates the galactose utilisation Leloir pathway

Studies of *S. pyogenes* indicate that the Zn-dependent defect in glycolysis may be circumvented by the utilisation of galactose via the T6P pathway (Ong *et al.*, 2015). In addition to the T6P pathway, *S. pneumoniae* can also metabolise galactose via the Leloir pathway.

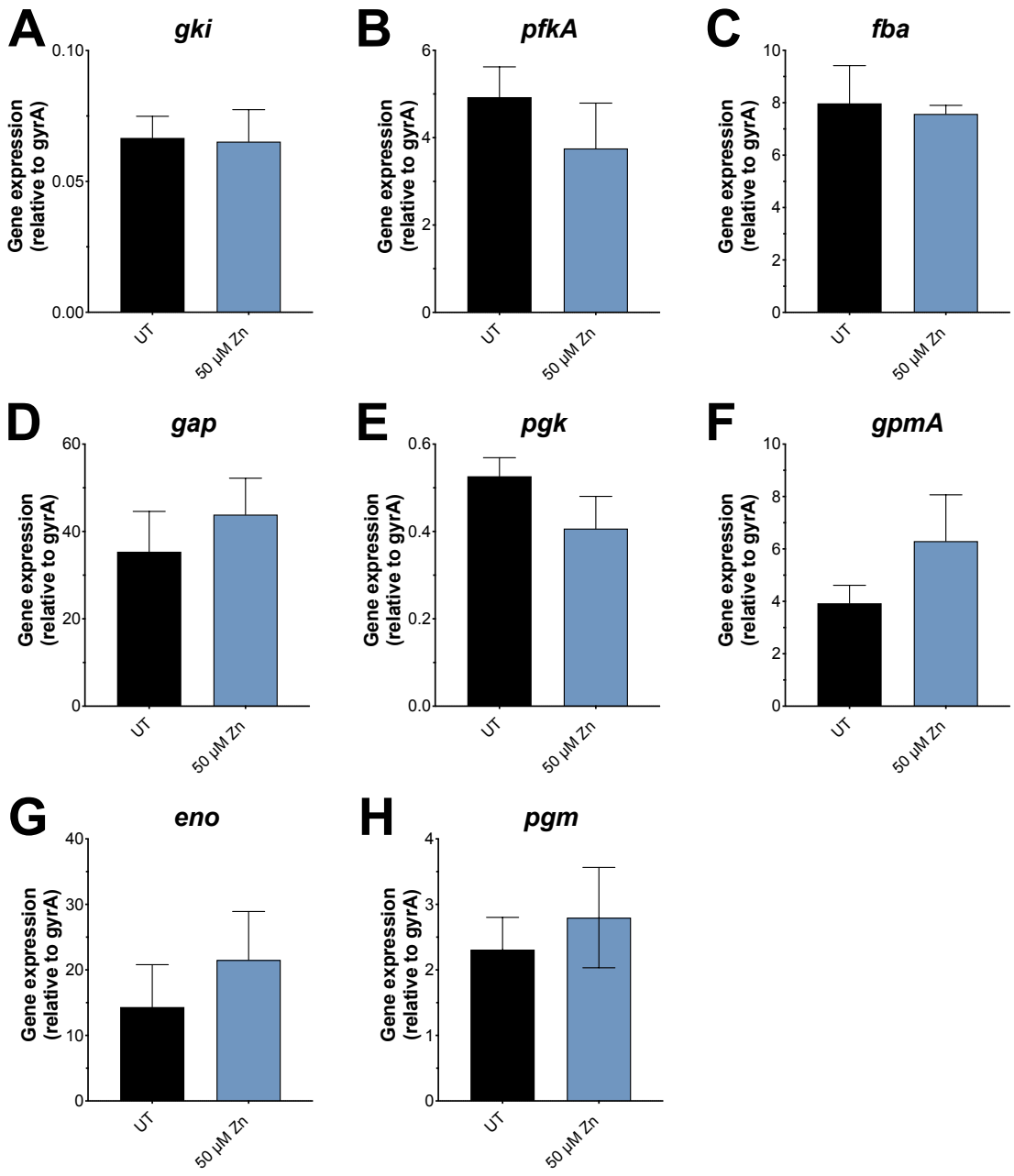


Figure 4.6 Transcription of *S. pneumoniae* glycolytic genes in the presence of zinc

S. pneumoniae were grown to mid-log phase (OD_{600} = 0.30) in the presence or absence of 50 µM $ZnSO_4$. Cells were harvested, RNA was extracted, and the transcription of genes in the glycolytic pathway were examined by qRT-PCR. The transcription of (A) *gki* (SPD_0580), (B) *pfkA* (SPD_0789), (C) *fba* (SPD_0526), (D) *gap* (SPD_1823), (E) *pgk* (SPD_0445), (F) *gpmA* (SPD_1468), (G) *eno* (SPD_1012), and (H) *pgm* (SPD_1326) were determined and expressed relative to the transcription of the *gyrA* (SPD_1077) internal control. Data are the mean ± SEM, n = 3. Statistical significance was assessed using the Student's two-tailed unpaired *t*-test.

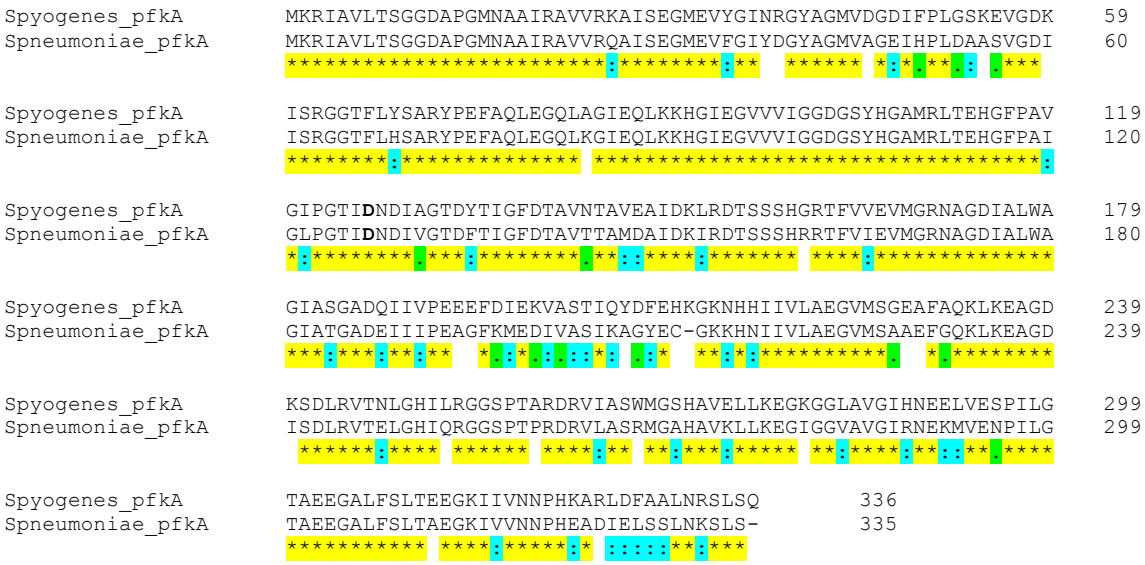


Figure 4.7 Amino acid sequence alignment of PfkA from *S. pneumoniae* and *S. pyogenes*

Amino acid sequences of *S. pneumoniae* PfkA (SPD_0789; GI: 122278840) and *S. pyogenes* PfkA (GI: 1019981227) were obtained from NCBI and aligned using Clustal Omega (Sievers *et al.*, 2011). Yellow shading denotes fully conserved residue (*), blue shading denotes conservation between groups of strongly similar properties (:), and green shading denotes conservation between groups of weakly similar properties (.).

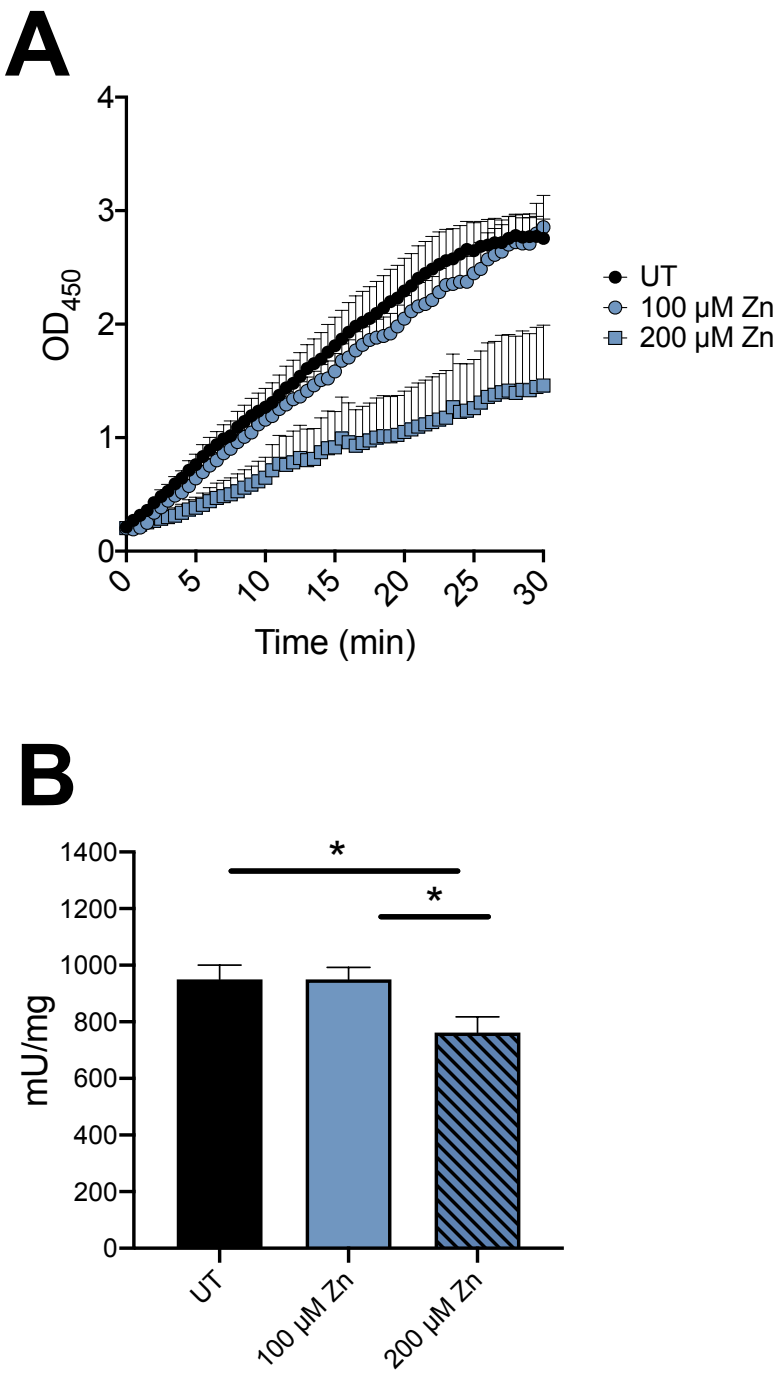


Figure 4.8 Zinc decreases *S. pneumoniae* phosphofructokinase activity

S. pneumoniae were grown to mid-log phase (OD_{600} = 0.30) and cell lysates were incubated with 0, 100 or 200 µM $ZnSO_4$ for 10 min prior to assessing the phosphofructokinase (PFK) activity by a colorimetric assay. The data are the mean + SEM NADH production over time (A), and the derived mean + SEM interpolated PFK activity based on a NADH standard curve, where one unit of PFK is the amount of enzyme that generates 1.0 µmol of NADH per min (B). Data are from n ≥ 4 biological replicates. Statistical significance was assessed using the Student's two-tailed unpaired *t*-test where * represents $P < 0.05$.

The transcriptomic analyses of the previous chapter revealed that Zn induced an upregulation of the genes involved in the Leloir galactose metabolism pathway but, contrary to *S. pyogenes,* showed no alteration to the T6P galactose metabolic genes. To assess whether the expression levels of these genes were significantly altered following exposure to Zn, targeted transcriptional analyses were performed. Consistent with the transcriptomic analyses, treatment with Zn significantly upregulated the transcription of *galK* by 13-fold ($P < 0.05$, two-tailed unpaired *t*-test) and *galT-2* by 7-fold ($P < 0.0001$, two-tailed unpaired *t*-test) compared to untreated, while *galM, lacA, lacC* and *lacD* transcription remained unchanged (Figure 4.9). Based on these data, it was hypothesised that although glucose was the primary carbon source in the medium, Zn induced a shift towards the metabolism of galactose. Thus, the impact of Zn supplementation on the growth of *S. pneumoniae* D39 when glucose or galactose are the dominant carbon source was examined further. When glucose was the dominant carbon source, the addition of 50 μM Zn did not significantly alter the growth kinetics. However, growth with 100 μM Zn showed a reduction in maximal growth yield (OD_{600} ~0.15 compared with ~0.20) and a reduced growth rate during logarithmic phase (Figure 4.10A and Appendix 3). In contrast, when galactose was the primary carbon source, no significant changes in the growth rate were observed (Figure 4.10B and Appendix 3). However, *S. pneumoniae* supplemented with 50 μM and 100 μM Zn showed in an increase in maximal absorbance values (OD_{600} ~0.25 and ~0.20, respectively) compared to untreated (OD_{600} ~0.15) [Figure 4.10B]. Collectively, these data suggest that Zn promotes the growth of *S. pneumoniae* when galactose is the primary carbon source but impairs growth when glucose is the dominant carbon source.

The results of the transcriptional and growth studies indicate that Zn treatment favours the utilisation of galactose via the Leloir pathway. However, the mechanism behind the Zn-dependent shift in carbon metabolism genes is unknown. In *S. pneumoniae*, the transcription of the genes associated with carbon metabolism can be regulated by carbon catabolite protein A (CcpA), which controls the expression of 19% of the *S. pneumoniae* genome by binding to the catabolite response elements to either repress or activate transcription (Carvalho *et al.*, 2011). As a result, the contribution of CcpA to the Zn-dependent upregulation in the Leloir pathway genes was assessed. An isogenic deletion strain of *ccpA* was generated in the *S. pneumoniae* D39 strain, by replacing the *ccpA* gene with a kanamycin resistance cassette. Following transformation, this region was amplified by PCR from the *S. pneumoniae* D39 wild-type strain and four putative Δ*ccpA* clones. The successful generation of the *S. pneumoniae* D39 Δ*ccpA*

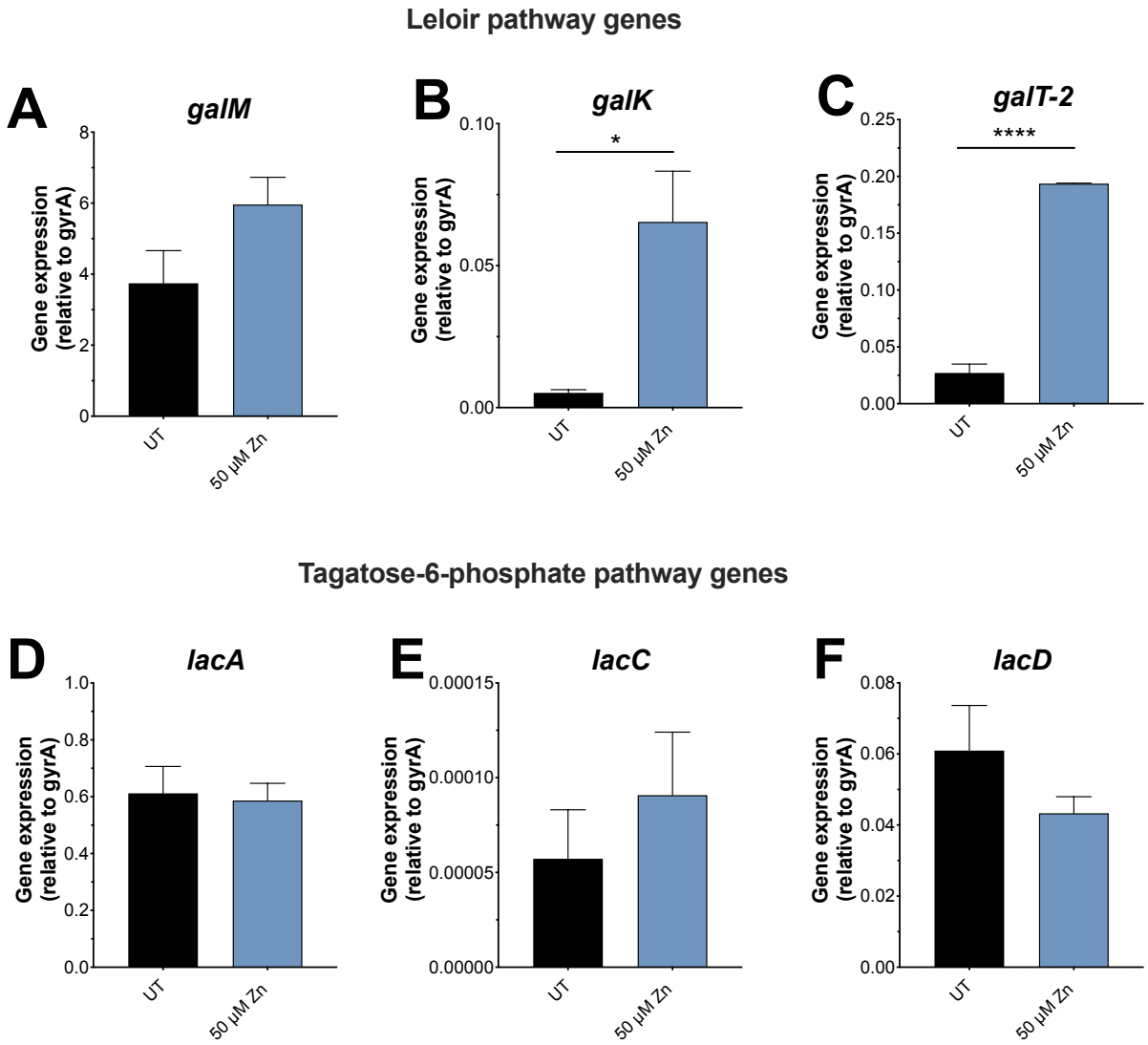


Figure 4.9 Transcription of *S. pneumoniae* galactose utilisation genes in the presence of zinc

S. pneumoniae were grown to mid-log phase (OD_{600} = 0.30) in C+Y medium or C+Y medium supplemented with 50 µM $ZnSO_4$. Cells were harvested, RNA extracted, and the transcription of genes in the Leloir and tagatose-6-phosphate pathways examined by qRT-PCR. The transcription of (A) *galM* (SPD_0071), (B) *galK* (SPD_1634), (C) *galT-2* (SPD_1633), (D) *lacA* (SPD_1053), (E) *lacC* (SPD_1051) and (F) *lacD* (SPD_1050) were determined and expressed relative to the transcription of the *gyrA* (SPD_1077) internal control. Data are the mean + SEM, n = 3 biological replicates. Statistical significance was assessed using the Student's two-tailed unpaired *t*-test, where * represents $P < 0.05$ and **** represents $P < 0.0001$.

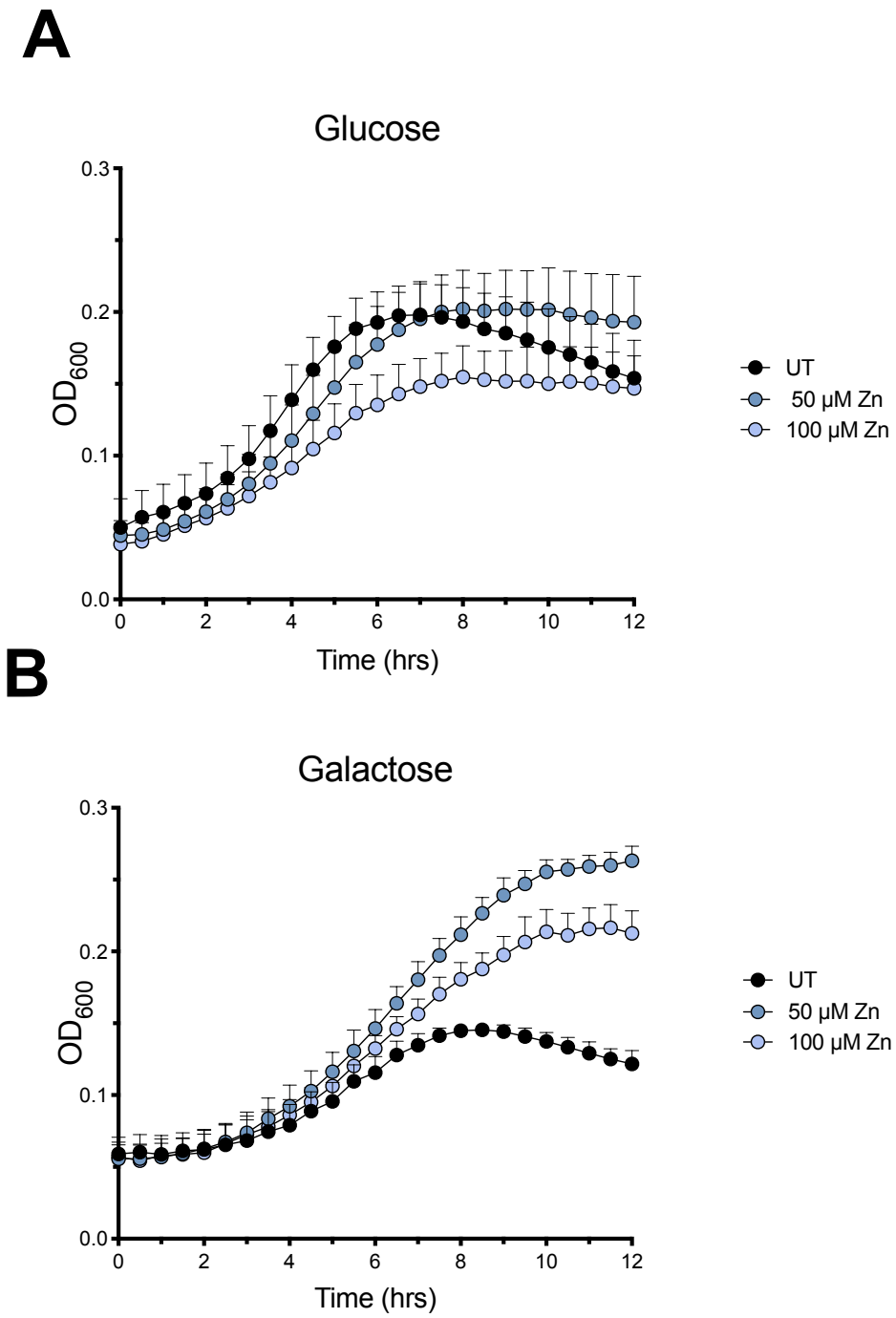


Figure 4.10 Carbon source influences growth kinetics of *S. pneumoniae* treated with zinc

S. pneumoniae from overnight blood agar plates were used to inoculate (A) glucose-free C+Y medium supplemented with 0.2% (w/v) glucose, with or without 50 or 100 µM $ZnSO_4$ supplementation, or (B) glucose-free C+Y medium supplemented with 0.2% (w/v) galactose, with or without 50 or 100 µM $ZnSO_4$. Growth was monitored by readings of the optical density at 600 nm (OD_{600}) every 30 mins. The data are the mean absorbance + SEM, n = 3 biological replicates.

strain was confirmed based on amplicon size (Figure 4.11) and Sanger sequencing. All clones tested displayed the correct insertion of the kanamycin resistance cassette in the *ccpA* gene. As a result, subsequent analyses were performed with clone 1. Analysis of the growth of this strain in C+Y media revealed that the Δ*ccpA* strain showed reduced growth compared to the wild-type strain (Figure 4.12). Due to the reduced growth of the Δ*ccpA* mutant, the transcriptional analyses of the wild-type and Δ*ccpA* mutant were performed at a lower cell density (OD_{600} = 0.15) to mitigate the impact of altered growth time on the Leloir gene transcription. The transcription of the Leloir pathway genes was assessed in the *S. pneumoniae* D39 and Δ*ccpA* strains following growth in C+Y glucose media in the presence and absence of 50 μM Zn. Treatment of the *S. pneumoniae* D39 wild-type strain with Zn induced a significant increase in the transcription of *galK* and *galT-2* (Figure 4.13A-B; $P < 0.01$, two-tailed unpaired *t*-test). Following growth in un-supplemented media, the Δ*ccpA* mutant displayed significantly increased *galK* and *galT-2* transcription compared to wild-type (Figure 4.13A-B; $P < 0.001$, two-tailed unpaired *t*-test). This indicates that *ccpA* contributes to the repression of the Leloir pathway genes during growth in the presence of glucose. Interestingly, treatment of the Δ*ccpA* mutant with Zn induced a further significant increase in the transcription of *galK* and *galT-2* (Figure 4.13A-B; $P < 0.05$, two-tailed unpaired *t*-test). Taken together, these data show that the upregulation of the *galK* and *galT-2* genes in response to Zn occurs independently of CcpA.

The Leloir pathway feeds directly into the capsule biosynthesis pathway due to the production of the key capsule precursor, UDP-glucose. In a previous study, the upregulation of the Leloir pathway in *S. pneumoniae* has been shown to increase capsule production and induce a hypervirulent phenotype (Trappetti *et al.*, 2017). Here, the metabolomics results revealed that levels of UDP-glucose were enriched in Zn-treated cells (Figure 4.14; $P < 0.001$, two-tailed unpaired *t*-test). Taken together, these data indicate the Zn-dependent shift in carbon metabolism may also increase capsule production. As a result, the levels of capsule in Zn-treated *S. pneumoniae* were explored, following growth with glucose or galactose as the dominant carbon source. Surprisingly, despite the increase in UDP-glucose when glucose was the primary carbon source, *S. pneumoniae* treated with Zn displayed a significant 50% reduction in total capsule, compared with untreated (Figure 4.15; $P < 0.05$, two-tailed unpaired *t*-test). However, when galactose was the primary carbon source, capsule production was unaltered by Zn treatment (Figure 4.15). Thus, Zn treatment when glucose is dominant reduces total capsule production, but this change is negated when galactose is the dominant carbon source.

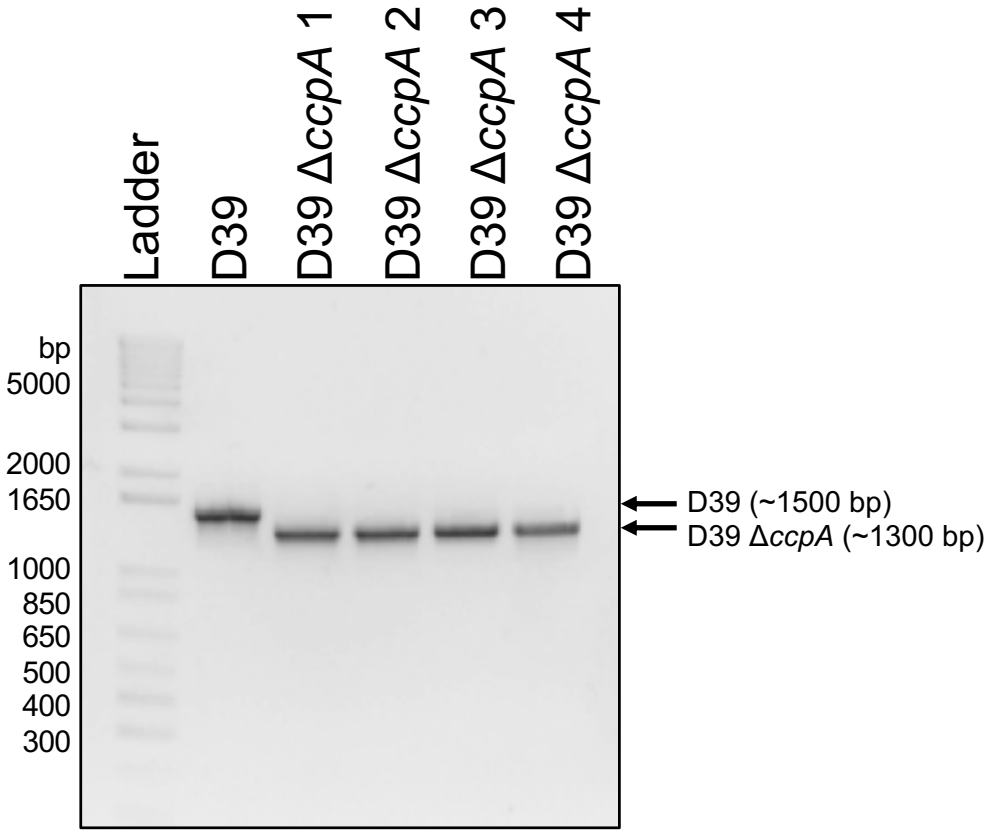


Figure 4.11 Confirmation of *S. pneumoniae ccpA* mutagenesis

Agarose gel of polymerase chain reaction amplification of D39 wild-type (1507 bp) *ccpA* or four D39 Δ*ccpA* clones following replacement with a kanamycin resistance cassette (1291 bp), with 200 bp upstream and downstream flanking regions. The 1 kb Plus DNA ladder was used to approximate the size of the PCR products.

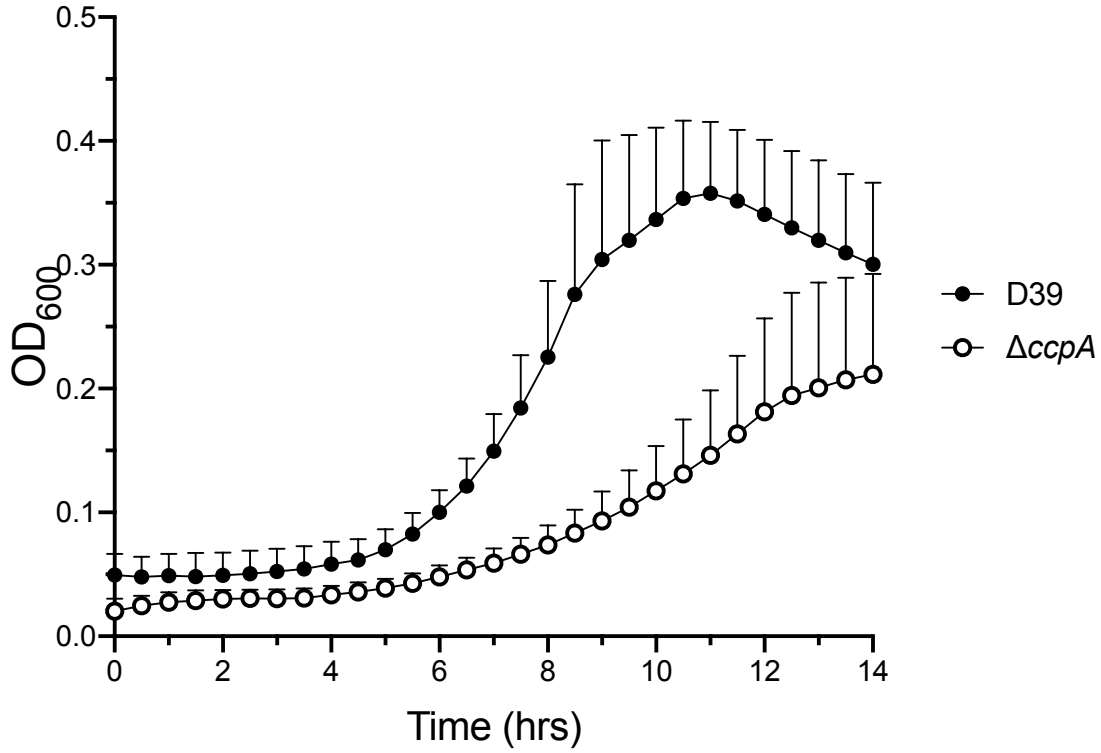


Figure 4.12 Growth kinetics of the *S. pneumoniae* D39 wild-type and Δ*ccpA* strains

S. pneumoniae D39 wild-type and Δ*ccpA* from overnight blood-agar plates were inoculated into C+Y media at OD_{600} = 0.05. Growth was monitored by readings of the optical density at 600 nm (OD_{600}) every 30 mins. Data are the mean + SEM n = 3 biological replicates.

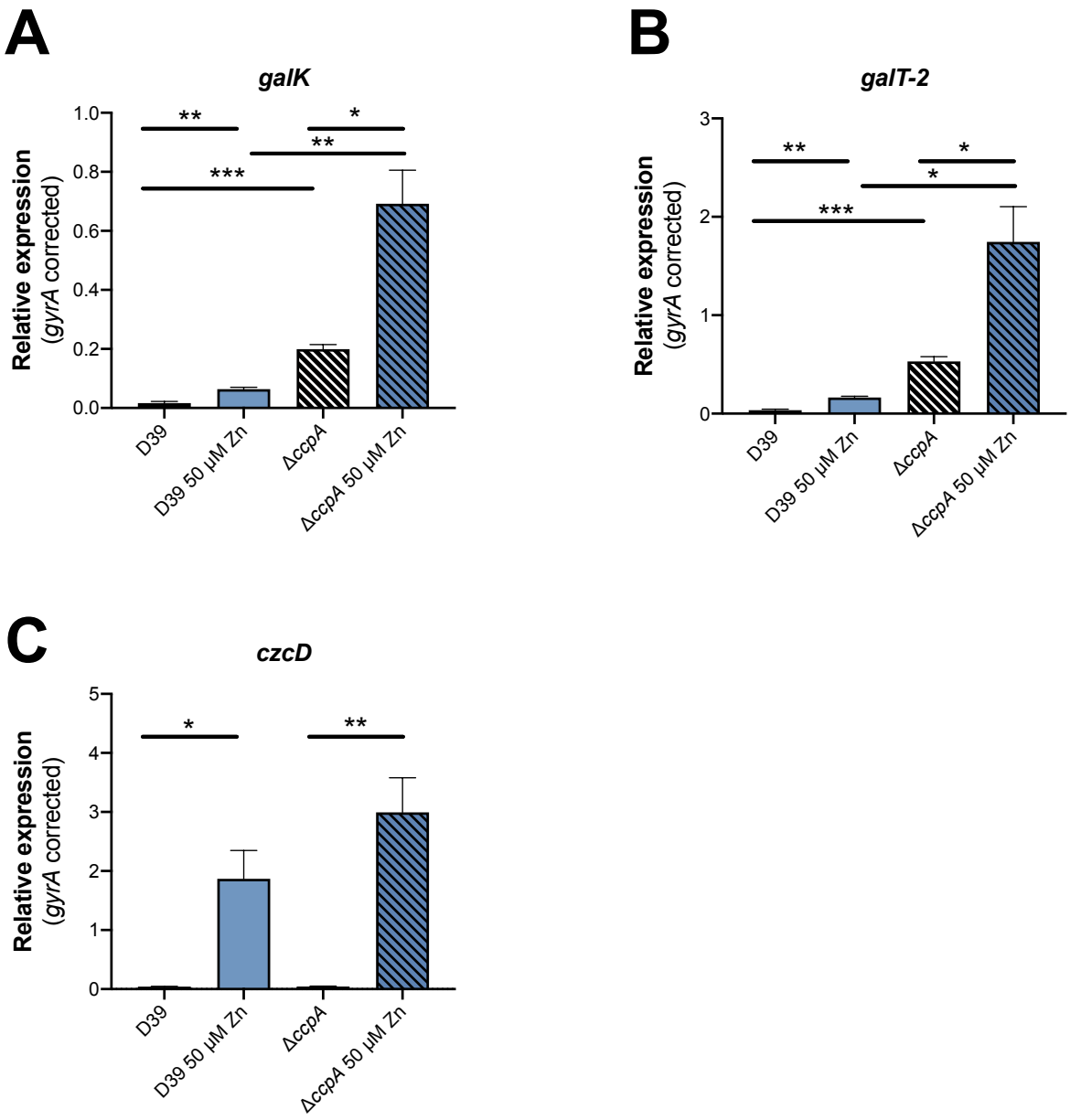


Figure 4.13 Transcription of galactose utilisation genes in the presence of zinc in *S. pneumoniae* D39 and Δ*ccpA*

S. pneumoniae were grown to mid-log phase (OD_{600} = 0.15) in C+Y media with or without supplementation with 50 µM $ZnSO_4$. Cells were harvested, RNA extracted, and the transcription of genes in the Leloir and Zn efflux pathway examined by qRT-PCR. Transcription of (A) *galK* (SPD_1634), (B) *galT-2* (SPD_1633), (C) *czcD* (SPD_1638) were determined and expressed relative to the transcription of the *gyrA* (SPD_1077) internal control. Data are the mean + SEM, n > 3 biological replicates. Statistical significance was assessed using the Student's two-tailed unpaired *t*-test, where * represents $P < 0.05$ ** represents $P < 0.01$, *** represents $P < 0.001$, and **** represents $P < 0.0001$.

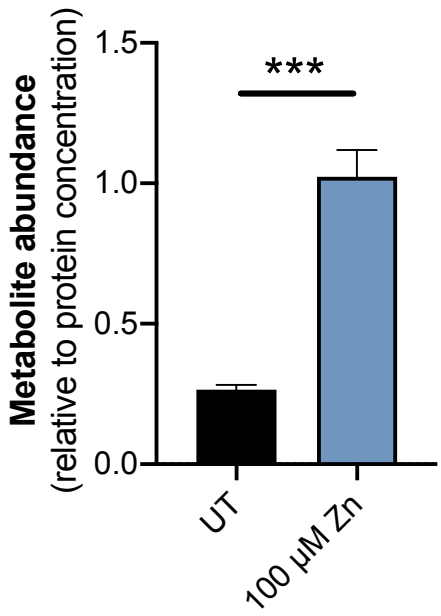


Figure 4.14 Zinc treatment increases the abundance of UDP-glucose in *S. pneumoniae*

S. pneumoniae were grown to mid-log phase (OD_{600} = 0.30) in the presence or absence of 100 µM $ZnSO_4$. Samples were harvested, the metabolic profile was examined by Metabolon®. Data are the mean + SEM, n = 4 biological replicates, of the median-adjusted abundance of 6-phosphogluconate relative to protein concentration. Statistical significance was assessed using the Student's two-tailed unpaired *t*-test, where *** represents $P < 0.001$.

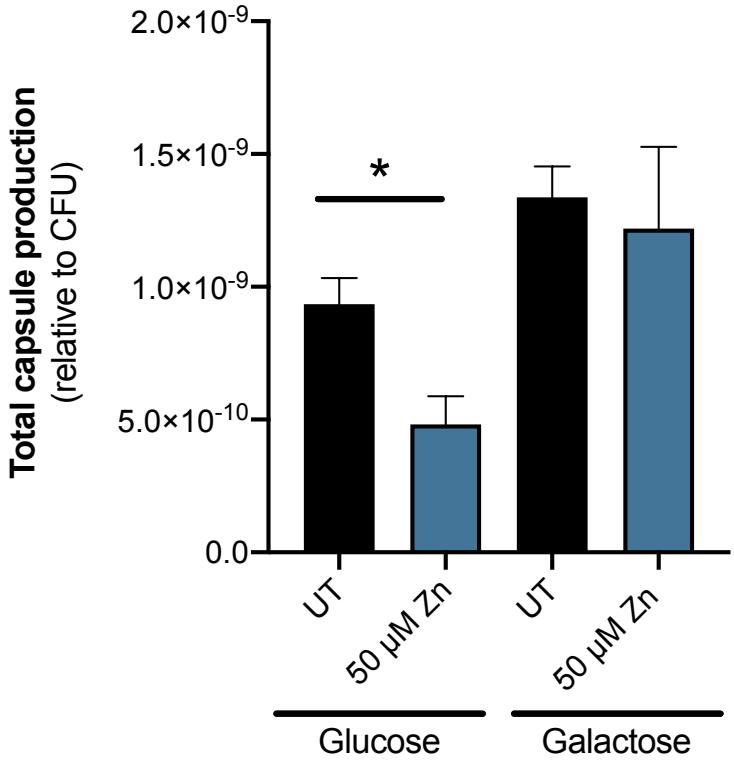


Figure 4.15 Zinc reduces *S. pneumoniae* total capsule production when glucose is dominant carbon source

S. pneumoniae were grown in glucose-free C+Y supplemented with 0.2% (w/v) glucose or 0.2% (w/v) galactose, with or without 50 µM $ZnSO_4$ supplementation. Total capsular polysaccharide production was determined by quantitation of uronic acid. Data are the mean + SEM capsule production relative to colony forming units (CFU), n = 3 biological replicates. Statistical significance was assessed using the Student's two-tailed unpaired *t*-test, where * represents $P < 0.05$.

4.2.4 Zinc alters the pentose phosphate pathway

The most substantial alteration observed in the metabolomic studies was the 70-fold increase in 6-phosphogluconate (Figure 4.16; $P < 0.0001$, two-tailed unpaired *t*-test). This metabolite is a key component of the core carbon metabolic process, the pentose phosphate pathway (PPP). This pathway generates NADPH, erythrose-4-phosphate and ribose-5-phosphate, which are required for reductase reactions, amino acid synthesis and nucleotide synthesis, respectively. Due to the unbiased approach employed for the metabolomics studies, data for the abundance of metabolites upstream and downstream in this pathway were lacking. As a result, the increased abundance of 6-phosphogluconate may be a consequence of enhanced activity and flux through this pathway or a consequence of enzyme inhibition by Zn. The conversion of 6-phosphogluconate to ribulose-5-phosphate is catalysed by a 6-phosphogluconate dehydrogenase (6-PGD) enzyme. Here, it was hypothesised that Zn may inhibit the activity of the putative 6-PGD, annotated as *gnd*, in *S. pneumoniae.* The transcriptomic analyses were confirmed by targeted analysis of *gnd* transcription, which showed that this gene was unaltered by Zn treatment (Figure 4.17). This indicates that Gnd may be altered at the level of protein expression or inhibited by Zn. In a previous study of the yeast opportunistic pathogen, *Cryptococcus neoformans*, 6-PGD activity was inhibited by Zn (Niehaus *et al.*, 1996). As a result, the activity of 6-PGD was assessed in the presence and absence of Zn. *S. pneumoniae* D39 was grown in C+Y media and enzymatically lysed. The cell lysates were untreated or treated with Zn prior to assessment of the 6-PGD activity (Figure 4.18A). Relative to total protein concentration, treatment of the cell lysates with 100 μM Zn did not significantly alter the 6-PGD activity. However, compared to untreated, treatment with 200 or 300 μM Zn significantly reduced the 6-PGD activity by 48% (Figure 4.18B; $P < 0.05$, two-tailed unpaired *t*-test) and 86% ($P < 0.01$, two-tailed unpaired *t*-test), respectively. Together these data indicate that the PPP of *S. pneumoniae* may be impaired by the Zn-dependent disruption of 6-PGD activity, which may have detrimental downstream effects on the production of NADPH, nucleotides and amino acids. Although the levels and NADPH were not assessed in the metabolomics analysis, Zn-treated cells displayed differences in the levels of nucleotides. A 2.8-fold increase in cytidine 5'-monophosphate and 1.74-fold increase in uridine 5'-diphosphate (Table 4.1) was accompanied by a 3.4-fold decrease in adenosine 5'-diphosphate and 1.5-fold decrease in uridine 5'-triphosphate (Table 4.2). However, the levels of the aromatic amino acids, histidine, tryptophan, phenylalanine, and tyrosine were unchanged in Zn-treated *S. pneumoniae*. Taken together, although 6-PGD may be susceptible

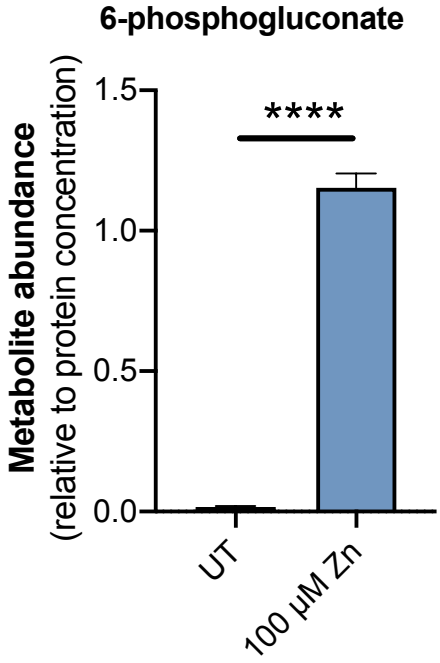


Figure 4.16 Zinc-treated *S. pneumoniae* display increased 6-phosphogluconate levels

S. pneumoniae was grown to mid-log phase (OD_{600} 0.30) in the presence or absence of 100 µM $ZnSO_4$. Samples were harvested, the metabolic profile was examined by Metabolon®. Data are the mean + SEM, n = 4 biological replicates, of the median-adjusted abundance of 6-phosphogluconate relative to sample protein concentration. Statistical significance was assessed using the Student's two-tailed unpaired *t*-test, where **** represents $P < 0.0001$.

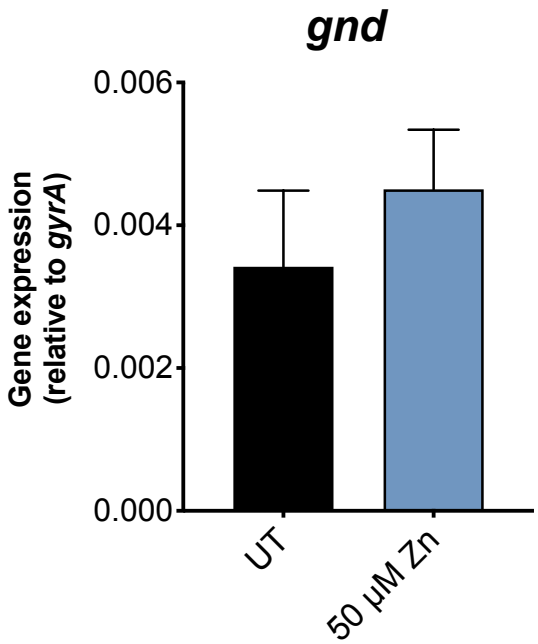


Figure 4.17 Zinc does not alter the transcription of *S. pneumoniae gnd*

S. pneumoniae was grown to mid-log phase (OD_{600} = 0.30) in C+Y medium with or without 50 µM $ZnSO_4$. Cells were harvested, RNA extracted, and transcription of *gnd* (SPD_0343) was examined by qRT- PCR. Gene expression is presented as the mean + SEM transcription relative to the transcription of the *gyrA* (SPD_1077) internal control, n = 3 biological replicates. Statistical significance was assessed using the Student's two-tailed unpaired *t*-test.

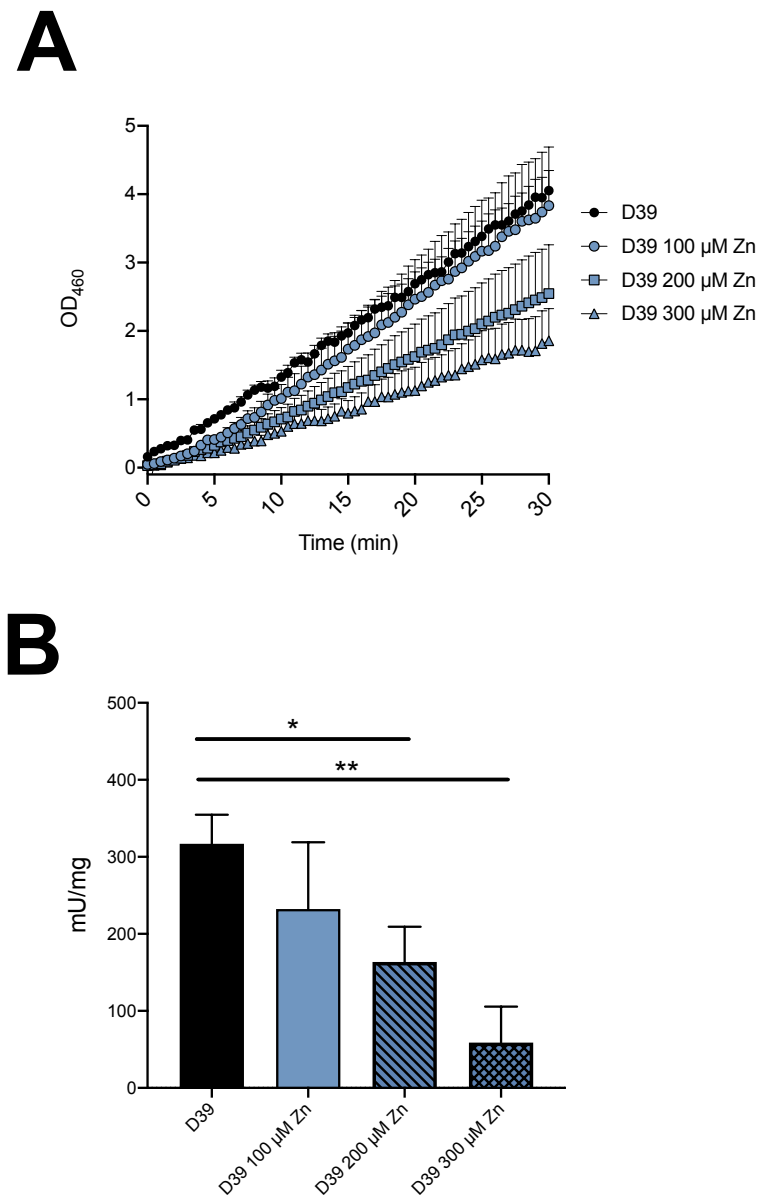


Figure 4.18 Zinc impairs *S. pneumoniae* 6-phosphogluconate dehydrogenase activity

S. pneumoniae was grown to mid-log phase (OD_{600} = 0.30) and lysed by treatment with sodium deoxycholate. (A) Whole cell lysates were untreated or incubated with 100, 200 or 300 µM $ZnSO_4$ for 10 min and then the 6-phosphogluconate dehydrogenase (6-PGD) activity was measured by the generation of NADPH in a colorimetric assay (BioVision). (B) The 6-PGD activity was interpolated based on the results of (A) using a standard curve of known NADPH concentrations, where one unit of 6-PGD is the amount of enzyme that generates 1.0 µmole of NADPH per min. Data are the mean + SEM n = 4 biological replicates. Statistical significance was assessed using the Student's two-tailed unpaired *t*-test where * represents $P < 0.05$ and ** represents $P < 0.01$.

to inhibition by Zn, the level of mismetallation in a cellular context may be negligible at the concentration tested.

4.2.5 Zinc stress disrupts the cell wall biosynthesis pathway

The metabolomics data revealed alterations in the abundance of metabolites in the peptidoglycan biosynthesis pathway. Notably, Zn-treated *S. pneumoniae* displayed a 4.9-fold increased abundance of fructose-6-phosphate (Figure 4.19A; $P < 0.01$, two-tailed unpaired *t*-test) and a 5.2-fold increase in glucosamine-6-phosphate (Figure 4.19B; $P < 0.05$, two-tailed unpaired *t*-test). Exposure to Zn also induced a 2.6-fold decrease in the abundance of N-acetyl-glucosamine-1-phosphate (Figure 4.19C; $P < 0.01$, two-tailed unpaired *t*-test) and a 1.5-fold decrease in UDP-N-acetyl-glucosamine (Figure 4.19D; $P < 0.01$, two-tailed unpaired *t*-test). An analysis of the transcription of genes in this pathway, *glmS*, *glmM,* and *glmU* (Figure 4.20A-C) corroborate the transcriptomic findings that showed no alteration in expression upon treatment with Zn. In the cell wall biosynthesis pathway, the enzyme responsible for the conversion of glucosamine 6-phosphate to N-acetylglucosamine-6-phosphate and the subsequent generation of UDP-N-acetyl-glucosamine is GlmU (Figure 4.3). GlmU is a metal-dependent enzyme, harbouring a magnesium ion in the uridyltransferase domain and calcium ion within the acetyltransferase domain (Kostrewa *et al.*, 2001; Sulzenbacher *et al.*, 2001). Thus, it was hypothesised that GlmU activity may be perturbed by the binding of Zn. Structural studies of GlmU were performed in the laboratory of collaborator, Associate Professor Megan Maher, by Mwilye Sikanyika and Dr Saumya Udagedara, (La Trobe University). Structural analyses revealed that Zn bound in the acetyltransferase domain of GlmU (Figure 4.21), with this metal ion coordinated by residues Glu315 and His330, and two water ligands (data not shown). Despite an interaction of GlmU with Zn, superimposition of the Zn-bound and apo structures of GlmU revealed that Zn binding at this site did not induce major structural rearrangements (data not shown). Further biochemical studies of purified GlmU, performed by Dr Saumya Udagedara (La Trobe University), revealed that Zn treatment decreased the acetyltransferase activity of GlmU (Figure 4.22A) while uridyltransferase activity was unaltered by Zn (data not shown). Furthermore, abrogation of Zn binding to GlmU by mutating residues Glu315 and His330 to alanine residues, reduced the observed Zn-dependent inhibition on acetyltransferase activity (Figure 4.22B). Together, these data indicate that the inhibition of acetyltransferase activity is due to Zn binding at this site.

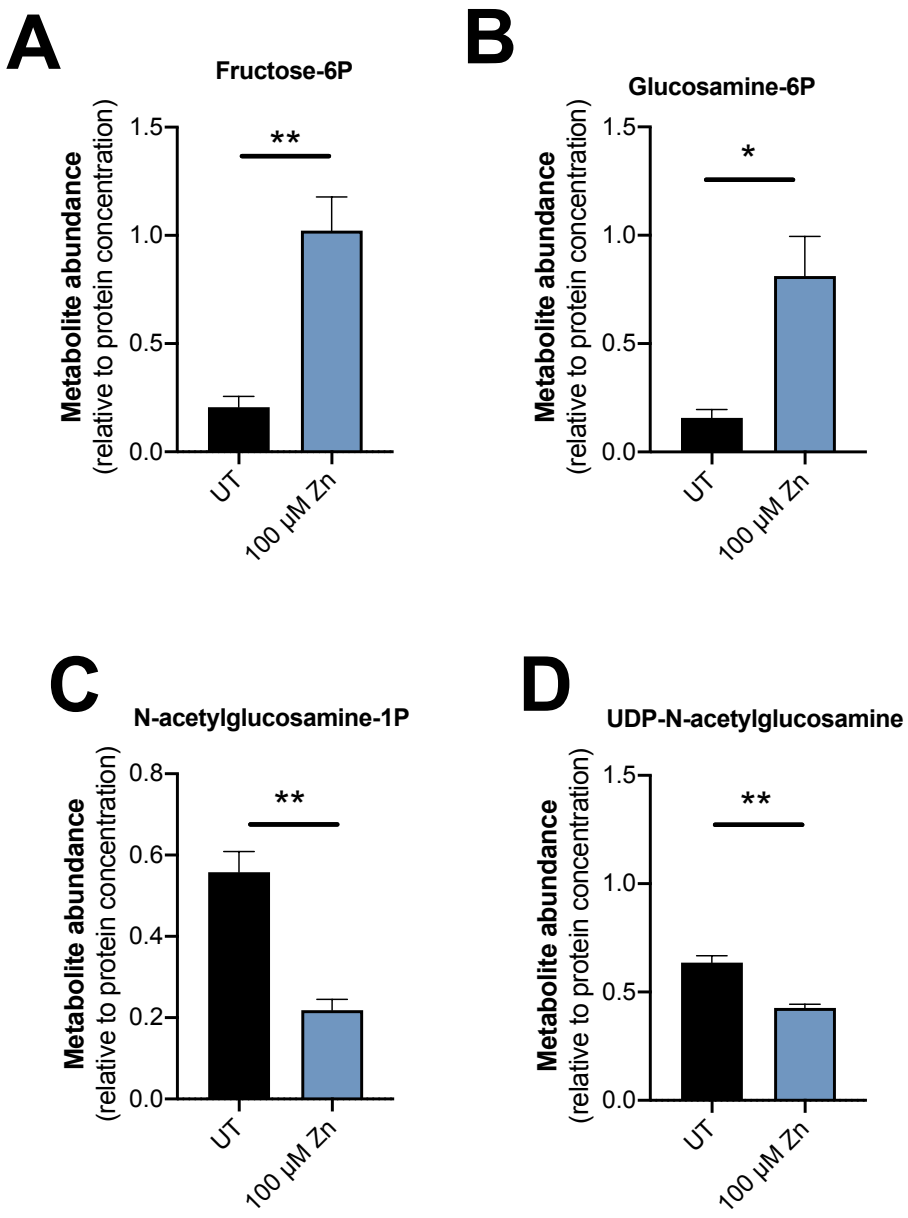


Figure 4.19 Zinc alters the abundance of metabolites in the cell wall biosynthesis pathway

S. pneumoniae was grown to mid-log phase (OD_{600} = 0.30) in C+Y medium supplemented with or without 100 µM $ZnSO_4$. Samples were harvested, the metabolic profile was examined by Metabolon®. Data are the mean + SEM, n = 4 biological replicates, of the median-adjusted abundance of (A) fructose-6-phosphate, (B) glucosamine-6-phosphate, (C) N-acetylglucosamine-1-phosphate and (D) UDP-N-acetylglucosamine relative to sample protein concentration. Statistical significance was assessed using the Student's two-tailed unpaired *t*-test, where * represents $P < 0.05$, and ** represents $P < 0.01$.

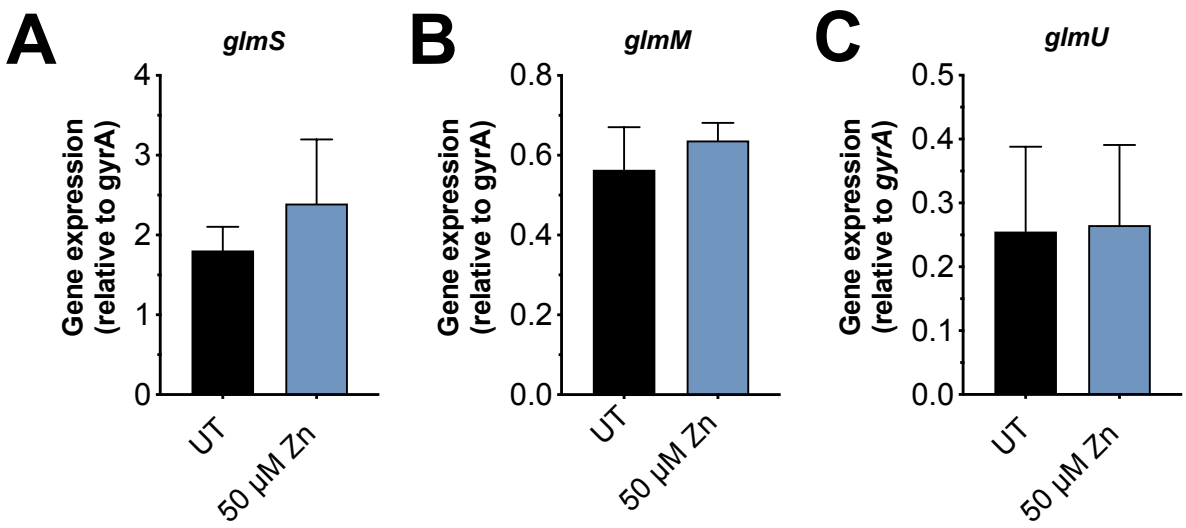


Figure 4.20 Zinc does not alter the transcription of the *S. pneumoniae* peptidoglycan biosynthesis genes

S. pneumoniae was grown to mid-log phase (OD_{600} = 0.30) in the presence or absence of 50 µM $ZnSO_4$. Cells were harvested, RNA was extracted, and the transcription of (A) *glmS* (SPD_0248) and (B) *glmM* (SPD_1390) and (C) *glmU* (SPD_0874) was examined by qRT-PCR. Data are the mean + SEM transcription relative to the transcription of the *gyrA* (SPD_1077) internal control, n = 3 biological replicates. Statistical significance was assessed using the Student's two-tailed unpaired *t*-test.

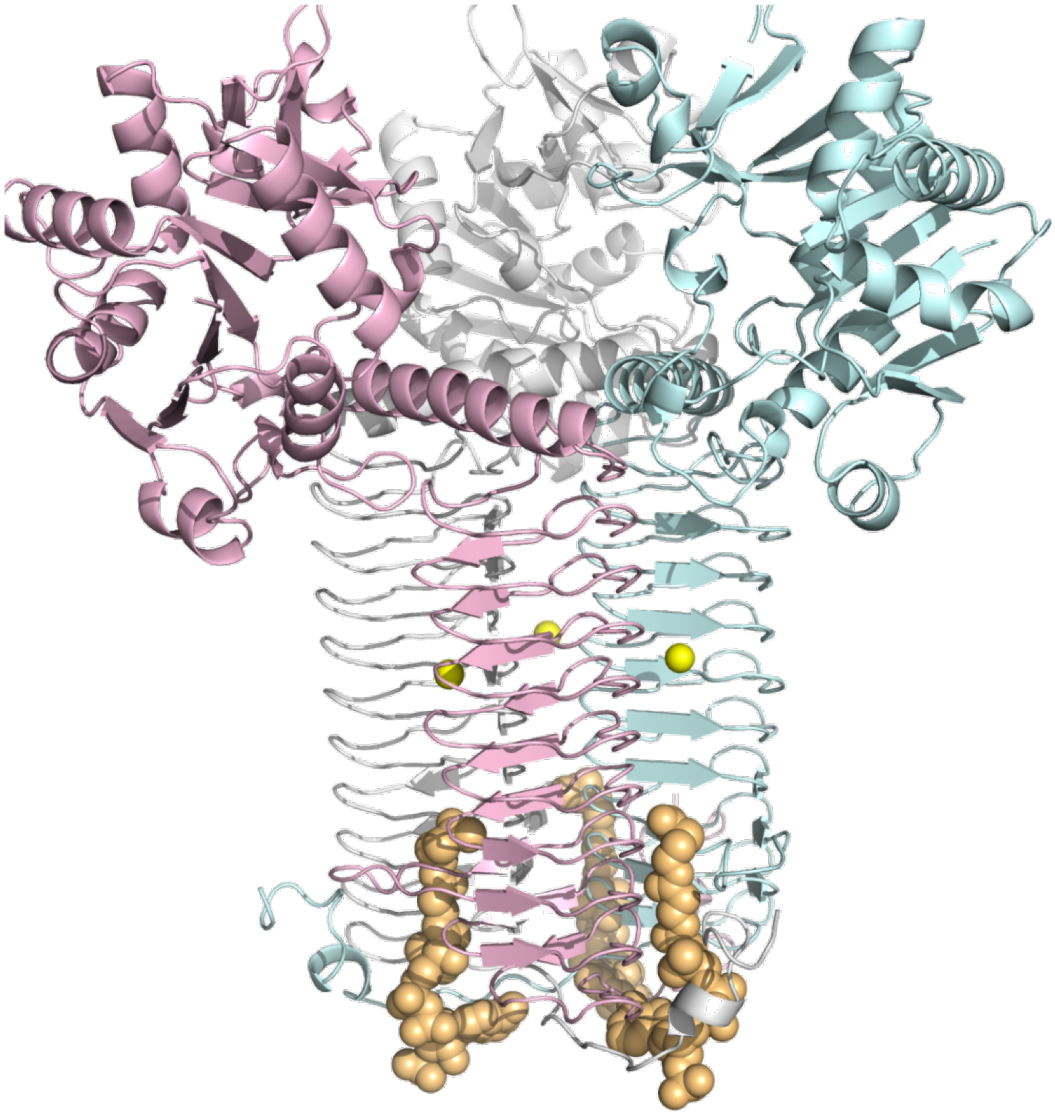


Figure 4.21 Zinc binds the acetyltransferase domain of GlmU

The 2.08 Å trimeric structure of purified GlmU presented as a cartoon diagram in complex with acetyl-CoA (light orange spheres) and Zn (yellow sphere).

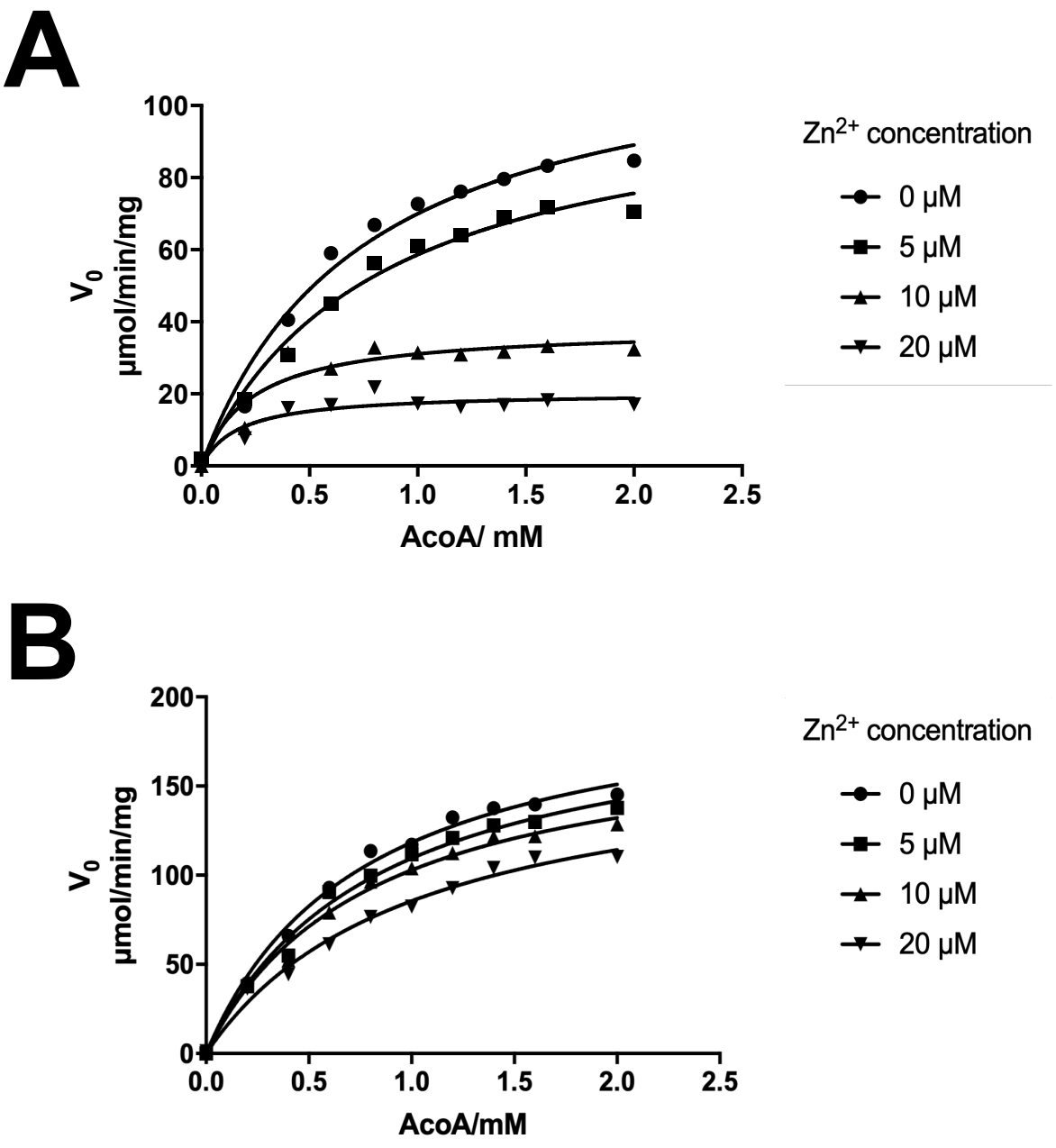


Figure 4.22 Zinc impacts the activity of *S. pneumoniae* GlmU

The acetyltransferase activity of purified (A) GlmU or (B) GlmU E315A/H330A, was assessed in following incubation with or without 5, 10 and 20 µM $ZnCl_4$. The data are the mean, from n = 3 biological replicates.

These data show that Zn disrupts GlmU, consistent with the findings of the metabolomics, and likely perturbs peptidoglycan biosynthesis. The hypothesis that Zn impacted cell wall biosynthesis was tested by examining the impact of Zn on the action of the cell wall-targeting antibiotic, penicillin. Survival of *S. pneumoniae* D39 wild-type and Δ*czcD* following treatment with 100 μM Zn, 0.1 μg/ml penicillin, singly or in combination was examined (Figure 4.23). At the concentration tested, exposure to Zn did not significantly alter the survival of the D39 or Δ*czcD* strain. Consistent with the antibiotic sensitivity profile, treatment with 0.1 μg/ml penicillin significantly reduced the survival of the D39 and Δ*czcD* strains (Figure 4.20; $P < 0.01$, two-tailed unpaired *t*-test). However, following treatment with Zn and penicillin, the Δ*czcD* strain showed significantly reduced survival compared with the wild-type strain under the same conditions ($P < 0.05$, two-tailed unpaired *t*-test), and compared with penicillin alone ($P < 0.01$, two-tailed unpaired *t*-test). Taken together, these data suggest that intracellular Zn enhances the susceptibility of *S. pneumoniae* to penicillin.

4.2.6 Intracellular zinc alters *S. pneumoniae* membrane physiology

The metabolic profile revealed Zn induced changes in the pathways associated with lipid metabolism. A heatmap of metabolites related to lipid metabolism was constructed to present the alterations in cellular abundance following exposure to Zn (Figure 4.24). Of the metabolites altered in these pathways, a significant 3.1-fold decrease was observed for acetyl-CoA (Figure 4.25A; $P < 0.001$, two-tailed unpaired *t*-test). Acetyl-CoA is a precursor for the *de novo* synthesis of fatty acids for the cell membrane via the type II fatty acid synthase (FASII) pathway (Zhang and Rock, 2008). Direct alterations in phospholipid abundance were also observed upon Zn treatment. Zn-treated cells displayed an increased abundance of 1,2-dipalmitoyl-GPG (16:0/16:0) (Figure 4.25B; $P < 0.001$, two-tailed unpaired *t*-test) and a decreased abundance of 1,2-dipalmitoleoyl-GPG (16:1/16:1) (Figure 4.25C; $P < 0.0001$, two-tailed unpaired *t*-test), 1-myristoyl-2-palmitoleoyl-GPG (14:0/16:1) (Figure 4.25D; $P < 0.0001$, two-tailed unpaired *t*-test) and 1-palmitoyl-2-palmitoleoyl-GPG (16:0/16:1) (Figure 4.25E; $P < 0.001$, two-tailed unpaired *t*-test). As a result of these broad impacts on lipid metabolism, the impact of Zn on phospholipid abundance and membrane physiology was further explored. As the untargeted metabolomic analyses were not optimised for the assessment of phospholipid abundance, the membrane fatty acid abundance was analysed by gas chromatography.

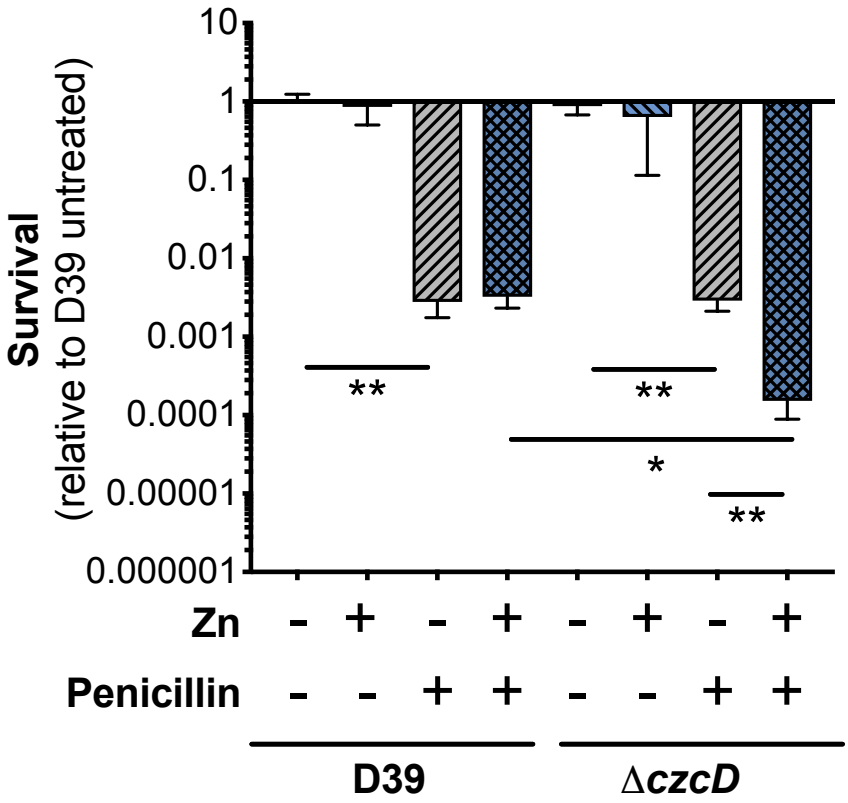


Figure 4.23 Zinc can enhance the susceptibility of *S. pneumoniae* to penicillin

S. pneumoniae D39 wild-type and Δ*czcD* were grown to mid-log phase (OD_{600} = 0.30) in C+Y medium and treated with 100 μM $ZnSO_4$, 0.1 μg/ml penicillin, either singly or in combination. Colony forming units were enumerated after 5 hrs treatment and the data are the mean + SEM survival relative to the D39 untreated sample, n = 5 biological replicates. Statistical significance was assessed using the Student's two-tailed *t*-test, where * represents $P < 0.05$ and ** represents $P < 0.01$.

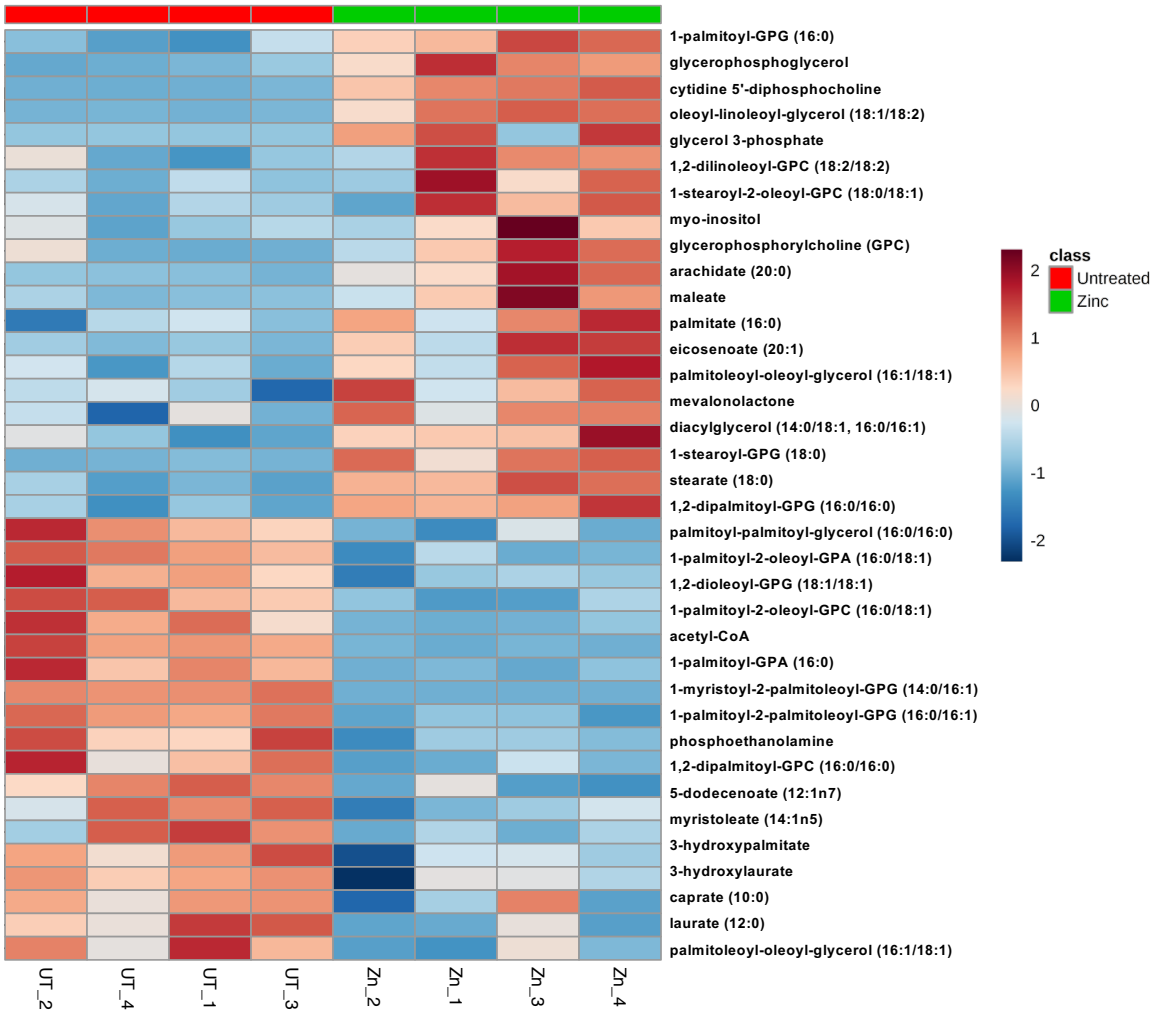


Figure 4.24 Changes in lipid metabolites in *S. pneumoniae* induced by zinc

S. pneumoniae were grown to mid-log phase (OD_{600} = 0.30) in the presence or absence of 100 µM $ZnSO_4$. Samples were harvested and the metabolic profile was examined by Metabolon®. A heatmap was generated by analysis of the normalised abundance of lipid metabolites using MetaboAnalyst 4.0 (Chong *et al.*, 2018). Each row represents a metabolite and each column represents a sample. The scaled expression value of each sample metabolite is plotted in red-blue colour scale, where the red colour of the tile represents high abundance and blue indicates low abundance, n = 4 biological replicates.

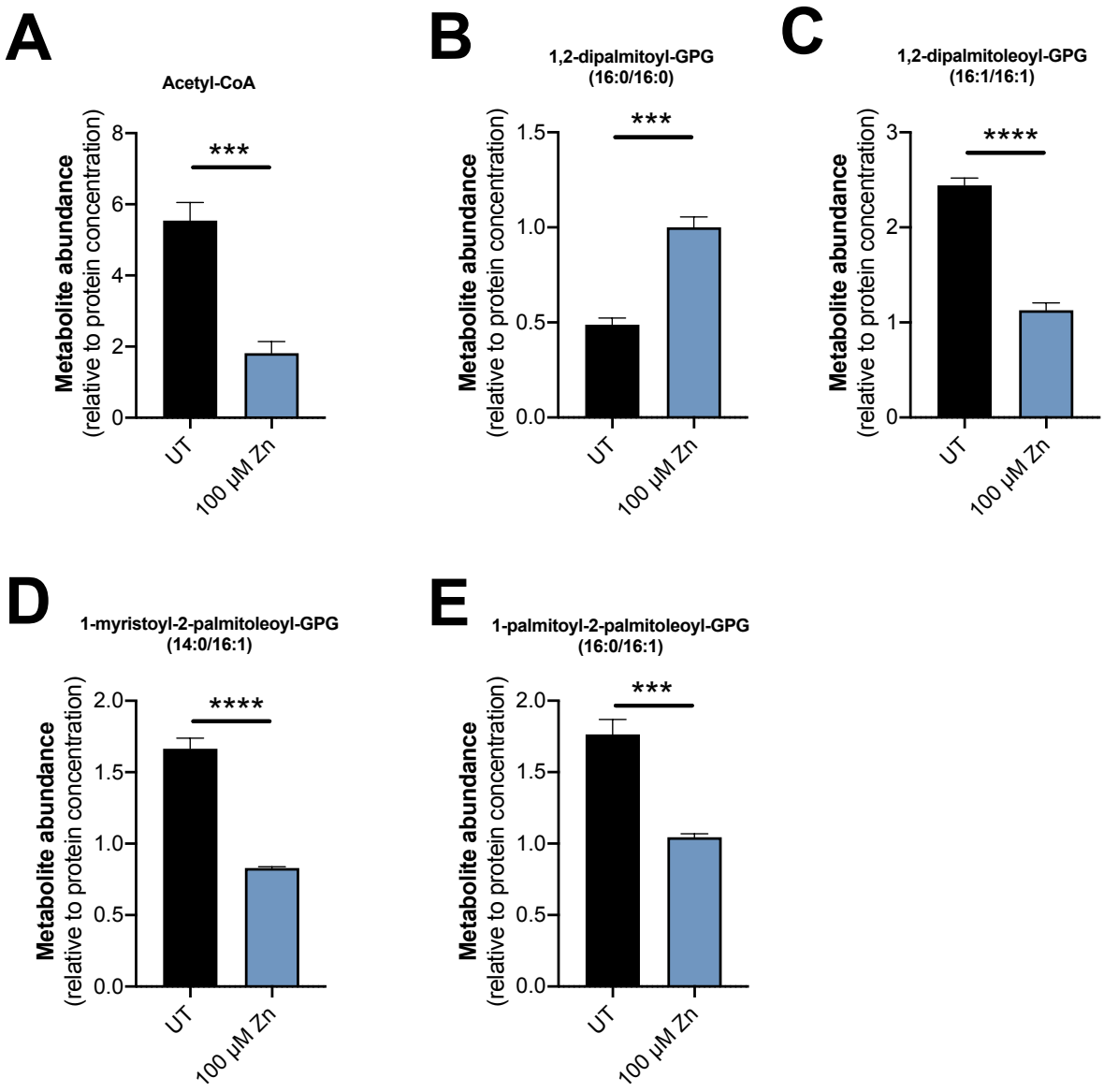


Figure 4.25 Zinc alters the abundance of lipids and lipid precursor metabolites in *S. pneumoniae*

S. pneumoniae was grown to mid-log phase (OD_{600} = 0.30) in C+Y medium with or without 100 µM $ZnSO_4$. Samples were harvested and the metabolic profile was examined by Metabolon®. The median-adjusted abundance of (A) acetyl-CoA, (B) 1,2-dipalmitoyl-GPG (16:0/16:0), (C) 1,2-dipalmitoleoyl-GPG (16:1/16:1) and (D) 1-myristoyl-2-palmitoleoyl-GPG (14:0/16:1) and (E) 1-palmitoyl-2-palmitoleoyl-GPG (16:0/16:1) was determined relative to sample protein concentration. Data are the mean + SEM, n = 4 biological replicates. Statistical significance was assessed using the Student's two-tailed unpaired *t*-test, where *** represents $P < 0.001$ and **** represents $P < 0.0001$.

S. pneumoniae D39 wild-type and Δ*czcD* were grown in the presence and absence of 50 μM Zn, the lipids were extracted, and the membrane fatty acid abundance was determined. In these analyses, the saturated fatty acids, 14:0, 16:0 and 18:0, and the monounsaturated fatty acids, 16:1n-7, 18:1n-7 and 18:1n-9 were detected in *S. pneumoniae* D39 (Figure 4.26). Zn-treated *S. pneumoniae* D39 displayed no significant alterations in the phospholipid composition compared to untreated. However, analysis of the Zn-treated Δ*czcD* mutant, which lacks the capacity to efflux Zn, revealed a significant increase in 14:0 (Figure 4.23A; $P < 0.05$, two-tailed unpaired *t*-test) and decrease in 18:1n-7 abundance compared to the untreated mutant (Figure 4.26E; $P < 0.01$, two-tailed unpaired *t*-test). Furthermore, the Zn-treated Δ*czcD* mutant displayed an increased abundance of 16:0 fatty acids compared to the Zn-treated wild-type strain (Figure 4.26B; $P < 0.01$, two-tailed unpaired *t*-test).

Overall these changes corresponded to a significant shift in the ratio of saturated to unsaturated phospholipids, such that Zn-overloaded *S. pneumoniae* Δ*czcD* possessed a higher proportion (ratio of 2.6 to 1) of saturated membrane fatty acids relative to unsaturated compared to untreated (ratio of 1.8 to 1) (Figure 4.27; $P < 0.05$, two-tailed unpaired *t*-test). To assess the physiological impact of the altered phospholipid composition, the fluidity of the membrane measured using the membrane probe, 1,6-diphenyl-1,3,5-hexatriene (DPH). The fluorescence polarization detected the relative movement of the probe in the membrane, which was used as a measure of rotational diffusion and thus membrane fluidity. Treatment of the *S. pneumoniae* D39 wild-type with Zn did not significantly alter the fluidity of the membrane, however, the Zn-overloaded Δ*czcD* mutant displayed a 6.4% decrease in membrane fluidity compared with the untreated Δ*czcD* mutant (Figure 4.28; $P < 0.05$, two-tailed unpaired *t*-test). Overall, these data indicate that *S. pneumoniae* overloaded with Zn display increased membrane saturation and rigidity. Based on these data, it was hypothesised that Zn may alter the FASII pathway. The transcription of candidate genes as representatives of the three open reading frames of the FASII pathway were examined in D39 and Δ*czcD* following growth in the presence or absence of 50 μM Zn. Treatment of either strain with Zn did not significantly alter the transcription of the regulator, *fabT*, or *fabK*, a representative of the biosynthetic genes in this pathway (Figure 4.29A-B).

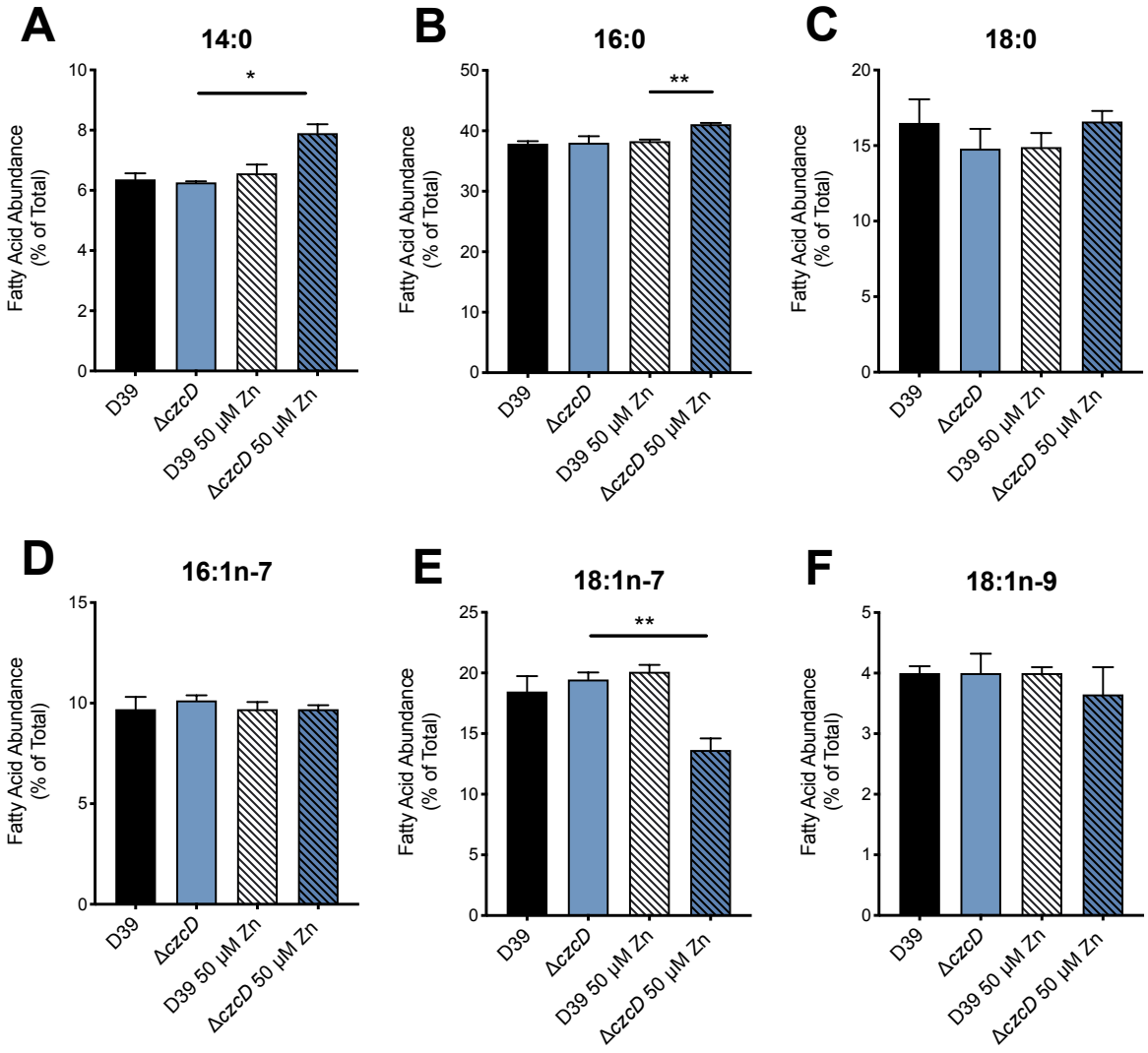


Figure 4.26 Excess intracellular zinc alters the fatty acid composition of the *S. pneumoniae* membrane

S. pneumoniae D39 and Δ*czcD* were grown to mid-log phase (OD_{600} = 0.30) in C+Y medium with or without 50 μM $ZnSO_4$. Cells were lysed by sonication and the fatty acid constituents were determined by gas chromatography. The abundance of each fatty acid is expressed as the percentage of total fatty acids. Data are the mean + SEM, n = 3 biological replicates. Statistical significance was assessed using the Student's two-tailed unpaired *t*-test, where * represents $P < 0.05$ and ** represents $P < 0.01$.

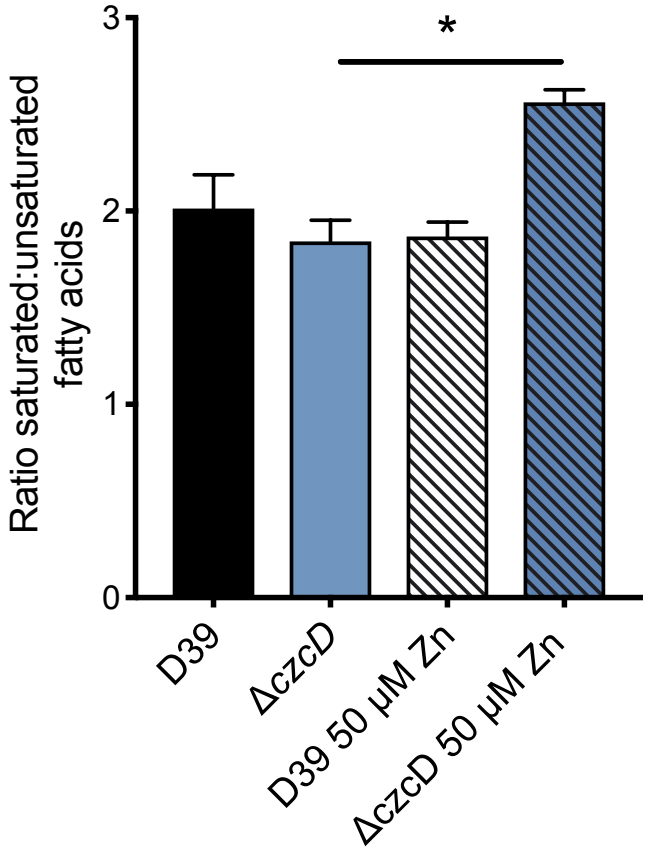


Figure 4.27 Intracellular zinc increases the relative abundance of membrane saturated fatty acids in *S. pneumoniae*

S. pneumoniae D39 and Δ*czcD* were grown to mid-log phase (OD_{600} = 0.30) in C+Y medium with or without 50 μM $ZnSO_4$. Cells were lysed by sonication and the fatty acid constituents were determined by gas chromatography. The ratio of saturated to unsaturated fatty acids was determined based on the percentage of saturated and unsaturated fatty acids. Data are the mean + SEM, n = 3. Statistical significance was assessed using the Student's two-tailed unpaired *t*-test, where * represents $P < 0.05$ and ** represents $P < 0.01$.

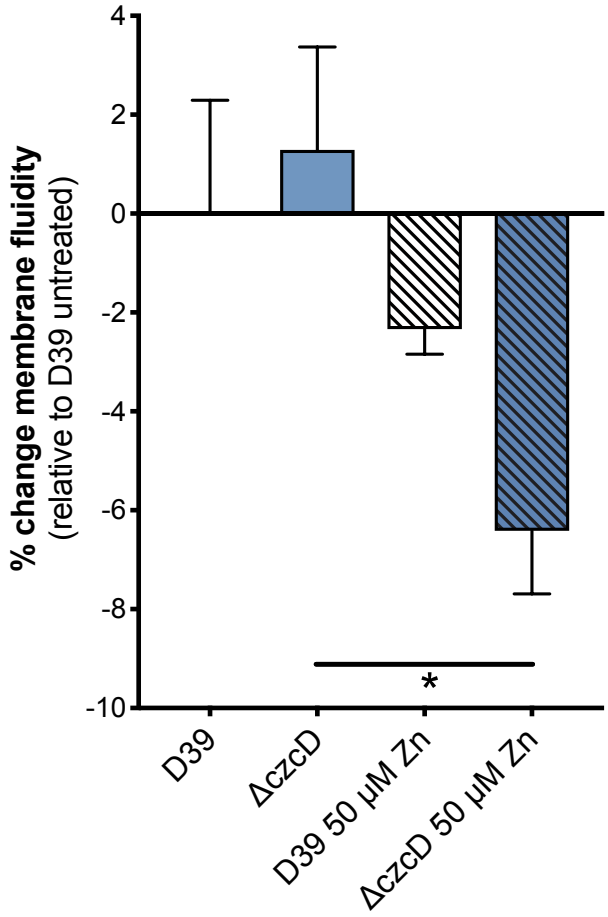


Figure 4.28 Zinc treatment alters the fluidity of the *S. pneumoniae* membrane

S. pneumoniae D39 and Δ*czcD* were grown to mid-log phase (OD_{600} = 0.30) in C+Y medium with or without 50 μM $ZnSO_4$. The membrane fluidity was assessed by examining the fluorescence polarization of DPH in the cellular membrane. The change in fluorescence polarisation was determined relative to D39 untreated and the data are the presented as the percentage change in membrane fluidity compared to D39 untreated. Data are the mean + SEM, n > 3. Statistical significance was assessed using the Student's two-tailed unpaired *t*-test, where * represents $P < 0.05$.

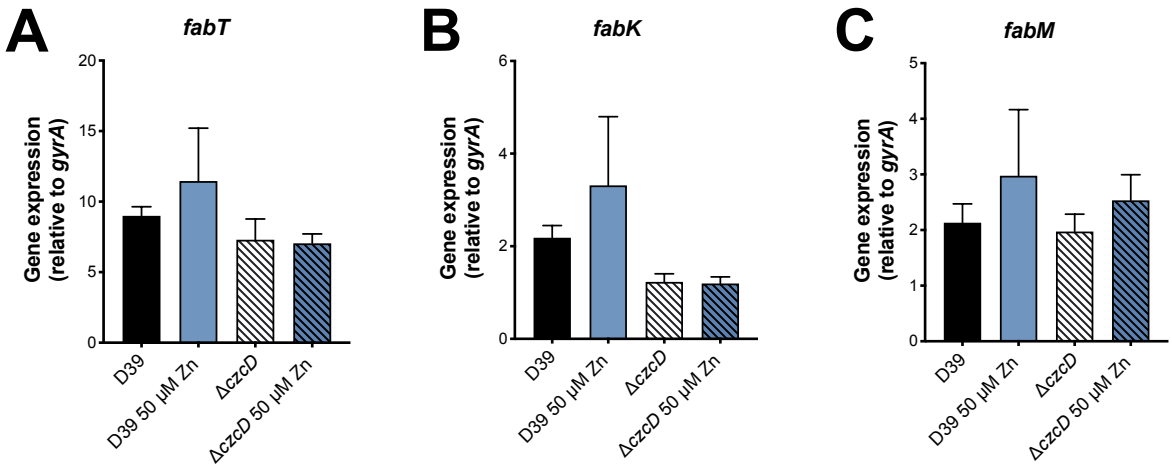


Figure 4.29 Zinc does not alter the transcription of genes in the *S. pneumoniae* fatty acid synthase II pathway

S. pneumoniae D39 and Δ*czcD* were grown to mid-log phase (OD_{600} = 0.30) in C+Y medium with or without 50 µM $ZnSO_4$. Cells were harvested, RNA extracted, and transcription of (A) *fabT* (SPD_0380), (B) *fabK* (SPD_0382) and (C) *fabM* (SPD_0378), was examined by quantitative reverse transcription PCR. Gene expression is presented as the mean + SEM transcription relative to the transcription of the *gyrA* (SPD_1077) internal control, n = 3 biological replicates. Statistical significance was assessed using the Student's two-tailed unpaired *t*-test.

Importantly, Zn treatment did not alter the transcription of the *fabM* gene (Figure 4.29C), which encodes a trans-2-decanoyl-ACP isomerase responsible for the formation of monounsaturated fatty acids through the incorporation of a double bond. These data indicate that the observed change in membrane composition and increase in membrane saturation is not a consequence of differential transcription of the FASII pathway genes.

4.3 Discussion

Although the toxicity of Zn towards bacteria is known, the specific pathways disrupted have remained elusive. The present study aimed to explore the metabolic pathways impacted by Zn to characterise novel targets of Zn stress in *S. pneumoniae.* A global metabolomic approach coupled with the transcriptomic analyses of the previous chapter identified several pathways influenced by Zn. As a fermentative organism, residing exclusively within the human host, *S. pneumoniae* energy production depends on the uptake of carbohydrates from host niches (Buckwalter & King, 2012). However, there are niche-dependent differences in the relative abundance of carbohydrates. The preferred carbon source of *S. pneumoniae* is glucose, which is the primary carbon source in the blood and inflamed tissues (Paixao *et al.*, 2015). However, galactose is the dominant carbon source in the nasopharynx and upper respiratory tract, where the pneumococcus typically resides as a commensal organism. When glucose is available, the expression of the pathways for the catabolism of non-dominant sugars are controlled by CcpA, which binds to catabolite response elements to regulate gene expression (Carvalho *et al.*, 2011). The present study indicates that, despite the dominance of glucose, Zn treatment resulted in a shift in pneumococcal metabolism towards galactose. Mutational analyses suggest that the Zn-dependent increase in Leloir pathway gene expression occurs independently of CcpA. The transcription of the *galK* and *galT-2* genes are also controlled at the transcriptional level by the regulatory protein GalR (Afzal *et al.*, 2015), which acts as an activator of these genes to increase the expression of *galK* and *galT-2* in the presence of galactose. Together, the results of this study indicate that Zn may interact directly with GalR or indirectly via an alteration in galactose abundance, which may influence its interaction with the operator sequence for the Leloir pathway genes. Further studies, such as electromobility shift and Zn binding studies of GalR, as well as quantification of cellular galactose abundance in the presence of Zn, are required to dissect the role of Zn in mediating Leloir pathway gene expression. *S. pneumoniae* is highly adapted to the environment of the human host. As a result, the Zn-dependent induction of Leloir pathway expression may constitute an adaptation response that facilitates host colonisation. Zn levels display significant niche-dependent differences in abundance. In mice, Zn levels are more than 2.5-fold higher in the nasopharynx and lungs compared to the blood, although the levels of Zn are significantly altered during systemic disease (McDevitt *et al.*, 2011). As the Zn levels in tissues correlate with the levels of galactose, Zn may be used as a signalling strategy to sense typically galactose-rich environments. These metabolic changes, concomitant with the upregulation of the genes

responsible for the cleavage of galactose from glycoconjugates and the PTS uptake pathways, may enable *S. pneumoniae* to harness galactose in the presence of Zn. The improved growth in the presence of Zn in galactose-supplemented media further supports the role of Zn in altering carbohydrate metabolism in a way that may be beneficial during a commensal lifestyle. Further studies directed towards elucidation of the impact of Zn on infection and asymptomatic colonisation of the nasopharynx are required to examine the contribution of host Zn levels on the survival of *S. pneumoniae.*

A previous study has shown that the upregulation of the Leloir pathway increases capsule production, resulting in a hypervirulent phenotype (Trappetti *et al.*, 2017). Surprisingly, despite the Zn-dependent upregulation of the Leloir pathway and increase in UDP-glucose levels, capsule levels were reduced in Zn-treated cells when glucose was the dominant carbon source. The lack of observed transcriptional changes to the genes in the capsule locus upon Zn treatment suggests that the alteration in capsule production may be due to changes at the post-transcriptional level, possibly due to Zn mismetallation. Zn treatment has been shown to impair capsule production in *S. pyogenes*, which the authors propose is due to inhibition of Pgm by Zn (Ong *et al.*, 2015). Pgm is a phosphoglucomutase enzyme that facilitates the interconversion of glucose-6-phosphate to glucose-1-phosphate (Shackelford *et al.*, 2004). As this enzyme is highly conserved between *S. pneumoniae* and *S. pyogenes*, (83% identity, 91% similarity; Appendix 4), it is possible that the inhibition of Pgm may be responsible for the decrease in capsule production. However, due to the presence of the genes encoding the Leloir pathway, the mechanism underlying the capsule defect in *S. pneumoniae* has a greater level of complexity. In addition to capsule production via glucose metabolism, the Leloir pathway enables capsule production to be mediated by galactose metabolism. In contrast, *S. pyogenes* relies on glucose metabolism for the generation of capsule intermediates (Ong *et al.*, 2015). Furthermore, Pgm inhibition and lack of flux into the capsule biosynthesis pathway is not consistent with the enrichment of UDP-glucose, which indicates that an alternative mechanism may be at play. Although there is no evidence for metal binding, Zn may interfere with Cps2K, the UDP-glucose-6-dehydrogenase responsible for the conversion of UDP-glucose to UDP-glucouronic acid. Zn may impair translation of Cps2K or interact directly with this protein to impair its function. Further studies, including PGM activity assays in the presence of Zn, as well as protein immunoblot and enzymatic activity assays of Cps2K are required to further dissect the impact of Zn on capsule production.

The impairment of *S. pneumoniae* PfkA activity is likely responsible for the Zn-dependent accumulation of glycolytic metabolites upstream of fructose 1,6-bisphosphate (ie. Glucose-6-phosphate and fructose-6-phosphate). The capacity for Zn to impair glycolytic enzymes, including PFK, has been observed previously in rat skeletal muscle (Ikeda *et al.*, 1980). In a more recent study, Zn treatment during growth or in cell free extracts, impaired PFK activity in *S. pyogenes* (Ong *et al.*, 2015). The authors proposed that the energy defect imparted by the inhibition of PFK activity could be circumvented by upregulation of the T6P pathway, the sole route for the utilisation of galactose in this bacterium. In contrast, *S. pneumoniae* possesses the genes for two galactose metabolic pathways; the T6P pathway and the Leloir pathway. While it is tempting to speculate that *S. pneumoniae* employs a similar metabolic route to bypass the requirement on PfkA, no altered expression of the T6P pathway genes were observed, and the Leloir pathway does not bypass the reliance on PfkA for energy production. Thus, the inhibition of PfkA may be contribute to the growth delay observed upon Zn treatment when glucose is dominant. Despite the lack of upregulation of the T6P pathway genes, there is evidence that Zn increases the activity of this pathway in *S. pyogenes* (Ong *et al.*, 2015). The activity of the tagatose-6-phosphate kinase, LacC.2, which is responsible for the conversion of tagatose 6-phosphate to tagatose1,6-bisphosphate in *S. pyogenes,* is increased following treatment of cell lysates with Zn. *S. pneumoniae lacC* displays a high degree of homology with the *S. pyogenes lacC.2* gene (67% identity, 80% similarity; Appendix 5). Thus, despite the lack of transcriptional upregulation, this pathway may display increased activity in *S. pneumoniae* in the presence of Zn. Further tagatose-6-phosphate kinase activity assays in *S. pneumoniae* are required to directly assess the influence of Zn on the activity of *S. pneumoniae* LacC. Furthermore, although changes in the glycolytic metabolites are observed when glucose is dominant, the degree of a PfkA inhibition and influence of Zn on metabolism when galactose is dominant remains unknown. Given the enhanced growth upon Zn treatment when galactose is dominant, further transcriptional analyses are required to assess whether Zn treatment in the presence of galactose further alters the expression of the Leloir and T6P pathway genes.

Zn treatment in *S. pneumoniae* induced an increase in 6-phosphogluconate abundance and activity assays corroborated a Zn-dependent inhibition of the 6-PGD enzyme. A previous study has shown that Zn impairs 6-PGD activity in the RAW264 murine macrophage cell line and a metalloproteomic screen revealed that this protein is susceptible to Zn binding (Triboulet *et al.*, 2014). This enzyme is highly conserved, with 51% identity and 70% similarity between the RAW264 6-PGD and the *S. pneumoniae* Gnd protein. Although this protein was susceptible

to Zn mismetallation in this murine macrophage cell line, the capacity for cellular Zn levels to be sufficiently high in *S. pneumoniae* for this to occur remains unknown. Further activity and metalloproteomic studies in *S. pneumoniae* grown in the presence of Zn are required to elucidate the impact of intracellular Zn on 6-PGD activity. Nevertheless, these data indicate that Zn may disrupt the PPP.

The PPP is highly conserved and serves three major functions: the generation of NADPH, ribose-5-phosphate and erythrose-4-phosphate [reviewed in (Stincone *et al.*, 2015)]. Although the levels of NADPH were not assessed in the present study, NADPH is involved in pathways that require reductive biosynthesis reactions, such as the fatty acid biosynthesis pathway (Agledal *et al.*, 2010). NADPH is required for a number of enzymatic steps in the FASII pathway, which is required for the *de novo* synthesis of fatty acids. NADPH is required for the FabG-dependent reduction of β-ketoacyl-ACP to β-hydroxyacyl-ACP, and the FabK-dependent formation of saturated fatty acids via the conversion of trans-2-enoyl-ACP to acyl-ACP (Price *et al.*, 2001). It follows that if NADPH levels are depleted in Zn-treated cells, this may limit fatty acid synthesis or the formation of saturated fatty acids. However, as a relative proportion, Zn-overloaded *S. pneumoniae* displayed higher levels of saturated fatty acids and reduced levels of the monounsaturated fatty acid, 18:1n-7. These findings were supported by the decreased membrane fluidity observed under Zn stress, as the acyl chains of fatty acids are key determinants of membrane fluidity (Eijkelkamp *et al.*, 2018).

Together, the membrane physiology data indicate that Zn induces an increase in the abundance of saturated phospholipids, which altered the biophysical properties of the membrane. The altered membrane fluidity is likely to translate into a significant change in membrane microviscosity, as alterations in fluidity of 10% have previously been proposed to be indicative of a change of up to 25% in viscosity (Aricha *et al.*, 2004; Shinitzky & Barenholz, 1978). Changes to the lipid composition, comprising an increased membrane saturation and decreased membrane fluidity have previously been proposed to constitute a stress response to enable bacteria to save energy and survive (Dubois-Brissonnet *et al.*, 2016). Given the potential for Zn to interfere with energy production, these changes in membrane physiology may constitute a strategy to overcome this limitation. However, the mechanism underlying this increase in membrane rigidity is not understood. Given the lack of transcriptional changes in the fatty acid biosynthesis genes, it is possible that Zn may impair the activity of FabM, the enzyme responsible for the formation of unsaturated fatty acids (Marrakchi *et al.*, 2002). While

there is no evidence for metal binding in this enzyme, future experiments assessing the activity of this enzyme in the presence of Zn may reveal further insight into the Zn-dependent increase in membrane saturation. Zn-stressed pneumococci also displayed a marked depletion in acetyl-CoA, which is a key precursor for the synthesis of fatty acids. This indicates that *S. pneumoniae* may display an overall reduction in fatty acid synthesis. Future studies to elucidate the total phospholipid abundance in Zn-stressed cells may provide further insight into this phenomenon.

The PPP also produces ribose-5-phosphate, which is required for the synthesis of nucleic acids. Thus, it is possible that the inhibition of 6-PGD has downstream consequences for the generation of nucleotides, which are required for the synthesis and repair of DNA. Although ribose-5-phosphate abundance was not assessed in the metabolomics analyses, this study revealed changes in the abundance of metabolites associated with nucleotide synthesis. However, the data do not highlight any clear detrimental impact on nucleotide abundance and the precise contribution of Zn treatment on nucleotide synthesis, if any, remains unclear. Future studies to directly examine the impact of Zn treatment on *S. pneumoniae* DNA synthesis and repair are required. The PPP is also responsible for the production of erythrose-4-phosphate, a key precursor for the synthesis of the aromatic amino acids. However, Zn did not induce changes in the abundance of aromatic amino acids.

The production of NADPH via the PPP is also required for the regeneration of GSH, which serves a role in resistance to oxidative stress and metal stress. Thus, a Zn-dependent impairment of 6-PGD activity may increase the susceptibility of pneumococci to oxidative and Zn stress. However, a link between Mn starvation and the PPP has previously been described (Ogunniyi *et al.*, 2010). Mn depletion has been associated with impairment of the Mn-dependent superoxide dismutase enzyme, SodA, which is also impaired under conditions of excess Zn (Eijkelkamp *et al.*, 2014). The impairment of SodA has been shown to induce a shift to a glutathione-based oxidative stress response, which requires the regeneration of GSH by NADPH produced by the PPP. Taken together, it is possible that the observed change in 6-phosphogluconate is instead a consequence of increased flux through the PPP due to a shift towards a glutathione-based defence. A comprehensive dissection of the impact of Zn on the PPP was hindered by insufficient insight into all metabolic intermediates in this pathway. It is possible that although 6-PGD activity may be impaired with *in vitro* Zn supplementation, the levels of Zn intracellularly following Zn treatment may not reach sufficient concentrations to impart significant PPP inhibition. Alternatively, it remains possible that the observed increase

in 6-phosphogluconate is a consequence of increased flux through this pathway, as is observed under conditions of Mn starvation. The quantification of all metabolites in this pathway in Zn-treated *S. pneumoniae,* as well as additional activity assays to assess 6-PGD activity following Zn treatment during growth, may yield further insight into the impact of Zn on the PPP.

Treatment with Zn revealed an alteration in the abundance of key intermediates in the peptidoglycan biosynthesis pathway. The bacterial cell wall is important for maintaining the structural integrity of the cell and is the target of a range of successful antibiotic classes, such as β-lactams and glycopeptides (Park & Strominger, 1957; Reynolds, 1989). GlmU is an essential bifunctional enzyme that possesses two catalytic domains (Mengin-Lecreulx & van Heijenoort, 1994; Sulzenbacher *et al.*, 2001). First, an acetyltransferase domain that catalyses the transfer of an acetyl group from acetyl-CoA to glucosamine-1-phosphate, followed by the transfer of uridine 5-monophosphate via the uridyltransferase domain, to convert N-acetylglucosamine-1-phosphate to UDP-N-acetylglucosamine (Gehring *et al.*, 1996; Mengin-Lecreulx & van Heijenoort, 1993). Although the observed depletion of cellular acetyl-CoA may influence the function of GlmU, the present study identified a direct Zn-dependent inhibition of GlmU acetyltransferase activity. Structural studies elucidated the Zn-binding site of GlmU and showed that Zn was coordinated by the C-terminal acetyltransferase domain residues, Glu315 and His330. The binding of Zn to these residues may directly impede an interaction required for acetyltransferase activity or indirectly elicit a change in the conformation of critical residues in acetyltransferase activity. Interestingly, although the Glu315 and His330 residues reside in the acetyltransferase domain, there is no evidence to suggest that these residues directly contribute to the substrate binding or acetyltransferase activity of this enzyme (Wang, 2017). Substitution of these residues to alanines to abrogate Zn binding reduced the impact of Zn on acetyltransferase activity, which indicates that the inhibition was due to Zn binding at this site. The essentiality and specificity of GlmU in bacteria has led to the study of this protein for its utility as an antibiotic target (Buurman *et al.*, 2011; Sharma & Khan, 2017). The increased susceptibility to penicillin observed in Zn-overloaded *S. pneumoniae* indicate that Zn may be used in combination with traditional antibiotics to enhance their efficacy. However, these data highlight the need to adequately raise intracellular Zn levels in order to observe enhanced antibiotic efficacy, as no change in susceptibility was observed when *S. pneumoniae* was capable of Zn efflux via CzcD. Taken together, these data suggest that an increase in cytosolic Zn levels may render this pathogen more susceptible to treatment with cell wall-targeting antibiotics. Thus, strategies that inhibit Zn efflux or promote the uptake of Zn may be

used in combination with traditional cell wall-targeting antibiotics to enhance their efficacy. Given the broad and highly conserved pathways impaired by Zn treatment, Zn co-treatment strategies may be employed to enhance the efficacy of a range of antibiotic classes. In addition to improved antibiotic efficacy, this approach may have broader implications for the treatment of antibiotic resistant pathogens, where Zn overloading strategies may render resistant strains susceptible to treatment. Further studies are required to examine the viability of such co-treatment strategies *in vitro* and *in vivo*.

Collectively, this chapter has highlighted the broad impacts of Zn on *S. pneumoniae* metabolism. The identification of novel targets of Zn toxicity provides the foundation for future biochemical and mechanistic studies to determine the molecular basis of Zn toxicity in *S. pneumoniae*. In the context of disease, this study delivered new insights into the pathways that may be impaired by host-imposed Zn stress and revealed many conserved targets that may inform the rational development of future Zn-based therapeutics. This study also revealed the potential for Zn to augment the action of penicillin, which has the potential to be exploited in a novel therapeutic approach.

CHAPTER 5: Exploiting zinc to improve antibiotic efficacy

5.1. Introduction

The discovery of antibiotics in the 20th century played a defining role in shaping modern medicine. Mortality due to infectious diseases plummeted, dangerous medical procedures became routine, and the average life expectancy increased by 20 years (Adedeji, 2016). Today, bacterial pathogens harbouring resistance determinants to one or more antibiotic classes are increasingly detected in the clinic (Fair & Tor, 2014). However, at the current rate, the deployment of novel antimicrobial therapeutics into the clinic is insufficient to balance the surge in resistance. Consequently, immediate action towards the discovery and development of alternative treatment strategies is imperative.

Antibiotic resistance is becoming an increasing issue for the treatment of pneumococcal disease (Whitney *et al.*, 2000). The global dissemination of antibiotic resistant pandemic strains has led to widespread resistance, particularly against β-lactams, macrolides, fluoroquinolones and third generation cephalosporin antibiotics (Linares *et al.*, 2010). As new antibiotics are limited, enhancing or restoring the efficacy of existing antibiotics is an attractive strategy to combat disease. The previous chapter provided insight into the molecular targets of Zn toxicity in *S. pneumoniae*. This work showed that bacterial cell wall biosynthesis may be disrupted via the interaction of Zn with essential protein GlmU. Interestingly, the cell wall is also the target of existing antibiotics, such as β-lactams (Park & Strominger, 1957). This class of antibiotics acts at a later stage in the cell wall biosynthetic process to inhibit the transpeptidase that catalyses the cross linking of peptidoglycan (Yocum *et al.*, 1980). In line with these findings, high intracellular Zn augmented the action of the cell wall targeting antibiotic, penicillin. However, a key finding of this study was that Zn treatment alone was insufficient to enhance the action of penicillin. Nevertheless, this work indicates that pneumococci with sufficiently elevated cellular Zn levels may also display an enhanced susceptibility to penicillin. Given the broad cellular targets of Zn stress, it was hypothesised that Zn may augment the action of an even greater range of antibiotics. Furthermore, as the targets of Zn stress are conserved and independent of pneumococcal antibiotic resistance pathways, the enhanced susceptibility may extend to drug resistant strains. In this chapter, strategies to increase the cellular Zn abundance and thus the susceptibility of pneumococci to antibiotics were examined.

This study explored strategies to elevate pneumococcal intracellular Zn levels in strains with functional efflux pathways. It is possible that targeting of bacterial metal transport

proteins, such as importers and exporters, or interfering with metal sensing via regulatory proteins may increase cellular Zn abundance. Although the targeting of Zn homeostasis may be achieved via inhibitors of the Zn metalloregulators, SczA and AdcR, these proteins are localised in the cytoplasm, which necessitates the cellular uptake of an inhibitor. Alternatively, the pneumococcal Zn efflux protein, CzcD, is localised in the cell membrane and the development of an inhibitor targeting CzcD may circumvent the need for cellular uptake. As Zn abundance is modulated during disease (McDevitt *et al.*, 2011), an inhibitor targeting the primary Zn export pathway in pneumococci may be exploited in combination with antibiotics to enhance their efficacy. However, this strategy is not without risk as humans possess a collection of CDF family Zn transporter (ZnT/SLC30A) proteins. Although the roles of these proteins are not fully understood, these transporters are critical for maintaining cytosolic Zn concentrations and may contribute to the alteration of metal abundance in various tissues (Huang & Tepaamorndech, 2013). While bacterial Zn resistance is primarily mediated by cellular efflux of Zn, eukaryotic CDF transporters contribute to Zn redistribution into distinct subcellular compartments. To date, ten mammalian Zn-transporting CDF proteins have been identified. Of these, only ZnT1 is localised to the plasma membrane, functioning in a manner akin to bacterial Zn efflux CDF proteins, such as CzcD (Palmiter & Huang, 2004). ZnT1 plays an essential role in development, as homozygous knockouts are embryonic lethal in mice (Andrews *et al.*, 2004). The remaining nine human CDF family proteins are localised in intracellular organelle membranes. These proteins aid in the sequestration of Zn into the Golgi apparatus and cytoplasmic vesicles [ZnT5 (Jackson *et al.*, 2007), ZnT6 (Huang *et al.*, 2002), ZnT7 (Kirschke & Huang, 2003) and ZnT10 (Bosomworth *et al.*, 2012)], endosomes, lysosomes and secretory vesicles [ZnT2 (Guo *et al.*, 2010; Lopez & Kelleher, 2009)] and ZnT4 (McCormick & Kelleher, 2012; Ranaldi *et al.*, 2002)], secretory granules [ZnT8 (Chimienti *et al.*, 2004)), endoplasmic reticulum [ZnT9 (Perez *et al.*, 2017)] or synaptic vesicles [ZnT3 (Wenzel *et al.*, 1997)]. Studies have revealed both overlapping and unique expression patterns for these transporters, with many possessing a broad tissue distribution, such as ZnT5 in the Golgi apparatus, vesicles, and plasma membrane (Jackson *et al.*, 2007), while others are restricted, such as ZnT9 in the endoplasmic reticulum (Perez *et al.*, 2017) [for a detailed review, see (Bafaro *et al.*, 2017)]. As an inhibitor against CzcD must be highly selective, this chapter employed a bioinformatics approach to examine the homology of CzcD with human ZnT proteins to assess the viability of *S. pneumoniae* CzcD as an antimicrobial target.

In addition to inhibiting pneumococcal Zn efflux, an alternative strategy to increase Zn uptake was explored. Zn is a charged ion unable to cross the cell membrane by passive diffusion. However, several metal-binding compounds can shield positively charged ions, thus rendering them permissive to membrane translocation. Here, the use of a metal-binding compound to increase pneumococcal intracellular Zn was examined. Metal binding drugs can be divided into three main subtypes; chelators, shuttles, and ionophores (Ding & Lind, 2009). Metal chelators bind and sequester metal ions, rendering these ions unavailable to cells. Conversely, metal shuttles interact with a metal ion to facilitate their uptake into cells. Metal ionophores also carry metal ions across biological membranes but can repeat this process, with the potential to continuously cycle metal ions into the cell. Thus, an increase in the metal concentration amplifies the effect of ionophores, while metal shuttles are self-limiting. Metal ionophores have been investigated for their potential to inhibit antibiotic resistance proteins. The ionophore, pyrithione, has previously been investigated in complex with Zn or Cu to enhance antibiotic activity. Studies have shown that Zn pyrithione can inhibit the aminoglycoside-modifying enzyme, aminoglycoside 6'-N-acetyltransferase type Ib (AAC[6']-Ib), which confers resistance to antibiotics, such as amikacin (Chiem *et al.*, 2015; Lin *et al.*, 2014). The authors showed that treatment with Zn pyrithione rendered *A. baumannii*, *Klebsiella pneumoniae* and *E. coli* harbouring the *aac(6')-Ib* gene susceptible to amikacin. However, these analyses were restricted to *in vitro* studies of strains harbouring the *aac(6')-Ib* gene and did not provide mechanistic evidence for the improved susceptibility. Another study showed that Cu pyrithione enhanced the susceptibility of *E. coli* to carbapenem antibiotics (Djoko *et al.*, 2018). Although the precise mechanism of action remains to be elucidated, the authors propose that high intracellular levels of Cu ions may displace the Zn ion from the resistance protein, metallo-β-lactamase NDM-1. However, pyrithione has been associated with acute oral toxicity, which precludes its utility in the present study as a treatment option for invasive *S. pneumoniae* disease (Black & Howes, 1978). A recent study explored the use of the hydroxyquinoline ionophore, clioquinol, for the reversal of amikacin resistance in *A. baumannii* and *E. coli in vitro* (Chiem *et al.*, 2018). Clioquinol was an over-the-counter drug used for treating diarrhea and indigestion but in the 1950s it was associated with the development of subacute myelo-optic neuropathy [SMON] (Oakley, 1973). The relationship between clioquinol and SMON is poorly understood and remains a topic of contention, but clioquinol was discontinued due to the severity of these adverse events. Recently, the hydroxyquinoline clioquinol derivative ionophore, PBT2, was developed as an orally administered drug for the treatment of Alzheimer's disease (AD) (Adlard *et al.*, 2008). In AD, the utility of PBT2 has been attributed to its capacity to cross the blood-

brain barrier to redistribute metal cations from amyloid beta plaques, without restricting the availability of these metal ions to cells. The successful progression of PBT2 to Phase II clinical trials demonstrated that this drug is safely tolerated orally in humans, up to a dosage of 250 mg/day for 26 weeks (Lannfelt *et al.*, 2008). Based on the metal-modulating mechanism proposed for AD, encouraging safety profile, and broad tissue distribution of PBT2, this study aimed to investigate the capacity of this drug to be repurposed *in vitro* and *in vivo* to increase the accumulation of Zn in pneumococci and thereby enhance antibiotic susceptibility. A recent study of a range of murine wound infection models has shown that topical administration of PBT2 and Zn can potentiate the impact of antibiotics to significantly reduce bacterial levels in the treatment of antibiotic resistant *S. aureus, S. pyogenes* and *Enterococcus faecium* (Bohlmann *et al.*, 2018). However, this study administered Zn and PBT2 topically at high concentrations, which are likely beyond the scope of feasibility for a systemic treatment due to toxicity issues. Although associated with additional complexities, the systemic administration of PBT2 with Zn may constitute a drug repurposing strategy to combat antibiotic resistant pneumococci and warrants investigation. The repurposing of an existing drug as a potential adjunct to current antibiotics may offer a relatively rapid and inexpensive solution to treat disease caused by antibiotic resistant *S. pneumoniae*.

One of the earliest penicillin-resistant clones to be identified was the *S. pneumoniae*^{Spain23F} sequence type 81 (ST81) strain (Croucher *et al.*, 2009). *S. pneumoniae*^{Spain23F} was initially isolated in 1987 in Barcelona, Spain, and rapidly disseminated globally (Munoz *et al.*, 1991). By the early 1990s, *S. pneumoniae*^{Spain23F} was established as the cause of almost 40% of penicillin-resistant disease isolates in the United States (Corso *et al.*, 1998). *S. pneumoniae*^{Spain23F} additionally harbours resistance to tetracycline and chloramphenicol and is increasingly associated with resistance to macrolides and fluoroquinolones (Croucher *et al.*, 2009). As this strain caused high rates of disease in children and exhibited extensive antibiotic resistance, the type 23F CPS was included in the 7-valent pneumococcal conjugate vaccine (PCV-7). Despite effective reductions in carriage of *S. pneumoniae*^{Spain23F} upon introduction of this vaccine, this lineage has undergone capsule switching and may be susceptible to vaccine evasion (Croucher *et al.*, 2009). This study aimed to use this multi-drug resistant strain as a clinically relevant model to assess the capacity of Zn to augment antibiotic action. The results presented in this chapter demonstrate the *in vitro* efficacy of Zn, PBT2 and antibiotic combinations and highlight the complexities associated with the translation of this strategy *in vivo.*

5.2. Results

5.2.1 Bioinformatic analyses of CzcD and human ZnT proteins

CDF family Zn transporters have crucial roles in mammals, as highlighted by disease-causing mutations, including transient neonatal Zn deficiency (ZnT2), diabetes mellitus (ZnT8), and Parkinsonism (ZnT10). Accordingly, inhibitors of *S. pneumoniae* CzcD must be highly selective towards bacterial orthologs in order to avoid possible off-target effects. Development of specific CzcD inhibitors required that the level of homology between *S. pneumoniae* CzcD and human ZnT proteins was assessed. BLASTp analyses revealed that CzcD has a moderate level of homology with many of the ZnT proteins (Table 5.1). Notably, ZnT3, ZnT4, ZnT5, ZnT8, and ZnT10 displayed 39-50% similarity with >80% coverage with *S. pneumoniae* CzcD. Primary sequence alignment with ZnT4, which shares the highest level of homology, showed that the similarity spanned the full length of CzcD and did not reveal any regions that may be selectively targeted (Figure 5.1). Functional analyses of CzcD have largely been restricted to the metal binding residues, which have established that many of these residues are essential for function (Martin & Giedroc, 2016). A primary sequence alignment of *S. pneumoniae* CzcD and the most extensively characterised CDF protein, *E. coli* YiiP, against the ten human ZnT proteins was performed to identify conservation among metal-binding residues (Appendix 6, summarised in Table 5.2). With the exception of *S. pneumoniae* CzcD Asn222, each metal-binding residue of CzcD was present in at least one of the human ZnT proteins. As a result, a primary sequence alignment of known bacterial Zn-transporting CDF proteins was performed against the human ZnT proteins to identify novel residues conserved across bacteria but absent in human proteins (Appendix 7). Although several residues displayed moderate levels of conservation, these spanned both bacterial and human proteins. As a result, these analyses did not identify candidate target regions for a bacterial-specific inhibitor. While an inhibitor that targets CzcD may be developed, the level of homology with human Zn-transporting CDF proteins necessitates a stringent structure-based drug design approach to ensure selectivity. While a previous chapter has generated a structure model of CzcD based on the structure of *E. coli* YiiP, detailed structural information of CzcD is lacking. As a result, an alternative strategy to increase pneumococcal Zn stress was explored.

Table 5.1 Sequence identity and similarity of *S. pneumoniae* CzcD with human ZnT zinc-transporting cation diffusion facilitator family members

Gene	Coverage	E-value	Identity	Positive	Matching segments
ZnT4	96%	1e-24	23%	46%	1
ZnT5	88%	3e-18	20%	39%	1
ZnT8	92%	1e-15	23%	48%	1
ZnT3	91%	2e-15	23%	42%	1
ZnT10	84%	8e-14	27%	52%	2
ZnT7	68%	1e-11	29%	51%	2
ZnT2	67%	9e-11	23%	47%	1
ZnT9	53%	1e-09	24%	45%	2
ZnT1	87%	6e-09	24%	47%	3
ZnT6	62%	4e-04	18%	37%	1

Amino acid sequences of *S. pneumoniae* CzcD (SPD_1638) and *Homo sapiens* ZnT1-10 were obtained from UniProt and homology was assessed by BLASTp analysis.

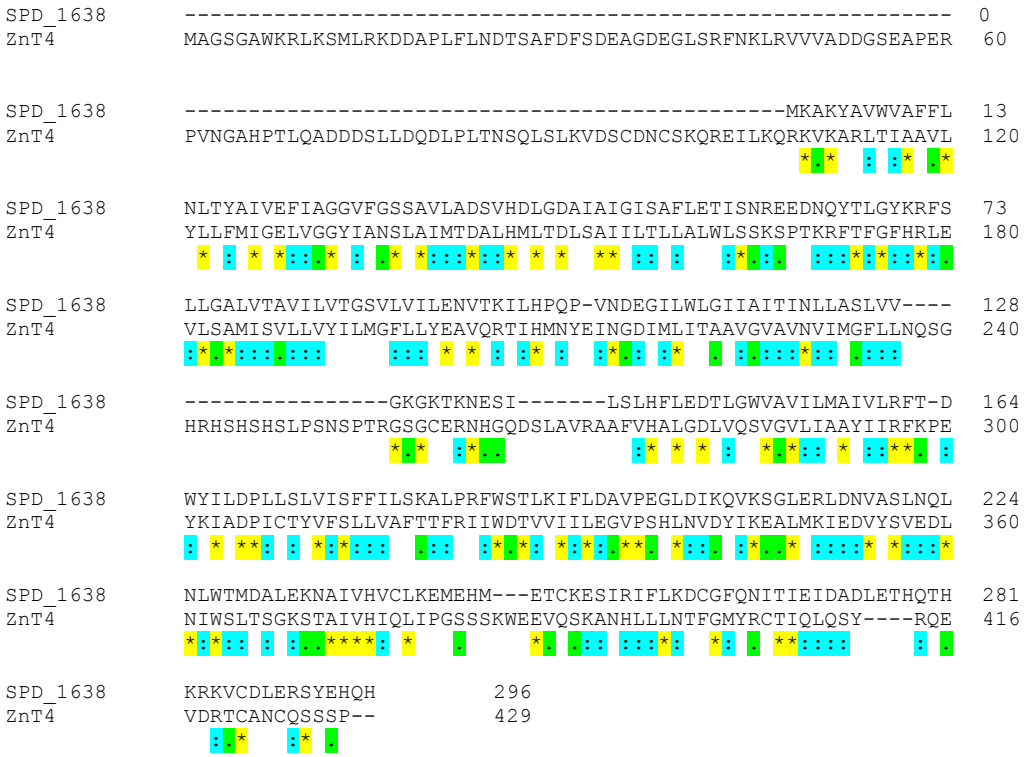


Figure 5.1 Primary sequence alignment of *S. pneumoniae* CzcD with human ZnT4

Amino acid sequences of *S. pneumoniae czcD* (SPD_1638; GI: 116077533) and *Homo sapiens* ZnT4 (GI: 2582415) were obtained from NCBI and aligned using Clustal Omega (Sievers *et al.*, 2011). ***** denotes fully conserved residue, **:** denotes conservation between groups of strongly similar properties, **.** denotes conservation between groups of weakly similar properties.

Table 5.2 Putative metal binding residues of *S. pneumoniae* CzcD and human ZnT family proteins

Protein	Site A				Site B			Site C1		Site C2	
CzcD	H	D	H	D	D	Y	Y	N	H	E	E
ZnT1	H	D	H	D	T	N	W	H	H	M	Q
ZnT2	-	-	H	D	-	-	-	H	H	Q	Q
ZnT3	H	D	H	D	T	M	W	H	H	E	Q
ZnT4	H	D	H	D	T	F	F	E	H	E	Q
ZnT5	H	D	H	D	T	F	Y	R	H	Q	Q
ZnT6	L	D	H	D	S	Y	F	R	H	Q	Q
ZnT7	H	D	H	D	N	F	Y	Q	K	R	Q
ZnT8	H	D	H	D	S	L	W	H	H	Q	Q
ZnT9	H	D	I	D	D	H	F	H	E	D	E
ZnT10	N	D	H	D	G	A	Y	H	H	Q	Q

Putative metal binding residues proposed based on a primary sequence alignment (Clustal Omega) of *S. pneumoniae* CzcD and the human ZnT proteins (Appendix 6). Residues of the ZnT proteins identical to CzcD are highlighted in yellow. '-' indicates regions that are present in CzcD but absent in ZnT2.

5.2.2 The ionophore PBT2 increases the potency of zinc stress

This study aimed to investigate whether PBT2 ionophore activity could increase Zn in *S. pneumoniae*. Here, the ability of PBT2 to enhance Zn toxicity was assessed based on a combination of growth and cellular Zn accumulation studies. Growth of *S. pneumoniae* D39 (Figure 5.2A) and the Δ*czcD* strain (Figure 5.2B), which lacks the gene encoding the Zn efflux protein, was assessed in the presence and absence of Zn and PBT2. Comparable growth was observed for untreated *S. pneumoniae* D39 and cells treated with 1 μM PBT2, while a minor growth perturbation was observed in the presence of 50 μM Zn. However, the combination of 50 μM Zn and 1 μM PBT2 resulted in a reduction in growth of the *S. pneumoniae* D39 strain. Growth of the Δ*czcD* strain displayed a similar growth pattern, although perturbation was also observed in the presence of either 1 μM PBT2 or 50 μM Zn. Significantly, the growth of the Δ*czcD* strain was severely compromised upon supplementation of the media with the combination of 50 μM Zn and 1 μM PBT2. As treatment with Zn or PBT2 in isolation had minimal impacts on growth, but in combination compromised growth, these data support the capacity of PBT2 to enhance the toxicity of Zn in pneumococci.

Based on these data, it was hypothesised that PBT2 could shuttle Zn into *S. pneumoniae* to raise intracellular Zn levels. To test the veracity of this hypothesis, the cellular Zn levels of *S. pneumoniae* D39 treated with PBT2, Zn, or a combination of both Zn and PBT2 was determined by ICP-MS (Figure 5.3). These data showed that treatment with PBT2 resulted in comparable levels of cellular Zn as the untreated pneumococci, while treatment with Zn significantly increased the cellular Zn relative to the untreated controls ($P < 0.0001$, two-tailed unpaired *t*-test). Consistent with the phenotypic studies, treatment with Zn and PBT2 significantly increased the cellular Zn relative to the single treatments ($P < 0.0001$, two-tailed unpaired *t*-test). Collectively, these data show that PBT2 increases the cellular Zn abundance of *S. pneumoniae.* Building on these data, the susceptibility of *S. pneumoniae* to antibiotics treated with PBT2 and Zn was investigated.

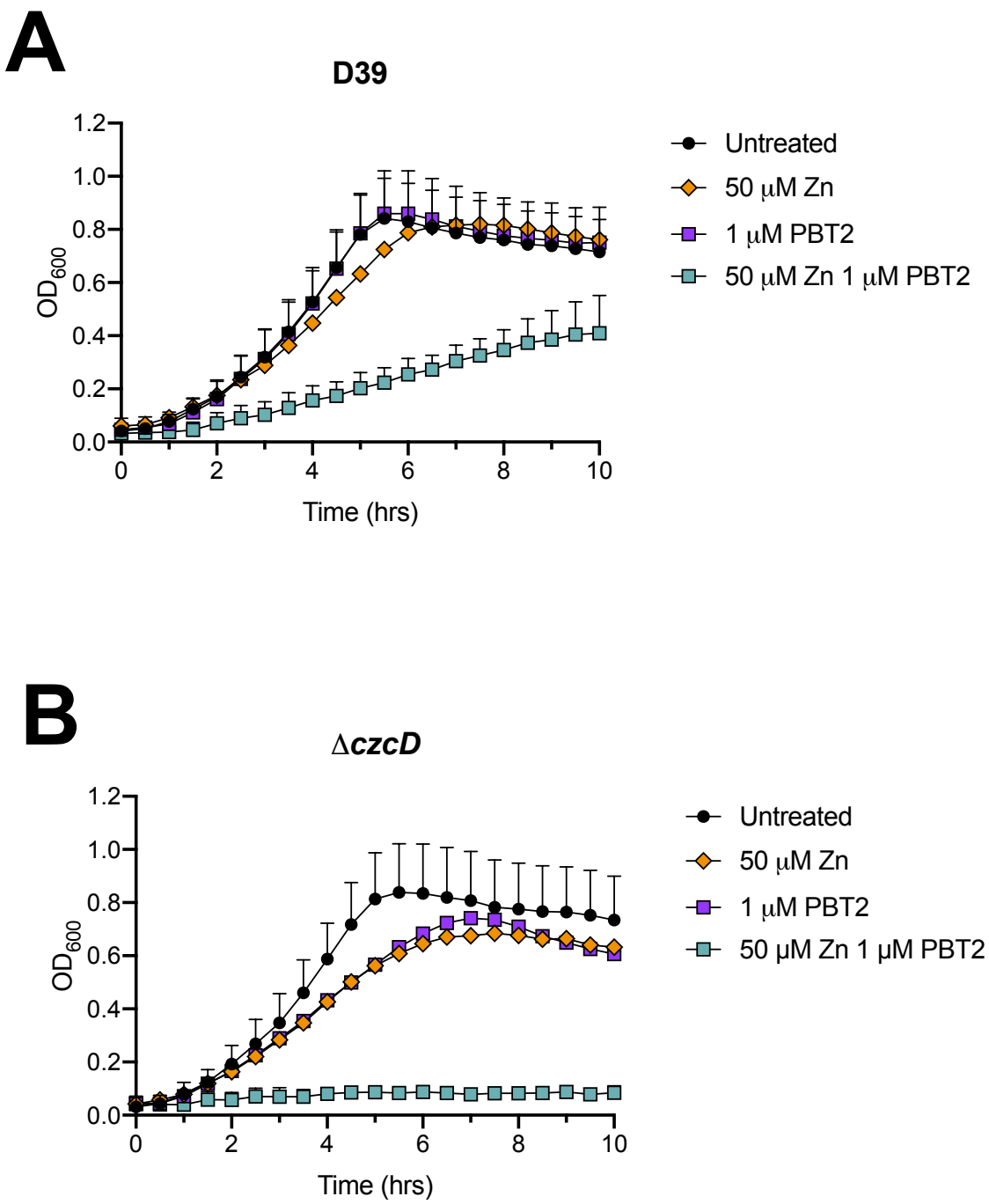


Figure 5.2 PBT2 enhances the toxicity of zinc against *S. pneumoniae*

Growth kinetics of were monitored by reading the optical density (OD_{600}) of *S. pneumoniae* D39 (A), and Δ*czcD* (B), at 30 min intervals over 10 hrs. Cells were grown in C+Y media or C+Y supplemented with 50 μM $ZnSO_4$, 0.5 μM PBT2.2HCl, or a combination of Zn sulphate and PBT2.2HCl. Data are the mean + SEM, from n = 3 biological replicates. Where not visible, the error bars are overlapped by the representative symbols.

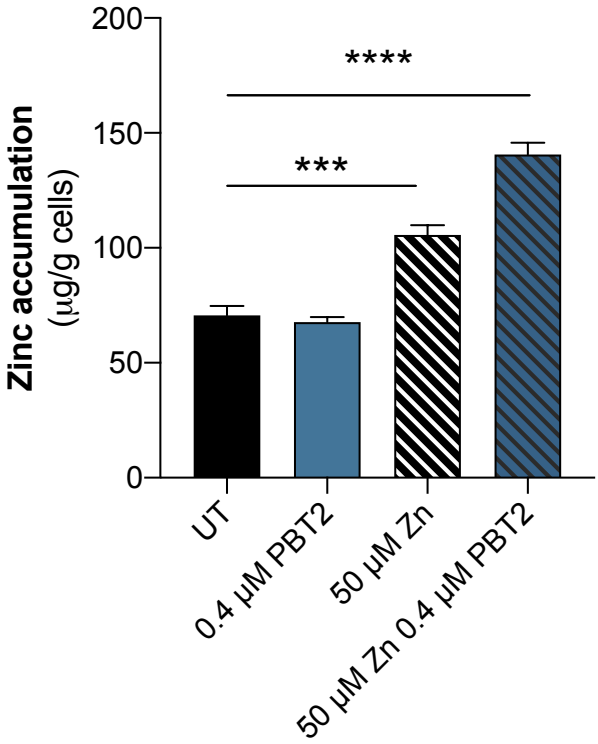


Figure 5.3 PBT2 increases *S. pneumoniae* cellular zinc accumulation

Cellular metal content was determined for the *S. pneumoniae* D39 strain grown in C+Y media, or C+Y media with 0.4 μM PBT2.2HCl, 50 μM $ZnSO_4$ or a combination of 0.4 μM PBT2.2HCl and 50 μM $ZnSO_4$. Metal content is expressed as the microgram of metal per gram of dry cells as determined by inductively coupled plasma-mass spectrometry. Data are the mean ± SEM, from n ≥ 3 biological replicates. Statistical significance was assessed by an ordinary one-way ANOVA with comparisons relative to untreated, where *** represents $P < 0.001$ and **** represents $P < 0.001$.

5.2.3 PBT2 and zinc enhances the antibiotic susceptibility of antibiotic resistant *S. pneumoniae*

The targets of Zn stress described in the previous chapter represent components of conserved pathways. Hence, Zn stress was predicted to impact drug-resistant *S. pneumoniae* strains in a similar manner to that of susceptible strains. In the previous chapter, the increase in antibiotic susceptibility by Zn was demonstrated in an antibiotic-sensitive strain. Consequently, the present chapter expanded these studies by investigating the impact of PBT2-mediated Zn overload on antibiotic susceptibility in the *S. pneumoniae*^{Spain23F} strain, which harbours resistance to penicillin, ampicillin, chloramphenicol, and tetracycline (Croucher *et al.*, 2009). First, the susceptibility of this strain to PBT2 was assessed in the presence and absence of varying concentrations of Zn by determining the Minimum Inhibitory Concentration (MIC), defined as the concentration at which no visible growth is observed (Wiegand *et al.*, 2008). A standardised protocol was established to determine the MIC based on the guidelines of the Clinical Laboratory Standards Institute [CLSI] (CLSI, 2015). In the absence of additional Zn, 32 μM PBT2 inhibited growth of *S. pneumoniae*^{Spain23F} (Table 5.3). In this assay format, no growth inhibition was observed following treatment with 8-64 μM Zn, either alone, or in combination with a vehicle control (data not shown). However, as anticipated, treatment with these sub-inhibitory Zn concentrations reduced the MIC of PBT2. The MIC of PBT2 in combination with 8, 16 and 32 μM Zn was reduced by 2-fold compared to without Zn, while 64 μM Zn reduced the MIC by 4-fold. As the inhibitory concentrations of Zn and PBT2 were defined, the impact of a sub-inhibitory concentration on antibiotic susceptibility was assessed. A sub-inhibitory combination of 32 μM Zn and 8 μM PBT2 (Zn-PBT2) was selected based on a lack of visible growth inhibition, corresponding to a concentration of PBT2 2-fold lower than the MIC with 32 μM Zn. The impact of sub-inhibitory Zn-PBT2 on pneumococcal survival in combination with penicillin, ampicillin, gentamicin, chloramphenicol and tetracycline was assessed. Interestingly, by comparison with untreated cells, *S. pneumoniae*^{Spain23F} treated with the sub-inhibitory concentration Zn-PBT2 displayed higher colony forming units (CFU) at the conclusion of the assay ($P < 0.05$, two-tailed unpaired *t*-test). Consistent with the antibiotic resistance profile of *S. pneumoniae*^{Spain23F}, at the concentrations tested, treatment with these antibiotics alone did not significantly alter the bacterial survival (Figure 5.4A-E). However, pneumococci treated with sub-inhibitory Zn-PBT2 displayed a significantly reduced survival

Table 5.3 PBT2 minimum inhibitory concentrations for the *S. pneumoniae*^{Spain23F} strain in the presence and absence of zinc

Zn concentration (μM)	Minimum inhibitory concentration (μM)
	PBT2
0	32
8	16
16	16
32	16
64	8

PBT2, PBT2.2HCl; Zn, $ZnSO_4$. Minimum inhibitory concentrations were determined according to the Clinical Laboratory Standard Institute Guidelines (CLSI, 2015).

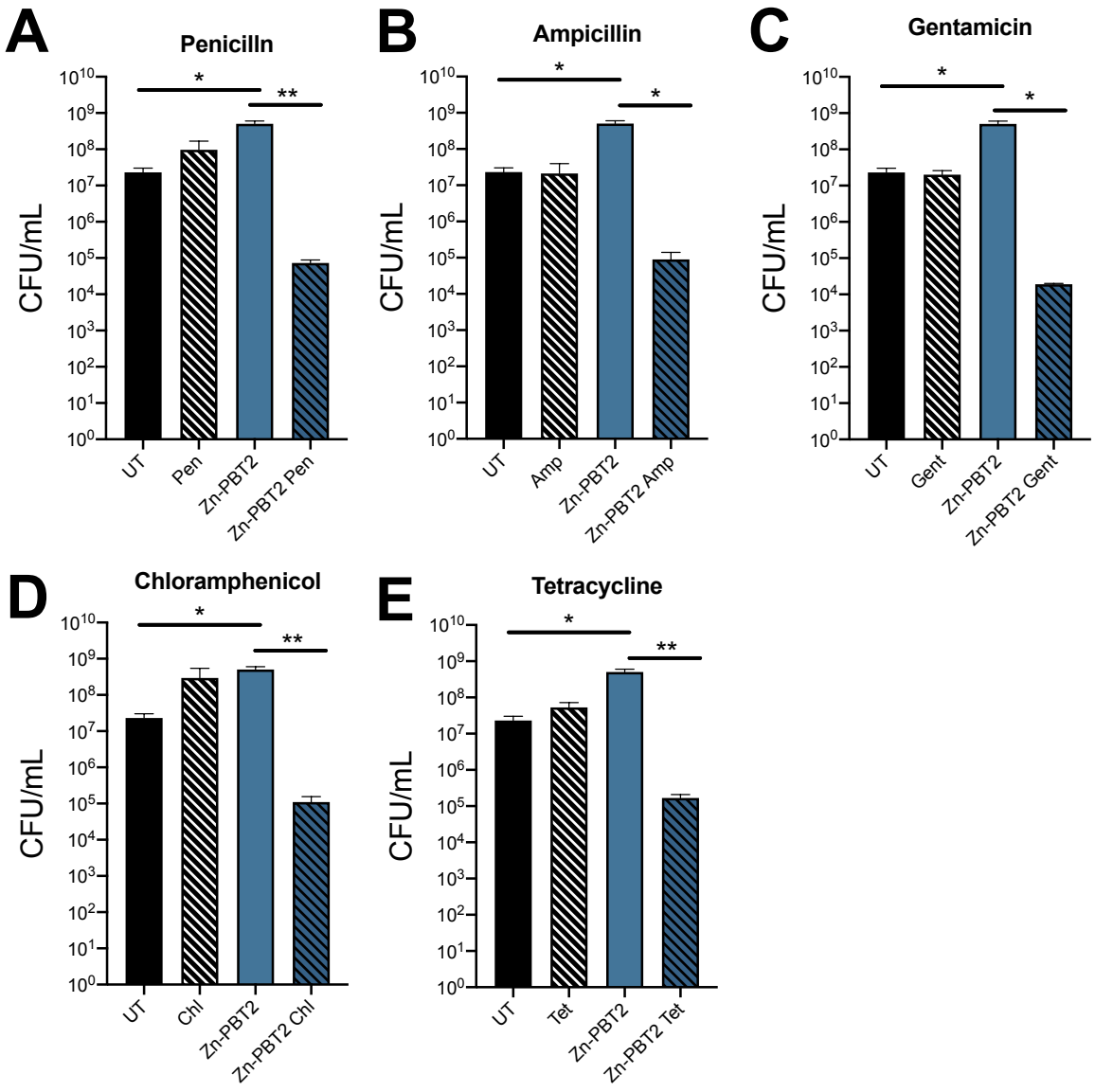


Figure 5.4 Treatment with sub-inhibitory zinc and PBT2 reduces survival of *S. pneumoniae*^{Spain23F} ST81 strain in the presence of antibiotics

Mueller Hinton broth with 5% lysed horse blood was inoculated with *S. pneumoniae*^{Spain23F} from overnight agar plates with or without supplementation with 8 μM PBT2.2HCl and 32 μM $ZnSO_4$. Suspensions were added to a series of 2-fold dilutions of (A) Pen; 1 mg/ml penicillin, (B) Amp; 4 mg/ml ampicillin, (C) Gent; 4 mg/ml gentamicin, (D) Chl; 2 mg/ml chloramphenicol, and (E) Tet; 16 mg/ml tetracycline, and incubated at 37 °C for 18 hrs. The bacterial survival was assessed by enumerating the colony forming units (CFU) by serial dilution and plating on blood agar plates. Data are the mean ± SEM, n ≥ 3 biological replicates. Statistical significance was assessed using the Student's two-tailed *t*-test, where * represents $P < 0.05$, and ** represents $P < 0.01$.

following treatment with penicillin ($P < 0.01$, two-tailed unpaired *t*-test; Figure 5.4A), ampicillin ($P < 0.05$, two-tailed unpaired *t*-test; Figure 5.4B), gentamicin ($P < 0.01$, two-tailed unpaired *t*-test; Figure 5.4C), chloramphenicol ($P < 0.01$, two-tailed unpaired *t*-test; Figure 5.4D) and tetracycline ($P < 0.01$, two-tailed unpaired *t*-test; Figure 5.4E). To assess the significance of these findings, the change in antibiotic MIC upon treatment with sub-inhibitory Zn-PBT2 was assessed (Table 5.4). Treatment with Zn, PBT2 or the vehicle control, either singly or in combination did not alter the MIC of penicillin, ampicillin, chloramphenicol or tetracycline. The MIC of penicillin for *S. pneumoniae*^{Spain23F} following the addition of Zn-PBT2 resulted in a 4-fold decrease in the MIC of penicillin. A similar trend was observed for ampicillin, whereby the MIC reduced by 8-fold upon Zn-PBT2 treatment. Treatment with Zn-PBT2 also dramatically decreased the MIC of the protein synthesis-targeting antibiotics. Treatment of *S. pneumoniae*^{Spain23F} with Zn-PBT2 induced a 32-fold decrease in the MIC of chloramphenicol and 16-fold reduction in the MIC of tetracycline. Interestingly, the results for gentamicin were distinct from the other antibiotics tested. The MIC of gentamicin was unchanged upon treatment Zn, the vehicle control, or the combination of Zn and a vehicle control. However, the addition of PBT2 resulted in a substantial decrease in the MIC of gentamicin by 16-fold, while treatment with Zn-PBT2 induced a 64-fold reduction in the MIC. Collectively, Zn-PBT2 treatment increased the susceptibility of *S. pneumoniae*^{Spain23F} to a range of antibiotic classes and most substantially to gentamicin by PBT2 with or without the addition of Zn.

5.2.4 The impact of zinc and PBT2 treatment on pneumococcal disease

Zn-PBT2 treatment increased bacterial cellular Zn while also reducing the amount of antibiotic required to inhibit growth *in vitro*. Although oral PBT2 administration has been investigated for the treatment of Alzheimer's Disease in murine models (doses of 10 or 30 mg/kg/day), the intraperitoneal (IP) administration of Zn in combination with PBT2 during bacterial infection had not yet been investigated (Adlard *et al.*, 2011; Adlard *et al.*, 2008). Here, the impact of Zn-PBT2 administration on weight loss, bacterial burden, and the capacity to induce bacterial Zn toxicity in a murine pneumococcal infection model was explored. Four-week-old Swiss mice were intranasally challenged with 2×10^7 CFU of *S. pneumoniae* D39 and treated with 8 mg/kg/day PBT2 and 0.25 mg/kg/day $ZnSO_4$ or a vehicle control for 48 hrs. As PBT2 was administered systemically with Zn in the present study, the dosage of PBT2 was

Table 5.4 Antibiotic minimum inhibitory concentrations for *S. pneumoniae*^{Spain23F} with sub-inhibitory zinc and PBT2

	Minimum inhibitory concentration (µg/ml)				
	Pen	**Amp**	**Chl**	**Tet**	**Gent**
Untreated	2	8	32	16	64
32 µM Zn	2	8	32	16	64
Vehicle	2	8	32	16	64
Vehicle + 32 µM Zn	2	8	32	16	64
8 µM PBT2	2	8	32	16	4
8 µM PBT2 + 32 µM Zn	0.5	1	1	2	1

Vehicle, dimethyl sulfoxide; Pen, penicillin; Amp, ampicillin; Gent, gentamicin; Chl, chloramphenicol; Tet, tetracycline; PBT2, PBT2.2HCl; Zn, $ZnSO_4$. Minimum inhibitory concentrations were determined according to the Clinical Laboratory Standard Institute Guidelines (CLSI, 2015).

reduced compared to previous studies (Adlard *et al.*, 2011; Adlard *et al.*, 2008). The body weight of each mouse was monitored during the course of disease to assess the impact of the Zn-PBT2 administration. No significant difference in body weight was observed for mice treated with Zn and PBT2 compared with the vehicle control (Figure 5.5). The bacterial burden and induction of Zn toxicity was also examined. Zn levels have been shown to increase in host niches upon infection in the blood and lungs, and the spleen is a niche with a high density of immune cells and may exploit Zn toxicity as an antimicrobial measure (McDevitt *et al.*, 2011; Ong *et al.*, 2014). As a result, the impact of Zn-PBT2 on pneumococci in the blood, lungs and spleen was assessed. The pneumococcal disease burden was examined at 48 hrs post infection by enumerating the colony forming units (CFU) in the blood, lungs and spleen (Figure 5.6). Mice treated with Zn-PBT2 showed no significant differences in disease burden compared to the vehicle control in the blood, lungs, or spleen. In parallel, the capacity of Zn-PBT2 treatment to induce bacterial Zn stress *in vivo* was assessed by measuring the expression levels of the pneumococcal Zn-responsive genes. At 48 hrs post infection, following treatment with Zn-PBT2 or a vehicle control, pneumococci were harvested from the blood, lungs and spleen, and the RNA was extracted. The expression of *czcD,* the gene encoding the Zn efflux protein that is expressed under Zn toxicity was used as a marker of Zn stress. No significant changes in *czcD* transcription in the blood, lungs, or spleen were observed following treatment of the mice with Zn-PBT2 compared with the vehicle control (Figure 5.7A). The expression of *phtE*, a gene that encodes a component of the Zn uptake pathway that is expressed under Zn limitation was also assessed. While no significant change was observed in the lungs, transcription of this gene was increased upon Zn-PBT2 treatment in the blood ($P < 0.01$, two-tailed unpaired *t*-test) and spleen ($P < 0.05$, two-tailed unpaired *t*-test) (Figure 5.7B). Collectively, these studies indicate that Zn-PBT2 treatment did not modulate Zn abundance in the lungs and elicited a pneumococcal Zn starvation response in the blood and spleen. Thus, at the concentrations used in this study, Zn-PBT2 IP administration did not induce pneumococcal Zn intoxication *in vivo*.

5.2.5 *In vivo* studies of PBT2 and gentamicin treatment

The *in vitro* studies revealed that PBT2 treatment significantly increased the susceptibility of *S. pneumoniae*^{Spain23F} to gentamicin. This suggests that the enhanced susceptibility arises via an alternative, Zn independent mechanism. Building on the above framework, the impact of PBT2 administration on pneumococcal gentamicin susceptibility in

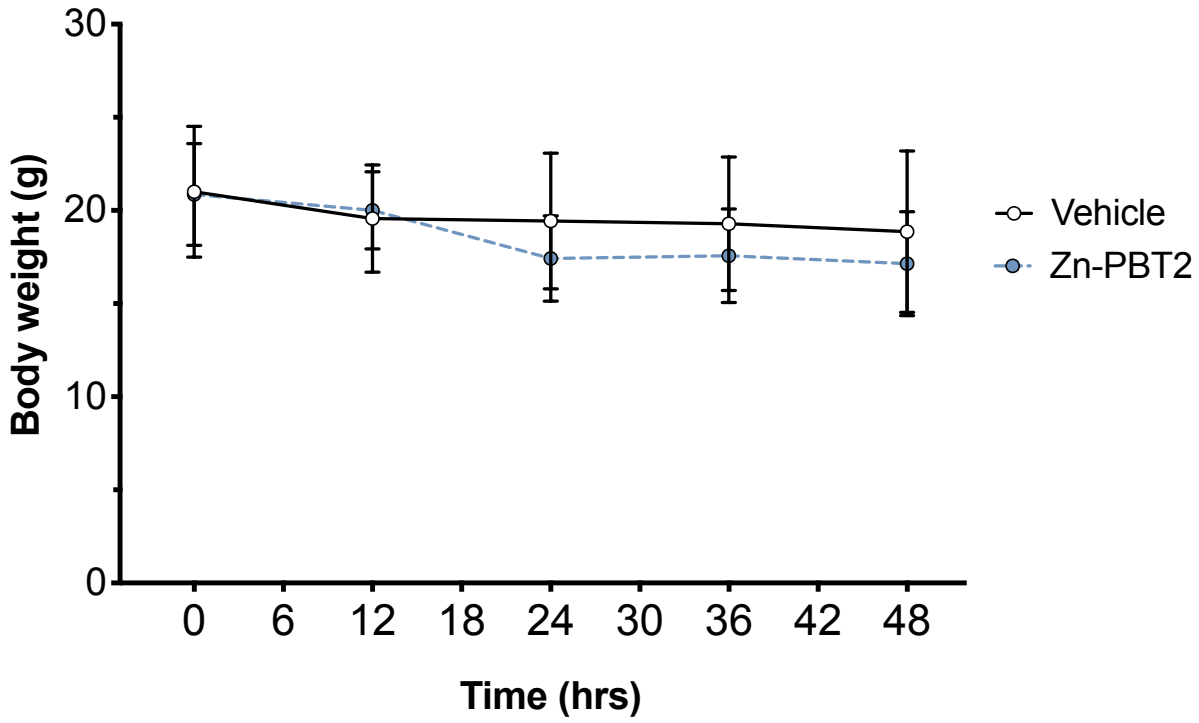


Figure 5.5 Changes in body weight induced by treatment with zinc and PBT2 treatment during *S. pneumoniae* infection

Mice were intranasally challenged with *S. pneumoniae* D39 and treated with IP administration of either 8 mg/kg/day PBT2.2HCl and 0.25 mg/kg/day $ZnSO_4$ (Zn-PBT2) or a vehicle control (phosphate buffered saline [PBS] and dimethyl sulfoxide [DMSO]). Body weight was measured prior to infection and monitored at 12 hr intervals for 48 hrs post challenge. Data points are the average weight in grams of the mice from each treatment group and lines depict the change in weight over time, from n = 7 mice per group. Statistical significance was assessed using the Student's two-tailed paired *t*-test.

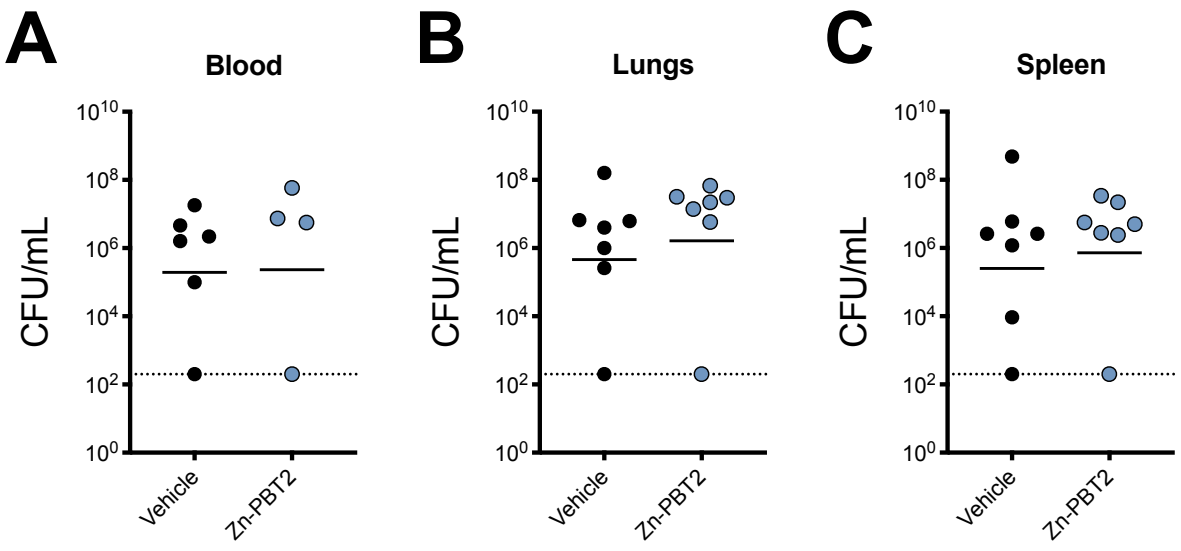


Figure 5.6 Impact of zinc and PBT2 treatment on *S. pneumoniae* infection

Mice were intranasally challenged with *S. pneumoniae* D39 and treated with IP administration of either 8 mg/kg/day PBT2.2HCl and 0.25 mg/kg/day $ZnSO_4$ (Zn-PBT2) or a vehicle control (phosphate buffered saline [PBS] and dimethyl sulfoxide [DMSO]). Bacterial colony forming units (CFU) were enumerated at 48 hrs post challenge in the (A) blood, (B) lungs, and (C) spleen. Replicate data are the CFU values from each tissue sample, the solid lines denote the geometric means of each group, and the dashed lines indicate the limit of detection. Statistical significance was assessed using the Student's two-tailed *t*-test.

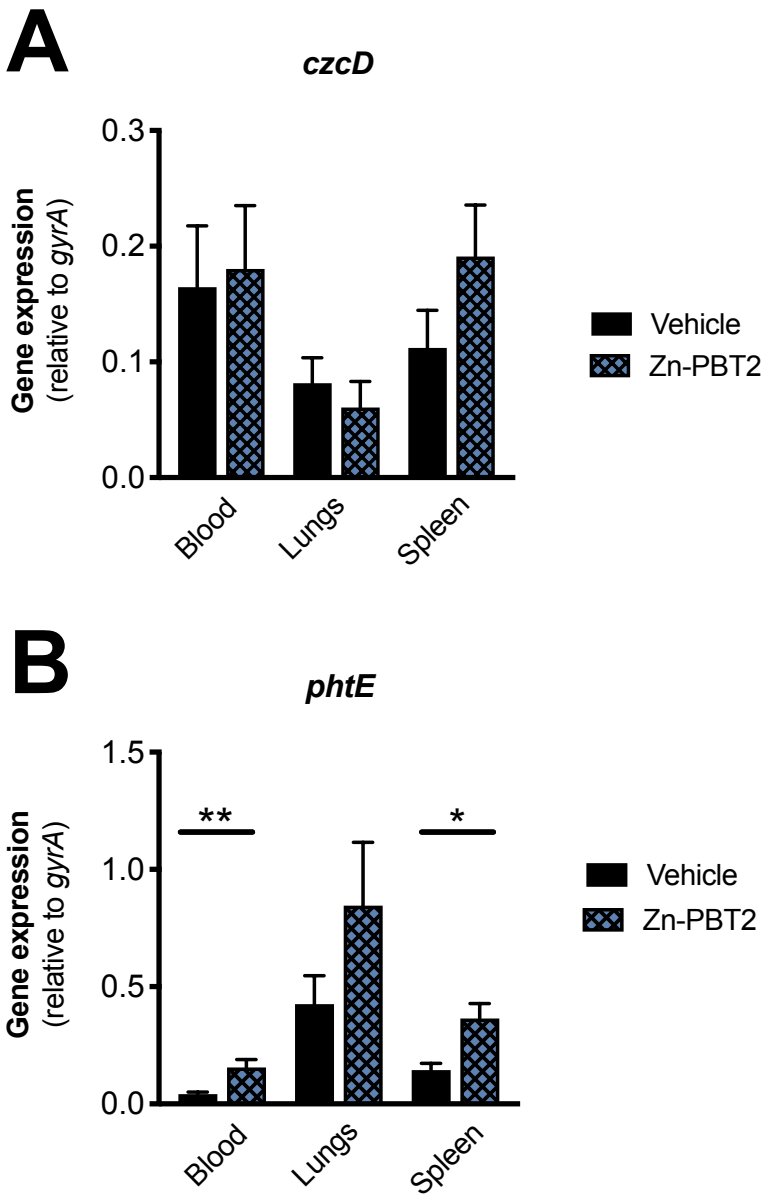


Figure 5.7 Impact of zinc and PBT2 treatment on transcription of *S. pneumoniae* zinc-responsive genes during infection

Mice were intranasally challenged with *S. pneumoniae* D39 and treated with IP administration of either 8 mg/kg/day PBT2 and 0.25 mg/kg/day $ZnSO_4$ (Zn-PBT2) or a vehicle control (phosphate buffered saline [PBS] and dimethyl sulfoxide [DMSO]). At 48 hrs post challenge, the blood, lungs, and spleen were collected, and the RNA was extracted. Transcription of *czcD* (SPD_1638) and *phtE* (SPD_0890) mRNA was determined by quantitative reverse transcription-PCR relative the transcription of the *gyrA* (SPD_1077). Data are the mean + SEM, n ≥ 6. Statistical significance was assessed using the Student's two-tailed *t*-test, where * represents $P < 0.05$ and ** represents $P < 0.01$.

the *S. pneumoniae* D39 murine infection model was investigated. First, the change in the MIC of gentamicin in the presence of PBT2 was examined for the *S. pneumoniae* D39 strain (Table 5.5). Compared to the *S. pneumoniae*^{Spain23F} strain, *S. pneumoniae* D39 possesses a lower MIC of 16 μg/ml. Treatment of this strain with a vehicle control and Zn, singly or in combination did not alter the MIC. However, treatment with PBT2 reduced the MIC by 4-fold, while Zn-PBT2 decreased the MIC by 8-fold. To examine the impact of PBT2 on gentamicin efficacy, mice were intranasally challenged with 2×10^7 CFU of *S. pneumoniae* D39 and treated with a vehicle control, 8 mg/kg/day PBT2, 40 mg/kg/day gentamicin, or PBT2 and gentamicin in combination for 48 hrs. The pneumococcal disease burden was assessed by enumerating the CFU in the blood, lungs, spleen, brain, and liver (Figure 5.8A-E). Treatment of the infected mice with gentamicin revealed niche-dependent impacts. Gentamicin treatment significantly reduced the bacterial burden in the blood ($P < 0.01$, two-tailed unpaired *t*-test; Figure 5.8A), spleen ($P < 0.01$, two-tailed unpaired *t*-test; Figure 5.8C) and liver ($P < 0.01$, two-tailed unpaired *t*-test; Figure 5.8E). In contrast, gentamicin treatment did not alter the disease burden in the lungs (Figure 5.8B) or the brain (Figure 5.8D). Similar to the findings for Zn-PBT2, treatment with PBT2 alone did not significantly alter the bacterial burden in any of these niches. Similarly, no significant difference was observed between the mice treated with gentamicin alone, compared with gentamicin and PBT2. This indicates that PBT2 does not enhance the efficacy of gentamicin *in vivo* at the concentrations tested. Further, despite the decrease in bacterial burden upon gentamicin treatment, a significant reduction in bacterial burden for mice treated with PBT2 and gentamicin was only observed in the blood ($P < 0.01$, two-tailed unpaired *t*-test; Figure 5.8A) and not the spleen (Figure 5.8C) or liver (Figure 5.8E). Therefore, at the concentrations used in this study, PBT2 treatment did not enhance pneumococcal susceptibility to gentamicin in *vivo*.

Table 5.5 Gentamicin minimum inhibitory concentrations for *S. pneumoniae* D39 with sub-inhibitory zinc and PBT2 treatment

	Minimum inhibitory concentration (µg/ml)
	Gentamicin
Untreated	16
32 µM Zn	16
Vehicle	16
Vehicle + 32 µM Zn	16
8 µM PBT2	4
8 µM PBT2 + 32 µM Zn	2

Vehicle, dimethyl sulfoxide; PBT2, PBT2.2HCl; Zn, $ZnSO_4$. Minimum inhibitory concentrations were determined according to the Clinical Laboratory Standard Institute Guidelines (CLSI, 2015).

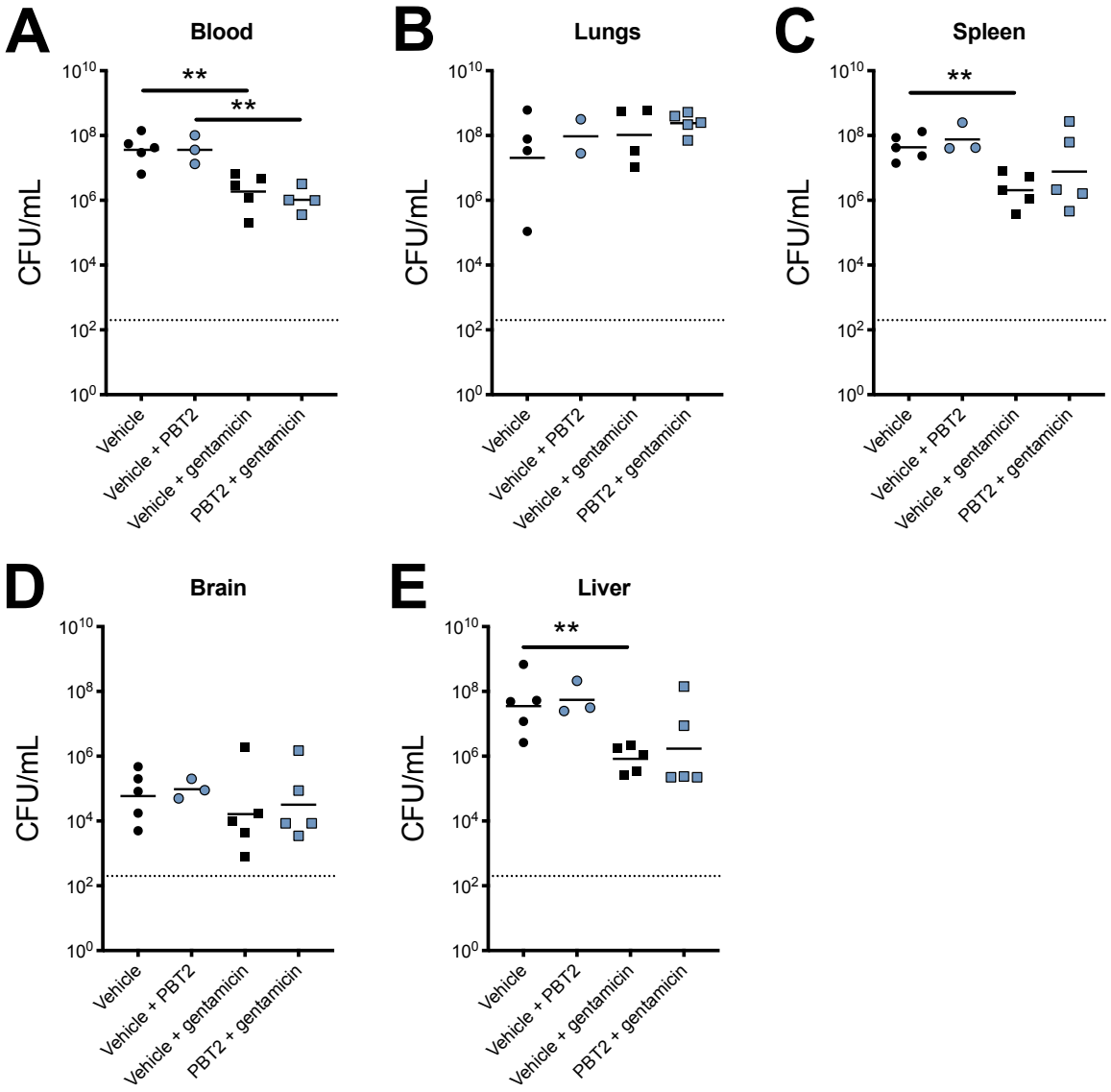


Figure 5.8 Host infection of *S. pneumoniae* following PBT2 and gentamicin treatment

Mice were intranasally challenged with *S. pneumoniae* D39 and treated with IP administration of 8 mg/kg/day PBT2.2HCl, or a vehicle control (Dimethyl sulfoxide), either individually, or in combination with 40 mg/kg/day gentamicin sulphate. Bacterial colony forming units (CFU) were enumerated at 48 hrs post challenge in the blood (A), lungs (B), spleen (C), brain (D) and liver (E). Replicate data are the CFU values from each tissue sample, the solid lines denote the geometric means of each group, and the dashed lines indicate the limit of detection. Statistical significance was assessed using the Student's two-tailed *t*-test, where ** represents $P < 0.01$.

5.3. Discussion

Antibiotic treatment failure is an urgent issue facing medicine. As rates of resistance to antibiotics rise, so too do the inherent risks associated with a range of medical procedures. Despite efforts towards the development of new antibacterial drugs, the deployment of novel antibiotics from conception to the clinic is a costly process requiring years of clinical trials. Repurposing existing drugs to target drug resistant pathogens may circumvent many of the challenges associated with the development of new drugs, such as the cost of Phase I trials and toxicity issues. The previous chapter showed that that high intracellular Zn levels disrupt cell wall biosynthesis and enhance the susceptibility of pneumococci to penicillin. These data highlight the therapeutic potential of Zn and antibiotics as a combination antimicrobial treatment strategy. The previous chapter also highlighted that the impact of Zn is multifactorial. Thus, these data suggested that the action of a wide range of antibiotics may be augmented by high intracellular Zn. The present study explored novel Zn-based therapeutic strategies for their potential to enhance the action of a range of antibiotics *in vitro* and *in vivo.*

The Zn export protein, CzcD, represented a possible candidate to induce bacterial Zn toxicity in *S. pneumoniae*. In a previous chapter, the importance of this protein in resisting high intracellular Zn levels was demonstrated. It was shown that *S. pneumoniae* incapable of Zn efflux via CzcD accumulated significantly more Zn than wild-type and displayed a heightened sensitivity to penicillin. In this chapter, to investigate the feasibility of targeting CzcD, the level of conservation between human and *S. pneumoniae* Zn-transporting CDF proteins was assessed. Bioinformatic studies showed a high degree of homology between these proteins, which emphasized potential specificity issues associated with the design of inhibitors targeting pneumococcal CzcD. The mammalian Zn transporters, ZnT4, ZnT5, ZnT8 and ZnT10, displayed high levels of overall sequence similarity with *S. pneumoniae* CzcD spanning a considerable proportion of CzcD. These human Zn transporters are localised to the lysosomes, endosomes, Golgi apparatus and intracellular vesicles, functioning to redistribute Zn stores among intracellular organelles (Bosomworth *et al.*, 2012; Chimienti *et al.*, 2004; Jackson *et al.*, 2007; McCormick & Kelleher, 2012; Ranaldi *et al.*, 2002). Thus, the potential cross-reactivity of inhibitors with these human ZnT proteins may have significant impacts. Mutations in these proteins have been associated with several pathologies. For example, a missense mutation in ZnT8 has been associated with an increased risk of developing type 2 diabetes (Sladek *et al.*, 2007), while frameshift, missense and nonsense mutations have been observed in ZnT10, which

have been associated with Parkinsonism and dystonia (Quadri *et al.*, 2012). Effective inhibitors must exhibit a high degree of specificity; however, the design of inhibitors targeting conserved regions of CzcD is hindered by a lack of detailed structural and functional information. While a previous study has characterised the role of the metal-binding residues in Zn resistance (Martin & Giedroc, 2016), the contribution of residues outside these metal-binding sites to transport remain poorly understood. The metal-binding residues of CzcD also exhibited a high degree of conservation in mammalian CDF transporters, with all but one Zn-binding residue of CzcD (Asn222) aligning with one or more of the human ZnT proteins. However, a previous study has shown that mutation of CzcD Asn222 does not alter the Zn resistance profile of *S. pneumoniae* (Martin & Giedroc, 2016), which indicates that this residue is dispensable for the function of CzcD. Overall, this indicates that the metal binding sites may not be suitable target regions for an inhibitor and that a selective inhibitor must bind in a region distinct from these residues. Excluding a number of CDF signature motifs that are present across species (Montanini *et al.*, 2007), CDF proteins generally exhibit a relatively low level of overall homology. However, the lack of conservation outside the metal binding sites may be an indicator of their dispensability. Attempts in the present study to identify regions conserved among prokaryotic CDF proteins, but absent in mammalian ZnT proteins yielded no candidate regions. While the similarity between *S. pneumoniae* CzcD and several of the human Zn-transporting CDF proteins raised issues of selectivity, sequence-based studies provide only limited information. Future studies providing detailed structural insight into CzcD and the mammalian ZnT proteins may enable the design of highly specific inhibitors of CzcD. A small molecule screening process may be employed to identify inhibitors that have the capacity to bind CzcD, which could be tested experimentally for inhibition of CzcD and for a lack of cross-reactivity towards mammalian cells. A small molecule screen has been applied for the identification of an inhibitor of the human metal-proton cotransporter protein, divalent metal transporter 1 (DMT1) (Buckett & Wessling-Resnick, 2009). DMT1 is primarily an Fe uptake protein in humans that has a critical role in mediating the uptake of Fe in the small intestine. While these inhibitor screens were performed to identify tools for the study of Fe transport, a similar approach may be employed to identify CzcD inhibitors for use as therapeutics.

In view of issues associated with CzcD inhibitors, an alternative Zn-modulating strategy was examined. In this study, PBT2, an ionophore initially developed for AD, showed promising *in vitro* results. Crucially, treatment with Zn-PBT2 induced similar levels of cellular Zn to those of the Δ*czcD* mutant incapable of Zn efflux. These findings indicate that PBT2 can be

successfully repurposed to increase pneumococcal cellular Zn levels *in vitro*. Consistent with the findings of the previous chapter for the efflux-deficient mutant, PBT2-induced Zn overload successfully augmented the action of antibiotics *in vitro*. The present study showed that Zn-PBT2 treatment altered the antibiotic resistance profile of the multidrug resistant *S. pneumoniae*^{Spain23F} strain. The reduction in MIC observed upon PBT2-induced Zn overload indicates that this strategy may alter treatment outcomes. While no data are available for ampicillin and gentamicin, Zn-PBT2 treatment shifts the MIC of penicillin and tetracycline against *S. pneumoniae*^{Spain23F} into the intermediate range, while chloramphenicol shifts into the susceptible range, as defined by CLSI (CLSI, 2015). This indicates that Zn-PBT2 treatment may significantly improve responses to chloramphenicol, while treatment outcomes for penicillin and tetracycline may exhibit a degree of variation. However, the MIC interpretive criteria provide only limited insight into the utility of Zn-PBT2 to alter antibiotic treatment outcomes, which necessitates the validation of this approach in the treatment disease.

Initial studies of the *in vivo* capacity of PBT2 to modulate pneumococcal Zn levels highlight the complexity associated with this drug combination strategy. The efficacy of Zn-PBT2 as a cotreatment with antibiotics is dependent on the successful delivery of these drugs to the sites of infection. Although PBT2 treatment in the absence of Zn has been studied in humans and murine AD models, these studies are focused primarily on the brain. Furthermore, the application of these findings in the present study is hindered by differences in treatment time and administration route (Adlard *et al.*, 2011; Adlard *et al.*, 2008). In the present study, no significant differences in body weight were observed following the administration of Zn-PBT2 compared with the vehicle control during infection, indicating that this treatment was well-tolerated in mice. At a cellular level, bacteria primarily rely on the efflux of Zn out of the cell, while eukaryotic cells can efflux and redistribute Zn within subcellular compartments. Thus, it is likely that despite the lack of specificity exhibited by ionophores towards bacteria, eukaryotic cells may have a greater propensity to overcome ionophore-induced Zn toxicity. The expression of pneumococcal Zn efflux and uptake genes provided insight into the induction of Zn toxicity in each niche. At the concentrations tested, this study suggests that Zn-PBT2 did not increase Zn levels of pneumococci during disease. Rather, these data showed that Zn-PBT2 treatment induced a Zn starvation response in the blood and spleen, which indicates that PBT2 may be acting as a chelator in these niches. These findings may be attributable to a lack of colocalization of Zn-PBT2 within these tissues, an inappropriately skewed ratio of Zn-PBT2 administration, or the preferential redistribution of Zn into human cells, such that the impact on

pneumococci is diminished. Previous studies of topical Zn-PBT2 treatment have shown enhancement of antibiotic efficacy in wound infection models, which demonstrates that this approach can be effective if colocalization occurs (Bohlmann *et al.*, 2018). The findings presented in this chapter highlight that systemic use of this treatment strategy is associated with further complexities, but revealed insight into key challenges. Although distinct from the desired outcome, the upregulation of the Zn uptake pathway indicates that the PBT2 is reaching the blood and spleen tissues. This suggests that Zn is likely the limiting factor and that increasing the Zn levels in tissues may improve the pneumococcal Zn-loading capacity of PBT2 *in vivo*. While the present study administered Zn via the IP route, analyses of pneumococci *in vivo* following oral Zn-PBT2 administration may be used to assess the influence of administration route on pneumococcal Zn-responsive genes. Furthermore, the development of novel PBT2 derivatives to alleviate potential Zn colocalization issues and improve the tissue distribution may enhance the *in vivo* efficacy of this treatment strategy.

Although the accumulation of Zn is likely the major contributor to the observed enhanced sensitivity, the improved gentamicin susceptibility indicates that PBT2 alone also has the potential to induce physiological changes. While gentamicin is not used as a treatment for pneumococcal disease, studies have shown that the activity of this antibiotic can be enhanced following treatment with compounds that alter cell wall integrity, such as penicillin (Darras-Joly *et al.*, 1996; Tateda *et al.*, 1999). It is possible that PBT2 interacts with the cell wall or membrane, which may be responsible for the improved gentamicin efficacy. However, the molecular basis for the interaction between PBT2 and gentamicin against pneumococci remains poorly understood. Future studies, such as the assessment of the transcriptomic profile and cell permeability of PBT2-treated pneumococci may reveal distinct changes induced in the presence of PBT2. Despite an interaction between PBT2 and gentamicin *in vitro*, this was not reflected in the *in vivo* studies. This may be a consequence of inadequate concentrations reaching the sites of infection. However, the upregulation of the Zn uptake pathway upon Zn-PBT2 treatment in the blood and spleen indicates that PBT2 is reaching these tissues. Future studies to optimise the PBT2 administration route and dosage to maximise tissue distribution may lead to improved treatment outcomes with gentamicin.

Understanding the mechanism behind the Zn-dependent improvement in antibiotic susceptibility may also help to improve provide insight into the broader applications of this treatment strategy. The previous chapter revealed that Zn treatment depleted cell wall

biosynthesis metabolites, impaired GlmU function and rendered *S. pneumoniae* more susceptible to penicillin. These data indicate that Zn is acting independently of the resistance pathway to increase antibiotic susceptibility. The *S. pneumoniae*^{Spain23F} strain possesses altered penicillin binding proteins (PBPs), which reduces the affinity of penicillin for its target. Despite the alterations in PBPs, a similar trend in penicillin survival was observed between the Zn-overloaded drug resistant *S. pneumoniae*^{Spain23F} strain and the sensitive *S. pneumoniae* D39 strain. Furthermore, as GlmU is a highly conserved bacterial protein, it is possible that this treatment strategy may extend to other bacterial species. Further collaborative studies have examined the broad utility of this treatment strategy in a range of other clinically significant bacterial pathogens (Bohlmann *et al.*, 2018). This work revealed that Zn-PBT2 substantially reduced the MIC of a range of antibiotic classes, including a range of cell wall targeting antibiotics. Interestingly, this work indicates that there may be mechanistic differences in the mode of action of Zn. For example, the MIC of oxacillin and ampicillin were reduced by 64-fold in the *S. aureus* USA300 strain when treated with Zn-PBT2 (Bohlmann *et al.*, 2018). However, Zn-PBT2 only marginally reduced the MIC (2-fold) of these cell wall-targeting antibiotics against the *S. pyogenes* HKU16 strain and the *Enterococcus faecium* RBWH1 strain. As these vast differences induced by Zn-PBT2 may be due to differences in the interaction between Zn and GlmU, the primary sequences of GlmU from these bacteria were examined. The previous chapter showed that in *S. pneumoniae*, Zn bound GlmU at Glu315 and His330. Surprisingly, while Glu315 and His330 were conserved between *S. pneumoniae, S. pyogenes* and *E. faecium, S. aureus* possessed asparagine and glutamine residues at these sites (Appendix 8). Although instances of Zn coordination have been observed via asparagine residues, it is less common than residues, such as histidine, glutamine and aspartate. Further studies are required to determine whether Zn is capable of binding at this site or altering the acetyltransferase activity of *S. aureus* GlmU. Nevertheless, it is possible that the enhanced susceptibility of *S. aureus* USA300 to oxacillin and ampicillin may occur via an alternative mechanism. Overall, while the interaction between Zn, GlmU and the susceptibility to β-lactam antibiotics is evident in *S. pneumoniae*, the mechanism in other species is unclear and warrants further investigation.

Collectively, the present study showed that ionophore-mediated Zn overload enhanced the efficacy of cell wall and protein synthesis-targeting antibiotics *in vitro*. Although this treatment did not induce bacterial Zn overload *in vivo*, this proof-of-concept study provides a foundation for future studies to optimise this strategy and improve the *in vivo* interaction of Zn-ionophores with antibiotics.

CHAPTER 6: Final Discussion

This thesis describes the characterisation of the Zn resistance pathway in *S. pneumoniae*, defines novel targets of Zn toxicity, and highlights a drug-repurposing approach to harness the toxicity of Zn, thereby heightening the sensitivity of *S. pneumoniae* to antibiotics.

6.1 The role of CzcD in *S. pneumoniae* zinc resistance

The generation of a model structure of CzcD based on YiiP from *E. coli*, revealed a number of negatively charged regions that likely accommodate the binding of a metal ion. Analyses of the primary sequence of CzcD identified several putative metal-binding residues that align with the metal-binding residues of YiiP. With the exception of Asn222, these residues have since been shown to be critical for Zn resistance (Martin & Giedroc, 2016). Although largely absent in *E. coli* YiiP, *S. pneumoniae* CzcD also possesses a large number of putative Zn-binding histidine, aspartate, and glutamate residues in its cytoplasmic CTD that may contribute to CzcD function, possibly in the recruitment of cytoplasmic Zn to the transporter, which warrants further investigation. These findings have broader implications for the function of CDF proteins. Although YiiP is the only CDF for which structural data is available, the possibility that other CDF family members employ distinct mechanisms of metal ion transport cannot be excluded. Although *czcD* is upregulated in response to Zn, Co, Cd and Ni, the substrates of CzcD are restricted to Zn and Co (Begg *et al.*, 2015; Kloosterman *et al.*, 2007). The exclusion of Cd as a substrate of CzcD is most likely attributable the most N-terminal histidine residue of metal binding site A, as was observed for *E. coli* YiiP upon mutation of this aspartate residue to histidine (Hoch *et al.*, 2012). *E. coli* YiiP and *S. pneumoniae* CzcD possess a similar tetrahedral geometry at metal-binding site A. However, the steric bulk of the histidine residue may contribute to the selectivity of CzcD towards Zn and Co. As a host-adapted organism, it is unlikely that there is selective pressure for evolution of Cd resistance, as Cd is not a physiological metal ion commonly found in the host environment. Accordingly, the majority of the human ZnT transporters also possess the same HD-HD site A motif as *S. pneumoniae* CzcD. The exclusion of Cd efflux via CzcD renders the pneumococcus particularly susceptible to Cd toxicity due to its capacity to deplete cellular Zn stores by inducing the expression of *czcD,* presumably via SczA (Begg *et al.*, 2015). Further biochemical, structural and mutational analyses are required to determine the mechanism of metal transport by CzcD.

The work presented herein highlights that efflux of Zn via CzcD is critical for *S. pneumoniae* to achieve fine homeostatic balance of intracellular Zn. The antibacterial action of Zn is facilitated by the mobilisation of Zn in phagocytic cells. Consistent with findings in other bacterial species, *S. pneumoniae* CzcD was critical for survival in macrophages (Botella *et al.*, 2011; Kapetanovic *et al.*, 2016; Ong *et al.*, 2014). These findings are similar to the decreased survival observed for an isogenic *sczA* deletion strain, which lacks the capacity to upregulate *czcD* (Martin *et al.*, 2017). This indicates that pneumococci are exposed to high concentrations of Zn in the macrophage environment, although the precise concentrations of Zn encountered remain unknown. Insights into the abundance of Zn are hindered a lack of tractable methods to spatially quantify labile cellular Zn concentrations. Total Zn levels in macrophages infected with *S. pneumoniae* may be assessed by ICP-MS; however, this method would be unable to reveal the cellular localisation of Zn or discern labile Zn from Zn tightly associated with host proteins (Winters *et al.*, 2010). Zn-responsive fluorophores have been used to track Zn mobilisation in macrophages in response to the uptake of other bacterial species. However, these are limited by their relative affinity for the metal ion and are not strictly selective for Zn (Botella *et al.*, 2011; Kapetanovic *et al.*, 2016; Ong *et al.*, 2014). Although future studies may use Zn-responsive fluorophores to visualise the flux of Zn in the phagolysosome upon *S. pneumoniae* uptake, it is difficult to translate these observations to infer the relative toxicity imparted upon internalised pneumococci. An alternative method to investigate the impact of macrophage Zn mobilisation on bacteria is via fluorescent reporter strains responsive to bacterial Zn abundance (Stocks *et al.*, 2019). Future studies to address this could be achieved by the introduction of fluorescent signals at Zn-responsive genes, such as a fusion to the *czcD* promotor region, to monitor the intracellular abundance of Zn in *S. pneumoniae* following uptake by macrophages. Nevertheless, this work suggests that the mobilisation of Zn in macrophages is sufficient to raise the labile cytoplasmic Zn levels in *S. pneumoniae* such that the deployment of CzcD is required. The importance of Zn in macrophage-mediated clearance of *S. pneumoniae* may provide a basis for the increased susceptibility to respiratory disease associated with dietary Zn deficiency (Bahl *et al.*, 1998; Black & Sazawal, 2001). In accordance with this hypothesis, recent work showed that dietary Zn contributed to the control of pneumococcal disease in mice and demonstrated that PMN Zn status and function, but not recruitment, was impaired in Zn-deficient mice (Eijkelkamp *et al.*, 2019). Despite the importance of Zn at the host-pathogen interface, the pathways affected and thus the basis for its antibacterial action against *S. pneumoniae* remained poorly defined.

6.2 The cellular targets of *S. pneumoniae* zinc toxicity

Zn toxicity can arise due to its ability to readily interact with a wide range of proteins, which has the potential to perturb or inhibit protein function (Laitaoja *et al.*, 2013). Investigation of the cellular targets of Zn stress revealed changes in essential pneumococcal pathways. Most notably, in central carbon metabolism, where a Zn-dependent perturbation of PfkA appeared to occur. In support of this finding, disruption of PFK activity by Zn has previously been described in the closely related bacterium, *S. pyogenes* (Ong *et al.*, 2015). Impairment of PFK activity in *S. pneumoniae* has the potential to impede energy production via the glycolytic pathway. Despite this, only a minimal growth delay was observed at this concentration of Zn. Thus, it is possible that this concentration of Zn induced only a partial obstruction at this glycolytic step or that carbon flux was diverted such that energy production may be preserved. In contrast to *S. pyogenes*, the Zn-dependent impairment of PFK activity in *S. pneumoniae* is not offset via the upregulation of the T6P pathway for galactose metabolism (Ong *et al.*, 2015). Rather, *S. pneumoniae* galactose metabolic genes of the Leloir pathway and galactose importers were highly expressed in response to Zn stress. The precise mechanism behind the Zn-dependent upregulation of this pathway is not clear, although evidence presented herein suggests that it occurs independently of the global metabolic regulator, CcpA. It is possible that Zn is capable of upregulating the transcription of these genes via a direct interaction with GalR or SczA, or indirectly, via changes in the abundance of cellular galactose (Afzal *et al.*, 2015). However, further analyses are required to elucidate whether Zn influences cellular galactose abundance, whether Zn is capable of interacting with GalR or SczA, or whether an interaction may be capable of influencing the transcription of the Leloir pathway genes.

The upregulation of the Leloir pathway genes in response to Zn may have an evolutionary basis, as Zn may enhance the capacity of *S. pneumoniae* to grow in galactose-rich environments. Supporting this idea are the high concentrations of both galactose and Zn found in the nasopharynx and upper respiratory tract, which constitute the major ecological niches for *S. pneumoniae* (Al-Bayati *et al.*, 2017; McDevitt *et al.*, 2011). However, a limitation of this study is the lack of transcriptional information for these genes upon Zn treatment when galactose is dominant. Future studies to assess whether Zn induces a significant upregulation of the Leloir pathway when galactose is the primary carbon source and in host niches are

required. Nevertheless, it is possible that Zn serves as a signal to direct the upregulation of the galactose metabolism genes to harness the increased availability of galactose in the nasopharynx. In line with this observation, strains with defects in galactose catabolism display reduced colonisation of the nasopharynx (van Opijnen & Camilli, 2012). Increased expression of the Leloir pathway has also been associated with increased capsule production and virulence (Trappetti *et al.*, 2017). However, in the present study, Zn treatment induced a decline in total capsule production when glucose was dominant, while no difference was observed when galactose was the primary carbon source. Carbon flux can be directed from glycolysis into the capsule biosynthesis pathway via the conversion of glucose-6-phosphate to glucose-1-phosphate by the phosphoglucomutase enzyme, Pgm (Hardy *et al.*, 2000). Elevated Zn induced the accumulation of glucose-6-phosphate, which suggests that this enzyme may also be susceptible to Zn mismetallation, which has been proposed to occur in *S. pyogenes* (Ong *et al.*, 2015). Further studies are required to assess the impact of Zn on Pgm activity in *S. pneumoniae* to discern whether a similar inhibition may be at play. It is possible that the changes in galactose metabolism induced by excess Zn may have broader implications, with the potential to influence tissue tropism and the growth of *S. pneumoniae* in specific host niches. A study of dietary Zn on pneumococcal burden suggests the opposite is true, as reduced survival of pneumococci in the nasopharynx was observed following intranasal challenge with the virulent *S. pneumoniae* D39 strain (Eijkelkamp *et al.*, 2019). However, this study used a highly virulent strain and a high bacterial challenge dose, and so this is likely a consequence of improved phagocytic cell-mediated killing following inflammation and recruitment of immune cells to this niche. It remains possible that Zn may promote the survival of pneumococci during asymptomatic nasopharyngeal colonisation. Future studies, such as the assessment of pneumococcal burden in the nasopharynx of a murine Zn deficiency colonisation model, may address this issue. A decrease in capsule production by Zn may also influence the susceptibility of *S. pneumoniae* to the host immune system, modulate the capacity to adhere to host cells, or influence the protection afforded by CPS-based vaccine strategies, and therefore warrants further investigation. Despite the upregulation of the Leloir pathway genes, Zn may induce alternative diversions in carbon flux, as this pathway does not circumvent a possible inhibition of glycolysis at PfkA.

Understanding the compensatory changes to offset the Zn-dependent glycolytic defect was limited by a lack of data for the abundance of all metabolic pathway intermediates. However, there is sufficient data to propose models of action for further investigation. The

metabolomic data show that Zn also induced changes in the PPP. However, it remains unclear whether this is a result of inhibition and/or a diversion of carbon flux through this pathway. Mn abundance has previously been shown to drive utilisation of the PPP (Ogunniyi *et al.*, 2010). Zn-induced Mn depletion in *S. pneumoniae* impacts the Mn-dependent superoxide dismutase enzyme, SodA, which may induce a switch to a glutathione-based stress response (Couñago *et al.*, 2014; Eijkelkamp *et al.*, 2014; McDevitt *et al.*, 2011; Ogunniyi *et al.*, 2010; Yesilkaya *et al.*, 2000). As this process is reliant on NADPH for the regeneration of reduced glutathione, increased flux through the PPP may facilitate NADPH production. Therefore, it is possible that the observed change in 6-phosphogluconate abundance in Zn-treated cells may be due to increased carbon flux through this pathway due to Mn depletion. The observation that 6-PGD activity may be sensitive to Zn confounds this hypothesis. However, no notable changes in the abundance of downstream products of this pathway, such as aromatic amino acids and nucleotides were observed, and the impact of Zn on NADPH levels remains to be determined. The quantification of all intermediates in the PPP in cells treated with Zn and Mn would provide further insight to broaden the scope of these interpretations, while further activity and metalloproteomic studies may reveal whether Zn influences 6-PGD activity in a cellular context.

The central metabolic intermediate, acetyl-CoA was also depleted in Zn-treated cells. Depletion of acetyl-CoA may occur via the Zn-dependent upregulation of the *adhC* gene, which has a putative role in the conversion of acetyl-CoA to ethanol. Future studies that compare the levels of acetyl-CoA and ethanol in *S. pneumoniae* wild-type and an isogenic *adhC* deletion strain may reveal whether the depletion of acetyl-CoA is mediated by AdhC. The *adhC* gene is located on the same transcript as *czcD* and has been shown to be upregulated by SczA in the presence of Zn (Kloosterman *et al.*, 2007). AdhC has previously been implicated in resistance to oxidative stress (Potter *et al.*, 2010). As SodA-mediated oxidative stress tolerance is compromised by Zn-induced Mn depletion, AdhC may provide an alternative strategy to overcome oxidative stress in *S. pneumoniae* (Eijkelkamp *et al.*, 2014). Previous work has also proposed that AdhC may contribute to the regeneration of GSH through the formation of a glutathione-aldehyde adduct, which may aid in resistance to Zn and oxidative stress (Potter *et al.*, 2010). Thus, AdhC may aid in resistance to Zn through an increase in Zn buffering via the regeneration of the GSH, albeit at the expense of acetyl-CoA depletion. Acetyl-CoA is a key intermediate for fatty acid biosynthesis (Parsons & Rock, 2011). Changes in the composition of the membrane were observed upon treatment with Zn, with an increase in the proportion of

saturated phospholipids in the membrane. Although the mechanism behind the Zn-dependent increase in membrane saturation remains undefined, these findings are consistent with the observed increase in membrane rigidity, which may constitute a stress response mediating energy conservation and survival in pneumococci (Dubois-Brissonnet *et al.*, 2016). Further studies to examine the total abundance of phospholipids in Zn-treated cells compared to untreated and the influence of Zn on FabM activity are required to discern whether the changes in membrane physiology may be due to depletion of acetyl-CoA or altered FASII enzyme activity and impaired fatty acid double bond formation.

Zn treatment also resulted in the upregulation of genes involved in genetic competence, including the type II bacteriocin system and associated immunity factor that are required for the lysis of neighbouring non-competent cells (Rice & Bayles, 2008). In support of these findings, a competence defect has previously been reported in Zn-starved *S. pneumoniae*, which can be restored by the addition of Zn (Dintilhac *et al.*, 1997). An increase in competence may contribute to the genetic plasticity of *S. pneumoniae* and drive the acquisition of novel resistance and virulence determinants. The mechanism behind the Zn-dependent modulation of these genes is unclear; however, Zn may alter the response to CSP by influencing the phosphorylation state of the ComE response regulator, which may promote DNA uptake in the Zn-rich nasopharyngeal environment (Dintilhac *et al.*, 1997). Nevertheless, a recent study of the pneumococcal transcriptome in response to a range of infection-relevant conditions showed that genes of the competence pathway are highly dynamic in their expression pattern, displaying high upregulation in response to a range of experimental conditions (Aprianto *et al.*, 2018). Thus, the upregulation of the competence pathway genes may constitute a general stress response rather than a Zn-specific alteration. Further studies are required to assess whether excess Zn enhances DNA uptake and recombination and whether the higher levels of Zn in the nasopharynx influences interactions between *S. pneumoniae* strains during colonisation.

The cell wall biosynthesis pathway was susceptible to Zn as a consequence of mismetallation of GlmU by Zn. This disruption is proposed to be mediated through the binding of Zn within the acetyltransferase domain of GlmU, which perturbed the function of this highly conserved enzyme *in vitro*. The Glu315 and His330 residues are conserved among pneumococcal strains and across a range of bacterial species, including *S. pyogenes, Streptococcus mutans, Streptococcus agalactiae, S. aureus, and Enterococcus faecium* GlmU. This indicates that GlmU may also be a target of Zn stress in these species. Nevertheless, these

residues are not strictly conserved. For example, the glutamate residue is substituted with a histidine (*B. cereus*), asparagine (*B. subtilis*) or serine (*M. tuberculosis*), while the histidine residue is substituted with a tyrosine (*M. tuberculosis*) or arginine (*Salmonella* Typhimurium and *E. coli*). Although the coordination of a Zn ion may be maintained upon the glutamate to histidine substitution observed in *B. cereus*, the other substitutions likely abolish the capacity for Zn to interact with this site. This may indicate that the Glu315 and His330 residues of *S. pneumoniae* GlmU are not essential for function or that the other species have evolved to exclude Zn binding at this site, possibly due to increased exposure to Zn. Despite the coordination of Zn in the acetyltransferase domain, structural studies show that the Glu315 and His330 residues are not associated with substrate binding (Kostrewa *et al.*, 2001). This is further supported by the maintenance of acetyltransferase activity upon substitution of these residues to alanine to abolish Zn binding. As a result, the inhibitory mechanism of Zn at this site remains unclear. Superimposition of the structures of apo-GlmU and Zn-GlmU revealed no major structural rearrangements upon Zn binding, although there is a minor shift in Glu315 and His330 to accommodate the binding of the Zn ion. It is possible that minor shifts in the spatial localisation of these residues upon Zn binding may alter the interaction of GlmU with its substrates. Additional insight via biophysical or computational analyses are required to assess possible minor structural rearrangements upon Zn binding. Furthermore, analyses of Zn stress in a GlmU Glu315Ala and His330Ala substitution mutant of *S. pneumoniae* would provide insight into whether this phenomenon is observed in a cellular context. The influence of Zn on GlmU and the downstream contribution to peptidoglycan biosynthesis provided the basis for investigation of the therapeutic potential of Zn to augment the action of cell wall-targeting antibiotics.

6.3 Exploiting zinc stress in a novel treatment strategy against *S. pneumoniae*

This thesis described a potential novel therapeutic strategy, where Zn toxicity can be exploited to enhance the action of traditional antibiotics. Although the antimicrobial action of metals is harnessed in a range of topical treatment strategies today, significant challenges are associated with their application in the treatment of invasive diseases such as pneumonia, meningitis and sepsis. The major barriers restricting the success of metals in invasive disease are related to administration route and formulation issues that hinder adequate tissue

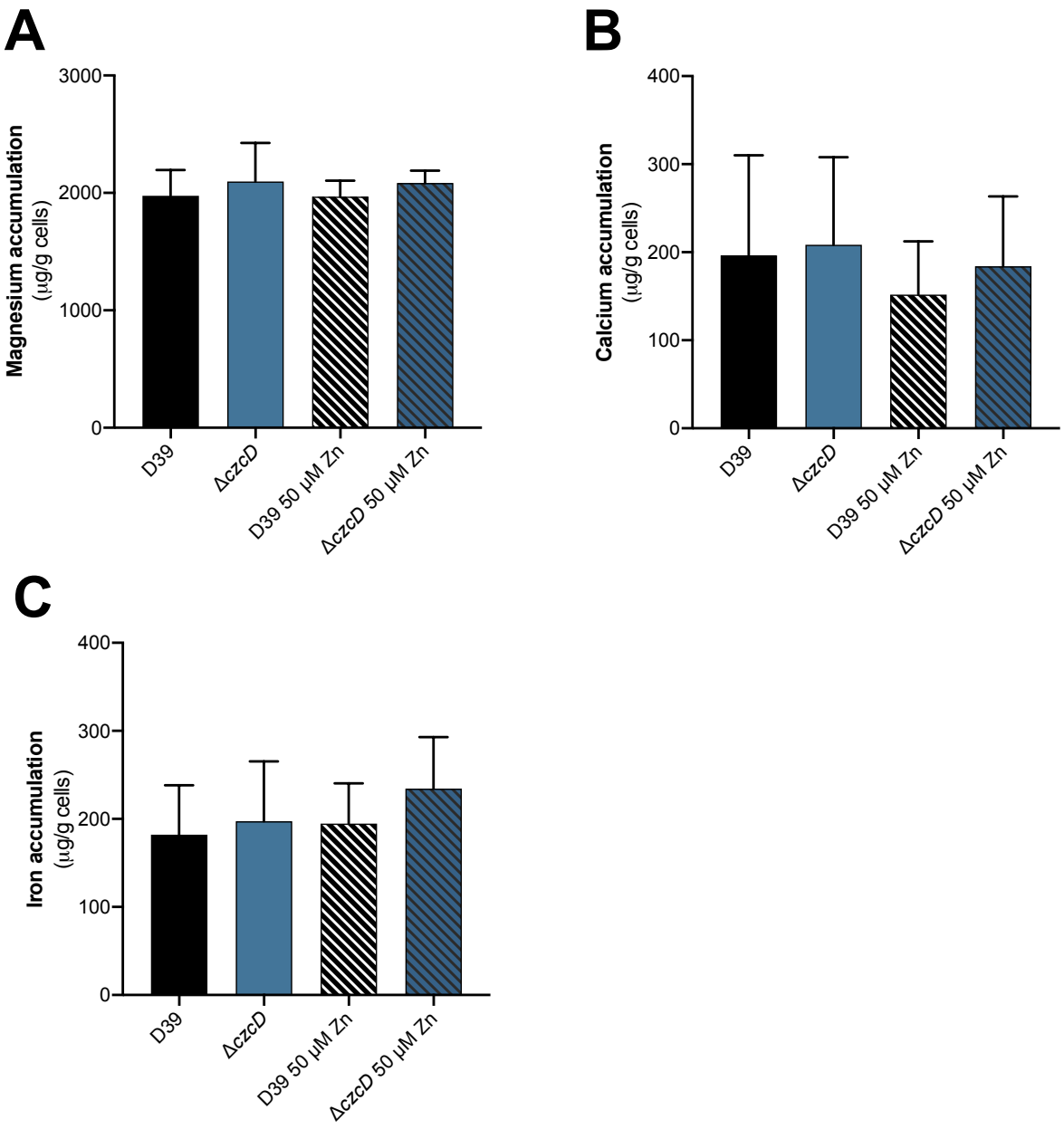
distribution, as well as the high concentration of metals typically required for antibacterial action, which may expose the patient to metal toxicity.

As the only known Zn efflux pathway in *S. pneumoniae,* the development of inhibitors targeting CzcD represented a possible strategy to induce high Zn levels and potentiate antibiotic activity. However, CzcD possesses a high degree of similarity with human CDF transporters, which limited its utility as a drug target. Furthermore, the absence of detailed structural information for CzcD and the human ZnT proteins limits structure aided drug design approaches. The safe for human use neuropathology drug PBT2 was repurposed to overcome this challenge (Lannfelt *et al.*, 2008). PBT2 was successfully exploited for its capacity to enhance the toxicity and intracellular abundance of Zn in *S. pneumoniae in vitro*. The increased cellular Zn mediated by PBT2 enhanced the susceptibility of a multi-drug resistant pneumococcal strain to a range of cell wall and protein synthesis-targeting antibiotics. Further collaborative studies of a range of other clinically significant bacterial pathogens, including *S. aureus, Enterococcus faecium* and *S. pyogenes* have now demonstrated the broad utility of this strategy in potentiating the action of antibiotics (Bohlmann *et al.*, 2018). Despite *in vitro* success, the translation of this strategy to increase pneumococcal Zn in a murine model of infection was accompanied with significant challenges. The lack of pneumococcal *czcD* induction indicated that IP administration of Zn-PBT2 at the dose tested was not capable of inducing Zn stress in pneumococci within host tissues. Rather, this work suggested that treatment induced a Zn starvation response by upregulation the Zn uptake machinery. Issues associated with the localisation of Zn with PBT2 may be overcome with the development of PBT2 derivatives that exhibit a higher affinity for Zn or by tuning the ratio or route of Zn and PBT2 administration. Future studies examining the impact of Zn with PBT2 or novel derivatives at a range of doses and administration routes may highlight the optimal treatment schedule to enhance tissue and pneumococcal Zn abundance. Nevertheless, this work provides a foundation for future studies into the therapeutic capacity of metals with ionophores to enhance antibiotic activity *in vivo*. These findings are of clinical significance, as antibiotic treatment failure contributes to the high mortality attributable to invasive pneumococcal disease (Lujan *et al.*, 2004). Once the challenges associated with imparting pneumococcal Zn stress *in vivo* are overcome, this may represent a viable treatment strategy to enhance antibiotic action and combat disease caused by antibiotic resistant strains. Together, this approach has the potential to extend the shelf life of currently available antibiotics against *S. pneumoniae,* which may be expanded for the treatment of a range of other bacterial pathogens.

6.4 Conclusions

The work presented in this thesis exploited molecular insights into Zn stress to aid in the development of a novel treatment strategy for *S. pneumoniae*. Together, this work conducted a detailed analysis of Zn toxicity and revealed the diverse metabolic pathways affected by excess Zn. The influence of Zn on *S. pneumoniae* was complex and the molecular mechanisms underpinning the changes induced by Zn require further elucidation. Nevertheless, this study indicates that *S. pneumoniae* responds to the perturbations induced by Zn via the upregulation of efflux by CzcD and through the diversion of metabolic flux. This work also highlighted several protein targets that may be susceptible to mismetallation, including the cell wall biosynthetic protein, GlmU. This led to the development of a potential novel therapeutic strategy where Zn may be used to augment the action of antibiotics. The intrinsic Zn homeostatic pathways could be overcome by repurposing a Phase II neuropathology drug, which raised cellular Zn abundance, concomitantly rendering *S. pneumoniae* highly sensitive to antibiotic treatment. Taken together, this work provides a foundation for future studies into the capacity of ionophore-induced Zn stress to improve antibiotic treatment outcomes for bacterial disease.

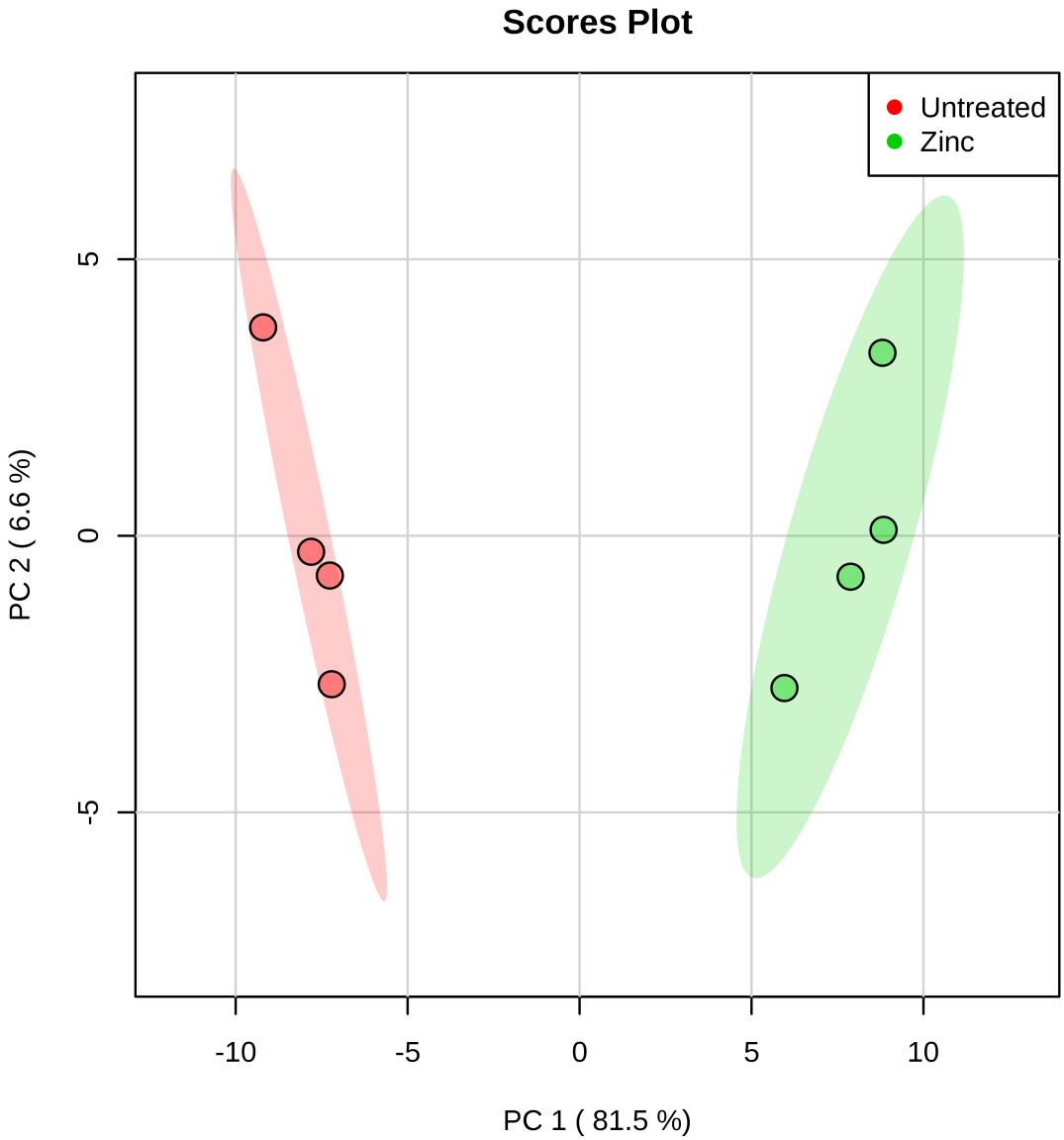
APPENDIX 1



Appendix 1: Cellular magnesium, calcium and iron accumulation in *S. pneumoniae* D39 and D39 Δ*czcD*

Mg, Ca and Fe content were assessed in *S. pneumoniae* D39 wild-type and the mutant strain Δ*czcD* following growth in the presence of absence of 50 µM $ZnSO_4$. Content of (A) Mg (B) Ca and (C) Fe were determined based on the dried cell pellets of cells grown to mid-log phase by ICP-MS. Data are the mean + SEM, from n ≥ 3 biological replicates. Statistical significance was assessed using the Student's two-tailed *t*-test.

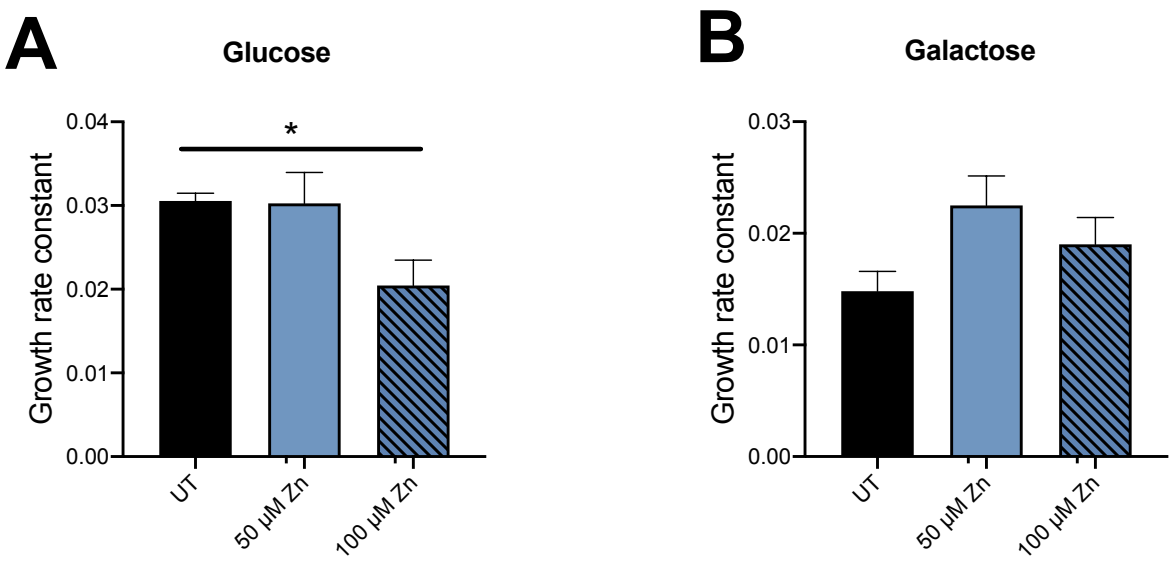
APPENDIX 2



Appendix 2: Principal component analysis (PCA) score plot of metabolic profiles in *S. pneumoniae* treated with or without zinc

S. pneumoniae were grown to mid-log phase (OD_{600} 0.30) in the presence or absence of 100 µM $ZnSO_4$. Samples were harvested and the metabolic profile was examined by Metabolon®, The PCA plot was generated using MetaboAnalyst following the exclusion of samples with low protein yield, from n = 4 biological replicates. The clustering of Zn treated samples (green) and untreated samples (red) in the PCA plot suggest significant metabolic differences in *S. pneumoniae* induced by Zn.

APPENDIX 3



Appendix 3: Carbon source influences growth kinetics of *S. pneumoniae* treated with zinc

S. pneumoniae from overnight blood agar plates were used to inoculate (A) glucose-free C+Y medium supplemented with 0.2% (w/v) glucose, with or without 50 or 100 µM $ZnSO_4$ supplementation, or (B) glucose-free C+Y medium supplemented with 0.2% (w/v) galactose, with or without 50 or 100 µM $ZnSO_4$. Growth rates were determined based on the rate of change in optical density at 600 nm (OD_{600}) during logarithmic growth (2-6hrs post inoculation). The data are the mean absorbance + SEM, from n = 3 biological replicates. Statistical significance was assessed using the Student's two-tailed *t*-test, where * represents $P < 0.05$.

APPENDIX 4

```
S.pneumoniae_pgm      MSYQENYQKWVDFVELPDYLRQDLENMDEKTKEDAFYTNLEFGTAGMRGLVGAGTNRINI   60
S.pyogenes_pgmA       MTYTENFQKWLDFEQLPDYLRQELLSMDEKTKEDAFYTNLEFGTAGMRGYIGAGTNRINI   60
                      *:* **:***:** :*******:* .********************** :*********

S.pneumoniae_pgm      YVVRQATEGLARLIESKGGNEKERGVAIAYDSRHFSPEFAFESAAVLAKHGIKSYVFESL   120
S.pyogenes_pgmA       YVVRQATEGLAKLIETKGEEAKKRGVAIAYDSRHFSPEFAFESAQVLAQHGIKSYVFEAL   120
                      ***********:***:** : *:********************* ***:*********:*

S.pneumoniae_pgm      RPTPELSFAVRHLNCFAGIMVTASHNPAPFNGYKVYGEDGGQMPPHDADALTTYIRAIEN   180
S.pyogenes_pgmA       RPTPELSFAVRHLNAYAGIMVTASHNPAPFNGYKVYGQDGGQLPPADADALTDFIRAIEN   180
                      **************.:*********************:****:** ****** :******

S.pneumoniae_pgm      PFAVEVADVETEKASGLIEVIGEAVDIEYLKEVKDININPALIEEFGKDMKIVYTPLHGT   240
S.pyogenes_pgmA       PFAVELADLDENKSSGLIQVIGEDVDMEYLREVKDVNINQDLINNFGKDMKIVYTPLHGT   240
                      *****:**:: :*:****:**** **:***:****:***  **::***************

S.pneumoniae_pgm      GEMLARRALAQAGFDSVQVVEAQATADPDFSTVTSPNPESQAAFALAEELGRQVGADVLV   300
S.pyogenes_pgmA       GEMLTRRALAQAGFESVVVVESQAKADPDFSTVKSPNPESQAAFALAEELGREVEADVLV   300
                      ****:**********:** ***:**.********.******************:* *****

S.pneumoniae_pgm      ATDPDADRVGVEVLQKDGSYLNLSGNQIGAIMAKYILEAHKNAGTLPENAALCKSIVSTD   360
S.pyogenes_pgmA       ATDPDADRLGVEIRQPDGSYKNLSGNQIGAIIAKYILEAHKTAGTLPENAALAKSIVSTE   360
                      ********:***: * **** **********:*********.**********.******:

S.pneumoniae_pgm      LVTKIAESYGATMFNVLTGFKFIAEKIQEFEEKHNHTYMMGFEESFGYLIKPFVRDKDAI   420
S.pyogenes_pgmA       LVTKIAESYGATMFNVLTGFKFIAEKIQEFEEKHNHTYMFGFEESFGYLIKPFVRDKDAI   420
                      ************************************:********************

S.pneumoniae_pgm      QAVLVVAELAAYYRSRGLTLADGIEEIYKEYGYYAEKTISVTLSGVDGAEQIKAIMAKFR   480
S.pyogenes_pgmA       QAVLLVAEIAAYYRSRGLTLADGIDEIYKEYGYFAEKTISVTLSGVDGAAEIKKIMDKFR   480
                      ****:***:***************:********:*************** :** ** ***

S.pneumoniae_pgm      NNAPTEWNATAITVVEDFKAQTATVADGTVTNLTTPPSDVLKYTLADGSWIAVRPSGTEP   540
S.pyogenes_pgmA       ENGPKQFNNTDIVLLEDFQKQTATKNDGTISNLTTPPSNVLKYTLADDSWIAVRPSGTEP   540
                      :*.*.*.::* * *.::***: ****  ***:*******:********.************

S.pneumoniae_pgm      KIKFYIAVVGETNEESQAKIANIEAEINAFVK       572
S.pyogenes_pgmA       KIKFYIATIGDTLDIAQEKIANIETEINTFVG       572
                      *******.:*:* : :* ******:***:**
```

Appendix 4: Primary sequence alignment of the phosphoglucomutase genes, *S. pneumoniae* Pgm and *S. pyogenes* PgmA

Amino acid sequences of *S. pneumoniae* Pgm (SPD_1326; GI: 4442743) and *S. pyogenes* PgmA (GI: 901328) were obtained from NCBI and aligned using Clustal Omega (Sievers *et al.*, 2011). Yellow shading denotes fully conserved residue (*), blue shading denotes conservation between groups of strongly similar properties (:), and green shading denotes conservation between groups of weakly similar properties (.).

APPENDIX 5

```
Spneumoniae_lacC      MILTVTMNPSIDISYPLDELKIDTVNRVVDVTKTAGGKGLNVTRVLSEFGDSVLATGLVG    60
Spyogenes_lacC2       MILTVTLNPAIDVSYPLDELKCDTVNRVVDVTKTPGGKGLNVSRVLNEFGETVKATGCVG    60
                      ******:**.**:******** ************ *******:***.***::* *** **

Spneumoniae_lacC      GKLGEFLVEHIDNQVKKDFFSIQGETRNCIAILHGDNQTEVLEKGPEVLEQEGQDFLEHF    120
Spyogenes_lacC2       GESGDFIINHLPDSILSRFYKISGDTRTCIAILHEGNQTEILEKGPMLSVDEIDGFTHHF    120
                      *: *:*:::*: :.:: . *:.*.*:**.****** .****:***** :  :* :.* .**

Spneumoniae_lacC      KKLLESVEVVAISGSLPAGLPVDYYASLVELANQAGKPVVLDCSGAALQAVLESPHKPTV    180
Spyogenes_lacC2       KYLLNDVDVVTLSGSLPAGMPDDYYQKLIKIANLNGKKTVLDCSGNALEAVLKGDSKPTV    180
                      * **:.*:**::******:* *** .*:::** ** .****** **:***:.  ****

Spneumoniae_lacC      IKPNNEELSQLLGREVSEDLDELKEVLQEPLFAGIEWIIVSLGANGTFAKHGDTFYKVDI    240
Spyogenes_lacC2       IKPNLEELSQLLGKEMTKDFDALKEVLQDELFDGIEWIIVSLGADGVFAKHKDTFYNVDI    240
                      **** ********:*:::*:* ******: ** ***********:*.**** ****:***

Spneumoniae_lacC      PRIQVVNPVGSGDSTVAGISSGLLHKESDAELLIKANVLGMLNAQEKMTGHVNMANYQAL    300
Spyogenes_lacC2       PKIKIVSAVGSGDSTVAGIASGLANDEDDRALLTKANVLGMLNAQEKTTGHVNMANYDKL    300
                      *:*::*. ***********:*** :.*.*  ** ************* *********: *

Spneumoniae_lacC      YDQLIVKEV       309
Spyogenes_lacC2       YQSIKVKEV       309
                      *:.: ****
```

Appendix 5: Primary sequence alignment of the tagatose-6-phosphate kinase genes, *S. pneumoniae* LacC and *S. pyogenes* LacC.2

Amino acid sequences of *S. pneumoniae* LacC (SPD_1051; GI: 116076615) and *S. pyogenes* LacC.2 (GI: 15675729) were obtained from NCBI and aligned using Clustal Omega (Sievers *et al.*, 2011). Yellow shading denotes fully conserved residue (*), blue shading denotes conservation between groups of strongly similar properties (:), and green shading denotes conservation between groups of weakly similar properties (.).

APPENDIX 6

```
ZnT9       ------------------------------------------------------------     0
YiiP       ------------------------------------------------------------     0
ZnT4       ------------------------------------------------------------     0
ZnT3       ------------------------------------------------------------     0
ZnT2       ------------------------------------------------------------     0
ZnT8       ------------------------------------------------------------     0
ZnT1       ------------------------------------------------------------     0
ZnT10      ------------------------------------------------------------     0
ZnT6       ------------------------------------------------------------     0
CzcD       ------------------------------------------------------------     0
ZnT5       MEEKYGGDVLAGPGGGGGLGPVDVPSARLTKYIVLLCFTKFLKAVGLFESYDLLKAVHIV     60
ZnT7       ------------------------------------------------------------     0

ZnT9       ------------------------------------------------------------     0
YiiP       ------------------------------------------------------------     0
ZnT4       ------------------------------------------------------------     0
ZnT3       ------------------------------------------------------------     0
ZnT2       ------------------------------------------------------------     0
ZnT8       ------------------------------------------------------------     0
ZnT1       ------------------------------------------------------------     0
ZnT10      ------------------------------------------------------------     0
ZnT6       ------------------------------------------------------------     0
CzcD       ------------------------------------------------------------     0
ZnT5       QFIFILKLGTAFFMVLFQKPFSSGKTITKHQWIKIFKHAVAGCIISLLWFFGLTLCGPLR     120
ZnT7       ------------------------------------------------------------     0

ZnT9       ------------------------------------------------------------     0
YiiP       ------------------------------------------------------------     0
ZnT4       ------------------------------------------------------------     0
ZnT3       ------------------------------------------------------------     0
ZnT2       ------------------------------------------------------------     0
ZnT8       ------------------------------------------------------------     0
ZnT1       ------------------------------------------------------------     0
ZnT10      ------------------------------------------------------------     0
ZnT6       ------------------------------------------------------------     0
CzcD       ------------------------------------------------------------     0
ZnT5       TLLLFEHSDIVVISLLSVLFTSSGGGPAKTRGAAFFIIAVICLLLFDNDDLMAKMAEHPE     180
ZnT7       ------------------------------------------------------------     0

ZnT9       ---------------MLPGL-----------------------------------------     5
YiiP       ------------------------------------------------------------     0
ZnT4       ------------------------------------------------------------     0
ZnT3       ------------------------------------------------------------     0
ZnT2       ------------------------------------------------------------     0
ZnT8       ------------------------------------------------------------     0
ZnT1       ------------------------------------------------------------     0
ZnT10      ------------------------------------------------------------     0
ZnT6       ------------------------------------------------------------     0
CzcD       ------------------------------------------------------------     0
ZnT5       GHHDSALTHMLYTAIAFLGVADHKGGVLLLVLALCCKVGFHTASRKLSVDVGGAKRLQAL     240
ZnT7       ------------------------------------------------------------     0

ZnT9       --AAAAAHRCSWSSLCRLRLRCRAAACNPSDRQEWQNLV-TFGSFSNMVPCSHPYIGTLS     62
YiiP       ------------------------------------------------------------     0
ZnT4       ------------------------------------------------------------     0
ZnT3       ------------------------------------------------------------     0
ZnT2       ------------------------------------------------------------     0
ZnT8       ------------------------------------------------------------     0
ZnT1       ------------------------------------------------------------     0
ZnT10      ------------------------------------------------------------     0
ZnT6       ------------------------------------------------------------     0
CzcD       ------------------------------------------------------------     0
ZnT5       SHLVSVLLLCPWVIVLSVT--------TESKVESWFSLIMPFATVIFFVMILDFYVDSIC     292
ZnT7       ------------------------------------------------------------     0

ZnT9       QVKLYSTNVQKEGQGSQTLRVEKVPSFETAEGIGTELKAPLKQEPLQVRVKAVLKKREYG     122
YiiP       ------------------------------------------------------------     0
ZnT4       -------------------------------MAGSGAWKRL---------------------     10
ZnT3       ------------------------------------------------------------     0
ZnT2       ------------------------------------------------------------     0
ZnT8       ------------------------------------------------------------     0
ZnT1       ------------------------------------------------------------     0
```

```
ZnT10      ------------------------------------------------------------      0
ZnT6       ------------------------------------------------------------      0
CzcD       ------------------------------------------------------------      0
ZnT5       SVKMEVS---------KCARYGSFPIFISALLFGNFWTHPI--------------------      324
ZnT7       ------------------------------------------------------------      0


ZnT9       SKYTQNNFITGVRAINEFCLKSSDLEQLRKIRRRSPHEDTESFTVYLRSDVEA----KSL      178
YiiP       ------------------------------------------------------------      0
ZnT4       ------------------------KSMLRKDDAPLFLNDTSAFDFSDEAGDEGLSRFNKL      46
ZnT3       --------------------------MEPSPAAGGLETTRLVSPRDRG-GAG----GSL      28
ZnT2       ----------------------------------MEAKEKQHLLDARPAIRSYT----GSL      23
ZnT8       ----------------------------------MEFLERTYLVNDKA-AKMYA----FTL      22
ZnT1       ------------------------------------------------------------      0
ZnT10      ------------------------------------------------------------      0
ZnT6       ------------------------------------------------------------      0
CzcD       ------------------------------------------------------------      0
ZnT5       ------------------------TDQLRAMNKAAHQESTEHV---LSGGVVVSAIFFIL      357
ZnT7       ------------------------------------------------------------      0


ZnT9       E------VWGSPEA-LAREK----KLRKEAEI-----------EYRERLFR--NQKILRE      214
YiiP       ------------------------------------------------------MNQSY---      5
ZnT4       RVVVADDGSEAPERPVNGAH-PTLQADDDSLLDQDLPLTNSQLSLKVDSCD--NCSKQRE      103
ZnT3       RLKS---LFTEPSEPLPEES--------------------KPVEMPFHHCH--RDPLPPP      63
ZnT2       WQEG---A---GWIPLPRPG-LDLQAI-------------ELAAQSNHHCH--AQKGPDS      61
ZnT8       ESVE---L---QQKPVNKDQCPRERPE-------------ELESGGMYHCH--SGSKPTE      61
ZnT1       ------------------------------------------------------------      0
ZnT10      ------------------------------------------------------------      0
ZnT6       ---------------------------------------------MGTIHLFRKPQRSFFGK      17
CzcD       ------------------------------------------------------------      0
ZnT5       SA----NILSSP----------SKRGQKGTLIGY-SPEGTPLYNFMGDAFQHSSQSIPRF      402
ZnT7       ------------------------------ML---------PLSIKDDEYKPPKFNLFGK      21


ZnT9       YRDFLGNTKPRSRTASVFFKGPGKVVMVAICINGLNCFFKFLAWIYTGSASMFSEAIHSL      274
YiiP       -G-----------------RLVSRAAIAATAMASLLLLIKIFAWWYTGSVSILAALVDSL      47
ZnT4       IL---------------KQRKVKARLTIAAVLYLLFMIGELVGGYIANSLAIMTDALHML      148
ZnT3       GL----TP---------ERLHARRQLYAACAVCFVFMAGEVVGGYLAHSLAIMTDAAHLL      110
ZnT2       HC----DP---------KKGKAQRQLYVASAICLLFMIGEV--------------------      89
ZnT8       KG----AN---------EYAYAKWKLCSASAICFIFMIAEVVGGHIAGSLAVVTDAAHLL      108
ZnT1       MGCW---------------GRNRGRLLCMLALTFMFMVLEVVVSRVTSSLAMLSDSFHML      45
ZnT10      MGRY---------------SGKTCRLLFMLVLTVAFFVAELVSGYLGNSIALLSDSFNML      45
ZnT6       LLREFRLV---------AADRRSWKILLFGVINLICTGFLLMWCSSTNSIALTAYTYLTI      68
CzcD       --------------------MKAKYAVWVAFFLNLTYAIVEFIAGGVFGSSAVLADSVHDL      41
ZnT5       IKESLKQI---------LEESDSRQIFYFLCLNLLFTFVELFYGVLTNSLGLISDGFHML      453
ZnT7       ISGWFRSI---------LSDKTSRNLFFFLCLNLSFAFVELLYGIWSNCLGLISDSFHMF      72
                                           :         .

ZnT9       SDTCNQGLLALGISKSVQTP-DPSHPYGFSNMRYISSLISGVGIFMMGAGLSWYHGVMGL      333
YiiP       VDIGASLTNLLVVRYSLQPA-DDNHSFGHGKAESLAALAQSMFIS-GSALFLFLTGIQHL      105
ZnT4       TDLSAIILTLLALWLSSKSP-TKRFTFGFHRLEVLSAMISVLLVY-ILMGFLLYEAVQRT      206
ZnT3       ADVGSMMGSLFSLWLSTRPA-TRTMTFGWHRSETLGALASVVSLW-MVTGILLYLAFVRL      168
ZnT2       ------------------------------VEILGALVSVLSIW-VVTGVLVYLAVERL      117
ZnT8       IDLTSFLLSLFSLWLSSKPP-SKRLTFGWHRAEILGALLSILCIW-VVTGVLVYLACERL      166
ZnT1       SDVLALVVALVAERFARRTHATQKNTFGWIRAEVMGALVNAIFLT-GLCFAILLEAIERF      104
ZnT10      SDLISLCVGLSAGYIARRPTRGFSATYGYARAEVVGALSNAVFLT-ALCFTIFVEAVLRL      104
ZnT6       FDLFSLMTCLISYWVTLRKP-SPVYSFGFERLEVLAVFASTVLAQ-LGALFILKESAERF      126
CzcD       GDAIAIGISAFLETISNREE-DNQYTLGYKRFSLLGALVTAVILV-TGSVLVILENVTKI      99
ZnT5       FDCSALVMGLFAALMSRWKA-TRIFSYGYGRIEILSGFINGLFLI-VIAFFVFMESVARL      511
ZnT7       FDSTAILAGLAASVISKWRD-NDAFSYGYVRAEVLAGFVNGLFLI-FTAFFIFSEGVERA      130
                                              :.  :    :

ZnT9       LHPQPIESLLWAYCI-LAGSLVSEGATLLVAVN----------------------------      365
YiiP       VSPTPMTDPGVGVIVTIVALICTIILVS-FQRW----VVR----------------------      140
ZnT4       IHMNYEINGDIMLITAAVGVAVNVIMGFLLNQSGHRHSHSHS------LP-----------      250
ZnT3       LHSDYHIEGGAMLLTASIAVCANLLMAFVLHQAGPPHSHGSR------GA-----------      212
ZnT2       ISGDYEIDGGTMLITSGCAVAVNIIMGLTLHQSGHGHSHGTT------NQ-----------      161
ZnT8       LYPDYQIQATVMIIVSSCAVAANIVLTVVLHQRCLGHNHKE----------------------      207
ZnT1       IEPHEMQQPLVVLGVGVAGLLVNVLGLCLFHHH-SGFSQDSGHGHSHGGH-------GHG      156
ZnT10      ARPERIDDPELVLIVGVLGLLVNVVGLLIFQDC-AAWFACCLRGRSRRLQQRQQLAEGCV      163
ZnT6       LEQPEIHTGR-LLVGTFVALCFNLFTMLSIRNKPFAYVSEAAS---TSWL-----------      172
CzcD       LHPQPVNDEG-ILWLGIIAITINLLASLVVGKG----------------------------      131
ZnT5       IDPPELDTHM-LTPVSVGGLIVNLIGICAFSHA-HSHAHGASQGSCHSS------------      558
ZnT7       LAPPDVHHER-LLLVSILGFVVNLIGIFVFKHGGHGHSHGSGHGHSHSLF-----------      179
                          .    .       .
```

```
ZnT9        ----------------------------------ELR---------------RNARAKGM     376
YiiP        ------------------------------------------------------------     140
ZnT4        ---------------------------------------------------SNSPTRGS     258
ZnT3        ---------------------------------------------------EYAPLE-E     219
ZnT2        ------------------------------------------------------------     161
ZnT8        ------------------------------------------------------------     207
ZnT1        HGLPKGPRVKSTRPGSSDINVAPGEQGPDQEETNTLVANTSNSNGLKLDPADPENPRSGD     216
ZnT10       PGAFGGPQGAE-DPRRAADPTAPGSD-----SAVTLR-------GTSV----ERKREKGA     206
ZnT6        ---------------------------------------------------QEHVA     177
CzcD        ------------------------------------------------------------     131
ZnT5        ---------------------------------------DHSHSHHMH------GHSDHGH     574
ZnT7        ----NGALDQA-----------HGHV------------DHCHSHEVKHGAAHSHDHAHGH     212

ZnT9        SFYKYV--------------ME-------SRDPSTNVILLEDTAAVLGVIIAATCMGLTS     415
YiiP        -------------------------RTQSQAVRADMLHYQSDVMMNGAILLALGLSWYG-     174
ZnT4        G-------------------CERNHGQDSLAVRAAFVHALGDLVQSVGVLIAAYIIRFKP     299
ZnT3        G-------------------PEEPLPLGNTSVRAAFVHVLGDLLQSFGVLAASILIYFKP     260
ZnT2        -------------------------QEENPSVRAAFIHVIGDFMQSMGVLVAAYILYFKP     196
ZnT8        -------------------------VQANASVRAAFVHALGDLFQSISVLISALIIYFKP     242
ZnT1        TVEVQVNG---NLVREPDHMELEEDRAGQLNMRGVFLHVLGDALGSVIVVVNALVFYFSW     273
ZnT10       TVFANVAGDSFNTQNEPEDMMKKEKKSEALNIRGVLLHVMGDALGSVVVVITAIIFYVLP     266
ZnT6        DLSRSL--------------CGIIPGLSSIFLPRMNPFVLIDLAGAFALCITYMLIEINN     223
CzcD        --------------------------KTKNESILSLHFLEDTLGWVAVILMAIVLRFTD     164
ZnT5        GHSHGS-----------------AGGGMNANMRGVFLHVLADTLGSIGVIVSTVLIEQFG     617
ZnT7        GHFHSHDGPS----------LKETTGPSRQILQGVFLHILADTLGSIGVIASAIMMQNFG     262
                                                 *      :

ZnT9        IT-------GNPL--------------------YDSL--GSLGVGTLLGMVSAFLIYT---     444
YiiP        ----------------------------------------W-HRADALFALGIGIYILYSAL     195
ZnT4        ---------------------------------------EYKIADPICTYVFSLLVAFTTF     321
ZnT3        ---------------------------------------QYKAADPISTFLFSICALGSTA     282
ZnT2        ---------------------------------------EYKYVDPICTFVFSILVLGTTL     218
ZnT8        ---------------------------------------EYKIADPICTFIFSILVLASTI     264
ZnT1        KGCSEGDFCVNPCFPDPCKAFVEIINSTHASVYEAGPCWVLYLDPTLCVVMVCILLYTTY     333
ZnT10       LK-----------------------------SEDPCNWQCYIDPSLTVLMVIIILSSAF     296
ZnT6        ----------------------------------------Y-FAVDTASAIAIALMTFGTMY     244
CzcD        ----------------------------------------W-YILDPLLSLVISFFILSKAL     185
ZnT5        ----------------------------------------W-FIADPLCSLFIAILIFLSVV     638
ZnT7        ---------------------------------------L-MIADPICSILIAILIVVSVI     283
                                                      .

ZnT9        ----NTEALLGRSIQPE-Q--VQRLTELLENDPSVRAIHDVKATDLGLGKVRFKAEVDFD     497
YiiP        RMGYEAVQSLLDRALPDEER--QEIIDIVTSWPGVSGAHDLRTRQSGPTRFIQ-IHLEME     252
ZnT4        RIIWDTVVIILEGVPSHLNV--DYIKEALMKIEDVYSVEDLNIWSLTSGKSTAIVHIQLI     379
ZnT3        PTLRDVLRILMEGTPRNVGF--EPVRDTLLSVPGVRATHELHLWALTLTYHVASAHLAID     340
ZnT2        TILRDVILVLMEGTPKGVDF--TAVRDLLLSVEGVEALHSLHIWALTVAQPVLSVHIAIA     276
ZnT8        TILKDFSILLMEGVPKSLNY--SGVKELILAVDGVLSVHSLHIWSLTMNQVILSAHVATA     322
ZnT1        PLLKESALILLQTVPKQIDI--RNLIKELRNVEGVEEVHELHVWQLAGSRIIATAHIKCE     391
ZnT10       PLIKETAAILLQMVPKGVNM--EELMSKLSAVPGISSVHEVHIWELVSGKIIATLHIKYP     354
ZnT6        PMSVYSGKVLLQTTPPHVIGQLDKLIREVSTLDGVLEVRNEHFWTLGFGSLAGSVHVRIR     304
CzcD        PRFWSTLKIFLDAVPEGLDI--KQVKSGLERLDNVASLNQLNLWTMDALEKNAIVHVCLK     243
ZnT5        PLIKDACQVLLLRLPPEYEKELHIALEKIQKIEGLISYRDPHFWRHSASIVAGTIHIQVT     698
ZnT7        PLLRESVGILMQRTPPLLENSLPQCYQRVQQLQGVYSLQEQHFWTLCSDVYVGTLKLIVA     343
                  :                    :    .:    .. .            .:

ZnT9        GRVVTRSYL-----------EKQDFDQMLQEIQE--VKTPEELETFML------------     532
YiiP        DSLPLVQAHMVADQVEQAILRRFPGSDVII-------------------------HQDPC     287
ZnT4        PGS-SSKWEEVQSKANHLLLNTFGMYRCTIQLQSYRQEV---DRTCA-------NCQSSS     428
ZnT3        --S-TADPEAVLAEASSRLYSRFGFSSCTLQVEQYQPE----MAQCL-------RCQEPP     386
ZnT2        --Q-NTDAQAVLKTASSRLQGKFHFHTVTIQIEDYSED----MKDCQ-------ACQGPS     322
ZnT8        --A-SRDSQVVRREIAKALSKSFTMHSLTIQMESPVDQ----DPDCL-------FCEDPC     368
ZnT1        --D-PTSYMEVAKTIKD-VFHNHGIHATTIQPEFASVGSKSSVVPCEL------ACRTQC     441
ZnT10       --K-DRGYQDASTKIRE-IFHHAGIHNVTIQFENVDLKEPLEQKDLLL------LCNSPC     404
ZnT6        --R-DANEQMVLAHVTN-RLYT-LVSTLTVQIFKDDWIRPALLSGPVAANVLNFSDHHVI     359
CzcD        --E-MEHMETCKESIRI-FLKDCGFQNITIEIDADLETHQTHK-------------RKVC     286
ZnT5        --S-DVLEQRIVQQVTG-ILKDAGVNNLTIQVEKEAYFQHMSGLST--------GFHDVL     746
ZnT7        --P-DADARWILSQTHN-IFTQAGVRQLYVQIDFAAM-----------------------     376

ZnT9        --KH-----GENIIDTLGAEVDR------LEKELKKRNPEVRHV----------------     563
YiiP        SVVPREGKRSML---S-----------------------------------------     300
ZnT4        P-------------------------------------------------------     429
ZnT3        QA------------------------------------------------------     388
ZnT2        D-------------------------------------------------------     323
ZnT8        D-------------------------------------------------------     369
ZnT1        ALKQ---CCG-----TLPQAPSG--------KDAEK-TPAVSIS----CLELSNNLEKKP     480
```

```
ZnT10      ISKG---CAK-----QLCCPPGAL-PLAHVNGCAEH-NGGPSLD----TYG-SDGLSRRD     449
ZnT6       PMPLLKGTDDLNPVTSTPAKPSSPPPEFSFNTPGKNVNPVILLNTQTRPYGFGLNHGHTP     419
CzcD       DLER--SYEH-----------------QH-------------------------------     296
ZnT5       AMTK--QMES-----------------MKYCKDGTYIM----------------------     765
ZnT7       ------------------------------------------------------------     376

ZnT9       -----DLEIL----------------------------------    568
YiiP       -----------------------------------------      300
ZnT4       -----------------------------------------      429
ZnT3       -----------------------------------------      388
ZnT2       -----------------------------------------      323
ZnT8       -----------------------------------------      369
ZnT1       RRTK-AENI--PAVVIEIKNMPNKQPESSL------------     507
ZnT10      AREV-AIEVSLDSCLSDHGQSLNKTQEDQCYVNRTHF-----     485
ZnT6       YSSMLNQGLGVPGIGATQGLRTGFTNIPSRYGTNNRIGQPRP    461
CzcD       -----------------------------------------      296
ZnT5       -----------------------------------------      765
ZnT7       -----------------------------------------      376
```

Appendix 6: Primary sequence alignment of human ZnT proteins with *S. pneumoniae* CzcD and *E. coli* YiiP

Amino acid sequences of *E. coli* YiiP (GI: 60392291*), S. pneumoniae* CzcD (SPD_1638; GI: 116077533), *H. sapiens* ZnT1 (GI: 52352803), ZnT2 (GI: 14210520), ZnT3 (GI: 21361112), ZnT4 (GI: 2582415), ZnT5 (GI: 20070323), ZnT6 (GI: 21687224), ZnT7 (GI: 222080086), ZnT8 (GI: 64762489), ZnT9 (GI: 57164948) and ZnT10 (GI: 52351208) were obtained from NCBI and aligned using Clustal Omega (Sievers *et al.*, 2011). * denotes fully conserved residue, : denotes conservation between groups of strongly similar properties, . denotes conservation between groups of weakly similar properties.

APPENDIX 7

```
ZnT9                    ------------------------------------------------------------ 0
E.coli_yiiP             ------------------------------------------------------------ 0
ZnT6                    ------------------------------------------------------------ 0
ZnT5                    MEEKYGGDVLAGPGGGGGLGPVDVPSARLTKYIVLLCFTKFLKAVGLFESYDLLKAVHIV 60
ZnT7                    ------------------------------------------------------------ 0
S.pneumoniae_czcD       ------------------------------------------------------------ 0
S.pyogenes_czcD         ------------------------------------------------------------ 0
ZnT4                    ------------------------------------------------------------ 0
ZnT3                    ------------------------------------------------------------ 0
ZnT2                    ------------------------------------------------------------ 0
ZnT8                    ------------------------------------------------------------ 0
E.coli_zitB             ------------------------------------------------------------ 0
A.baumannii_czcD        ------------------------------------------------------------ 0
C.metallidurans_czcD    ------------------------------------------------------------ 0
ZnT1                    ------------------------------------------------------------ 0
ZnT10                   ------------------------------------------------------------ 0

ZnT9                    ------------------------------------------------------------ 0
E.coli_yiiP             ------------------------------------------------------------ 0
ZnT6                    ------------------------------------------------------------ 0
ZnT5                    QFIFILKLGTAFFMVLFQKPFSSGKTITKHQWIKIFKHAVAGCIISLLWFFGLTLCGPLR 120
ZnT7                    ------------------------------------------------------------ 0
S.pneumoniae_czcD       ------------------------------------------------------------ 0
S.pyogenes_czcD         ------------------------------------------------------------ 0
ZnT4                    ------------------------------------------------------------ 0
ZnT3                    ------------------------------------------------------------ 0
ZnT2                    ------------------------------------------------------------ 0
ZnT8                    ------------------------------------------------------------ 0
E.coli_zitB             ------------------------------------------------------------ 0
A.baumannii_czcD        ------------------------------------------------------------ 0
C.metallidurans_czcD    ------------------------------------------------------------ 0
ZnT1                    ------------------------------------------------------------ 0
ZnT10                   ------------------------------------------------------------ 0

ZnT9                    ------------------------------------------------------------ 0
E.coli_yiiP             ------------------------------------------------------------ 0
ZnT6                    ------------------------------------------------------------ 0
ZnT5                    TLLLFEHSDIVVISLLSVLFTSSGGGPAKTRGAAFFIIAVICLLLFDNDDLMAKMAEHPE 180
ZnT7                    ------------------------------------------------------------ 0
S.pneumoniae_czcD       ------------------------------------------------------------ 0
S.pyogenes_czcD         ------------------------------------------------------------ 0
ZnT4                    ------------------------------------------------------------ 0
ZnT3                    ------------------------------------------------------------ 0
ZnT2                    ------------------------------------------------------------ 0
ZnT8                    ------------------------------------------------------------ 0
E.coli_zitB             ------------------------------------------------------------ 0
A.baumannii_czcD        ------------------------------------------------------------ 0
C.metallidurans_czcD    ------------------------------------------------------------ 0
ZnT1                    ------------------------------------------------------------ 0
ZnT10                   ------------------------------------------------------------ 0

ZnT9                    ---------------MLPGL------------------------------------- 5
E.coli_yiiP             ------------------------------------------------------------ 0
ZnT6                    ------------------------------------------------------------ 0
ZnT5                    GHHDSALTHMLYTAIAFLGVADHKGGVLLLVLALCCKVGFHTASRKLSVDVGGAKRLQAL 240
ZnT7                    ------------------------------------------------------------ 0
S.pneumoniae_czcD       ------------------------------------------------------------ 0
S.pyogenes_czcD         ------------------------------------------------------------ 0
ZnT4                    ------------------------------------------------------------ 0
ZnT3                    ------------------------------------------------------------ 0
ZnT2                    ------------------------------------------------------------ 0
ZnT8                    ------------------------------------------------------------ 0
E.coli_zitB             ------------------------------------------------------------ 0
A.baumannii_czcD        ------------------------------------------------------------ 0
C.metallidurans_czcD    ------------------------------------------------------------ 0
ZnT1                    ------------------------------------------------------------ 0
ZnT10                   ------------------------------------------------------------ 0

ZnT9                    --AAAAAHRCSWSSLCRLRLRCRAAACNPSDRQEWQNLV-TFGSFSNMVPCSHPYIGTLS 62
E.coli_yiiP             ------------------------------------------------------------ 0
ZnT6                    ------------------------------------------------------------ 0
ZnT5                    SHLVSVLLLCPWVIVLSVT--------TESKVESWFSLIMPFATVIFFVMILDFYVDSIC 292
ZnT7                    ------------------------------------------------------------ 0
S.pneumoniae_czcD       ------------------------------------------------------------ 0
S.pyogenes_czcD         ------------------------------------------------------------ 0
ZnT4                    ------------------------------------------------------------ 0
ZnT3                    ------------------------------------------------------------ 0
ZnT2                    ------------------------------------------------------------ 0
ZnT8                    ------------------------------------------------------------ 0
E.coli_zitB             ------------------------------------------------------------ 0
A.baumannii_czcD        ------------------------------------------------------------ 0
C.metallidurans_czcD    ------------------------------------------------------------ 0
ZnT1                    ------------------------------------------------------------ 0
ZnT10                   ------------------------------------------------------------ 0
```

```
ZnT9                    QVKLYSTNVQKEGQGSQTLRVEKVPSFETAEGIGTELKAPLKQEPLQVRVKAVLKKREYG 122
E.coli_yiiP             ------------------------------------------------------------ 0
ZnT6                    ------------------------------------------------------------ 0
ZnT5                    SVKMEVS---------KCARYGSFPIFISALLFGNFWTHPIT------------------ 325
ZnT7                    ------------------------------------------------------------ 0
S.pneumoniae_czcD       ------------------------------------------------------------ 0
S.pyogenes_czcD         ------------------------------------------------------------ 0
ZnT4                    ----------------------------MAGSGAWKRL-K------------------ 11
ZnT3                    ------------------------------------------------------------ 0
ZnT2                    ------------------------------------------------------------ 0
ZnT8                    ------------------------------------------------------------ 0
E.coli_zitB             ------------------------------------------------------------ 0
A.baumannii_czcD        ------------------------------------------------------------ 0
C.metallidurans_czcD    ------------------------------------------------------------ 0
ZnT1                    ------------------------------------------------------------ 0
ZnT10                   ------------------------------------------------------------ 0

ZnT9                    SKYTQNNFITGVRAINEFCLKSSDLEQLRKIRRRSPHEDTESFTVYLRSDVEAKSLEVWG 182
E.coli_yiiP             ------------------------------------------------------------ 0
ZnT6                    ------------------------------------------------------------ 0
ZnT5                    ------------------------DQLRAMNKAAHQESTEHVL---SGGVVV--SAIFF 355
ZnT7                    ------------------------------------------------------------ 0
S.pneumoniae_czcD       ------------------------------------------------------------ 0
S.pyogenes_czcD         ------------------------------------------------------------ 0
ZnT4                    ------------------------SMLRKDDAPLFLNDTSAFDFSDEAGDEG--LSRFN 44
ZnT3                    --------------------------MEPSPAAGGLETTRLVSPRDRG-GAG------G 26
ZnT2                    ----------------------------------MEAKEKQHLLDARPAIRSYT------G 21
ZnT8                    ----------------------------------MEFLERTYLVNDKA-AKMYA------F 20
E.coli_zitB             ------------------------------------------------------------ 0
A.baumannii_czcD        ------------------------------------------------------------ 0
C.metallidurans_czcD    ------------------------------------------------------------ 0
ZnT1                    ------------------------------------------------------------ 0
ZnT10                   ------------------------------------------------------------ 0

ZnT9                    SPEAL-------AREKKLRKEAEIEYR----------ERLFRNQK--I------L----- 212
E.coli_yiiP             ------------------------------------------------------------ 0
ZnT6                    ------------------------------------------------------MGTIHL 6
ZnT5                    ILSAN----ILSSPSKRGQKGTLIGYSPEGTPLYNFMGDAFQHSSQSI------PRFI-- 403
ZnT7                    ----------------------ML--------PLSIKDDEYKPPKFNL------FGKI-- 22
S.pneumoniae_czcD       ------------------------------------------------------------ 0
S.pyogenes_czcD         ------------------------------------------------------------ 0
ZnT4                    KLRVVVADDGSEAPERPVN--------GAH-PTLQADDDSLLDQDLPLTNSQLSLKVDSC 95
ZnT3                    SLRLKS---LFTEPSEPLP--------EES--------------------KPVEMPFHHC 55
ZnT2                    SLWQEG---A---GWIPLP--------RPG-LDLQAI-------------ELAAQSNHHC 53
ZnT8                    TLESVE---L---QQKPVN--------KDQCPRERPE-------------ELESGGMYHC 53
E.coli_zitB             ----------------------------------------------------MAHSHS 6
A.baumannii_czcD        ----------------------------------------------------MGGHHG 6
C.metallidurans_czcD    ----------------------------------------------------MGAGHS 6
ZnT1                    ------------------------------------------------------------ 0
ZnT10                   ------------------------------------------------------------ 0

ZnT9                    --REYRDFLGNTKPRSRTASVFFKGPGKVVMVAICINGLNCFFKFLAWIYTGSASMFSEA 270
E.coli_yiiP             ----MN-------------QSYGRLVSRAAIAATAMASLLLLIKIFAWWYTGSVSILAAL 43
ZnT6                    FRKPQRSFFGKL-LREFRLVAADRR-SWKILLFGVINLICTGFLLMWCSSTNSIALTAYT 64
ZnT5                    --KE-------S-LKQ---ILEESD-SRQIFYFLCLNLLFTFVELFYGVLTNSLGLISDG 449
ZnT7                    --SG-------W-FRS---ILSDKT-SRNLFFFLCLNLSFAFVELLYGIWSNCLGLISDS 68
S.pneumoniae_czcD       ----------------------MKA-KYAVWVAFFLNLTYAIVEFIAGGVFGSSAVLADS 37
S.pyogenes_czcD         ----------------------MPA-SKKVTIIFILNLSFSLIEFIFGTLFFSGAILADA 37
ZnT4                    DNCS-------K-QREIL--KQRKV-KARLTIAAVLYLLFMIGELVGGYIANSLAIMTDA 144
ZnT3                    HRDP-------L-PPPGLTPERLHA-RRQLYAACAVCFVFMAGEVVGGYLAHSLAIMTDA 106
ZnT2                    HAQK-------G-PDSHCDPKKGKA-QRQLYVASAICLLFMIGEV---------------- 89
ZnT8                    HSGS-------K-PTEKGANEYAYA-KWKLCSASAICFIFMIAEVVGGHIAGSLAVVTDA 104
E.coli_zitB             HTSS-------H-------LPEDNN-ARRLLYAFGVTAGFMLVEVVGGFLSGSLALLADA 51
A.baumannii_czcD        HDHS-------H-A-----VVTEGN-AKKLTIALALTTTFLIVEVIAGLITQSLALLSDA 52
C.metallidurans_czcD    HDH------------------PGGN-ERSLKIALALTGTFLIAEVVGGVMTKSLALISDA 47
ZnT1                    -------------M-----GCWGRN-RGRLLCMLALTFMFMVLEVVVSRVTSSLAMLSDS 41
ZnT10                   -------------M-----GRYSGK-TCRLLFMLVLTVAFFVAELVSGYLGNSIALLSDS 41
                                                 :         .

ZnT9                    IHSLSDTCNQGLLALGISKSVQTP-DPSHPYGFSNMRYISSLISGVGIFMMGAGLSWYHG 329
E.coli_yiiP             VDSLVDIGASLTNLLVVRYSLQPA-DDNHSFGHGKAESLAALAQSMFIS-GSALFLFLTG 101
ZnT6                    YLTIFDLFSLMTCLISYWVTLRKP-SPVYSFGFERLEVLAVFASTVLAQ-LGALFILKES 122
ZnT5                    FHMLFDCSALVMGLFAALMSRWKA-TRIFSYGYGRIEILSGFINGLFLI-VIAFFVFMES 507
ZnT7                    FHMFFDSTAILAGLAASVISKWRD-NDAFSYGYVRAEVLAGFVNGLFLI-FTAFFIFSEG 126
S.pneumoniae_czcD       VHDLGDAIAIGISAFLETISNREE-DNQYTLGYKRFSLLGALVTAVILV-TGSVLVILEN 95
S.pyogenes_czcD         VHDFGDAIAIGISAILERKAIKKE-SPNFSLGYKRFSLLGALTTNLILI-SGSLLVMIET 95
ZnT4                    LHMLTDLSAIILTLLALWLSSKSP-TKRFTFGFHRLEVLSAMISVLLVY-ILMGFLLYEA 202
ZnT3                    AHLLADVGSMMGSLFSLWLSTRPA-TRTMTFGWHRSETLGALASVVSLW-MVTGILLYLA 164
ZnT2                    ----------------------------------VEILGALVSVLSIW-VVTGVLVYLA 113
ZnT8                    AHLLIDLTSFLLSLFSLWLSSKPP-SKRLTFGWHRAEILGALLSILCIW-VVTGVLVYLA 162
E.coli_zitB             GHMLTDTAALLFALLAVQFSRRPP-TIRHTFGWLRLTTLAAFVNAIALV-VITILIVWEA 109
A.baumannii_czcD        AHMFTDAAALAIALVAIQISKRPA-DNKRTFGYQRFEILAALFNALMLF-VVAIYILYEA 110
C.metallidurans_czcD    AHMLTDTVALAIALAAIAIAKRPA-DKKRTFGYYRFEILAAAFNALLLF-GVAIYILYEA 105
```

```
ZnT1                    FHMLSDVLALVVALVAERFARRTHATQKNTFGWIRAEVMGALVNAIFLT-GLCFAILLEA 100
ZnT10                   FNMLSDLISLCVGLSAGYIARRPTRGFSATYGYARAEVVGALSNAVFLT-ALCFTIFVEA 100
                                                      ::     :

ZnT9                    VMGLLHPQPIESLLWAYCILAGSLVSEGATLLVAVNE-------LRR------------- 369
E.coli_yiiP             IQHLISPTPMTDPGVGVIVTIVALICTIILVS-FQRW---VV------------------ 139
ZnT6                    AERFLEQPEIHTGR-LLVGTFVALCFNLFTMLSIRNKPFAYVSEAASTSWLQEH------ 175
ZnT5                    VARLIDPPELDTHM-LTPVSVGGLIVNLIGICAFSHA--------HSHAHGASQ------ 552
ZnT7                    VERALAPPDVHHER-LLLVSILGFVVNLIGIFVFKHG-------GHGHSHGSGH------ 172
S.pneumoniae_czcD       VTKILHPQPVNDEG-ILWLGIIAITINLLASLVVGKG----------------------- 131
S.pyogenes_czcD         IPKLWHPTIVNYDG-MFVLAIFAIIINGFASFIIHSN----------------------- 131
ZnT4                    VQRTIHMNYEINGDIMLITAAVGVAVNVIMGFLLNQS-------GHRHSHSHSL------ 249
ZnT3                    FVRLLHSDYHIEGGAMLLTASIAVCANLLMAFVLHQA-------GPPHSHGSRG------ 211
ZnT2                    VERLISGDYEIDGGTMLITSGCAVAVNIIMGLTLHQS-------GHGHSHGTTN------ 160
ZnT8                    CERLLYPDYQIQATVMIIVSSCAVAANIVLTVVLHQR-------CLGHNHKE-------- 207
E.coli_zitB             IERFRTPRPVEGGM-MMAIAVAGLLANILSFWLLHHG----------------------- 145
A.baumannii_czcD        YIRFSQPPEIQSVG-MLIVATIGLVINLISMKILMSS----------------------- 146
C.metallidurans_czcD    YLRLKSPPQIESTG-MFVVAVLGLIINLISMRMLSSG----------------------- 141
ZnT1                    IERFIEPHEMQQPLVVLGVGVAGLLVNVLGLCLFHHHSGFSQDSGHGHSHGGH------- 153
ZnT10                   VLRLARPERIDDPELVLIVGVLGLLVNVVGLLIFQDCAAWFACCLRGRSRRLQQRQQLAE 160
                                          ..

ZnT9                    ------------------------------------------------------NARA 373
E.coli_yiiP             ------------------------------------------------------------ 139
ZnT6                    ------------------------------------------------------------ 175
ZnT5                    GSCHSS--------------DHS--------------------HSHHMH------GHSD 571
ZnT7                    GHSHSLFNGALDQAHGHV--DHC--------------------HSHEVKHGAAHSHDHA 209
S.pneumoniae_czcD       ------------------------------------------------------------ 131
S.pyogenes_czcD         ------------------------------------------------------------ 131
ZnT4                    ------------PSNSPTRGSGC---------------------------------------- 260
ZnT3                    ------------AEYAPLE-EGP----------------------------------------- 221
ZnT2                    ------------Q------------------------------------------------- 161
ZnT8                    ------------------------------------------------------------ 207
E.coli_zitB             ------------------------------------------------------------ 145
A.baumannii_czcD        ------------------------------------------------------------ 146
C.metallidurans_czcD    ------------------------------------------------------------ 141
ZnT1                    GHGHGLPKGPRVKSTRPGSSDINVAPGEQGPDQEETNTLVANTSNSNGLKLDPADPENPR 213
ZnT10                   GCVPGAFGGPQGAE-DPRRAADPTAPGSD-----SAVTLR-------GTSV----ERKRE 203


ZnT9                    KGMSFYKYV----------------------MESRDPSTNVILLEDTAAVLGVIIAATCMG 412
E.coli_yiiP             ---------------------------RRTQSQAVRADMLHYQSDVMMN-GAILLALGLS 171
ZnT6                    -VADLSRSLCG--------------IIPGLSSIFLPRMNPFVLIDLAGAFALCITYMLIE 220
ZnT5                    HGHGHSHGS-----------------AGGGMNANMRGVFLHVLADTLGSIGVIVSTVLIE 614
ZnT7                    HGHGHFHSHDG----------PSLKETTGPSRQILQGVFLHILADTLGSIGVIASAIMMQ 259
S.pneumoniae_czcD       ----------------------------KTKNESILSLHFLEDTLGWVAVILMAIVLR 161
S.pyogenes_czcD         ----------------------------QTKNEEILSLHFLEDILGWLAIIILSLILK 161
ZnT4                    ------------------------ERNHGQDSLAVRAAFVHALGDLVQSVGVLIAAYIIR 296
ZnT3                    ----------------------EEPLPLGNTSVRAAFVHVLGDLLQSFGVLAASILIY 257
ZnT2                    ---------------------------QEENPSVRAAFIHVIGDFMQSMGVLVAAYILY 193
ZnT8                    ---------------------------VQANASVRAAFVHALGDLFQSISVLISALIIY 239
E.coli_zitB             --------------------------SEEKNLNVRAAALHVLGDLLGSVGAIIAALIII 178
A.baumannii_czcD        -------------------------ANNSLNVKGAYLEVLSDALGSVGVIIGAIIIY 178
C.metallidurans_czcD    ---------------------------QSSSLNVKGAYLEVWSDLLGSVGVIAGAIIIR 173
ZnT1                    SGDTVEVQVNG---NLVREPDHMELEEDRAGQLNMRGVFLHVLGDALGSVIVVVNALVFY 270
ZnT10                   KGATVFANVAGDSFNTQNEPEDMMKKEKKSEALNIRGVLLHVMGDALGSVVVVITAIIFY 263
                                                        *          :

ZnT9                    LTSITGNPLYDSLGS--------------------------------LGVGTLLGMVSA 439
E.coli_yiiP             WYGW-----H-------------------------------------RADALFALGIG 187
ZnT6                    INNY-----F-------------------------------------AVDTASAIAIA 236
ZnT5                    QFGW-----F-----------------------------------IADPLCSLFIA 630
ZnT7                    NFGL-----M-----------------------------------IADPICSILIA 275
S.pneumoniae_czcD       FTDW-----Y-----------------------------------ILDPLLSLVIS 177
S.pyogenes_czcD         WKPW-----Y-----------------------------------ILDPLLSIAIA 177
ZnT4                    FKPE-----Y-----------------------------------KIADPICTYVFS 313
ZnT3                    FKPQ-----Y-----------------------------------KAADPISTFLFS 274
ZnT2                    FKPE-----Y-----------------------------------KYVDPICTFVFS 210
ZnT8                    FKPE-----Y-----------------------------------KIADPICTFIFS 256
E.coli_zitB             WTGW-----------------------------------------TPADPILSILVS 194
A.baumannii_czcD        FTNW-----------------------------------------YWIDTLIAVLIG 194
C.metallidurans_czcD    FTGW-----------------------------------------AWVDSAIAVLIG 189
ZnT1                    FSWK-----GCSEGDFCVNPCFPDPCKAFVEIINSTHASVYEAGPCWVLYLDPTLCVVMV 325
ZnT10                   VLPL-----K--------------------------------SEDPCNWQCYIDPSLTVLMV 288
                                                                    .

ZnT9                    FLIYTNTEALLGRSI------QPEQV--QR--LTELLE-NDPSVRAIHDVKATDLGLGKV 488
E.coli_yiiP             IYILYSALRMGYEAVQSLLDRALPDEERQE--IIDIVT-SWPGVSGAHDLRTRQSGPTRF 244
ZnT6                    LMTFGTMYPMSVYSGKVLLQTTPPHVIGQLDKLIREVS-TLDGVLEVRNEHFWTLGFGSL 295
ZnT5                    ILIFLSVVPLIKDACQVLLLRLPPEYEKELHIALEKIQ-KIEGLISYRDPHFWRHSASIV 689
ZnT7                    ILIVVSVIPLLRESVGILMQRTPPLLENSLPQCYQRVQ-QLQGVYSLQEQHFWTLCSDVY 334
S.pneumoniae_czcD       FFILSKALPRFWSTLKIFLDAVPEGLDIKQ--VKSGLE-RLDNVASLNQLNLWTMDALEK 234
S.pyogenes_czcD         SFILSKALSKLVATANIFLDGVPDSIDYCA--LHHELS-QLPHIVSVNQLNVWSMDGIDH 234
ZnT4                    LLVAFTTFRIIWDTVVIILEGVPSHLNVDY--IKEALM-KIEDVYSVEDLNIWSLTSGKS 370
ZnT3                    ICALGSTAPTLRDVLRILMEGTPRNVGFEP--VRDTLL-SVPGVRATHELHLWALTLTYH 331
ZnT2                    ILVLGTTLTILRDVILVLMEGTPKGVDFTA--VRDLLL-SVEGVEALHSLHIWALTVAQP 267
ZnT8                    ILVLASTITILKDFSILLMEGVPKSLNYSG--VKELIL-AVDGVLSVHSLHIWSLTMNQV 313
E.coli_zitB             LLVLRSAWRLLKDSVNELLEGAPVSLDIAE--LKRRMCREIPEVRNVHHVHVWMVGEKPV 252
```

```
A.baumannii_czcD          FWVLPRTWVLLKQSINILLEGVPEEVDIEK--LRADLL-SLNGVESIHQLKVWAITSKNI 251
C.metallidurans_czcD      LWVLPRTWILLKSSLNVLLEGVPDDVDLAE--VEKQIL-ATPGVKSFHDLHIWALTSGKA 246
ZnT1                      CILLYTTYPLLKESALILLQTVPKQIDIRN--LIKELR-NVEGVEEVHELHVWQLAGSRI 382
ZnT10                     IIILSSAFPLIKETAAILLQMVPKGVNMEE--LMSKLS-AVPGISSVHEVHIWELVSGKI 345
                                                          :     :   . .

ZnT9                      R-FKAEVDFD--GR-------V---VTRSYLEKQDFDQMLQEIQEV--KTPEELE----- 528
E.coli_yiiP               I--QIHLEME-DSLPLVQAHMVADQVEQAILRRFPGSDVIIHQD---------------- 285
ZnT6                      A-GSVHVRIRRDAN--E--QMVLAHVTNRLYTLV--STLTVQIFKDDWIRPALLSGPVAA 348
ZnT5                      A-GTIHIQVTSDVL--E--QRIVQQ-VTGILKDAGVNNLTIQVEKEAYFQHMSGL-S--- 739
ZnT7                      V-GTLKLIVAPDAD--A--RWILSQ-THNIFTQAGVRQLYVQIDFAAM------------ 376
S.pneumoniae_czcD         N-AIVHVCLK--EM---EHMETCKESIRIFLKDCGFQNITIEIDADLETHQ--------- 279
S.pyogenes_czcD           R-ATIHCCLK--ES---TTEKHCKKSIRLICQRYNINSVTVEIDTSLNEHQ--------- 279
ZnT4                      T-AIVHIQLIPGSS--SKWEEVQSKANHLLLNTFGMYRCTIQLQSYRQE----VD-R--- 419
ZnT3                      V-ASAHLAID--ST--ADPEAVLAEASSRLYSRFGFSSCTLQVEQYQPE-----M-A--- 377
ZnT2                      V-LSVHIAIA--QN--TDAQAVLKTASSRLQGKFHFHTVTIQIEDYSED-----M-K--- 313
ZnT8                      I-LSAHVATA--AS--RDSQVVRREIAKALSKSFTMHSLTIQMESPVDQ-----D-P--- 359
E.coli_zitB               MTLHVQVIPP-HDH-----DALLDQIQHYLMDHYQIEHATIQMEYQP------------- 293
A.baumannii_czcD          H-LTVHLFAP-EAD--RNK--LYQDAVEMLSHEHGIGEVTLQIEDDAEI----------- 294
C.metallidurans_czcD      S-LTVHVVND-TAV--NPEMEVLPELKQMLADKFDITHVTIQFELAP------------- 289
ZnT1                      I-ATAHIKCE-DPT---SYMEVAKTI-KDVFHNHGIHATTIQPEFASVGSKSSVV-P--- 432
ZnT10                     I-ATLHIKYP-KDR---GYQDASTKI-REIFHHAGIHNVTIQFENVDLKEPLEQK-D--- 395
                               .                           :

ZnT9                      ------------TFMLKH--GENIIDTLGAEVDRLE----KELKKRNPEVRHVDLEIL-- 568
E.coli_yiiP               ------------PCSVVPREGKRSMLS---------------------------------- 300
ZnT6                      NVLNFSDHHVIPMPLLKGTDDLNPVTSTPAKPSSPPP----EFSFNTPGKN-VNPVILLN 403
ZnT5                      --TGFHDV----LAMTKQMESM-----KYCKDGTYIM----------------------- 765
ZnT7                      ------------------------------------------------------------ 376
S.pneumoniae_czcD         ----THKR---KVCDLERSYEH-----QH------------------------------- 296
S.pyogenes_czcD           ----HHCS---SLSGIEVN----------------------------------------- 291
ZnT4                      --TCANCQ---SSSP--------------------------------------------- 429
ZnT3                      --QCLRCQ---EPPQA-------------------------------------------- 388
ZnT2                      --DCQACQ---GPSD--------------------------------------------- 323
ZnT8                      --DCLFCE---DPCD--------------------------------------------- 369
E.coli_zitB               ------CH---G----PDCHLN-----EGVS----G--H--SHHHH-------------- 313
A.baumannii_czcD          -----NCQ---H----IAQHAS-----HEHNDNDKT--H--SHQH-------------- 318
C.metallidurans_czcD      ------CE---Q----ADA-AQ-----HFNASPALV--G--SKSLAAGGN---------- 316
ZnT1                      --CELACR---TQCALKQCCGT-----LPQAPSG-------KDAEKTPAVS-ISCL---- 470
ZnT10                     --LLLLCN---SPCISKGCAKQ-----LCCPPGALPLAHVNGCAEHNGGPS-LDTY---- 440


ZnT9                      ------------------------------------------------------------  568
E.coli_yiiP               ------------------------------------------------------------  300
ZnT6                      TQTRPYGFGLNHGHTPYSSMLNQGLGVPGIGATQGLRTGFTNIPSRYGTNNRIGQPRP   461
ZnT5                      ------------------------------------------------------------  765
ZnT7                      ------------------------------------------------------------  376
S.pneumoniae_czcD         ------------------------------------------------------------  296
S.pyogenes_czcD           ------------------------------------------------------------  291
ZnT4                      ------------------------------------------------------------  429
ZnT3                      ------------------------------------------------------------  388
ZnT2                      ------------------------------------------------------------  323
ZnT8                      ------------------------------------------------------------  369
E.coli_zitB               ------------------------------------------------------------  313
A.baumannii_czcD          ------------------------------------------------------------  318
C.metallidurans_czcD      ------------------------------------------------------------  316
ZnT1                      ------ELSNNLEKKPRRT-KAENI--PAVVIEIKNMPNKQPESSL------------  507
ZnT10                     ------G-SDGLSRRDARE-VAIEVSLDSCLSDHGQSLNKTQEDQCYVNRTHF-----  485
```

Appendix 7: Primary sequence alignment of human ZnT proteins and bacterial zinc-transporting CDF proteins

Amino acid sequences of *E. coli* YiiP *(*GI: 60392291*), S. pneumoniae* CzcD (SPD_1638; GI: 116077533), *S. pyogenes* CzcD (GI: 94547648), *E. coli* ZitB (GI: 16128720), *A. baumannii* CzcD (GI: 672214288) *C. metallidurans* CzcD (GI: 3170388), and *H. sapiens* ZnT1 (GI: 52352803), ZnT2 (GI: 14210520), ZnT3 (GI: 21361112), ZnT4 (GI: 2582415), ZnT5 (GI: 20070323), ZnT6 (GI: 21687224), ZnT7 (GI: 222080086), ZnT8 (GI: 64762489), ZnT9 (GI: 57164948) and ZnT10 (GI: 52351208) were obtained from NCBI and aligned using Clustal Omega (Sievers *et al.*, 2011). * denotes fully conserved residue, : denotes conservation between groups of strongly similar properties, . denotes conservation between groups of weakly similar properties.

APPENDIX 8

```
Salmonella_glmU          -MLNSAMSVVILAAGKGTRMYSDIPKVLHTLAGKPMVQHVIDAATKLGAAQVHLVYGHGG  59
Ecoli_glmU               -MLNNAMSVVILAAGKGTRMYSDLPKVLHTLAGKAMVQHVIDAANELGAAHVHLVYGHGG  59
Mtuberculosis_glmU       MTFPGDTAVLVLAAGPGTRMRSDTPKVLHTLAGRSMLSHVLHAIAKLAPQRLIVVLGHDH  60
Spyogenes_glmU           ----MTNYAIILAAGKGTRMTSDLPKVLHKVSGLTMLEHVFRSVKAISPEKAVTVIGHKS  56
Saureus_glmU             ----MTNYAIILAAGKGTRMKSDLPKVLHHVSGLTMLEHVFRSVAAIEPEQNVTVIGHKA  56
Smutans_glmU             ----MTNYAIILAAGKGTRMKSDLPKVLHQVAGLTMLEHVKRAVDTMNPAKTVTVVGHKA  56
Spneumoniae_glmU         ----MSNFAIILAAGKGTRMKSDLPKVLHKVAGISMLEHVFRSVGAIQPEKTVTVVGHKA  56
Sagalactiae_glmU         ----MTNYAIILAAGKGTRMKSDLPKVMHQVAGITMLEHVFRAVSAIQPEKTVTVIGHKA  56
Efaecium_glmU            ---MENRYAIILAAGKGTRMKSKLYKVLHPVAGKPMVEHILDQVEQTEPTEIVTIVGHGA  57
Bcereus_glmU             ---MSNRFAVILAAGKGTRMKSKLYKVLHPVCGKPMVQHVVDQVSQLGLQKLVTVVGHGA  57
Bsubtilis_glmU           ---MDKRFAVILAAGKGTRMKSKLYKVLHPVCGKPMVEHVADEALKLSLAKLVTIVGHGA  57

Salmonella_glmU          ELLKQTL------KDDKLNWVLQAEQLGTGHAMQQAAPFFSDD--EDILMLYGDVPLISV  111
Ecoli_glmU               DLLKQAL------KDDNLNWVLQAEQLGTGHAMQQAAPFFADD--EDILMLYGDVPLISV  111
Mtuberculosis_glmU       QRIAPLVGELADTLGRTIDVALQDRPLGTGHAVLCGLSALPDDYAGNVVVTSGDTPLLDA  120
Spyogenes_glmU           EMVRAV-------LADQSAFVHQTEQLGTGHAVMMAETQLE-GLEGHTLVIAGDTPLITG  108
Saureus_glmU             DMVRAV-------LADQSEFVLQTEQLGTGHAVMMAEEKLA-GLEGHTLVIAGDTPLITG  108
Smutans_glmU             ELVQKV-------LEDQSEFVLQSEQLGTGHAVMMAESALA-ELEGQTLVIAGDTPLIRG  108
Spneumoniae_glmU         ELVEEV-------LAEQTEFVTQSEQLGTGHAVMMTEPILE-GLSGHTLVIAGDTPLITG  108
Sagalactiae_glmU         ELVKEV-------LGEQSLFALQTDQLGTGHAVMMAEAELA-GLEGQTLVIAGDTPLITG  108
Efaecium_glmU            EMIKSH-------LGERSQYALQAEQLGTGHAVMQAQELLG-GKQGTTLVITGDTPLLTA  109
Bcereus_glmU             EMVQEQ-------LGNVSEFALQAEQLGTAHAVDQAASVLA-NEEGTTLVICGDTPLITA  109
Bsubtilis_glmU           EDVKKQ-------LGQKSDYALQAEQLGTAHAVKQAKPFLQ-GEKGVTIVICGDTPLLTA  109

Salmonella_glmU          ETLQRLRDAKPQ--GGIGLLTVKLDDPSGYGRITR-ENGKVTGIVEHKDATDEQRQIQEI  168
Ecoli_glmU               ETLQRLRDAKPQ--GGIGLLTVKLDDPTGYGRITR-ENGKVTGIVEHKDATDEQRQIQEI  168
Mtuberculosis_glmU       DTLADLIATHRAVSAAVTVLTTTLDDPFGYGRILRTQDHEVMAIVEQTDATPSQREIREV  180
Spyogenes_glmU           ESLKSLIDFHVNHKNVATILTATAQDPFGYGRIVRNKDGEVIKIVEQKDANEYEQQLKEI  168
Saureus_glmU             QSLKSLIDFHVNHKNVATILTATAQDPFGYGRIIRNKDGEVIKIVEQKDASDFEQQIKEI  168
Smutans_glmU             ESLKNLLHYHKSHKNVATILTAEADDPFGYGRIIRNQNAEVIKIVEQKDASDYEQQVKEI  168
Spneumoniae_glmU         ESLKNLIDFHINHKNVATILTAETDNPFGYGRIVRNDNAEVLRIVEQKDATDFEKQIKEI  168
Sagalactiae_glmU         DSLQSLIEYHVSHKNVATILTAEADNPFGYGRIVRNKDQEVTKIVEQKDANDYEQAITEI  168
Efaecium_glmU            ETLKNLFDYHQGKNASATILTAHAEDPTGYGRIIRDHVGIVERIVEQKDASEEEARVQEI  169
Bcereus_glmU             ETMEALLQQHKEAGAMATVLTAYIEEPAGYGRIVRNENGHVEKIVEHKDANEKELAIKEI  169
Bsubtilis_glmU           ETMEAMLNEHTDKGAKATVLTAVADDPAGYGRIIRSEDGAVQKIVEHKDASEQERLVKEI  169

Salmonella_glmU          NTGILIANGADMKRWLSKLTNNNAQGEYYITDIIALAYQEGREIAAVHPARISETDGVNN  228
Ecoli_glmU               NTGILIANGADMKRWLAKLTNNNAQGEYYITDIIALAYQEGREIVAVHPQRLSEVEGVNN  228
Mtuberculosis_glmU       NAGVYAFDIAALRSALSRLSSNNAQQELYLTDVIAILRSDGQTVHASHVDDSALVAGVNN  240
Spyogenes_glmU           NTGTYVFDNKRLFEALKCITTNNAQGEYYLTDVVAIFRANKEKVGAYILRDFNESLGVND  228
Saureus_glmU             NTGTYVFDNKRLFEALKNITTNNAQGEYYLTDVISIFRDHKEKVGAYTLRDFNESLGVND  228
Smutans_glmU             NTGTYVFDNKRLFEALKEINTNNAQGEYYLTDVISIFKEADEKVGAYKLADFDESLGVND  228
Spneumoniae_glmU         NTGTYVFDNERLFEALKNINTNNAQGEYYITDVIGIFRETGEKVGAYTLKDFDESLGVND  228
Sagalactiae_glmU         NTGTYLFDNKRLFEALKNINTNNAQGEYYLTDVIGIFKEAGEKVGAYKLRDFDESLGVND  228
Efaecium_glmU            NTGTFCFDNESLFEALAKTDTNNTQGEYYLTDIIEILKKEGKAVAAYQMADFDEAMGVND  229
Bcereus_glmU             NTGTYCFDNKALFASLSKVSNDNVQGEYYLPDVIEILKNEGHIVSAYQTEHFDETLGVND  229
Bsubtilis_glmU           NTGTYCFDNEALFRVIEQVSNENAQGEYYLPDVIEILKDEGETVAAYQTGNFQETLGVND  229

Salmonella_glmU          RLQLSRLERIYQAEQAEKLLLSGVMLRDPARFDLRGTLHCGMDVEIDANVIIEGYVTLGH  288
Ecoli_glmU               RLQLSRLERVYQSEQAEKLLLAGVMLRDPARFDLRGTLTHGRDVEIDTNVIIEGNVTLGH  288
Mtuberculosis_glmU       RVQLAELASELNRRVVAAHQLAGVTVVDPATTWIDVDVTIGRDTVIHPGTQLLGRTQIGG  300
Spyogenes_glmU           RVALATAETVMRQRITQKHMVNGVTFQNPETVYIESDVEIAPDVLIEGNVTLKGRTHIGS  288
Saureus_glmU             RVALATAEAVMRQRITKKHMVNGVTFQNPETVYIESDVEIAPDVLIEGNVTLKGKTRIAA  288
Smutans_glmU             RVALAKAEKVMRRRINHAHMVNGVTLTNPASTYIDSDVIIAPDVVIEANVTLKGQTKIET  288
Spneumoniae_glmU         RVALATAESVMRRRINHKHMVNGVSFVNPEATYIDIDVEIAPEVQIEANVILKGQTKIGA  288
Sagalactiae_glmU         RVALATAERVMRRRINHNHMVKGVSFQNPDSAYIDIDVEIAEEVVVEANVTLKGQTKIGR  288
Efaecium_glmU            RVALSTANKIMHRRLNEMHMRNGVTFIDPDTTYIDEGVVIGSDTVIEAGVTIKGKTVIGE  289
Bcereus_glmU             RVALSQAEIIMKNRINRKNMVNGVTIIDPSNTYISADAIIGSDTVLHPGTIIEGNTVIGS  289
Bsubtilis_glmU           RVALSQAEMYMKERINKRHMQNGVTLIDPMNTYISPDARIGQDTVIYPGTVLKGQAEIGD  289

Salmonella_glmU          RVKIGAGCIIKNSVIGDDCEISPYSVVEDAHLEAACTIGPFARLRPGAELLAGAHVGNFV  348
Ecoli_glmU               RVKIGTGCVIKNSVIGDDCEISPYTVVEDANLAAACTIGPFARLRPGAELLEGAHVGNFV  348
Mtuberculosis_glmU       RCVVGPDTTLTDVAVGDGASVV-RTHGSSSSIGDGAAVGPFTYLRPGTALGADGKLGAFV  359
Spyogenes_glmU           GTVLTNGTYIVDSEIGQGSIIT-NSMIESSVLAAGVTVGPYAHLRPGTTLGREVHIGNFV  347
Saureus_glmU             ECVLTNGTYIVDSEIGQGSIIT-NSMIESSTLASGVTVGPYAHIRPGTSLAKDVHIGNFV  347
Smutans_glmU             GSVLTNGTYIVDSVIGENTVIT-HSMIEASRIEKNVTVGPYAHLRPNSVLEEAVHVGNFV  347
Spneumoniae_glmU         ETVLTNGTYVVDSTIGAGAVIT-NSMIEESSVADGVTVGPYAHIRPNSSLGAQVHIGNFV  347
Sagalactiae_glmU         ETVLTNGTYIVDSEVGANAVIT-NSMIEESQLDDGVTIGPYAHIRPGSDLAKNVHIGNFV  347
Efaecium_glmU            DCLIGAHSEIVDSHIGNQVVVK-QSVIEESVVREGADVGPYAHLRPKADVGANVHIGNFV  348
Bcereus_glmU             DCEIGPHTVIRDSEIGDRTTIR-QSTVHDSKLGTEVSVGPFAHIRPDSVIGDEVRVGNFV  348
Bsubtilis_glmU           ECVIGPHTEIEDSSIGSRTVIK-QSVVNRSKVGNDVNIGPFAHIRPDSAIGNEVKIGNFV  348
```

```
Salmonella_glmU         EMKKARLGKGSKAGHLTYLGDAEIGDNVNIGAGTITCNYDGANKFKTVIGDDVFVGSDTQ  408
Ecoli_glmU              EMKKARLGKGSKAGHLTYLGDAEIGDNVNIGAGTITCNYDGANKFKTIIGDDVFVGSDTQ  408
Mtuberculosis_glmU      EVKNSTIGTGTKVPHLTYVGDADIGEYSNIGASSVFVNYDGTSKRRTTVGSHVRTGSDTM  419
Spyogenes_glmU          EVKGSHIGEKTKAGHLTYIGNAQVGSSVNVGAGTITVNYDGQNKYETVIGDHAFIGSNST  407
Saureus_glmU            EVKGSHIGEKTKAGHLTYIGNAQVGSKVNVGAGTITVNYDGQNKYQTVIGDYAFIGSNST  407
Smutans_glmU            EVKASTLGKETKAGHLTYIGNAEVGHDVNFGAGTITVNYDGQNKYKTIIGNHVFVGSNST  407
Spneumoniae_glmU        EVKGSSIGENTKAGHLTYIGNCEVGSNVNFGAGTITVNYDGKNKYKTVIGDNVFVGSNST  407
Sagalactiae_glmU        EVKGSKLGENTKSGHLTYLGNAEIGKDVNIGAGTITVNYDGQHKFKTIIGDNAFVGSHST  407
Efaecium_glmU           EVKNATIDEGTKVGHLTYVGDATLGKDINVGCGVVFVNYDGKNKHQTVVGDHAFIGSATN  408
Bcereus_glmU            EIKKTVFGNRSKASHLSYIGDAQVGEDVNLGCGSITVNYDGKNKFKTVIGNGVFIGCNSN  408
Bsubtilis_glmU          EIKKTQFGDRSKASHLSYIGDAEVGTDVNLGCGSITVNYDGKKKYLTKIEDGAFIGCNSN  408
                          *:** : :.  :*  **:*:*:. :*   *.*.. :  **** *  * : . .  *. :

Salmonella_glmU         LVAPVTVGKGATIAAGTTVTRNVADNELVLSRVPQVHKQGWQRPVKKK------------  456
Ecoli_glmU              LVAPVTVGKGATIAAGTTVTRNVGENALAISRVPQTQKEGWRRPVKKK------------  456
Mtuberculosis_glmU      FVAPVTIGDGAYTGAGTVVREDVPPGALAVSAGPQRNIENWVQRKRPGSPAAQASKRASE  479
Spyogenes_glmU          LIAPLEVGDNALTAAGSTISKTVPADSIVIGRSRQVTKEGYAKRLAHHP-SRSK------  460
Saureus_glmU            LIAPLEVGDNALTAAGSTISKTVPADSIAIGRSRQVTKEDYAKRLPHHP-SRSK------  460
Smutans_glmU            IIAPVTIGDNALTAAGSTIHKDVPVDSIAIGRGRQVNKEGYAKKKPHHP-NNK-------  459
Spneumoniae_glmU        IIAPVELGDNSLVGAGSTITKDVPADAIAIGRGRQINKDEYATRLPHHP-KNQ*------  459
Sagalactiae_glmU        LIAPLEVGDNALTAAGSTITKDVPKDSVAIGRSRQENKEFYALKLPHHP-SRK-------  459
Efaecium_glmU           IVAPVTIGDHAVTAAGSTITEDVPSEDLAIARARQVNKEGYAKKLPYMK-D---------  458
Bcereus_glmU            LVAPVTVEDGAYVAAGSTITENVPSKALSVARARQVNKEDYVDQLLNKK-KS--------  459
Bsubtilis_glmU          LVAPVTVGEGAYVAAGSTVTEDVPGEALAIARARQVNKEDYVKNIHKK------------  456
                          ::**: : . :  .**:.:: . *    : :.   *   : :

Salmonella_glmU         ----------------        456
Ecoli_glmU              ----------------        456
Mtuberculosis_glmU      MACQQPTQPPDADQTP        495
Spyogenes_glmU          ----------------        460
Saureus_glmU            ----------------        460
Smutans_glmU            ----------------        459
Spneumoniae_glmU        ----------------        459
Sagalactiae_glmU        ----------------        459
Efaecium_glmU           ----------------        458
Bcereus_glmU            ----------------        459
Bsubtilis_glmU          ----------------        456
```

Appendix 8: Primary sequence alignment bacterial GlmU sequences

Amino acid sequences of *S.* Typhimurium GlmU (GI: 81521142), *E. coli* GlmU *(*GI: 81175326*), M. tuberculosis* GlmU (GI: 378544276), *S. pyogenes* GlmU (GI: 1757876988), *S. aureus* GlmU (GI: 669034937), *S. mutans* GlmU (GI: 557670921), *S. pneumoniae* GlmU (SPD_0874; GI: 122278758), *S. agalactiae* GlmU (GI: 1325413198) *E. faecium* GlmU (GI: 1150409197), *B. cereus* GlmU (GI: 728882518), *B. subtilis* GlmU (GI: 349592935) were obtained from NCBI and aligned using Clustal Omega (Sievers *et al.*, 2011). * denotes fully conserved residue, : denotes conservation between groups of strongly similar properties, . denotes conservation between groups of weakly similar properties.

REFERENCES

Aas, J. A., Paster, B. J., Stokes, L. N., Olsen, I., & Dewhirst, F. E. (2005). Defining the normal bacterial flora of the oral cavity. *J Clin Microbiol, 43*(11), 5721-5732. doi: 10.1128/JCM.43.11.5721-5732.2005

Adedeji, W. A. (2016). The Treasure Called Antibiotics. *Ann Ib Postgrad Med, 14*(2), 56-57.

Adetifa, I. M., Antonio, M., Okoromah, C. A., Ebruke, C., Inem, V., Nsekpong, D., Bojang, A., & Adegbola, R. A. (2012). Pre-vaccination nasopharyngeal pneumococcal carriage in a Nigerian population: epidemiology and population biology. *PLoS One, 7*(1), e30548. doi: 10.1371/journal.pone.0030548

Adlard, P. A., Bica, L., White, A. R., Nurjono, M., Filiz, G., Crouch, P. J., Donnelly, P. S., Cappai, R., Finkelstein, D. I., & Bush, A. I. (2011). Metal ionophore treatment restores dendritic spine density and synaptic protein levels in a mouse model of Alzheimer's disease. *PLoS One, 6*(3), e17669. doi: 10.1371/journal.pone.0017669

Adlard, P. A., Cherny, R. A., Finkelstein, D. I., Gautier, E., Robb, E., Cortes, M., Volitakis, I., Liu, X., Smith, J. P., Perez, K., Laughton, K., Li, Q. X., Charman, S. A., Nicolazzo, J. A., Wilkins, S., Deleva, K., Lynch, T., Kok, G., Ritchie, C. W., Tanzi, R. E., Cappai, R., Masters, C. L., Barnham, K. J., & Bush, A. I. (2008). Rapid restoration of cognition in Alzheimer's transgenic mice with 8-hydroxy quinoline analogs is associated with decreased interstitial Abeta. *Neuron, 59*(1), 43-55. doi: 10.1016/j.neuron.2008.06.018

Adler, H., Ferreira, D. M., Gordon, S. B., & Rylance, J. (2017). Pneumococcal Capsular Polysaccharide Immunity in the Elderly. *Clin Vaccine Immunol, 24*(6). doi: 10.1128/CVI.00004-17

Afzal, M., Shafeeq, S., Manzoor, I., & Kuipers, O. P. (2015). GalR Acts as a Transcriptional Activator of galKT in the Presence of Galactose in *Streptococcus pneumoniae*. *J Mol Microbiol Biotechnol, 25*(6), 363-371. doi: 10.1159/000439429

Agledal, L., Niere, M., & Ziegler, M. (2010). The phosphate makes a difference: cellular functions of NADP. *Redox Rep, 15*(1), 2-10. doi: 10.1179/174329210X12650506623122

Al-Bayati, F. A., Kahya, H. F., Damianou, A., Shafeeq, S., Kuipers, O. P., Andrew, P. W., & Yesilkaya, H. (2017). Pneumococcal galactose catabolism is controlled by multiple regulators acting on pyruvate formate lyase. *Sci Rep, 7*, 43587. doi: 10.1038/srep43587

Anders, S., & Huber, W. (2010). Differential expression analysis for sequence count data. *Genome Biol, 11*(10), R106. doi: 10.1186/gb-2010-11-10-r106

Andreini, C., Banci, L., Bertini, I., & Rosato, A. (2006). Counting the zinc-proteins encoded in the human genome. *J Proteome Res, 5*(1), 196-201. doi: 10.1021/pr050361j

Andreini, C., Bertini, I., Cavallaro, G., Holliday, G. L., & Thornton, J. M. (2008). Metal ions in biological catalysis: from enzyme databases to general principles. *J Biol Inorg Chem, 13*(8), 1205-1218. doi: 10.1007/s00775-008-0404-5

Andreini, C., Bertini, I., & Rosato, A. (2009). Metalloproteomes: a bioinformatic approach. *Acc Chem Res, 42*(10), 1471-1479. doi: 10.1021/ar900015x

Andrew, P. W., Mitchell, T. J., & Morgan, P. J. (1997). Relationship of structure to function in pneumolysin. *Microb Drug Resist, 3*(1), 11-17. doi: 10.1089/mdr.1997.3.11

Andrews, G. K., Wang, H., Dey, S. K., & Palmiter, R. D. (2004). Mouse zinc transporter 1 gene provides an essential function during early embryonic development. *Genesis, 40*(2), 74-81. doi: 10.1002/gene.20067

Anton, A., Grosse, C., Reissmann, J., Pribyl, T., & Nies, D. H. (1999). CzcD is a heavy metal ion transporter involved in regulation of heavy metal resistance in Ralstonia sp. strain CH34. *J Bacteriol, 181*(22), 6876-6881.

Anton, A., Weltrowski, A., Haney, C. J., Franke, S., Grass, G., Rensing, C., & Nies, D. H. (2004). Characteristics of zinc transport by two bacterial cation diffusion facilitators from Ralstonia metallidurans CH34 and *Escherichia coli*. *J Bacteriol, 186*(22), 7499-7507. doi: 10.1128/JB.186.22.7499-7507.2004

Aprianto, R., Slager, J., Holsappel, S., & Veening, J. W. (2018). High-resolution analysis of the pneumococcal transcriptome under a wide range of infection-relevant conditions. *Nucleic Acids Res, 46*(19), 9990-10006. doi: 10.1093/nar/gky750

Arguello, J. M. (2003). Identification of ion-selectivity determinants in heavy-metal transport P1B-type ATPases. *J Membr Biol, 195*(2), 93-108. doi: 10.1007/s00232-003-2048-2

Arguello, J. M., Eren, E., & Gonzalez-Guerrero, M. (2007). The structure and function of heavy metal transport P1B-ATPases. *Biometals, 20*(3-4), 233-248. doi: 10.1007/s10534-006-9055-6

Arguello, J. M., Gonzalez-Guerrero, M., & Raimunda, D. (2011). Bacterial transition metal P(1B)-ATPases: transport mechanism and roles in virulence. *Biochemistry, 50*(46), 9940-9949. doi: 10.1021/bi201418k

Aricha, B., Fishov, I., Cohen, Z., Sikron, N., Pesakhov, S., Khozin-Goldberg, I., Dagan, R., & Porat, N. (2004). Differences in membrane fluidity and fatty acid composition between phenotypic variants of *Streptococcus pneumoniae*. *J Bacteriol, 186*(14), 4638-4644. doi: 10.1128/JB.186.14.4638-4644.2004

Artini, M., Papa, R., Cellini, A., Tilotta, M., Barbato, G., Koverech, A., & Selan, L. (2014). Effect of betamethasone in combination with antibiotics on gram positive and gram negative bacteria. *Int J Immunopathol Pharmacol, 27*(4), 675-682. doi: 10.1177/039463201402700426

AURA. (2019). Australian Use and Resistance in Australia. *Australian Commission on Safetu and Quality in Health Care*.

Axelsen, K. B., & Palmgren, M. G. (1998). Evolution of substrate specificities in the P-type ATPase superfamily. *J Mol Evol, 46*(1), 84-101. doi: 10.1007/pl00006286

Babb, R., Chen, A., Hirst, T. R., Kara, E. E., McColl, S. R., Ogunniyi, A. D., Paton, J. C., & Alsharifi, M. (2016). Intranasal vaccination with gamma-irradiated *Streptococcus pneumoniae* whole-cell vaccine provides serotype-independent protection mediated by B-cells and innate IL-17 responses. *Clin Sci (Lond), 130*(9), 697-710. doi: 10.1042/CS20150699

Babb, R., Chen, A., Ogunniyi, A. D., Hirst, T. R., Kara, E. E., McColl, S. R., Alsharifi, M., & Paton, J. C. (2017). Enhanced protective responses to a serotype-independent pneumococcal vaccine when combined with an inactivated influenza vaccine. *Clin Sci (Lond), 131*(2), 169-180. doi: 10.1042/CS20160475

Bafaro, E., Liu, Y., Xu, Y., & Dempski, R. E. (2017). The emerging role of zinc transporters in cellular homeostasis and cancer. *Signal Transduct Target Ther, 2*. doi: 10.1038/sigtrans.2017.29

Bahl, R., Bhandari, N., Hambidge, K. M., & Bhan, M. K. (1998). Plasma zinc as a predictor of diarrheal and respiratory morbidity in children in an urban slum setting. *Am J Clin Nutr, 68*(2 Suppl), 414S-417S. doi: 10.1093/ajcn/68.2.414S

Bajaj, M., Mamidyala, S. K., Zuegg, J., Begg, S. L., Ween, M. P., Luo, Z., Huang, J. X., McEwan, A. G., Kobe, B., Paton, J. C., McDevitt, C. A., & Cooper, M. A. (2015). Discovery of novel pneumococcal surface antigen A (PsaA) inhibitors using a fragment-based drug design approach. *ACS Chem Biol, 10*(6), 1511-1520. doi: 10.1021/cb501032x

Bakal, S. N., Bereswill, S., & Heimesaat, M. M. (2017). Finding Novel Antibiotic Substances from Medicinal Plants - Antimicrobial Properties of Nigella Sativa Directed against Multidrug-resistant Bacteria. *Eur J Microbiol Immunol (Bp), 7*(1), 92-98. doi: 10.1556/1886.2017.00001

Baker, N. A., Sept, D., Joseph, S., Holst, M. J., & McCammon, J. A. (2001). Electrostatics of nanosystems: application to microtubules and the ribosome. *Proc Natl Acad Sci U S A, 98*(18), 10037-10041. doi: 10.1073/pnas.181342398

Banin, E., Hughes, D., & Kuipers, O. P. (2017). Editorial: Bacterial pathogens, antibiotics and antibiotic resistance. *FEMS Microbiol Rev, 41*(3), 450-452. doi: 10.1093/femsre/fux016

Baquero, F. (1996). Trends in antibiotic resistance of respiratory pathogens: an analysis and commentary on a collaborative surveillance study. *J Antimicrob Chemother, 38 Suppl A*, 117-132. doi: 10.1093/jac/38.suppl_a.117

Baquero, F. (1999). Evolving resistance patterns of *Streptococcus pneumoniae*: a link with long-acting macrolide consumption? *J Chemother, 11 Suppl 1*, 35-43. doi: 10.1179/joc.1999.11.Supplement-2.35

Barnham, K. J., & Bush, A. I. (2014). Biological metals and metal-targeting compounds in major neurodegenerative diseases. *Chem Soc Rev, 43*(19), 6727-6749. doi: 10.1039/c4cs00138a

Bayle, L., Chimalapati, S., Schoehn, G., Brown, J., Vernet, T., & Durmort, C. (2011). Zinc uptake by *Streptococcus pneumoniae* depends on both AdcA and AdcAII and is essential for normal bacterial morphology and virulence. *Mol Microbiol, 82*(4), 904-916. doi: 10.1111/j.1365-2958.2011.07862.x

Becker, K. W., & Skaar, E. P. (2014). Metal limitation and toxicity at the interface between host and pathogen. *FEMS Microbiol Rev, 38*(6), 1235-1249. doi: 10.1111/1574-6976.12087

Begg, S. L., Eijkelkamp, B. A., Luo, Z., Counago, R. M., Morey, J. R., Maher, M. J., Ong, C. L., McEwan, A. G., Kobe, B., O'Mara, M. L., Paton, J. C., & McDevitt, C. A. (2015). Dysregulation of transition metal ion homeostasis is the molecular basis for cadmium toxicity in *Streptococcus pneumoniae*. *Nat Commun, 6*, 6418. doi: 10.1038/ncomms7418

Bentley, S. D., Aanensen, D. M., Mavroidi, A., Saunders, D., Rabbinowitsch, E., Collins, M., Donohoe, K., Harris, D., Murphy, L., Quail, M. A., Samuel, G., Skovsted, I. C., Kaltoft, M. S., Barrell, B., Reeves, P. R., Parkhill, J., & Spratt, B. G. (2006). Genetic analysis of the capsular biosynthetic locus from all 90 pneumococcal serotypes. *PLoS Genet, 2*(3), e31. doi: 10.1371/journal.pgen.0020031

Bergmann, S., Rohde, M., Chhatwal, G. S., & Hammerschmidt, S. (2001). alpha-Enolase of *Streptococcus pneumoniae* is a plasmin(ogen)-binding protein displayed on the bacterial cell surface. *Mol Microbiol, 40*(6), 1273-1287. doi: 10.1046/j.1365-2958.2001.02448.x

Biasini, M., Bienert, S., Waterhouse, A., Arnold, K., Studer, G., Schmidt, T., Kiefer, F., Gallo Cassarino, T., Bertoni, M., Bordoli, L., & Schwede, T. (2014). SWISS-MODEL: modelling protein tertiary and quaternary structure using evolutionary information. *Nucleic Acids Res, 42*(Web Server issue), W252-258. doi: 10.1093/nar/gku340

Bidossi, A., Mulas, L., Decorosi, F., Colomba, L., Ricci, S., Pozzi, G., Deutscher, J., Viti, C., & Oggioni, M. R. (2012). A functional genomics approach to establish the complement of carbohydrate transporters in *Streptococcus pneumoniae*. *PLoS One, 7*(3), e33320. doi: 10.1371/journal.pone.0033320

Black, J. G., & Howes, D. (1978). Toxicity of pyrithiones. *Clin Toxicol, 13*(1), 1-26. doi: 10.3109/15563657808988226

Black, R. E., & Sazawal, S. (2001). Zinc and childhood infectious disease morbidity and mortality. *Br J Nutr, 85 Suppl 2*, S125-129. doi: 10.1079/bjn2000304

Bogaert, D., De Groot, R., & Hermans, P. W. (2004). *Streptococcus pneumoniae* colonisation: the key to pneumococcal disease. *Lancet Infect Dis, 4*(3), 144-154. doi: 10.1016/S1473-3099(04)00938-7

Bohlmann, L., De Oliveira, D. M. P., El-Deeb, I. M., Brazel, E. B., Harbison-Price, N., Ong, C. Y., Rivera-Hernandez, T., Ferguson, S. A., Cork, A. J., Phan, M. D., Soderholm, A. T., Davies, M. R., Nimmo, G. R., Dougan, G., Schembri, M. A., Cook, G. M., McEwan, A. G., von Itzstein, M., McDevitt, C. A., & Walker, M. J. (2018). Chemical Synergy between Ionophore PBT2 and Zinc Reverses Antibiotic Resistance. *MBio, 9*(6). doi: 10.1128/mBio.02391-18

Bonvehi, P., Weber, K., Busman, T., Shortridge, D., & Notario, G. (2003). Comparison of Clarithromycin and Amoxicillin/Clavulanic Acid for Community-Acquired Pneumonia in an Era of Drug-Resistant *Streptococcus pneumoniae*. *Clin Drug Investig, 23*(8), 491-501. doi: 10.2165/00044011-200323080-00001

Bosomworth, H. J., Thornton, J. K., Coneyworth, L. J., Ford, D., & Valentine, R. A. (2012). Efflux function, tissue-specific expression and intracellular trafficking of the Zn transporter ZnT10 indicate roles in adult Zn homeostasis. *Metallomics, 4*(8), 771-779. doi: 10.1039/c2mt20088k

Botella, H., Peyron, P., Levillain, F., Poincloux, R., Poquet, Y., Brandli, I., Wang, C., Tailleux, L., Tilleul, S., Charriere, G. M., Waddell, S. J., Foti, M., Lugo-Villarino, G., Gao, Q., Maridonneau-Parini, I., Butcher, P. D., Castagnoli, P. R., Gicquel, B., de Chastellier, C., & Neyrolles, O. (2011). Mycobacterial p(1)-type ATPases mediate resistance to zinc poisoning in human macrophages. *Cell Host Microbe, 10*(3), 248-259. doi: 10.1016/j.chom.2011.08.006

Botella, H., Stadthagen, G., Lugo-Villarino, G., de Chastellier, C., & Neyrolles, O. (2012). Metallobiology of host-pathogen interactions: an intoxicating new insight. *Trends Microbiol, 20*(3), 106-112. doi: 10.1016/j.tim.2012.01.005

Boulnois, G. J., Paton, J. C., Mitchell, T. J., & Andrew, P. W. (1991). Structure and function of pneumolysin, the multifunctional, thiol-activated toxin of *Streptococcus pneumoniae*. *Mol Microbiol, 5*(11), 2611-2616. doi: 10.1111/j.1365-2958.1991.tb01969.x

Braun, J. S., Sublett, J. E., Freyer, D., Mitchell, T. J., Cleveland, J. L., Tuomanen, E. I., & Weber, J. R. (2002). Pneumococcal pneumolysin and H(2)O(2) mediate brain cell apoptosis during meningitis. *J Clin Invest, 109*(1), 19-27. doi: 10.1172/JCI12035

Brinkmann, V., Reichard, U., Goosmann, C., Fauler, B., Uhlemann, Y., Weiss, D. S., Weinrauch, Y., & Zychlinsky, A. (2004). Neutrophil extracellular traps kill bacteria. *Science, 303*(5663), 1532-1535. doi: 10.1126/science.1092385

Brooks, L. R. K., & Mias, G. I. (2018). *Streptococcus pneumoniae*'s Virulence and Host Immunity: Aging, Diagnostics, and Prevention. *Front Immunol, 9*, 1366. doi: 10.3389/fimmu.2018.01366

Brooks, W. A., Chang, L. J., Sheng, X., Hopfer, R., & Team, P. P. R. S. (2015). Safety and immunogenicity of a trivalent recombinant PcpA, PhtD, and PlyD1 pneumococcal protein vaccine in adults, toddlers, and infants: A phase I randomized controlled study. *Vaccine, 33*(36), 4610-4617. doi: 10.1016/j.vaccine.2015.06.078

Brooks, W. A., Yunus, M., Santosham, M., Wahed, M. A., Nahar, K., Yeasmin, S., & Black, R. E. (2004). Zinc for severe pneumonia in very young children: double-blind placebo-controlled trial. *Lancet, 363*(9422), 1683-1688. doi: 10.1016/S0140-6736(04)16252-1

Brophy, M. B., Hayden, J. A., & Nolan, E. M. (2012). Calcium ion gradients modulate the zinc affinity and antibacterial activity of human calprotectin. *J Am Chem Soc, 134*(43), 18089-18100. doi: 10.1021/ja307974e

Brown, J. S., Gilliland, S. M., & Holden, D. W. (2001a). A *Streptococcus pneumoniae* pathogenicity island encoding an ABC transporter involved in iron uptake and virulence. *Mol Microbiol, 40*(3), 572-585. doi: 10.1046/j.1365-2958.2001.02414.x

Brown, J. S., & Holden, D. W. (2002). Iron acquisition by Gram-positive bacterial pathogens. *Microbes Infect, 4*(11), 1149-1156.

Brown, J. S., Ogunniyi, A. D., Woodrow, M. C., Holden, D. W., & Paton, J. C. (2001b). Immunization with components of two iron uptake ABC transporters protects mice against systemic *Streptococcus pneumoniae* infection. *Infect Immun, 69*(11), 6702-6706. doi: 10.1128/IAI.69.11.6702-6706.2001

Brown, L. R., Caulkins, R. C., Schartel, T. E., Rosch, J. W., Honsa, E. S., Schultz-Cherry, S., Meliopoulos, V. A., Cherry, S., & Thornton, J. A. (2017). Increased Zinc Availability Enhances Initial Aggregation and Biofilm Formation of *Streptococcus pneumoniae*. *Front Cell Infect Microbiol, 7*, 233. doi: 10.3389/fcimb.2017.00233

Buckett, P. D., & Wessling-Resnick, M. (2009). Small molecule inhibitors of divalent metal transporter-1. *Am J Physiol Gastrointest Liver Physiol, 296*(4), G798-804. doi: 10.1152/ajpgi.90342.2008

Buckwalter, C. M., & King, S. J. (2012). Pneumococcal carbohydrate transport: food for thought. *Trends Microbiol, 20*(11), 517-522. doi: 10.1016/j.tim.2012.08.008

Burnaugh, A. M., Frantz, L. J., & King, S. J. (2008). Growth of *Streptococcus pneumoniae* on human glycoconjugates is dependent upon the sequential activity of bacterial exoglycosidases. *J Bacteriol, 190*(1), 221-230. doi: 10.1128/JB.01251-07

Buurman, E. T., Andrews, B., Gao, N., Hu, J., Keating, T. A., Lahiri, S., Otterbein, L. R., Patten, A. D., Stokes, S. S., & Shapiro, A. B. (2011). In vitro validation of acetyltransferase

activity of GlmU as an antibacterial target in Haemophilus influenzae. *J Biol Chem, 286*(47), 40734-40742. doi: 10.1074/jbc.M111.274068

Campo, J. J., Le, T. Q., Pablo, J. V., Hung, C., Teng, A. A., Tettelin, H., Tate, A., Hanage, W. P., Alderson, M. R., Liang, X., Malley, R., Lipsitch, M., & Croucher, N. J. (2018). Panproteome-wide analysis of antibody responses to whole cell pneumococcal vaccination. *Elife, 7*. doi: 10.7554/eLife.37015

Capdevila, D. A., Edmonds, K. A., & Giedroc, D. P. (2017). Metallochaperones and metalloregulation in bacteria. *Essays Biochem, 61*(2), 177-200. doi: 10.1042/EBC20160076

Capdevila, D. A., Wang, J., & Giedroc, D. P. (2016). Bacterial Strategies to Maintain Zinc Metallostasis at the Host-Pathogen Interface. *J Biol Chem, 291*(40), 20858-20868. doi: 10.1074/jbc.R116.742023

Capocci, S., & Lipman, M. (2013). Respiratory infections in HIV-infected adults: epidemiology, clinical features, diagnosis and treatment. *Curr Opin Pulm Med, 19*(3), 238-243. doi: 10.1097/MCP.0b013e32835f1b5c

Cardoso, A. I., Beauverger, P., Gerlier, D., Wild, T. F., & Rabourdin-Combe, C. (1995). Formaldehyde inactivation of measles virus abolishes CD46-dependent presentation of nucleoprotein to murine class I-restricted CTLs but not to class II-restricted helper T cells. *Virology, 212*(1), 255-258. doi: 10.1006/viro.1995.1479

Carvalho, S. M., Kloosterman, T. G., Kuipers, O. P., & Neves, A. R. (2011). CcpA ensures optimal metabolic fitness of *Streptococcus pneumoniae*. *PLoS One, 6*(10), e26707. doi: 10.1371/journal.pone.0026707

CDC. (2012). Centers for Disease Control and Prevention, Active Bacterial Core Surveillance Report, Emerging Infections Program Network, *Streptococcus pneumoniae*, 2010.

CDC. (2019). Centers for Disease Control and Prevention, Vaccine Price List. *National Center for Immunization and Respiratory Diseases*.

Chambers, H. F. (1999). Penicillin-binding protein-mediated resistance in pneumococci and staphylococci. *J Infect Dis, 179 Suppl 2*, S353-359. doi: 10.1086/513854

Chandrangsu, P., Rensing, C., & Helmann, J. D. (2017). Metal homeostasis and resistance in bacteria. *Nat Rev Microbiol, 15*(6), 338-350. doi: 10.1038/nrmicro.2017.15

Chao, Y., & Fu, D. (2004). Thermodynamic studies of the mechanism of metal binding to the *Escherichia coli* zinc transporter YiiP. *J Biol Chem, 279*(17), 17173-17180. doi: 10.1074/jbc.M400208200

Chen, C., Cervero Liceras, F., Flasche, S., Sidharta, S., Yoong, J., Sundaram, N., & Jit, M. (2019). Effect and cost-effectiveness of pneumococcal conjugate vaccination: a global

modelling analysis. *Lancet Glob Health, 7*(1), e58-e67. doi: 10.1016/S2214-109X(18)30422-4

Chen, V. B., Arendall, W. B., 3rd, Headd, J. J., Keedy, D. A., Immormino, R. M., Kapral, G. J., Murray, L. W., Richardson, J. S., & Richardson, D. C. (2010). MolProbity: all-atom structure validation for macromolecular crystallography. *Acta Crystallogr D Biol Crystallogr, 66*(Pt 1), 12-21. doi: 10.1107/S0907444909042073

Cherazard, R., Epstein, M., Doan, T. L., Salim, T., Bharti, S., & Smith, M. A. (2017). Antimicrobial Resistant *Streptococcus pneumoniae*: Prevalence, Mechanisms, and Clinical Implications. *Am J Ther, 24*(3), e361-e369. doi: 10.1097/MJT.0000000000000551

Chiem, K., Fuentes, B. A., Lin, D. L., Tran, T., Jackson, A., Ramirez, M. S., & Tolmasky, M. E. (2015). Inhibition of aminoglycoside 6'-N-acetyltransferase type Ib-mediated amikacin resistance in Klebsiella pneumoniae by zinc and copper pyrithione. *Antimicrob Agents Chemother, 59*(9), 5851-5853. doi: 10.1128/AAC.01106-15

Chiem, K., Hue, F., Magallon, J., & Tolmasky, M. E. (2018). Inhibition of aminoglycoside 6'-N-acetyltransferase type Ib-mediated amikacin resistance by zinc complexed with clioquinol, an ionophore active against tumors and neurodegenerative diseases. *Int J Antimicrob Agents, 51*(2), 271-273. doi: 10.1016/j.ijantimicag.2017.08.002

Chimienti, F., Devergnas, S., Favier, A., & Seve, M. (2004). Identification and cloning of a beta-cell-specific zinc transporter, ZnT-8, localized into insulin secretory granules. *Diabetes, 53*(9), 2330-2337.

Chong, J., Soufan, O., Li, C., Caraus, I., Li, S., Bourque, G., Wishart, D. S., & Xia, J. (2018). MetaboAnalyst 4.0: towards more transparent and integrative metabolomics analysis. *Nucleic Acids Res, 46*(W1), W486-W494. doi: 10.1093/nar/gky310

Choo, S., & Finn, A. (2001). New pneumococcal vaccines for children. *Arch Dis Child, 84*(4), 289-294. doi: 10.1136/adc.84.4.289

Cilloniz, C., Rodriguez-Hurtado, D., & Torres, A. (2018). Characteristics and Management of Community-Acquired Pneumonia in the Era of Global Aging. *Med Sci (Basel), 6*(2). doi: 10.3390/medsci6020035

Claverys, J. P., & Havarstein, L. S. (2002). Extracellular-peptide control of competence for genetic transformation in *Streptococcus pneumoniae*. *Front Biosci, 7*, d1798-1814. doi: 10.2741/claverys

CLSI. (2015). Performance standards for antimicrobial susceptibility testing; approved standard; 25th informational supplement. CLSI document M100-S25. Clinical and Laboratory Standards Institute, Wayne, PA.

Cockeran, R., Theron, A. J., Steel, H. C., Matlola, N. M., Mitchell, T. J., Feldman, C., & Anderson, R. (2001). Proinflammatory interactions of pneumolysin with human neutrophils. *J Infect Dis, 183*(4), 604-611. doi: 10.1086/318536

Coffey, T. J., Enright, M. C., Daniels, M., Morona, J. K., Morona, R., Hryniewicz, W., Paton, J. C., & Spratt, B. G. (1998). Recombinational exchanges at the capsular polysaccharide biosynthetic locus lead to frequent serotype changes among natural isolates of *Streptococcus pneumoniae*. *Mol Microbiol, 27*(1), 73-83. doi: 10.1046/j.1365-2958.1998.00658.x

Cohen, J. M., Khandavilli, S., Camberlein, E., Hyams, C., Baxendale, H. E., & Brown, J. S. (2011). Protective contributions against invasive *Streptococcus pneumoniae* pneumonia of antibody and Th17-cell responses to nasopharyngeal colonisation. *PLoS One, 6*(10), e25558. doi: 10.1371/journal.pone.0025558

Corbin, B. D., Seeley, E. H., Raab, A., Feldmann, J., Miller, M. R., Torres, V. J., Anderson, K. L., Dattilo, B. M., Dunman, P. M., Gerads, R., Caprioli, R. M., Nacken, W., Chazin, W. J., & Skaar, E. P. (2008). Metal chelation and inhibition of bacterial growth in tissue abscesses. *Science, 319*(5865), 962-965. doi: 10.1126/science.1152449

Correa, R. A., Costa, A. N., Lundgren, F., Michelin, L., Figueiredo, M. R., Holanda, M., Gomes, M., Teixeira, P. J. Z., Martins, R., Silva, R., Athanazio, R. A., Silva, R. M. D., & Pereira, M. C. (2018). 2018 recommendations for the management of community acquired pneumonia. *J Bras Pneumol, 44*(5), 405-423. doi: 10.1590/S1806-37562018000000130

Corso, A., Severina, E. P., Petruk, V. F., Mauriz, Y. R., & Tomasz, A. (1998). Molecular characterization of penicillin-resistant *Streptococcus pneumoniae* isolates causing respiratory disease in the United States. *Microb Drug Resist, 4*(4), 325-337. doi: 10.1089/mdr.1998.4.325

Coudray, N., Valvo, S., Hu, M., Lasala, R., Kim, C., Vink, M., Zhou, M., Provasi, D., Filizola, M., Tao, J., Fang, J., Penczek, P. A., Ubarretxena-Belandia, I., & Stokes, D. L. (2013). Inward-facing conformation of the zinc transporter YiiP revealed by cryoelectron microscopy. *Proc Natl Acad Sci U S A, 110*(6), 2140-2145. doi: 10.1073/pnas.1215455110

Couñago, R. M., Ween, M. P., Begg, S. L., Bajaj, M., Zuegg, J., O'Mara, M. L., Cooper, M. A., McEwan, A. G., Paton, J. C., Kobe, B., & McDevitt, C. A. (2014). Imperfect coordination chemistry facilitates metal ion release in the Psa permease. *Nat Chem Biol, 10*(1), 35-41. doi: 10.1038/nchembio.1382

Crisostomo, M. I., Vollmer, W., Kharat, A. S., Inhulsen, S., Gehre, F., Buckenmaier, S., & Tomasz, A. (2006). Attenuation of penicillin resistance in a peptidoglycan O-acetyl transferase mutant of *Streptococcus pneumoniae*. *Mol Microbiol, 61*(6), 1497-1509. doi: 10.1111/j.1365-2958.2006.05340.x

Croucher, N. J., Walker, D., Romero, P., Lennard, N., Paterson, G. K., Bason, N. C., Mitchell, A. M., Quail, M. A., Andrew, P. W., Parkhill, J., Bentley, S. D., & Mitchell, T. J. (2009). Role of conjugative elements in the evolution of the multidrug-resistant pandemic clone *Streptococcus pneumoniae*Spain23F ST81. *J Bacteriol, 191*(5), 1480-1489. doi: 10.1128/JB.01343-08

Dagan, R., Melamed, R., Muallem, M., Piglansky, L., & Yagupsky, P. (1996). Nasopharyngeal colonization in southern Israel with antibiotic-resistant pneumococci during the first 2 years of life: relation to serotypes likely to be included in pneumococcal conjugate vaccines. *J Infect Dis, 174*(6), 1352-1355. doi: 10.1093/infdis/174.6.1352

Damo, S. M., Kehl-Fie, T. E., Sugitani, N., Holt, M. E., Rathi, S., Murphy, W. J., Zhang, Y., Betz, C., Hench, L., Fritz, G., Skaar, E. P., & Chazin, W. J. (2013). Molecular basis for manganese sequestration by calprotectin and roles in the innate immune response to invading bacterial pathogens. *Proc Natl Acad Sci U S A, 110*(10), 3841-3846. doi: 10.1073/pnas.1220341110

Darras-Joly, C., Bedos, J. P., Sauve, C., Moine, P., Vallee, E., Carbon, C., & Azoulay-Dupuis, E. (1996). Synergy between amoxicillin and gentamicin in combination against a highly penicillin-resistant and -tolerant strain of *Streptococcus pneumoniae* in a mouse pneumonia model. *Antimicrob Agents Chemother, 40*(9), 2147-2151.

David, S. C., Norton, T., Tyllis, T., Wilson, J. J., Singleton, E. V., Laan, Z., Davies, J., Hirst, T. R., Comerford, I., McColl, S. R., Paton, J. C., & Alsharifi, M. (2019). Direct interaction of whole-inactivated influenza A and pneumococcal vaccines enhances influenza-specific immunity. *Nat Microbiol, 4*(8), 1316-1327. doi: 10.1038/s41564-019-0443-4

Davidson, A. L., Shuman, H. A., & Nikaido, H. (1992). Mechanism of maltose transport in *Escherichia coli*: transmembrane signaling by periplasmic binding proteins. *Proc Natl Acad Sci U S A, 89*(6), 2360-2364. doi: 10.1073/pnas.89.6.2360

Davis, K. M., Akinbi, H. T., Standish, A. J., & Weiser, J. N. (2008). Resistance to mucosal lysozyme compensates for the fitness deficit of peptidoglycan modifications by *Streptococcus pneumoniae*. *PLoS Pathog, 4*(12), e1000241. doi: 10.1371/journal.ppat.1000241

Davis, K. M., Nakamura, S., & Weiser, J. N. (2011). Nod2 sensing of lysozyme-digested peptidoglycan promotes macrophage recruitment and clearance of S. pneumoniae colonization in mice. *J Clin Invest, 121*(9), 3666-3676. doi: 10.1172/JCI57761

Davis, S. M., Deloria-Knoll, M., Kassa, H. T., & O'Brien, K. L. (2013). Impact of pneumococcal conjugate vaccines on nasopharyngeal carriage and invasive disease among unvaccinated people: review of evidence on indirect effects. *Vaccine, 32*(1), 133-145. doi: 10.1016/j.vaccine.2013.05.005

Dawid, S., Roche, A. M., & Weiser, J. N. (2007). The blp bacteriocins of *Streptococcus pneumoniae* mediate intraspecies competition both in vitro and in vivo. *Infect Immun, 75*(1), 443-451. doi: 10.1128/IAI.01775-05

de Steenhuijsen Piters, W. A., Sanders, E. A., & Bogaert, D. (2015). The role of the local microbial ecosystem in respiratory health and disease. *Philos Trans R Soc Lond B Biol Sci, 370*(1675). doi: 10.1098/rstb.2014.0294

Diavatopoulos, D. A., Short, K. R., Price, J. T., Wilksch, J. J., Brown, L. E., Briles, D. E., Strugnell, R. A., & Wijburg, O. L. (2010). Influenza A virus facilitates *Streptococcus pneumoniae* transmission and disease. *FASEB J, 24*(6), 1789-1798. doi: 10.1096/fj.09-146779

Ding, W. Q., & Lind, S. E. (2009). Metal ionophores - an emerging class of anticancer drugs. *IUBMB Life, 61*(11), 1013-1018. doi: 10.1002/iub.253

Dintilhac, A., Alloing, G., Granadel, C., & Claverys, J. P. (1997). Competence and virulence of *Streptococcus pneumoniae*: Adc and PsaA mutants exhibit a requirement for Zn and Mn resulting from inactivation of putative ABC metal permeases. *Mol Microbiol, 25*(4), 727-739.

Djoko, K. Y., Achard, M. E. S., Phan, M. D., Lo, A. W., Miraula, M., Prombhul, S., Hancock, S. J., Peters, K. M., Sidjabat, H. E., Harris, P. N., Mitic, N., Walsh, T. R., Anderson, G. J., Shafer, W. M., Paterson, D. L., Schenk, G., McEwan, A. G., & Schembri, M. A. (2018). Copper Ions and Coordination Complexes as Novel Carbapenem Adjuvants. *Antimicrob Agents Chemother, 62*(2). doi: 10.1128/AAC.02280-17

Dockrell, D. H., & Brown, J. S. (2015). Chapter 21 – *Streptococcus pneumoniae* interactions with macrophages and mechanisms of immune evasion. In Brown J, Hammerschmidt S, Orihuela C, editors, *Streptococcus pneumoniae*, . *Amsterdam: Academic Press;* , 401–422.

Dowell, S. F., & Schwartz, B. (1997). Resistant pneumococci: protecting patients through judicious use of antibiotics. *Am Fam Physician, 55*(5), 1647-1654, 1657-1648.

Dubois-Brissonnet, F., Trotier, E., & Briandet, R. (2016). The Biofilm Lifestyle Involves an Increase in Bacterial Membrane Saturated Fatty Acids. *Front Microbiol, 7*, 1673. doi: 10.3389/fmicb.2016.01673

Durando, P., Faust, S. N., Fletcher, M., Krizova, P., Torres, A., & Welte, T. (2013). Experience with pneumococcal polysaccharide conjugate vaccine (conjugated to CRM197 carrier protein) in children and adults. *Clin Microbiol Infect, 19 Suppl 1*, 1-9. doi: 10.1111/1469-0691.12320

Eijkelkamp, B. A., Begg, S. L., Pederick, V. G., Trapetti, C., Gregory, M. K., Whittall, J. J., Paton, J. C., & McDevitt, C. A. (2018). Arachidonic Acid Stress Impacts

Pneumococcal Fatty Acid Homeostasis. *Front Microbiol, 9*, 813. doi: 10.3389/fmicb.2018.00813

Eijkelkamp, B. A., Morey, J. R., Neville, S. L., Tan, A., Pederick, V. G., Cole, N., Singh, P. P., Ong, C. Y., Gonzalez de Vega, R., Clases, D., Cunningham, B. A., Hughes, C. E., Comerford, I., Brazel, E. B., Whittall, J. J., Plumptre, C. D., McColl, S. R., Paton, J. C., McEwan, A. G., Doble, P. A., & McDevitt, C. A. (2019). Dietary zinc and the control of *Streptococcus pneumoniae* infection. *PLoS Pathog, 15*(8), e1007957. doi: 10.1371/journal.ppat.1007957

Eijkelkamp, B. A., Morey, J. R., Ween, M. P., Ong, C. L., McEwan, A. G., Paton, J. C., & McDevitt, C. A. (2014). Extracellular zinc competitively inhibits manganese uptake and compromises oxidative stress management in *Streptococcus pneumoniae*. *PLoS One, 9*(2), e89427. doi: 10.1371/journal.pone.0089427

Ellman, G. L. (1958). A colorimetric method for determining low concentrations of mercaptans. *Arch Biochem Biophys, 74*(2), 443-450. doi: 10.1016/0003-9861(58)90014-6

Emsley, P., Lohkamp, B., Scott, W. G., & Cowtan, K. (2010). Features and development of Coot. *Acta Crystallogr D Biol Crystallogr, 66*(Pt 4), 486-501. doi: 10.1107/S0907444910007493

Ewig, S., Ruiz, M., Torres, A., Marco, F., Martinez, J. A., Sanchez, M., & Mensa, J. (1999). Pneumonia acquired in the community through drug-resistant *Streptococcus pneumoniae*. *Am J Respir Crit Care Med, 159*(6), 1835-1842. doi: 10.1164/ajrccm.159.6.9808049

Fair, R. J., & Tor, Y. (2014). Antibiotics and bacterial resistance in the 21st century. *Perspect Medicin Chem, 6*, 25-64. doi: 10.4137/PMC.S14459

Fan, B., & Rosen, B. P. (2002). Biochemical characterization of CopA, the *Escherichia coli* Cu(I)-translocating P-type ATPase. *J Biol Chem, 277*(49), 46987-46992. doi: 10.1074/jbc.M208490200

Feikin, D. R., Kagucia, E. W., Loo, J. D., Link-Gelles, R., Puhan, M. A., Cherian, T., Levine, O. S., Whitney, C. G., O'Brien, K. L., Moore, M. R., & Serotype Replacement Study, G. (2013). Serotype-specific changes in invasive pneumococcal disease after pneumococcal conjugate vaccine introduction: a pooled analysis of multiple surveillance sites. *PLoS Med, 10*(9), e1001517. doi: 10.1371/journal.pmed.1001517

Feldman, C., & Anderson, R. (2014). Review: current and new generation pneumococcal vaccines. *J Infect, 69*(4), 309-325. doi: 10.1016/j.jinf.2014.06.006

Ferreira, D. M., Neill, D. R., Bangert, M., Gritzfeld, J. F., Green, N., Wright, A. K., Pennington, S. H., Bricio-Moreno, L., Moreno, A. T., Miyaji, E. N., Wright, A. D., Collins, A. M., Goldblatt, D., Kadioglu, A., & Gordon, S. B. (2013). Controlled human infection and rechallenge with *Streptococcus pneumoniae* reveals the protective efficacy of carriage

in healthy adults. *Am J Respir Crit Care Med, 187*(8), 855-864. doi: 10.1164/rccm.201212-2277OC

Fischer Walker, C., & Black, R. E. (2004). Zinc and the risk for infectious disease. *Annu Rev Nutr, 24*, 255-275. doi: 10.1146/annurev.nutr.23.011702.073054

Flannagan, R. S., Cosio, G., & Grinstein, S. (2009). Antimicrobial mechanisms of phagocytes and bacterial evasion strategies. *Nat Rev Microbiol, 7*(5), 355-366. doi: 10.1038/nrmicro2128

Foster, A. W., Osman, D., & Robinson, N. J. (2014). Metal preferences and metallation. *J Biol Chem, 289*(41), 28095-28103. doi: 10.1074/jbc.R114.588145

French, G. L. (2005). Clinical impact and relevance of antibiotic resistance. *Adv Drug Deliv Rev, 57*(10), 1514-1527. doi: 10.1016/j.addr.2005.04.005

Fu, Y., Tsui, H. C., Bruce, K. E., Sham, L. T., Higgins, K. A., Lisher, J. P., Kazmierczak, K. M., Maroney, M. J., Dann, C. E., 3rd, Winkler, M. E., & Giedroc, D. P. (2013). A new structural paradigm in copper resistance in *Streptococcus pneumoniae*. *Nat Chem Biol, 9*(3), 177-183. doi: 10.1038/nchembio.1168

Gammoh, N. Z., & Rink, L. (2017). Zinc in Infection and Inflammation. *Nutrients, 9*(6). doi: 10.3390/nu9060624

Garcia, Y. M., Barwinska-Sendra, A., Tarrant, E., Skaar, E. P., Waldron, K. J., & Kehl-Fie, T. E. (2017). A Superoxide Dismutase Capable of Functioning with Iron or Manganese Promotes the Resistance of *Staphylococcus aureus* to Calprotectin and Nutritional Immunity. *PLoS Pathog, 13*(1), e1006125. doi: 10.1371/journal.ppat.1006125

Gehring, A. M., Lees, W. J., Mindiola, D. J., Walsh, C. T., & Brown, E. D. (1996). Acetyltransfer precedes uridylyltransfer in the formation of UDP-N-acetylglucosamine in separable active sites of the bifunctional GlmU protein of *Escherichia coli*. *Biochemistry, 35*(2), 579-585. doi: 10.1021/bi952275a

Geno, K. A., Saad, J. S., & Nahm, M. H. (2017). Discovery of Novel Pneumococcal Serotype 35D, a Natural WciG-Deficient Variant of Serotype 35B. *J Clin Microbiol, 55*(5), 1416-1425. doi: 10.1128/JCM.00054-17

Gibson, R. S., & Ferguson, E. L. (1998). Assessment of dietary zinc in a population. *Am J Clin Nutr, 68*(2 Suppl), 430S-434S. doi: 10.1093/ajcn/68.2.430S

Gooyit, M., & Janda, K. D. (2016). Reprofiled anthelmintics abate hypervirulent stationary-phase Clostridium difficile. *Sci Rep, 6*, 33642. doi: 10.1038/srep33642

Grass, G., Otto, M., Fricke, B., Haney, C. J., Rensing, C., Nies, D. H., & Munkelt, D. (2005). FieF (YiiP) from *Escherichia coli* mediates decreased cellular accumulation of iron

and relieves iron stress. *Arch Microbiol, 183*(1), 9-18. doi: 10.1007/s00203-004-0739-4

Guerra, A. J., Dann, C. E., 3rd, & Giedroc, D. P. (2011). Crystal structure of the zinc-dependent MarR family transcriptional regulator AdcR in the Zn(II)-bound state. *J Am Chem Soc, 133*(49), 19614-19617. doi: 10.1021/ja2080532

Guffanti, A. A., Wei, Y., Rood, S. V., & Krulwich, T. A. (2002). An antiport mechanism for a member of the cation diffusion facilitator family: divalent cations efflux in exchange for K+ and H+. *Mol Microbiol, 45*(1), 145-153. doi: 10.1046/j.1365-2958.2002.02998.x

Guo, L., Lichten, L. A., Ryu, M. S., Liuzzi, J. P., Wang, F., & Cousins, R. J. (2010). STAT5-glucocorticoid receptor interaction and MTF-1 regulate the expression of ZnT2 (Slc30a2) in pancreatic acinar cells. *Proc Natl Acad Sci U S A, 107*(7), 2818-2823. doi: 10.1073/pnas.0914941107

Haase, H., & Rink, L. (2014). Zinc signals and immune function. *Biofactors, 40*(1), 27-40. doi: 10.1002/biof.1114

Haider, B. A., Lassi, Z. S., Ahmed, A., & Bhutta, Z. A. (2011). Zinc supplementation as an adjunct to antibiotics in the treatment of pneumonia in children 2 to 59 months of age. *Cochrane Database Syst Rev,* (10), CD007368. doi: 10.1002/14651858.CD007368.pub2

Hamaguchi, S., Zafar, M. A., Cammer, M., & Weiser, J. N. (2018). Capsule Prolongs Survival of *Streptococcus pneumoniae* during Starvation. *Infect Immun, 86*(3). doi: 10.1128/IAI.00802-17

Hammerschmidt, S., Wolff, S., Hocke, A., Rosseau, S., Muller, E., & Rohde, M. (2005). Illustration of pneumococcal polysaccharide capsule during adherence and invasion of epithelial cells. *Infect Immun, 73*(8), 4653-4667. doi: 10.1128/IAI.73.8.4653-4667.2005

Hansman, D., & Bullen, M. M. (1967). A resistant Pneumococcus. *The Lancet, 290*(7509), 264-265.

Hardy, G. G., Caimano, M. J., & Yother, J. (2000). Capsule biosynthesis and basic metabolism in *Streptococcus pneumoniae* are linked through the cellular phosphoglucomutase. *J Bacteriol, 182*(7), 1854-1863. doi: 10.1128/jb.182.7.1854-1863.2000

Hasan, R., Rink, L., & Haase, H. (2013). Zinc signals in neutrophil granulocytes are required for the formation of neutrophil extracellular traps. *Innate Immun, 19*(3), 253-264. doi: 10.1177/1753425912458815

Hatori, Y., Majima, E., Tsuda, T., & Toyoshima, C. (2007). Domain organization and movements in heavy metal ion pumps: papain digestion of CopA, a Cu+-transporting ATPase. *J Biol Chem, 282*(35), 25213-25221. doi: 10.1074/jbc.M703520200

Havarstein, L. S., Gaustad, P., Nes, I. F., & Morrison, D. A. (1996). Identification of the streptococcal competence-pheromone receptor. *Mol Microbiol, 21*(4), 863-869. doi: 10.1046/j.1365-2958.1996.521416.x

Helsel, M. E., & Franz, K. J. (2015). Pharmacological activity of metal binding agents that alter copper bioavailability. *Dalton Trans, 44*(19), 8760-8770. doi: 10.1039/c5dt00634a

Henriques-Normark, B., & Tuomanen, E. I. (2013). The pneumococcus: epidemiology, microbiology, and pathogenesis. *Cold Spring Harb Perspect Med, 3*(7). doi: 10.1101/cshperspect.a010215

Hentzer, M., & Givskov, M. (2003). Pharmacological inhibition of quorum sensing for the treatment of chronic bacterial infections. *J Clin Invest, 112*(9), 1300-1307. doi: 10.1172/JCI20074

Hirst, R. A., Kadioglu, A., O'Callaghan, C., & Andrew, P. W. (2004). The role of pneumolysin in pneumococcal pneumonia and meningitis. *Clin Exp Immunol, 138*(2), 195-201. doi: 10.1111/j.1365-2249.2004.02611.x

Hoch, E., Lin, W., Chai, J., Hershfinkel, M., Fu, D., & Sekler, I. (2012). Histidine pairing at the metal transport site of mammalian ZnT transporters controls Zn2+ over Cd2+ selectivity. *Proc Natl Acad Sci U S A, 109*(19), 7202-7207. doi: 10.1073/pnas.1200362109

Holmes, A. R., McNab, R., Millsap, K. W., Rohde, M., Hammerschmidt, S., Mawdsley, J. L., & Jenkinson, H. F. (2001). The pavA gene of *Streptococcus pneumoniae* encodes a fibronectin-binding protein that is essential for virulence. *Mol Microbiol, 41*(6), 1395-1408. doi: 10.1046/j.1365-2958.2001.02610.x

Hood, M. I., Mortensen, B. L., Moore, J. L., Zhang, Y., Kehl-Fie, T. E., Sugitani, N., Chazin, W. J., Caprioli, R. M., & Skaar, E. P. (2012). Identification of an Acinetobacter baumannii zinc acquisition system that facilitates resistance to calprotectin-mediated zinc sequestration. *PLoS Pathog, 8*(12), e1003068. doi: 10.1371/journal.ppat.1003068

Hood, M. I., & Skaar, E. P. (2012). Nutritional immunity: transition metals at the pathogen-host interface. *Nat Rev Microbiol, 10*(8), 525-537. doi: 10.1038/nrmicro2836

Howie, S., Bottomley, C., Chimah, O., Ideh, R., Ebruke, B., Okomo, U., Onyeama, C., Donkor, S., Rodrigues, O., Tapgun, M., Janneh, M., Oluwalana, C., Kuti, B., Enwere, G., Esangbedo, P., Doherty, C., Mackenzie, G., Greenwood, B., Corrah, T., Prentice, A., Adegbola, R., & Zaman, S. (2018). Zinc as an adjunct therapy in the management of severe pneumonia among Gambian children: randomized controlled trial. *J Glob Health, 8*(1), 010418. doi: 10.7189/jogh.08.010418

Huang, L., Kirschke, C. P., & Gitschier, J. (2002). Functional characterization of a novel mammalian zinc transporter, ZnT6. *J Biol Chem, 277*(29), 26389-26395. doi: 10.1074/jbc.M200462200

Huang, L., & Tepaamorndech, S. (2013). The SLC30 family of zinc transporters - a review of current understanding of their biological and pathophysiological roles. *Mol Aspects Med, 34*(2-3), 548-560. doi: 10.1016/j.mam.2012.05.008

Hung, H. C., & Chang, G. G. (2001). Differentiation of the slow-binding mechanism for magnesium ion activation and zinc ion inhibition of human placental alkaline phosphatase. *Protein Sci, 10*(1), 34-45. doi: 10.1110/ps.35201

Hussain, M., Melegaro, A., Pebody, R. G., George, R., Edmunds, W. J., Talukdar, R., Martin, S. A., Efstratiou, A., & Miller, E. (2005). A longitudinal household study of *Streptococcus pneumoniae* nasopharyngeal carriage in a UK setting. *Epidemiol Infect, 133*(5), 891-898. doi: 10.1017/S0950268805004012

Ikeda, T., Kimura, K., Morioka, S., & Tamaki, N. (1980). Inhibitory effects of Zn2+ on muscle glycolysis and their reversal by histidine. *J Nutr Sci Vitaminol (Tokyo), 26*(4), 357-366.

Irving, H., & Williams, R. J. P. (1948). Order of Stability of Metal Complexes. *Nature, 162*, 746–747.

Irving, H. W. R. J. P. (1953). The stability of transition-metal complexes. *Journal of the Chemical Society, 0*, 3192-3210. doi: 10.1039/JR9530003192

Jackson, K. A., Helston, R. M., McKay, J. A., O'Neill, E. D., Mathers, J. C., & Ford, D. (2007). Splice variants of the human zinc transporter ZnT5 (SLC30A5) are differentially localized and regulated by zinc through transcription and mRNA stability. *J Biol Chem, 282*(14), 10423-10431. doi: 10.1074/jbc.M610535200

Jacobsen, F. E., Kazmierczak, K. M., Lisher, J. P., Winkler, M. E., & Giedroc, D. P. (2011). Interplay between manganese and zinc homeostasis in the human pathogen *Streptococcus pneumoniae*. *Metallomics, 3*(1), 38-41.

Janoff, E. N., Breiman, R. F., Daley, C. L., & Hopewell, P. C. (1992). Pneumococcal disease during HIV infection. Epidemiologic, clinical, and immunologic perspectives. *Ann Intern Med, 117*(4), 314-324. doi: 10.7326/0003-4819-117-4-314

Jensch, I., Gamez, G., Rothe, M., Ebert, S., Fulde, M., Somplatzki, D., Bergmann, S., Petruschka, L., Rohde, M., Nau, R., & Hammerschmidt, S. (2010). PavB is a surface-exposed adhesin of *Streptococcus pneumoniae* contributing to nasopharyngeal colonization and airways infections. *Mol Microbiol, 77*(1), 22-43. doi: 10.1111/j.1365-2958.2010.07189.x

Johnston, J. W., Briles, D. E., Myers, L. E., & Hollingshead, S. K. (2006). Mn2+-dependent regulation of multiple genes in *Streptococcus pneumoniae* through PsaR and the resultant impact on virulence. *Infect Immun, 74*(2), 1171-1180. doi: 10.1128/IAI.74.2.1171-1180.2006

Johnston, J. W., Myers, L. E., Ochs, M. M., Benjamin, W. H., Jr., Briles, D. E., & Hollingshead, S. K. (2004). Lipoprotein PsaA in virulence of *Streptococcus pneumoniae*: surface accessibility and role in protection from superoxide. *Infect Immun, 72*(10), 5858-5867. doi: 10.1128/IAI.72.10.5858-5867.2004

Kadioglu, A., Gingles, N. A., Grattan, K., Kerr, A., Mitchell, T. J., & Andrew, P. W. (2000). Host cellular immune response to pneumococcal lung infection in mice. *Infect Immun, 68*(2), 492-501. doi: 10.1128/iai.68.2.492-501.2000

Kadioglu, A., Weiser, J. N., Paton, J. C., & Andrew, P. W. (2008). The role of *Streptococcus pneumoniae* virulence factors in host respiratory colonization and disease. *Nat Rev Microbiol, 6*(4), 288-301. doi: 10.1038/nrmicro1871

Kamtchoua, T., Bologa, M., Hopfer, R., Neveu, D., Hu, B., Sheng, X., Corde, N., Pouzet, C., Zimmermann, G., & Gurunathan, S. (2013). Safety and immunogenicity of the pneumococcal pneumolysin derivative PlyD1 in a single-antigen protein vaccine candidate in adults. *Vaccine, 31*(2), 327-333. doi: 10.1016/j.vaccine.2012.11.005

Kapetanovic, R., Bokil, N. J., Achard, M. E., Ong, C. L., Peters, K. M., Stocks, C. J., Phan, M. D., Monteleone, M., Schroder, K., Irvine, K. M., Saunders, B. M., Walker, M. J., Stacey, K. J., McEwan, A. G., Schembri, M. A., & Sweet, M. J. (2016). Salmonella employs multiple mechanisms to subvert the TLR-inducible zinc-mediated antimicrobial response of human macrophages. *FASEB J, 30*(5), 1901-1912. doi: 10.1096/fj.201500061

Kaplan, S. L., Mason, E. O., Jr., Wald, E. R., Schutze, G. E., Bradley, J. S., Tan, T. Q., Hoffman, J. A., Givner, L. B., Yogev, R., & Barson, W. J. (2004). Decrease of invasive pneumococcal infections in children among 8 children's hospitals in the United States after the introduction of the 7-valent pneumococcal conjugate vaccine. *Pediatrics, 113*(3 Pt 1), 443-449. doi: 10.1542/peds.113.3.443

Kehl-Fie, T. E., Chitayat, S., Hood, M. I., Damo, S., Restrepo, N., Garcia, C., Munro, K. A., Chazin, W. J., & Skaar, E. P. (2011). Nutrient metal sequestration by calprotectin inhibits bacterial superoxide defense, enhancing neutrophil killing of *Staphylococcus aureus*. *Cell Host Microbe, 10*(2), 158-164. doi: 10.1016/j.chom.2011.07.004

Kietzman, C. C., Gao, G., Mann, B., Myers, L., & Tuomanen, E. I. (2016). Dynamic capsule restructuring by the main pneumococcal autolysin LytA in response to the epithelium. *Nat Commun, 7*, 10859. doi: 10.1038/ncomms10859

Kilian, M., Poulsen, K., Blomqvist, T., Havarstein, L. S., Bek-Thomsen, M., Tettelin, H., & Sorensen, U. B. (2008). Evolution of *Streptococcus pneumoniae* and its close commensal relatives. *PLoS One, 3*(7), e2683. doi: 10.1371/journal.pone.0002683

Kilian, M., Riley, D. R., Jensen, A., Bruggemann, H., & Tettelin, H. (2014). Parallel evolution of *Streptococcus pneumoniae* and Streptococcus mitis to pathogenic and mutualistic lifestyles. *MBio, 5*(4), e01490-01414. doi: 10.1128/mBio.01490-14

King, J. C. (2011). Zinc: an essential but elusive nutrient. *Am J Clin Nutr, 94*(2), 679S-684S. doi: 10.3945/ajcn.110.005744

King, S. J., Hippe, K. R., & Weiser, J. N. (2006). Deglycosylation of human glycoconjugates by the sequential activities of exoglycosidases expressed by *Streptococcus pneumoniae*. *Mol Microbiol, 59*(3), 961-974. doi: 10.1111/j.1365-2958.2005.04984.x

Kirschke, C. P., & Huang, L. (2003). ZnT7, a novel mammalian zinc transporter, accumulates zinc in the Golgi apparatus. *J Biol Chem, 278*(6), 4096-4102. doi: 10.1074/jbc.M207644200

Kloosterman, T. G., van der Kooi-Pol, M. M., Bijlsma, J. J., & Kuipers, O. P. (2007). The novel transcriptional regulator SczA mediates protection against Zn2+ stress by activation of the Zn2+-resistance gene czcD in *Streptococcus pneumoniae*. *Mol Microbiol, 65*(4), 1049-1063. doi: 10.1111/j.1365-2958.2007.05849.x

Kloosterman, T. G., Witwicki, R. M., van der Kooi-Pol, M. M., Bijlsma, J. J., & Kuipers, O. P. (2008). Opposite effects of Mn2+ and Zn2+ on PsaR-mediated expression of the virulence genes pcpA, prtA, and psaBCA of *Streptococcus pneumoniae*. *J Bacteriol, 190*(15), 5382-5393. doi: 10.1128/JB.00307-08

Kolaj-Robin, O., Russell, D., Hayes, K. A., Pembroke, J. T., & Soulimane, T. (2015). Cation Diffusion Facilitator family: Structure and function. *FEBS Lett, 589*(12), 1283-1295. doi: 10.1016/j.febslet.2015.04.007

Kostrewa, D., D'Arcy, A., Takacs, B., & Kamber, M. (2001). Crystal structures of *Streptococcus pneumoniae* N-acetylglucosamine-1-phosphate uridyltransferase, GlmU, in apo form at 2.33 A resolution and in complex with UDP-N-acetylglucosamine and Mg(2+) at 1.96 A resolution. *J Mol Biol, 305*(2), 279-289. doi: 10.1006/jmbi.2000.4296

Krogh, A., Larsson, B., von Heijne, G., & Sonnhammer, E. L. (2001). Predicting transmembrane protein topology with a hidden Markov model: application to complete genomes. *J Mol Biol, 305*(3), 567-580. doi: 10.1006/jmbi.2000.4315

Kyaw, M. H., Lynfield, R., Schaffner, W., Craig, A. S., Hadler, J., Reingold, A., Thomas, A. R., Harrison, L. H., Bennett, N. M., Farley, M. M., Facklam, R. R., Jorgensen, J. H., Besser, J., Zell, E. R., Schuchat, A., Whitney, C. G., & Active Bacterial Core Surveillance of the Emerging Infections Program, N. (2006). Effect of introduction of the pneumococcal conjugate vaccine on drug-resistant *Streptococcus pneumoniae*. *N Engl J Med, 354*(14), 1455-1463. doi: 10.1056/NEJMoa051642

Lacks, S., & Hotchkiss, R. D. (1960). A study of the genetic material determining an enzyme in Pneumococcus. *Biochim Biophys Acta, 39*, 508-518. doi: 10.1016/0006-3002(60)90205-5

Lagousi, T., Basdeki, P., Routsias, J., & Spoulou, V. (2019). Novel Protein-Based Pneumococcal Vaccines: Assessing the Use of Distinct Protein Fragments Instead of Full-Length Proteins as Vaccine Antigens. *Vaccines (Basel), 7*(1). doi: 10.3390/vaccines7010009

Laitaoja, M., Valjakka, J., & Janis, J. (2013). Zinc coordination spheres in protein structures. *Inorg Chem, 52*(19), 10983-10991. doi: 10.1021/ic401072d

Langmead, B., & Salzberg, S. L. (2012). Fast gapped-read alignment with Bowtie 2. *Nat Methods, 9*(4), 357-359. doi: 10.1038/nmeth.1923

Lannfelt, L., Blennow, K., Zetterberg, H., Batsman, S., Ames, D., Harrison, J., Masters, C. L., Targum, S., Bush, A. I., Murdoch, R., Wilson, J., Ritchie, C. W., & group, P. E. s. (2008). Safety, efficacy, and biomarker findings of PBT2 in targeting Abeta as a modifying therapy for Alzheimer's disease: a phase IIa, double-blind, randomised, placebo-controlled trial. *Lancet Neurol, 7*(9), 779-786. doi: 10.1016/S1474-4422(08)70167-4

Larson, T. R., & Yother, J. (2017). *Streptococcus pneumoniae* capsular polysaccharide is linked to peptidoglycan via a direct glycosidic bond to beta-D-N-acetylglucosamine. *Proc Natl Acad Sci U S A, 114*(22), 5695-5700. doi: 10.1073/pnas.1620431114

LaSarre, B., & Federle, M. J. (2013). Exploiting quorum sensing to confuse bacterial pathogens. *Microbiol Mol Biol Rev, 77*(1), 73-111. doi: 10.1128/MMBR.00046-12

Lepore, C., Silver, L., Theuretzbacher, U., Thomas, J., & Visi, D. (2019). The small-molecule antibiotics pipeline: 2014-2018. *Nat Rev Drug Discov, 18*(10), 739. doi: 10.1038/d41573-019-00130-8

Leukert, N., Sorg, C., & Roth, J. (2005). Molecular basis of the complex formation between the two calcium-binding proteins S100A8 (MRP8) and S100A9 (MRP14). *Biol Chem, 386*(5), 429-434. doi: 10.1515/BC.2005.051

Lewinson, O., & Livnat-Levanon, N. (2017). Mechanism of Action of ABC Importers: Conservation, Divergence, and Physiological Adaptations. *J Mol Biol, 429*(5), 606-619. doi: 10.1016/j.jmb.2017.01.010

Li, H., Handsaker, B., Wysoker, A., Fennell, T., Ruan, J., Homer, N., Marth, G., Abecasis, G., Durbin, R., & Subgroup, G. P. D. P. (2009). The Sequence Alignment/Map format and SAMtools. *Bioinformatics, 25*(16), 2078-2079. doi: 10.1093/bioinformatics/btp352

Liberato, S. C., Singh, G., & Mulholland, K. (2015). Zinc supplementation in young children: A review of the literature focusing on diarrhoea prevention and treatment. *Clin Nutr, 34*(2), 181-188. doi: 10.1016/j.clnu.2014.08.002

Lim, L. E., Vilcheze, C., Ng, C., Jacobs, W. R., Jr., Ramon-Garcia, S., & Thompson, C. J. (2013). Anthelmintic avermectins kill Mycobacterium tuberculosis, including multidrug-resistant clinical strains. *Antimicrob Agents Chemother, 57*(2), 1040-1046. doi: 10.1128/AAC.01696-12

Limoli, D. H., Sladek, J. A., Fuller, L. A., Singh, A. K., & King, S. J. (2011). BgaA acts as an adhesin to mediate attachment of some pneumococcal strains to human epithelial cells. *Microbiology, 157*(Pt 8), 2369-2381. doi: 10.1099/mic.0.045609-0

Lin, D. L., Tran, T., Alam, J. Y., Herron, S. R., Ramirez, M. S., & Tolmasky, M. E. (2014). Inhibition of aminoglycoside 6'-N-acetyltransferase type Ib by zinc: reversal of amikacin resistance in Acinetobacter baumannii and *Escherichia coli* by a zinc ionophore. *Antimicrob Agents Chemother, 58*(7), 4238-4241. doi: 10.1128/AAC.00129-14

Linares, J., Ardanuy, C., Pallares, R., & Fenoll, A. (2010). Changes in antimicrobial resistance, serotypes and genotypes in *Streptococcus pneumoniae* over a 30-year period. *Clin Microbiol Infect, 16*(5), 402-410. doi: 10.1111/j.1469-0691.2010.03182.x

Ling, L. L., Schneider, T., Peoples, A. J., Spoering, A. L., Engels, I., Conlon, B. P., Mueller, A., Schaberle, T. F., Hughes, D. E., Epstein, S., Jones, M., Lazarides, L., Steadman, V. A., Cohen, D. R., Felix, C. R., Fetterman, K. A., Millett, W. P., Nitti, A. G., Zullo, A. M., Chen, C., & Lewis, K. (2015). A new antibiotic kills pathogens without detectable resistance. *Nature, 517*(7535), 455-459. doi: 10.1038/nature14098

Lisher, J. P., & Giedroc, D. P. (2013). Manganese acquisition and homeostasis at the host-pathogen interface. *Front Cell Infect Microbiol, 3*, 91. doi: 10.3389/fcimb.2013.00091

Lisher, J. P., Higgins, K. A., Maroney, M. J., & Giedroc, D. P. (2013). Physical characterization of the manganese-sensing pneumococcal surface antigen repressor from *Streptococcus pneumoniae*. *Biochemistry, 52*(43), 7689-7701. doi: 10.1021/bi401132w

Liu, J. Z., Jellbauer, S., Poe, A. J., Ton, V., Pesciaroli, M., Kehl-Fie, T. E., Restrepo, N. A., Hosking, M. P., Edwards, R. A., Battistoni, A., Pasquali, P., Lane, T. E., Chazin, W. J., Vogl, T., Roth, J., Skaar, E. P., & Raffatellu, M. (2012). Zinc sequestration by the neutrophil protein calprotectin enhances Salmonella growth in the inflamed gut. *Cell Host Microbe, 11*(3), 227-239. doi: 10.1016/j.chom.2012.01.017

Lonnerdal, B. (2000). Dietary factors influencing zinc absorption. *J Nutr, 130*(5S Suppl), 1378S-1383S. doi: 10.1093/jn/130.5.1378S

Lopez, V., & Kelleher, S. L. (2009). Zinc transporter-2 (ZnT2) variants are localized to distinct subcellular compartments and functionally transport zinc. *Biochem J, 422*(1), 43-52. doi: 10.1042/BJ20081189

Lopez-Redondo, M. L., Coudray, N., Zhang, Z., Alexopoulos, J., & Stokes, D. L. (2018). Structural basis for the alternating access mechanism of the cation diffusion facilitator YiiP. *Proc Natl Acad Sci U S A, 115*(12), 3042-3047. doi: 10.1073/pnas.1715051115

Lu, C., Maurer, C. K., Kirsch, B., Steinbach, A., & Hartmann, R. W. (2014). Overcoming the unexpected functional inversion of a PqsR antagonist in Pseudomonas aeruginosa: an in vivo potent antivirulence agent targeting pqs quorum sensing. *Angew Chem Int Ed Engl, 53*(4), 1109-1112. doi: 10.1002/anie.201307547

Lu, M., Chai, J., & Fu, D. (2009). Structural basis for autoregulation of the zinc transporter YiiP. *Nat Struct Mol Biol, 16*(10), 1063-1067. doi: 10.1038/nsmb.1662

Lu, M., & Fu, D. (2007). Structure of the zinc transporter YiiP. *Science, 317*(5845), 1746-1748. doi: 10.1126/science.1143748

Lu, Y. (2010). Metal ions as matchmakers for proteins. *Proc Natl Acad Sci U S A, 107*(5), 1811-1812. doi: 10.1073/pnas.0914008107

Lu, Y. J., Leite, L., Goncalves, V. M., Dias Wde, O., Liberman, C., Fratelli, F., Alderson, M., Tate, A., Maisonneuve, J. F., Robertson, G., Graca, R., Sayeed, S., Thompson, C. M., Anderson, P., & Malley, R. (2010). GMP-grade pneumococcal whole-cell vaccine injected subcutaneously protects mice from nasopharyngeal colonization and fatal aspiration-sepsis. *Vaccine, 28*(47), 7468-7475. doi: 10.1016/j.vaccine.2010.09.031

Lujan, M., Gallego, M., Fontanals, D., Mariscal, D., & Rello, J. (2004). Prospective observational study of bacteremic pneumococcal pneumonia: Effect of discordant therapy on mortality. *Crit Care Med, 32*(3), 625-631. doi: 10.1097/01.ccm.0000114817.58194.bf

Luo, P., & Morrison, D. A. (2003). Transient association of an alternative sigma factor, ComX, with RNA polymerase during the period of competence for genetic transformation in *Streptococcus pneumoniae*. *J Bacteriol, 185*(1), 349-358. doi: 10.1128/jb.185.1.349-358.2003

Lutsenko, S., & Kaplan, J. H. (1995). Organization of P-type ATPases: significance of structural diversity. *Biochemistry, 34*(48), 15607-15613. doi: 10.1021/bi00048a001

Lysenko, E. S., Ratner, A. J., Nelson, A. L., & Weiser, J. N. (2005). The role of innate immune responses in the outcome of interspecies competition for colonization of mucosal surfaces. *PLoS Pathog, 1*(1), e1. doi: 10.1371/journal.ppat.0010001

Ma, Z., Chandrangsu, P., Helmann, T. C., Romsang, A., Gaballa, A., & Helmann, J. D. (2014). Bacillithiol is a major buffer of the labile zinc pool in Bacillus subtilis. *Mol Microbiol, 94*(4), 756-770. doi: 10.1111/mmi.12794

Ma, Z., Jacobsen, F. E., & Giedroc, D. P. (2009). Coordination chemistry of bacterial metal transport and sensing. *Chem Rev, 109*(10), 4644-4681. doi: 10.1021/cr900077w

Makthal, N., Nguyen, K., Do, H., Gavagan, M., Chandrangsu, P., Helmann, J. D., Olsen, R. J., & Kumaraswami, M. (2017). A Critical Role of Zinc Importer AdcABC in Group A Streptococcus-Host Interactions During Infection and Its Implications for Vaccine Development. *EBioMedicine, 21*, 131-141. doi: 10.1016/j.ebiom.2017.05.030

Malley, R., Lipsitch, M., Stack, A., Saladino, R., Fleisher, G., Pelton, S., Thompson, C., Briles, D., & Anderson, P. (2001). Intranasal immunization with killed unencapsulated whole cells prevents colonization and invasive disease by capsulated pneumococci. *Infect Immun, 69*(8), 4870-4873. doi: 10.1128/IAI.69.8.4870-4873.2001

Malley, R., Trzcinski, K., Srivastava, A., Thompson, C. M., Anderson, P. W., & Lipsitch, M. (2005). CD4+ T cells mediate antibody-independent acquired immunity to pneumococcal colonization. *Proc Natl Acad Sci U S A, 102*(13), 4848-4853. doi: 10.1073/pnas.0501254102

Mandal, A. K., Cheung, W. D., & Arguello, J. M. (2002). Characterization of a thermophilic P-type Ag+/Cu+-ATPase from the extremophile Archaeoglobus fulgidus. *J Biol Chem, 277*(9), 7201-7208. doi: 10.1074/jbc.M109964200

Marrakchi, H., Choi, K. H., & Rock, C. O. (2002). A new mechanism for anaerobic unsaturated fatty acid formation in *Streptococcus pneumoniae*. *J Biol Chem, 277*(47), 44809-44816. doi: 10.1074/jbc.M208920200

Martin, J. E., Edmonds, K. A., Bruce, K. E., Campanello, G. C., Eijkelkamp, B. A., Brazel, E. B., McDevitt, C. A., Winkler, M. E., & Giedroc, D. P. (2017). The zinc efflux activator SczA protects *Streptococcus pneumoniae* serotype 2 D39 from intracellular zinc toxicity. *Mol Microbiol, 104*(4), 636-651. doi: 10.1111/mmi.13654

Martin, J. E., & Giedroc, D. P. (2016). Functional Determinants of Metal Ion Transport and Selectivity in Paralogous Cation Diffusion Facilitator Transporters CzcD and MntE in *Streptococcus pneumoniae*. *J Bacteriol, 198*(7), 1066-1076. doi: 10.1128/JB.00975-15

Martner, A., Dahlgren, C., Paton, J. C., & Wold, A. E. (2008). Pneumolysin released during *Streptococcus pneumoniae* autolysis is a potent activator of intracellular oxygen radical production in neutrophils. *Infect Immun, 76*(9), 4079-4087. doi: 10.1128/IAI.01747-07

Martner, A., Skovbjerg, S., Paton, J. C., & Wold, A. E. (2009). *Streptococcus pneumoniae* autolysis prevents phagocytosis and production of phagocyte-activating cytokines. *Infect Immun, 77*(9), 3826-3837. doi: 10.1128/IAI.00290-09

Matthias, K. A., Roche, A. M., Standish, A. J., Shchepetov, M., & Weiser, J. N. (2008). Neutrophil-toxin interactions promote antigen delivery and mucosal clearance of *Streptococcus pneumoniae*. *J Immunol, 180*(9), 6246-6254. doi: 10.4049/jimmunol.180.9.6246

McAllister, L. J., Tseng, H. J., Ogunniyi, A. D., Jennings, M. P., McEwan, A. G., & Paton, J. C. (2004). Molecular analysis of the psa permease complex of *Streptococcus pneumoniae*. *Mol Microbiol, 53*(3), 889-901. doi: 10.1111/j.1365-2958.2004.04164.x

McCool, T. L., Cate, T. R., Moy, G., & Weiser, J. N. (2002). The immune response to pneumococcal proteins during experimental human carriage. *J Exp Med, 195*(3), 359-365. doi: 10.1084/jem.20011576

McCormick, N. H., & Kelleher, S. L. (2012). ZnT4 provides zinc to zinc-dependent proteins in the trans-Golgi network critical for cell function and Zn export in mammary epithelial cells. *Am J Physiol Cell Physiol, 303*(3), C291-297. doi: 10.1152/ajpcell.00443.2011

McCoy, A. J., Grosse-Kunstleve, R. W., Adams, P. D., Winn, M. D., Storoni, L. C., & Read, R. J. (2007). Phaser crystallographic software. *J Appl Crystallogr, 40*(Pt 4), 658-674. doi: 10.1107/S0021889807021206

McCullers, J. A., McAuley, J. L., Browall, S., Iverson, A. R., Boyd, K. L., & Henriques Normark, B. (2010). Influenza enhances susceptibility to natural acquisition of and disease due to *Streptococcus pneumoniae* in ferrets. *J Infect Dis, 202*(8), 1287-1295. doi: 10.1086/656333

McCullers, J. A., & Rehg, J. E. (2002). Lethal synergism between influenza virus and *Streptococcus pneumoniae*: characterization of a mouse model and the role of platelet-activating factor receptor. *J Infect Dis, 186*(3), 341-350. doi: 10.1086/341462

McDevitt, C. A., Ogunniyi, A. D., Valkov, E., Lawrence, M. C., Kobe, B., McEwan, A. G., & Paton, J. C. (2011). A molecular mechanism for bacterial susceptibility to zinc. *PLoS Pathog, 7*(11), e1002357. doi: 10.1371/journal.ppat.1002357

McKinnell, J. C., P; Blumberg, P; Murty, S; Tillotson, G. . (2017). Clinical Predictors Of Antibiotic Failure In Adult Outpatients With Community-Acquired Pneumonia. *American Journal of Respiratory and Critical Care Medicine, 195*.

Mellroth, P., Sandalova, T., Kikhney, A., Vilaplana, F., Hesek, D., Lee, M., Mobashery, S., Normark, S., Svergun, D., Henriques-Normark, B., & Achour, A. (2014). Structural and functional insights into peptidoglycan access for the lytic amidase LytA of *Streptococcus pneumoniae*. *MBio, 5*(1), e01120-01113. doi: 10.1128/mBio.01120-13

Mengin-Lecreulx, D., & van Heijenoort, J. (1993). Identification of the glmU gene encoding N-acetylglucosamine-1-phosphate uridyltransferase in *Escherichia coli*. *J Bacteriol, 175*(19), 6150-6157. doi: 10.1128/jb.175.19.6150-6157.1993

Mengin-Lecreulx, D., & van Heijenoort, J. (1994). Copurification of glucosamine-1-phosphate acetyltransferase and N-acetylglucosamine-1-phosphate uridyltransferase activities of *Escherichia coli*: characterization of the glmU gene product as a bifunctional enzyme catalyzing two subsequent steps in the pathway for UDP-N-acetylglucosamine synthesis. *J Bacteriol, 176*(18), 5788-5795. doi: 10.1128/jb.176.18.5788-5795.1994

Miro-Canturri, A., Ayerbe-Algaba, R., & Smani, Y. (2019). Drug Repurposing for the Treatment of Bacterial and Fungal Infections. *Front Microbiol, 10*, 41. doi: 10.3389/fmicb.2019.00041

Mitchell, T. J., Andrew, P. W., Saunders, F. K., Smith, A. N., & Boulnois, G. J. (1991). Complement activation and antibody binding by pneumolysin via a region of the toxin homologous to a human acute-phase protein. *Mol Microbiol, 5*(8), 1883-1888. doi: 10.1111/j.1365-2958.1991.tb00812.x

Mocchegiani, E., & Fabris, N. (1995). Age-related thymus involution: zinc reverses in vitro the thymulin secretion defect. *Int J Immunopharmacol, 17*(9), 745-749. doi: 10.1016/0192-0561(95)00064-9

Mogensen, T. H. (2009). Pathogen recognition and inflammatory signaling in innate immune defenses. *Clin Microbiol Rev, 22*(2), 240-273, Table of Contents. doi: 10.1128/CMR.00046-08

Montanini, B., Blaudez, D., Jeandroz, S., Sanders, D., & Chalot, M. (2007). Phylogenetic and functional analysis of the Cation Diffusion Facilitator (CDF) family: improved signature and prediction of substrate specificity. *BMC Genomics, 8*, 107. doi: 10.1186/1471-2164-8-107

Mosser, J. L., & Tomasz, A. (1970). Choline-containing teichoic acid as a structural component of pneumococcal cell wall and its role in sensitivity to lysis by an autolytic enzyme. *J Biol Chem, 245*(2), 287-298.

Munoz, R., Coffey, T. J., Daniels, M., Dowson, C. G., Laible, G., Casal, J., Hakenbeck, R., Jacobs, M., Musser, J. M., Spratt, B. G., & et al. (1991). Intercontinental spread of a multiresistant clone of serotype 23F *Streptococcus pneumoniae*. *J Infect Dis, 164*(2), 302-306.

Murshudov, G. N., Skubak, P., Lebedev, A. A., Pannu, N. S., Steiner, R. A., Nicholls, R. A., Winn, M. D., Long, F., & Vagin, A. A. (2011). REFMAC5 for the refinement of macromolecular crystal structures. *Acta Crystallogr D Biol Crystallogr, 67*(Pt 4), 355-367. doi: 10.1107/S0907444911001314

Nairn, B. L., Lonergan, Z. R., Wang, J., Braymer, J. J., Zhang, Y., Calcutt, M. W., Lisher, J. P., Gilston, B. A., Chazin, W. J., de Crecy-Lagard, V., Giedroc, D. P., & Skaar, E. P. (2016). The Response of Acinetobacter baumannii to Zinc Starvation. *Cell Host Microbe, 19*(6), 826-836. doi: 10.1016/j.chom.2016.05.007

Navne, J. E., Borresen, M. L., Slotved, H. C., Andersson, M., Melbye, M., Ladefoged, K., & Koch, A. (2016). Nasopharyngeal bacterial carriage in young children in Greenland: a population at high risk of respiratory infections. *Epidemiol Infect, 144*(15), 3226-3236. doi: 10.1017/S0950268816001461

Nelson, A. L., Roche, A. M., Gould, J. M., Chim, K., Ratner, A. J., & Weiser, J. N. (2007). Capsule enhances pneumococcal colonization by limiting mucus-mediated clearance. *Infect Immun, 75*(1), 83-90. doi: 10.1128/IAI.01475-06

Niehaus, W. G., Richardson, S. B., & Wolz, R. L. (1996). Slow-binding inhibition of 6-phosphogluconate dehydrogenase by zinc ion. *Arch Biochem Biophys, 333*(2), 333-337. doi: 10.1006/abbi.1996.0399

Nies, D. H. (2003). Efflux-mediated heavy metal resistance in prokaryotes. *FEMS Microbiol Rev, 27*(2-3), 313-339. doi: 10.1016/S0168-6445(03)00048-2

Nowak, J. E., Harmon, K., Caldwell, C. C., & Wong, H. R. (2012). Prophylactic zinc supplementation reduces bacterial load and improves survival in a murine model of sepsis. *Pediatr Crit Care Med, 13*(5), e323-329. doi: 10.1097/PCC.0b013e31824fbd90

O'Brien, K. L., Wolfson, L. J., Watt, J. P., Henkle, E., Deloria-Knoll, M., McCall, N., Lee, E., Mulholland, K., Levine, O. S., Cherian, T., Hib, & Pneumococcal Global Burden of Disease Study, T. (2009). Burden of disease caused by *Streptococcus pneumoniae* in children younger than 5 years: global estimates. *Lancet, 374*(9693), 893-902. doi: 10.1016/S0140-6736(09)61204-6

O'Neill, J. (2014). Review on Antimicrobial Resistance Antimicrobial Resistance: Tackling a crisis for the health and wealth of nations. *London: Review on Antimicrobial Resistance*.

Oakley, G. P., Jr. (1973). The neurotoxicity of the halogenated hydroxyquinolines. A commentary. *JAMA, 225*(4), 395-397.

Ogunniyi, A. D., Mahdi, L. K., Jennings, M. P., McEwan, A. G., McDevitt, C. A., Van der Hoek, M. B., Bagley, C. J., Hoffmann, P., Gould, K. A., & Paton, J. C. (2010). Central role of manganese in regulation of stress responses, physiology, and metabolism in *Streptococcus pneumoniae*. *J Bacteriol, 192*(17), 4489-4497. doi: 10.1128/JB.00064-10

Ogunniyi, A. D., Mahdi, L. K., Trappetti, C., Verhoeven, N., Mermans, D., Van der Hoek, M. B., Plumptre, C. D., & Paton, J. C. (2012). Identification of genes that contribute to

the pathogenesis of invasive pneumococcal disease by in vivo transcriptomic analysis. *Infect Immun, 80*(9), 3268-3278. doi: 10.1128/IAI.00295-12

Ong, C. L., Gillen, C. M., Barnett, T. C., Walker, M. J., & McEwan, A. G. (2014). An antimicrobial role for zinc in innate immune defense against group A streptococcus. *J Infect Dis, 209*(10), 1500-1508. doi: 10.1093/infdis/jiu053

Ong, C. L., Walker, M. J., & McEwan, A. G. (2015). Zinc disrupts central carbon metabolism and capsule biosynthesis in *Streptococcus pyogenes*. *Sci Rep, 5*, 10799. doi: 10.1038/srep10799

Orihuela, C. J., Radin, J. N., Sublett, J. E., Gao, G., Kaushal, D., & Tuomanen, E. I. (2004). Microarray analysis of pneumococcal gene expression during invasive disease. *Infect Immun, 72*(10), 5582-5596. doi: 10.1128/IAI.72.10.5582-5596.2004

Paixao, L., Caldas, J., Kloosterman, T. G., Kuipers, O. P., Vinga, S., & Neves, A. R. (2015). Transcriptional and metabolic effects of glucose on *Streptococcus pneumoniae* sugar metabolism. *Front Microbiol, 6*, 1041. doi: 10.3389/fmicb.2015.01041

Pallares, R., Linares, J., Vadillo, M., Cabellos, C., Manresa, F., Viladrich, P. F., Martin, R., & Gudiol, F. (1995). Resistance to penicillin and cephalosporin and mortality from severe pneumococcal pneumonia in Barcelona, Spain. *N Engl J Med, 333*(8), 474-480. doi: 10.1056/NEJM199508243330802

Palmiter, R. D., & Huang, L. (2004). Efflux and compartmentalization of zinc by members of the SLC30 family of solute carriers. *Pflugers Arch, 447*(5), 744-751. doi: 10.1007/s00424-003-1070-7

Parihar, S. P., Guler, R., Khutlang, R., Lang, D. M., Hurdayal, R., Mhlanga, M. M., Suzuki, H., Marais, A. D., & Brombacher, F. (2014). Statin therapy reduces the mycobacterium tuberculosis burden in human macrophages and in mice by enhancing autophagy and phagosome maturation. *J Infect Dis, 209*(5), 754-763. doi: 10.1093/infdis/jit550

Park, J. T., & Strominger, J. L. (1957). Mode of action of penicillin. *Science, 125*(3238), 99-101.

Parsons, J. B., & Rock, C. O. (2011). Is bacterial fatty acid synthesis a valid target for antibacterial drug discovery? *Curr Opin Microbiol, 14*(5), 544-549. doi: 10.1016/j.mib.2011.07.029

Paton, J. C., Rowan-Kelly, B., & Ferrante, A. (1984). Activation of human complement by the pneumococcal toxin pneumolysin. *Infect Immun, 43*(3), 1085-1087.

Paulsen, I. T., & Saier, M. H., Jr. (1997). A novel family of ubiquitous heavy metal ion transport proteins. *J Membr Biol, 156*(2), 99-103.

Perez, Y., Shorer, Z., Liani-Leibson, K., Chabosseau, P., Kadir, R., Volodarsky, M., Halperin, D., Barber-Zucker, S., Shalev, H., Schreiber, R., Gradstein, L., Gurevich, E., Zarivach, R., Rutter, G. A., Landau, D., & Birk, O. S. (2017). SLC30A9 mutation affecting intracellular zinc homeostasis causes a novel cerebro-renal syndrome. *Brain, 140*(4), 928-939. doi: 10.1093/brain/awx013

Pestova, E. V., Havarstein, L. S., & Morrison, D. A. (1996). Regulation of competence for genetic transformation in *Streptococcus pneumoniae* by an auto-induced peptide pheromone and a two-component regulatory system. *Mol Microbiol, 21*(4), 853-862. doi: 10.1046/j.1365-2958.1996.501417.x

Peterson, S. N., Sung, C. K., Cline, R., Desai, B. V., Snesrud, E. C., Luo, P., Walling, J., Li, H., Mintz, M., Tsegaye, G., Burr, P. C., Do, Y., Ahn, S., Gilbert, J., Fleischmann, R. D., & Morrison, D. A. (2004). Identification of competence pheromone responsive genes in *Streptococcus pneumoniae* by use of DNA microarrays. *Mol Microbiol, 51*(4), 1051-1070. doi: 10.1046/j.1365-2958.2003.03907.x

Philips, B. J., Meguer, J. X., Redman, J., & Baker, E. H. (2003). Factors determining the appearance of glucose in upper and lower respiratory tract secretions. *Intensive Care Med, 29*(12), 2204-2210. doi: 10.1007/s00134-003-1961-2

Pinkner, J. S., Remaut, H., Buelens, F., Miller, E., Aberg, V., Pemberton, N., Hedenstrom, M., Larsson, A., Seed, P., Waksman, G., Hultgren, S. J., & Almqvist, F. (2006). Rationally designed small compounds inhibit pilus biogenesis in uropathogenic bacteria. *Proc Natl Acad Sci U S A, 103*(47), 17897-17902. doi: 10.1073/pnas.0606795103

Plumptre, C. D., Eijkelkamp, B. A., Morey, J. R., Behr, F., Counago, R. M., Ogunniyi, A. D., Kobe, B., O'Mara, M. L., Paton, J. C., & McDevitt, C. A. (2014). AdcA and AdcAII employ distinct zinc acquisition mechanisms and contribute additively to zinc homeostasis in *Streptococcus pneumoniae*. *Mol Microbiol, 91*(4), 834-851. doi: 10.1111/mmi.12504

Potter, A. J., Kidd, S. P., McEwan, A. G., & Paton, J. C. (2010). The MerR/NmlR family transcription factor of *Streptococcus pneumoniae* responds to carbonyl stress and modulates hydrogen peroxide production. *J Bacteriol, 192*(15), 4063-4066. doi: 10.1128/JB.00383-10

Potter, A. J., Trappetti, C., & Paton, J. C. (2012). *Streptococcus pneumoniae* uses glutathione to defend against oxidative stress and metal ion toxicity. *J Bacteriol, 194*(22), 6248-6254. doi: 10.1128/JB.01393-12

Prasad, A. S. (2013). Discovery of human zinc deficiency: its impact on human health and disease. *Adv Nutr, 4*(2), 176-190. doi: 10.3945/an.112.003210

Price, A. C., Zhang, Y. M., Rock, C. O., & White, S. W. (2001). Structure of beta-ketoacyl-[acyl carrier protein] reductase from *Escherichia coli*: negative cooperativity and its structural basis. *Biochemistry, 40*(43), 12772-12781.

Quadri, M., Federico, A., Zhao, T., Breedveld, G. J., Battisti, C., Delnooz, C., Severijnen, L. A., Di Toro Mammarella, L., Mignarri, A., Monti, L., Sanna, A., Lu, P., Punzo, F., Cossu, G., Willemsen, R., Rasi, F., Oostra, B. A., van de Warrenburg, B. P., & Bonifati, V. (2012). Mutations in SLC30A10 cause parkinsonism and dystonia with hypermanganesemia, polycythemia, and chronic liver disease. *Am J Hum Genet, 90*(3), 467-477. doi: 10.1016/j.ajhg.2012.01.017

Quinlan, A. R., & Hall, I. M. (2010). BEDTools: a flexible suite of utilities for comparing genomic features. *Bioinformatics, 26*(6), 841-842. doi: 10.1093/bioinformatics/btq033

Rajamuthiah, R., Fuchs, B. B., Conery, A. L., Kim, W., Jayamani, E., Kwon, B., Ausubel, F. M., & Mylonakis, E. (2015). Repurposing salicylanilide anthelmintic drugs to combat drug resistant *Staphylococcus aureus*. *PLoS One, 10*(4), e0124595. doi: 10.1371/journal.pone.0124595

Ramos-Sevillano, E., Ercoli, G., & Brown, J. S. (2019). Mechanisms of Naturally Acquired Immunity to *Streptococcus pneumoniae*. *Front Immunol, 10*, 358. doi: 10.3389/fimmu.2019.00358

Ranaldi, G., Perozzi, G., Truong-Tran, A., Zalewski, P., & Murgia, C. (2002). Intracellular distribution of labile Zn(II) and zinc transporter expression in kidney and MDCK cells. *Am J Physiol Renal Physiol, 283*(6), F1365-1375. doi: 10.1152/ajprenal.00094.2002

Rasko, D. A., Moreira, C. G., Li de, R., Reading, N. C., Ritchie, J. M., Waldor, M. K., Williams, N., Taussig, R., Wei, S., Roth, M., Hughes, D. T., Huntley, J. F., Fina, M. W., Falck, J. R., & Sperandio, V. (2008). Targeting QseC signaling and virulence for antibiotic development. *Science, 321*(5892), 1078-1080. doi: 10.1126/science.1160354

Rathinakumar, R., & Wimley, W. C. (2010). High-throughput discovery of broad-spectrum peptide antibiotics. *FASEB J, 24*(9), 3232-3238. doi: 10.1096/fj.10-157040

Regev-Yochay, G., Trzcinski, K., Thompson, C. M., Malley, R., & Lipsitch, M. (2006). Interference between *Streptococcus pneumoniae* and *Staphylococcus aureus*: In vitro hydrogen peroxide-mediated killing by *Streptococcus pneumoniae*. *J Bacteriol, 188*(13), 4996-5001. doi: 10.1128/JB.00317-06

Rensing, C., Ghosh, M., & Rosen, B. P. (1999). Families of soft-metal-ion-transporting ATPases. *J Bacteriol, 181*(19), 5891-5897.

Reyes-Caballero, H., Campanello, G. C., & Giedroc, D. P. (2011). Metalloregulatory proteins: metal selectivity and allosteric switching. *Biophys Chem, 156*(2-3), 103-114. doi: 10.1016/j.bpc.2011.03.010

Reyes-Caballero, H., Guerra, A. J., Jacobsen, F. E., Kazmierczak, K. M., Cowart, D., Koppolu, U. M., Scott, R. A., Winkler, M. E., & Giedroc, D. P. (2010). The metalloregulatory zinc site in *Streptococcus pneumoniae* AdcR, a zinc-activated MarR family repressor. *J Mol Biol, 403*(2), 197-216. doi: 10.1016/j.jmb.2010.08.030

Reynolds, P. E. (1989). Structure, biochemistry and mechanism of action of glycopeptide antibiotics. *Eur J Clin Microbiol Infect Dis, 8*(11), 943-950.

Rice, K. C., & Bayles, K. W. (2008). Molecular control of bacterial death and lysis. *Microbiol Mol Biol Rev, 72*(1), 85-109, table of contents. doi: 10.1128/MMBR.00030-07

Richard, A. L., Siegel, S. J., Erikson, J., & Weiser, J. N. (2014). TLR2 signaling decreases transmission of *Streptococcus pneumoniae* by limiting bacterial shedding in an infant mouse Influenza A co-infection model. *PLoS Pathog, 10*(8), e1004339. doi: 10.1371/journal.ppat.1004339

Richards, L., Ferreira, D. M., Miyaji, E. N., Andrew, P. W., & Kadioglu, A. (2010). The immunising effect of pneumococcal nasopharyngeal colonisation; protection against future colonisation and fatal invasive disease. *Immunobiology, 215*(4), 251-263. doi: 10.1016/j.imbio.2009.12.004

Riley, I. D., Tarr, P. I., Andrews, M., Pfeiffer, M., Howard, R., Challands, P., & Jennison, G. (1977). Immunisation with a polyvalent pneumococcal vaccine. Reduction of adult respiratory mortality in a New Guinea Highlands community. *Lancet, 1*(8026), 1338-1341. doi: 10.1016/s0140-6736(77)92552-1

Robert, A., Liu, Y., Nguyen, M., & Meunier, B. (2015). Regulation of copper and iron homeostasis by metal chelators: a possible chemotherapy for Alzheimer's disease. *Acc Chem Res, 48*(5), 1332-1339. doi: 10.1021/acs.accounts.5b00119

Roca, A., Hill, P. C., Townend, J., Egere, U., Antonio, M., Bojang, A., Akisanya, A., Litchfield, T., Nsekpong, D. E., Oluwalana, C., Howie, S. R., Greenwood, B., & Adegbola, R. A. (2011). Effects of community-wide vaccination with PCV-7 on pneumococcal nasopharyngeal carriage in the Gambia: a cluster-randomized trial. *PLoS Med, 8*(10), e1001107. doi: 10.1371/journal.pmed.1001107

Roca, I., Akova, M., Baquero, F., Carlet, J., Cavaleri, M., Coenen, S., Cohen, J., Findlay, D., Gyssens, I., Heuer, O. E., Kahlmeter, G., Kruse, H., Laxminarayan, R., Liebana, E., Lopez-Cerero, L., MacGowan, A., Martins, M., Rodriguez-Bano, J., Rolain, J. M., Segovia, C., Sigauque, B., Tacconelli, E., Wellington, E., & Vila, J. (2015). The global threat of antimicrobial resistance: science for intervention. *New Microbes New Infect, 6*, 22-29. doi: 10.1016/j.nmni.2015.02.007

Roche, P. W., Krause, V., Cook, H., Barralet, J., Coleman, D., Sweeny, A., Fielding, J., Giele, C., Gilmour, R., Holland, R., Kampen, R., Enhanced Invasive Pneumococcal Disease Surveillance Working, G., Brown, M., Gilbert, L., Hogg, G., Murphy, D., & Pneumococcal Working Party of the Communicable Diseases Network, A. (2008). Invasive pneumococcal disease in Australia, 2006. *Commun Dis Intell Q Rep, 32*(1), 18-30.

Rodionov, D. A., Hebbeln, P., Gelfand, M. S., & Eitinger, T. (2006). Comparative and functional genomic analysis of prokaryotic nickel and cobalt uptake transporters:

evidence for a novel group of ATP-binding cassette transporters. *J Bacteriol, 188*(1), 317-327. doi: 10.1128/JB.188.1.317-327.2006

Rosado, J. L., Lopez, P., Munoz, E., Martinez, H., & Allen, L. H. (1997). Zinc supplementation reduced morbidity, but neither zinc nor iron supplementation affected growth or body composition of Mexican preschoolers. *Am J Clin Nutr, 65*(1), 13-19. doi: 10.1093/ajcn/65.1.13

Rosch, J. W., Gao, G., Ridout, G., Wang, Y. D., & Tuomanen, E. I. (2009). Role of the manganese efflux system mntE for signalling and pathogenesis in *Streptococcus pneumoniae*. *Mol Microbiol, 72*(1), 12-25. doi: 10.1111/j.1365-2958.2009.06638.x

Rose, M. C., & Voynow, J. A. (2006). Respiratory tract mucin genes and mucin glycoproteins in health and disease. *Physiol Rev, 86*(1), 245-278. doi: 10.1152/physrev.00010.2005

Rowe, H. M., Karlsson, E., Echlin, H., Chang, T. C., Wang, L., van Opijnen, T., Pounds, S. B., Schultz-Cherry, S., & Rosch, J. W. (2019a). Bacterial Factors Required for Transmission of *Streptococcus pneumoniae* in Mammalian Hosts. *Cell Host Microbe, 25*(6), 884-891 e886. doi: 10.1016/j.chom.2019.04.012

Rowe, H. M., Meliopoulos, V. A., Iverson, A., Bomme, P., Schultz-Cherry, S., & Rosch, J. W. (2019b). Direct interactions with influenza promote bacterial adherence during respiratory infections. *Nat Microbiol, 4*(8), 1328-1336. doi: 10.1038/s41564-019-0447-0

Rulisek, L., & Vondrasek, J. (1998). Coordination geometries of selected transition metal ions (Co2+, Ni2+, Cu2+, Zn2+, Cd2+, and Hg2+) in metalloproteins. *J Inorg Biochem, 71*(3-4), 115-127. doi: 10.1016/s0162-0134(98)10042-9

Russell, D., & Soulimane, T. (2012). Evidence for zinc and cadmium binding in a CDF transporter lacking the cytoplasmic domain. *FEBS Lett, 586*(24), 4332-4338. doi: 10.1016/j.febslet.2012.10.043

Sa-Leao, R., Pinto, F., Aguiar, S., Nunes, S., Carrico, J. A., Frazao, N., Goncalves-Sousa, N., Melo-Cristino, J., de Lencastre, H., & Ramirez, M. (2011). Analysis of invasiveness of pneumococcal serotypes and clones circulating in Portugal before widespread use of conjugate vaccines reveals heterogeneous behavior of clones expressing the same serotype. *J Clin Microbiol, 49*(4), 1369-1375. doi: 10.1128/JCM.01763-10

Sabri, M., Houle, S., & Dozois, C. M. (2009). Roles of the extraintestinal pathogenic *Escherichia coli* ZnuACB and ZupT zinc transporters during urinary tract infection. *Infect Immun, 77*(3), 1155-1164. doi: 10.1128/IAI.01082-08

Salusso, A., & Raimunda, D. (2017). Defining the Roles of the Cation Diffusion Facilitators in Fe(2+)/Zn(2+) Homeostasis and Establishment of Their Participation in Virulence in Pseudomonas aeruginosa. *Front Cell Infect Microbiol, 7*, 84. doi: 10.3389/fcimb.2017.00084

Santini, C., Pellei, M., Gandin, V., Porchia, M., Tisato, F., & Marzano, C. (2014). Advances in copper complexes as anticancer agents. *Chem Rev, 114*(1), 815-862. doi: 10.1021/cr400135x

Sazawal, S., Black, R. E., Jalla, S., Mazumdar, S., Sinha, A., & Bhan, M. K. (1998). Zinc supplementation reduces the incidence of acute lower respiratory infections in infants and preschool children: a double-blind, controlled trial. *Pediatrics, 102*(1 Pt 1), 1-5. doi: 10.1542/peds.102.1.1

Scanlon, T. C., Dostal, S. M., & Griswold, K. E. (2014). A high-throughput screen for antibiotic drug discovery. *Biotechnol Bioeng, 111*(2), 232-243. doi: 10.1002/bit.25019

Schrag, S. J., Beall, B., & Dowell, S. F. (2000). Limiting the spread of resistant pneumococci: biological and epidemiologic evidence for the effectiveness of alternative interventions. *Clin Microbiol Rev, 13*(4), 588-601. doi: 10.1128/cmr.13.4.588-601.2000

Schrag, S. J., Pena, C., Fernandez, J., Sanchez, J., Gomez, V., Perez, E., Feris, J. M., & Besser, R. E. (2001). Effect of short-course, high-dose amoxicillin therapy on resistant pneumococcal carriage: a randomized trial. *JAMA, 286*(1), 49-56. doi: 10.1001/jama.286.1.49

Schrödinger, L. The PyMOL Molecular Graphics System. *Version 2*.

Seiberling, M., Bologa, M., Brookes, R., Ochs, M., Go, K., Neveu, D., Kamtchoua, T., Lashley, P., Yuan, T., & Gurunathan, S. (2012). Safety and immunogenicity of a pneumococcal histidine triad protein D vaccine candidate in adults. *Vaccine, 30*(52), 7455-7460. doi: 10.1016/j.vaccine.2012.10.080

Shackelford, G. S., Regni, C. A., & Beamer, L. J. (2004). Evolutionary trace analysis of the alpha-D-phosphohexomutase superfamily. *Protein Sci, 13*(8), 2130-2138. doi: 10.1110/ps.04801104

Shafeeq, S., Yesilkaya, H., Kloosterman, T. G., Narayanan, G., Wandel, M., Andrew, P. W., Kuipers, O. P., & Morrissey, J. A. (2011). The cop operon is required for copper homeostasis and contributes to virulence in *Streptococcus pneumoniae*. *Mol Microbiol, 81*(5), 1255-1270. doi: 10.1111/j.1365-2958.2011.07758.x

Shak, J. R., Vidal, J. E., & Klugman, K. P. (2013). Influence of bacterial interactions on pneumococcal colonization of the nasopharynx. *Trends Microbiol, 21*(3), 129-135. doi: 10.1016/j.tim.2012.11.005

Shankar, A. H., & Prasad, A. S. (1998). Zinc and immune function: the biological basis of altered resistance to infection. *Am J Clin Nutr, 68*(2 Suppl), 447S-463S. doi: 10.1093/ajcn/68.2.447S

Shanker, E., & Federle, M. J. (2017). Quorum Sensing Regulation of Competence and Bacteriocins in *Streptococcus pneumoniae* and mutans. *Genes (Basel), 8*(1). doi: 10.3390/genes8010015

Sharma, R., & Khan, I. A. (2017). Mechanism and Potential Inhibitors of GlmU: A Novel Target for Antimicrobial Drug Discovery. *Curr Drug Targets, 18*(14), 1587-1597. doi: 10.2174/1389450117666160502152011

Shinitzky, M., & Barenholz, Y. (1978). Fluidity parameters of lipid regions determined by fluorescence polarization. *Biochim Biophys Acta, 515*(4), 367-394.

Short, K. R., & Diavatopoulos, D. A. (2015). Nasopharyngeal Colonization with *Streptococcus pneumoniae*. *Streptococcus pneumoniae, Academic Press*, 279-291.

Sievers, F., Wilm, A., Dineen, D., Gibson, T. J., Karplus, K., Li, W., Lopez, R., McWilliam, H., Remmert, M., Soding, J., Thompson, J. D., & Higgins, D. G. (2011). Fast, scalable generation of high-quality protein multiple sequence alignments using Clustal Omega. *Mol Syst Biol, 7*, 539. doi: 10.1038/msb.2011.75

Sjostrom, K., Spindler, C., Ortqvist, A., Kalin, M., Sandgren, A., Kuhlmann-Berenzon, S., & Henriques-Normark, B. (2006). Clonal and capsular types decide whether pneumococci will act as a primary or opportunistic pathogen. *Clin Infect Dis, 42*(4), 451-459. doi: 10.1086/499242

Sladek, R., Rocheleau, G., Rung, J., Dina, C., Shen, L., Serre, D., Boutin, P., Vincent, D., Belisle, A., Hadjadj, S., Balkau, B., Heude, B., Charpentier, G., Hudson, T. J., Montpetit, A., Pshezhetsky, A. V., Prentki, M., Posner, B. I., Balding, D. J., Meyre, D., Polychronakos, C., & Froguel, P. (2007). A genome-wide association study identifies novel risk loci for type 2 diabetes. *Nature, 445*(7130), 881-885. doi: 10.1038/nature05616

Sobota, J. M., & Imlay, J. A. (2011). Iron enzyme ribulose-5-phosphate 3-epimerase in *Escherichia coli* is rapidly damaged by hydrogen peroxide but can be protected by manganese. *Proc Natl Acad Sci U S A, 108*(13), 5402-5407. doi: 10.1073/pnas.1100410108

Solioz, M., & Vulpe, C. (1996). CPx-type ATPases: a class of P-type ATPases that pump heavy metals. *Trends Biochem Sci, 21*(7), 237-241.

Stephan, J. R., & Nolan, E. M. (2016). Calcium-induced Tetramerization and Zinc Chelation Shield Human Calprotectin from Degradation by Host and Bacterial Extracellular Proteases. *Chem Sci, 7*(3), 1962-1975. doi: 10.1039/C5SC03287C

Stincone, A., Prigione, A., Cramer, T., Wamelink, M. M., Campbell, K., Cheung, E., Olin-Sandoval, V., Gruning, N. M., Kruger, A., Tauqeer Alam, M., Keller, M. A., Breitenbach, M., Brindle, K. M., Rabinowitz, J. D., & Ralser, M. (2015). The return

of metabolism: biochemistry and physiology of the pentose phosphate pathway. *Biol Rev Camb Philos Soc, 90*(3), 927-963. doi: 10.1111/brv.12140

Stocks, C. J., Phan, M. D., Achard, M. E. S., Nhu, N. T. K., Condon, N. D., Gawthorne, J. A., Lo, A. W., Peters, K. M., McEwan, A. G., Kapetanovic, R., Schembri, M. A., & Sweet, M. J. (2019). Uropathogenic *Escherichia coli* employs both evasion and resistance to subvert innate immune-mediated zinc toxicity for dissemination. *Proc Natl Acad Sci U S A, 116*(13), 6341-6350. doi: 10.1073/pnas.1820870116

Stone, V. N., & Xu, P. (2017). Targeted antimicrobial therapy in the microbiome era. *Mol Oral Microbiol, 32*(6), 446-454. doi: 10.1111/omi.12190

Strand, T. A., Hollingshead, S. K., Julshamn, K., Briles, D. E., Blomberg, B., & Sommerfelt, H. (2003). Effects of zinc deficiency and pneumococcal surface protein a immunization on zinc status and the risk of severe infection in mice. *Infect Immun, 71*(4), 2009-2013.

Strupat, K., Rogniaux, H., Van Dorsselaer, A., Roth, J., & Vogl, T. (2000). Calcium-induced noncovalently linked tetramers of MRP8 and MRP14 are confirmed by electrospray ionization-mass analysis. *J Am Soc Mass Spectrom, 11*(9), 780-788. doi: 10.1016/S1044-0305(00)00150-1

Sucher, A. J., Chahine, E. B., Nelson, M., & Sucher, B. J. (2011). Prevnar 13, the new 13-valent pneumococcal conjugate vaccine. *Ann Pharmacother, 45*(12), 1516-1524. doi: 10.1345/aph.1Q347

Sulzenbacher, G., Gal, L., Peneff, C., Fassy, F., & Bourne, Y. (2001). Crystal structure of *Streptococcus pneumoniae* N-acetylglucosamine-1-phosphate uridyltransferase bound to acetyl-coenzyme A reveals a novel active site architecture. *J Biol Chem, 276*(15), 11844-11851. doi: 10.1074/jbc.M011225200

Swiatlo, E., & Ware, D. (2003). Novel vaccine strategies with protein antigens of *Streptococcus pneumoniae*. *FEMS Immunol Med Microbiol, 38*(1), 1-7. doi: 10.1016/S0928-8244(03)00146-9

Swier, L. J., Guskov, A., & Slotboom, D. J. (2016). Structural insight in the toppling mechanism of an energy-coupling factor transporter. *Nat Commun, 7*, 11072. doi: 10.1038/ncomms11072

Talbot, U. M., Paton, A. W., & Paton, J. C. (1996). Uptake of *Streptococcus pneumoniae* by respiratory epithelial cells. *Infect Immun, 64*(9), 3772-3777.

Tan, T. Q. (2012). Pediatric invasive pneumococcal disease in the United States in the era of pneumococcal conjugate vaccines. *Clin Microbiol Rev, 25*(3), 409-419. doi: 10.1128/CMR.00018-12

Tateda, K., Matsumoto, T., Miyazaki, S., & Yamaguchi, K. (1999). Efficacy of beta-lactam antibiotics combined with gentamicin against penicillin-resistant pneumococcal pneumonia in CBA/J mice. *J Antimicrob Chemother, 43*(3), 367-371.

Tatusov, R. L., Galperin, M. Y., Natale, D. A., & Koonin, E. V. (2000). The COG database: a tool for genome-scale analysis of protein functions and evolution. *Nucleic Acids Res, 28*(1), 33-36.

ter Beek, J., Guskov, A., & Slotboom, D. J. (2014). Structural diversity of ABC transporters. *J Gen Physiol, 143*(4), 419-435. doi: 10.1085/jgp.201411164

Thangamani, S., Mohammad, H., Abushahba, M. F., Hamed, M. I., Sobreira, T. J., Hedrick, V. E., Paul, L. N., & Seleem, M. N. (2015a). Exploring simvastatin, an antihyperlipidemic drug, as a potential topical antibacterial agent. *Sci Rep, 5*, 16407. doi: 10.1038/srep16407

Thangamani, S., Younis, W., & Seleem, M. N. (2015b). Repurposing celecoxib as a topical antimicrobial agent. *Front Microbiol, 6*, 750. doi: 10.3389/fmicb.2015.00750

Tomasz, A. (1965). Control of the competent state in Pneumococcus by a hormone-like cell product: an example for a new type of regulatory mechanism in bacteria. *Nature, 208*(5006), 155-159. doi: 10.1038/208155a0

Totsika, M. (2017). Disarming pathogens: benefits and challenges of antimicrobials that target bacterial virulence instead of growth and viability. *Future Med Chem, 9*(3), 267-269. doi: 10.4155/fmc-2016-0227

Trappetti, C., McAllister, L. J., Chen, A., Wang, H., Paton, A. W., Oggioni, M. R., McDevitt, C. A., & Paton, J. C. (2017). Autoinducer 2 Signaling via the Phosphotransferase FruA Drives Galactose Utilization by *Streptococcus pneumoniae*, Resulting in Hypervirulence. *MBio, 8*(1). doi: 10.1128/mBio.02269-16

Triboulet, S., Aude-Garcia, C., Armand, L., Gerdil, A., Diemer, H., Proamer, F., Collin-Faure, V., Habert, A., Strub, J. M., Hanau, D., Herlin, N., Carriere, M., Van Dorsselaer, A., & Rabilloud, T. (2014). Analysis of cellular responses of macrophages to zinc ions and zinc oxide nanoparticles: a combined targeted and proteomic approach. *Nanoscale, 6*(11), 6102-6114. doi: 10.1039/c4nr00319e

Trzcinski, K., Thompson, C., Malley, R., & Lipsitch, M. (2005). Antibodies to conserved pneumococcal antigens correlate with, but are not required for, protection against pneumococcal colonization induced by prior exposure in a mouse model. *Infect Immun, 73*(10), 7043-7046. doi: 10.1128/IAI.73.10.7043-7046.2005

Uchiyama, S., Carlin, A. F., Khosravi, A., Weiman, S., Banerjee, A., Quach, D., Hightower, G., Mitchell, T. J., Doran, K. S., & Nizet, V. (2009). The surface-anchored NanA protein promotes pneumococcal brain endothelial cell invasion. *J Exp Med, 206*(9), 1845-1852. doi: 10.1084/jem.20090386

Ueda, A., Attila, C., Whiteley, M., & Wood, T. K. (2009). Uracil influences quorum sensing and biofilm formation in Pseudomonas aeruginosa and fluorouracil is an antagonist. *Microb Biotechnol, 2*(1), 62-74. doi: 10.1111/j.1751-7915.2008.00060.x

Ulijasz, A. T., Andes, D. R., Glasner, J. D., & Weisblum, B. (2004). Regulation of iron transport in *Streptococcus pneumoniae* by RitR, an orphan response regulator. *J Bacteriol, 186*(23), 8123-8136. doi: 10.1128/JB.186.23.8123-8136.2004

van der Eerden, M. M., Vlaspolder, F., de Graaff, C. S., Groot, T., Bronsveld, W., Jansen, H. M., & Boersma, W. G. (2005). Comparison between pathogen directed antibiotic treatment and empirical broad spectrum antibiotic treatment in patients with community acquired pneumonia: a prospective randomised study. *Thorax, 60*(8), 672-678. doi: 10.1136/thx.2004.030411

van der Heide, T., & Poolman, B. (2002). ABC transporters: one, two or four extracytoplasmic substrate-binding sites? *EMBO Rep, 3*(10), 938-943. doi: 10.1093/embo-reports/kvf201

van Opijnen, T., & Camilli, A. (2012). A fine scale phenotype-genotype virulence map of a bacterial pathogen. *Genome Res, 22*(12), 2541-2551. doi: 10.1101/gr.137430.112

Ventola, C. L. (2015). The antibiotic resistance crisis: part 1: causes and threats. *P T, 40*(4), 277-283.

Verhagen, L. M., de Jonge, M. I., Burghout, P., Schraa, K., Spagnuolo, L., Mennens, S., Eleveld, M. J., van der Gaast-de Jongh, C. E., Zomer, A., Hermans, P. W., & Bootsma, H. J. (2014). Genome-wide identification of genes essential for the survival of *Streptococcus pneumoniae* in human saliva. *PLoS One, 9*(2), e89541. doi: 10.1371/journal.pone.0089541

Vollmer, W., & Tomasz, A. (2000). The pgdA gene encodes for a peptidoglycan N-acetylglucosamine deacetylase in *Streptococcus pneumoniae*. *J Biol Chem, 275*(27), 20496-20501. doi: 10.1074/jbc.M910189199

Wagner, D., Maser, J., Lai, B., Cai, Z., Barry, C. E., 3rd, Honer Zu Bentrup, K., Russell, D. G., & Bermudez, L. E. (2005). Elemental analysis of Mycobacterium avium-, Mycobacterium tuberculosis-, and Mycobacterium smegmatis-containing phagosomes indicates pathogen-induced microenvironments within the host cell's endosomal system. *J Immunol, 174*(3), 1491-1500. doi: 10.4049/jimmunol.174.3.1491

Waldron, K. J., & Robinson, N. J. (2009). How do bacterial cells ensure that metalloproteins get the correct metal? *Nat Rev Microbiol, 7*(1), 25-35. doi: 10.1038/nrmicro2057

Walker, C. L. F., Rudan, I., Liu, L., Nair, H., Theodoratou, E., Bhutta, Z. A., O'Brien, K. L., Campbell, H., & Black, R. E. (2013). Global burden of childhood pneumonia and diarrhoea. *Lancet, 381*(9875), 1405-1416. doi: 10.1016/S0140-6736(13)60222-6

Walsh, R. L., & Camilli, A. (2011). *Streptococcus pneumoniae* is desiccation tolerant and infectious upon rehydration. *MBio, 2*(3), e00092-00011. doi: 10.1128/mBio.00092-11

Wang, M. H., M; Gu, H; Li, S; Ma, Y; Wang, J. (2017). Mutational analysis to identify the residues essential for the acetyltransferase activity of GlmU in Bacillus subtilis. *The Royal Society of Chemistry, 7*, 13858-13867. doi: 10.1039/C7RA00086C

Watson, K., Carville, K., Bowman, J., Jacoby, P., Riley, T. V., Leach, A. J., Lehmann, D., & Kalgoorlie Otitis Media Research Project, T. (2006). Upper respiratory tract bacterial carriage in Aboriginal and non-Aboriginal children in a semi-arid area of Western Australia. *Pediatr Infect Dis J, 25*(9), 782-790. doi: 10.1097/01.inf.0000232705.49634.68

Wei, Y., & Fu, D. (2005). Selective metal binding to a membrane-embedded aspartate in the *Escherichia coli* metal transporter YiiP (FieF). *J Biol Chem, 280*(40), 33716-33724. doi: 10.1074/jbc.M506107200

Weinberg, E. D. (1975). Nutritional immunity. Host's attempt to withold iron from microbial invaders. *JAMA, 231*(1), 39-41. doi: 10.1001/jama.231.1.39

Weinberger, D. M., Malley, R., & Lipsitch, M. (2011). Serotype replacement in disease after pneumococcal vaccination. *Lancet, 378*(9807), 1962-1973. doi: 10.1016/S0140-6736(10)62225-8

Weiser, J. N., Ferreira, D. M., & Paton, J. C. (2018). *Streptococcus pneumoniae*: transmission, colonization and invasion. *Nat Rev Microbiol, 16*(6), 355-367. doi: 10.1038/s41579-018-0001-8

Weiss, G. (2003). Antimicrobial combination therapy. *Wien Med Wochenschr, 153*(7-8), 153-155.

Wenzel, H. J., Cole, T. B., Born, D. E., Schwartzkroin, P. A., & Palmiter, R. D. (1997). Ultrastructural localization of zinc transporter-3 (ZnT-3) to synaptic vesicle membranes within mossy fiber boutons in the hippocampus of mouse and monkey. *Proc Natl Acad Sci U S A, 94*(23), 12676-12681.

Wessells, K. R., & Brown, K. H. (2012). Estimating the global prevalence of zinc deficiency: results based on zinc availability in national food supplies and the prevalence of stunting. *PLoS One, 7*(11), e50568. doi: 10.1371/journal.pone.0050568

White, C., Lee, J., Kambe, T., Fritsche, K., & Petris, M. J. (2009). A role for the ATP7A copper-transporting ATPase in macrophage bactericidal activity. *J Biol Chem, 284*(49), 33949-33956. doi: 10.1074/jbc.M109.070201

Whitney, C. G., Farley, M. M., Hadler, J., Harrison, L. H., Lexau, C., Reingold, A., Lefkowitz, L., Cieslak, P. R., Cetron, M., Zell, E. R., Jorgensen, J. H., Schuchat, A., & Active Bacterial Core Surveillance Program of the Emerging Infections Program, N. (2000).

Increasing prevalence of multidrug-resistant *Streptococcus pneumoniae* in the United States. *N Engl J Med, 343*(26), 1917-1924. doi: 10.1056/NEJM200012283432603

Wiegand, I., Hilpert, K., & Hancock, R. E. (2008). Agar and broth dilution methods to determine the minimal inhibitory concentration (MIC) of antimicrobial substances. *Nat Protoc, 3*(2), 163-175. doi: 10.1038/nprot.2007.521

Wilke, K. E., Francis, S., & Carlson, E. E. (2015). Inactivation of multiple bacterial histidine kinases by targeting the ATP-binding domain. *ACS Chem Biol, 10*(1), 328-335. doi: 10.1021/cb5008019

Williams, L. E., & Mills, R. F. (2005). P(1B)-ATPases--an ancient family of transition metal pumps with diverse functions in plants. *Trends Plant Sci, 10*(10), 491-502. doi: 10.1016/j.tplants.2005.08.008

Winn, M. D., Ballard, C. C., Cowtan, K. D., Dodson, E. J., Emsley, P., Evans, P. R., Keegan, R. M., Krissinel, E. B., Leslie, A. G., McCoy, A., McNicholas, S. J., Murshudov, G. N., Pannu, N. S., Potterton, E. A., Powell, H. R., Read, R. J., Vagin, A., & Wilson, K. S. (2011). Overview of the CCP4 suite and current developments. *Acta Crystallogr D Biol Crystallogr, 67*(Pt 4), 235-242. doi: 10.1107/S0907444910045749

Winters, M. S., Chan, Q., Caruso, J. A., & Deepe, G. S., Jr. (2010). Metallomic analysis of macrophages infected with Histoplasma capsulatum reveals a fundamental role for zinc in host defenses. *J Infect Dis, 202*(7), 1136-1145. doi: 10.1086/656191

Worthington, R. J., Blackledge, M. S., & Melander, C. (2013). Small-molecule inhibition of bacterial two-component systems to combat antibiotic resistance and virulence. *Future Med Chem, 5*(11), 1265-1284. doi: 10.4155/fmc.13.58

Worthington, R. J., & Melander, C. (2013). Combination approaches to combat multidrug-resistant bacteria. *Trends Biotechnol, 31*(3), 177-184. doi: 10.1016/j.tibtech.2012.12.006

Wright, A. K., Bangert, M., Gritzfeld, J. F., Ferreira, D. M., Jambo, K. C., Wright, A. D., Collins, A. M., & Gordon, S. B. (2013). Experimental human pneumococcal carriage augments IL-17A-dependent T-cell defence of the lung. *PLoS Pathog, 9*(3), e1003274. doi: 10.1371/journal.ppat.1003274

Wroe, P. C., Lee, G. M., Finkelstein, J. A., Pelton, S. I., Hanage, W. P., Lipsitch, M., Stevenson, A. E., Rifas-Shiman, S. L., Kleinman, K., Dutta-Linn, M. M., Hinrichsen, V. L., Lakoma, M., & Huang, S. S. (2012). Pneumococcal carriage and antibiotic resistance in young children before 13-valent conjugate vaccine. *Pediatr Infect Dis J, 31*(3), 249-254. doi: 10.1097/INF.0b013e31824214ac

Yeo, W. S., Arya, R., Kim, K. K., Jeong, H., Cho, K. H., & Bae, T. (2018). The FDA-approved anti-cancer drugs, streptozotocin and floxuridine, reduce the virulence of *Staphylococcus aureus*. *Sci Rep, 8*(1), 2521. doi: 10.1038/s41598-018-20617-5

Yesilkaya, H., Kadioglu, A., Gingles, N., Alexander, J. E., Mitchell, T. J., & Andrew, P. W. (2000). Role of manganese-containing superoxide dismutase in oxidative stress and virulence of *Streptococcus pneumoniae*. *Infect Immun, 68*(5), 2819-2826. doi: 10.1128/iai.68.5.2819-2826.2000

Yocum, R. R., Rasmussen, J. R., & Strominger, J. L. (1980). The mechanism of action of penicillin. Penicillin acylates the active site of Bacillus stearothermophilus D-alanine carboxypeptidase. *J Biol Chem, 255*(9), 3977-3986.

Yu, Y., Lu, L., Wang, R. L., Xi, L., Luo, X. G., & Liu, B. (2010). Effects of zinc source and phytate on zinc absorption by in situ ligated intestinal loops of broilers. *Poult Sci, 89*(10), 2157-2165. doi: 10.3382/ps.2009-00486

Zafar, M. A., Hamaguchi, S., Zangari, T., Cammer, M., & Weiser, J. N. (2017a). Capsule Type and Amount Affect Shedding and Transmission of *Streptococcus pneumoniae*. *MBio, 8*(4). doi: 10.1128/mBio.00989-17

Zafar, M. A., Wang, Y., Hamaguchi, S., & Weiser, J. N. (2017b). Host-to-Host Transmission of *Streptococcus pneumoniae* Is Driven by Its Inflammatory Toxin, Pneumolysin. *Cell Host Microbe, 21*(1), 73-83. doi: 10.1016/j.chom.2016.12.005

Zahner, D., & Hakenbeck, R. (2000). The *Streptococcus pneumoniae* beta-galactosidase is a surface protein. *J Bacteriol, 182*(20), 5919-5921. doi: 10.1128/jb.182.20.5919-5921.2000

Zeleny, R., Altmann, F., & Praznik, W. (1997). A capillary electrophoretic study on the specificity of beta-galactosidases from Aspergillus oryzae, *Escherichia coli*, *Streptococcus pneumoniae*, and Canavalia ensiformis (jack bean). *Anal Biochem, 246*(1), 96-101. doi: 10.1006/abio.1996.9973

Zhang, P. (2013). Structure and mechanism of energy-coupling factor transporters. *Trends Microbiol, 21*(12), 652-659. doi: 10.1016/j.tim.2013.09.009

Zygiel, E. M., & Nolan, E. M. (2018). Transition Metal Sequestration by the Host-Defense Protein Calprotectin. *Annu Rev Biochem, 87*, 621-643. doi: 10.1146/annurev-biochem-062917-012312